BIOPOLYMER BASED CARBON NANOCOMPOSITE FOR THE ELECTROCHEMICAL DETERMINATION OF SELECTED PAINKILLER DRUGS

MD.SHALAUDDIN

INSTITUTE FOR ADVANCED STUDIES
UNIVERSITY OF MALAYA
KUALA LUMPUR

2021

BIOPOLYMER BASED CARBON NANOCOMPOSITE FOR THE ELECTROCHEMICAL DETERMINATION OF SELECTED PAINKILLER DRUGS

MD.SHALAUDDIN

THESIS SUBMITTED IN FULFILMENT OF THE REQUIREMENTS FOR THE DEGREE OF DOCTOR OF PHILOSOPY

INSTITUTE FOR ADVANCED STUDIES
UNIVERSITY OF MALAYA
KUALA LUMPUR

2021

UNIVERSITY OF MALAYA

ORIGINAL LITERARY WORK DECLARATION

Name of Candidate: **Md.Shalauddin**

Matric No: **HHC150010/ 17043046**

Name of Degree: **Doctor of Philosophy (Ph.D.)**

Title of Thesis:

BIOPOLYMER BASED CARBON NANOCOMPOSITE FOR THE ELECTROCHEMICAL DETERMINATION OF SELECTED PAINKILLER DRUGS

Field of Study: **Nanotechnology**

I do solemnly and sincerely declare that:

(1) I am the sole author/writer of this Work;
(2) This Work is original;
(3) Any use of any work in which copyright exists was done by way of fair dealing and for permitted purposes and any excerpt or extract from, or reference to or reproduction of any copyright work has been disclosed expressly and sufficiently and the title of the Work and its authorship have been acknowledged in this Work;
(4) I do not have any actual knowledge nor do I ought reasonably to know that the making of this work constitutes an infringement of any copyright work;
(5) I hereby assign all and every rights in the copyright to this Work to the University of Malaya ("UM"), who henceforth shall be owner of the copyright in this Work and that any reproduction or use in any form or by any means whatsoever is prohibited without the written consent of UM having been first had and obtained;
(6) I am fully aware that if in the course of making this Work I have infringed any copyright whether intentionally or otherwise, I may be subject to legal action or any other action as may be determined by UM.

Candidate's Signature Date:

Subscribed and solemnly declared before,

Witness's Signature Date:

Name:

Designation:

BIOPOLYMER BASED CARBON NANOCOMPOSITE FOR THE ELECTROCHEMICAL DETERMINATION OF SELECTED PAINKILLER DRUGS

ABSTRACT

Biopolymers are naturally occurring polymers which have attained profound interest and are investigated widely due to their outstanding characteristics and several advantages such as cost efficiency, excellent hydrophilicity, film formation capability, chemical inertness, non-toxicity, high mechanical integrity and biocompatibility. Cellulose and chitosan are the two most abundant biopolymers in the world. Recently, the incorporation of nanocellulose and chitosan into electroconductive platform i.e nanostructured carbon such as- multiwall carbon nanotube (MWCNT) and nitrogen doped graphene (NDG) is the focus of this thesis for the fabrication of modified electrodes as electrochemical sensor for the detection of some common painkiller drugs. Nanocellulose (NC) and chitosan (CTS) possess excellent properties such as biocompatibility, non-toxicity, biodegradability, film formability, dispersion of nanomaterials and preventing leaching of nanomaterials. These biopolymers enhance the electrocatalytic activity of the carbon-based nanoparticles for the sensitive determination of commonly administered painkillers. Multiwall carbon nanotubes and nitrogen doped graphene both are nanostructured carbons and possess excellent features such as high dispersion, chemical and mechanical stability, high electrical conductivity, high surface area etc. These two nanomaterials are conducting scaffold in the presence of biopolymers for the homogenous dispersion of nanomaterials and ultimately enhances the electrons transfer process. A hybrid nanocomposite of NC and MWCNT was prepared, where NC was synthesized while the MWCNT was functionalized by acid hydrolysis method to afford the *f*-MWCNTs/NC/GCE for the electrochemical determination of widely used painkiller drug,

diclofenac sodium. The assimilation of NC and *f*-MWCNTs enhances the active surface area by proper dispersion of the nanomaterials which enhances the electrical conductivity, accelerates the electrons transfer rate and ultimately amplifies the electrochemical response towards the determination of the targeted analyte. While a nanocomposite comprising of nitrogen doped graphene (NDG), nanocellulose (NC) and sodium dodecyl sulphate (SDS) i.e (NDG-NC)-SDS was prepared for the simultaneous determination of two common painkillers paracetamol (PCT) and naproxen (NPX) in the presence of another painkiller, diclofenac sodium (DCF). Due to binding property of NC, the junction of NC with NDG establishes a good bonding with each other and could be embedded into the graphene nanosheets. Another nanocomposite composed of MWCNT, CTS and copper (Cu), *f*-MWCNTs/CTS-Cu was prepared for the determination of DCF. The excellent catalytic effect of *f*-MWCNTs, adsorption capacity and film formation ability of CTS and the incorporation of Cu by immobilization technique enhances the catalytic effect of CTS-Cu complex. The fabricated *f*-MWCNTs/CTS-Cu nanocomposite is a potential candidate for the analytical detection of DCF. While another conductive biopolymer nanocomposite containing NC and conductive polymer polypyrrole (PPY) was prepared for the simultaneous determination of paracetamol (PCT) and ciprofloxacin (CPR) in commercial dosage forms, biological media and water sample. It should be mentioned that the synthesized biopolymer based nanostructured carbon nanocomposite have been fabricated for the first time for the detection of some common used painkiller drugs in commercial dosage forms and biological fluids.

Keywords: Paracetamol; Diclofenac sodium; Naproxen; Biopolymers; Electrochemical sensor

Polimer-bio yang berasaskan kepada komposit karbon-nano untuk penentuan ubat penghapus kesakitan dengan kaedah elektrokimia

ABSTRAK

Polimer-bio adalah polimer semulajadi yang telah menarik fokus penyelidikan yang luas disebabkan oleh beberapa ciri seperti harga yang murah, hidrofilik, pembentukan filem, kelengaian kimia, ketoksikan rendah, integriti mekanik dan bio-penyesuaian. Selulosa dan kitosan adalah dua jenis polimer-bio yang paling banyak terdapat di dunia. Gabungan di antara selulosa dan kitosan untuk membentuk pentas kealiran elektrik atau karbon berstruktur nano seperti tiub nano karbon multi-dinding dan grafin didopkan nitrogen adalah fokus utama tesis ini untuk pembentukan elektrod termodifikasi sebagai penderia elektrokimia untuk mengesan kehadiran ubat penghapus kesakitan. Selulosa-nano dan kitosan mempunyai ciri ciri yang cemerlang seperti bio-penyesuaian, ketoksikan rendah, bio-terurai, pembentukan filem, kebolehan untuk penguraian dan menghalang perlunturan bahan nano. Polimer-bio tersebut boleh meningkatkan aktiviti elektro-pemangkinan bahan nano karbon untuk penentuan kepekatan ubatan yang sensitif. Tiub nano karbon multi-dinding dan grafin didopkan nitrogen adalah bahan karbon nanostruktur yang mempunyai ciri cemerlang seperti penyebaran tinggi, kestabilan mekanik dan kimia yang tinggi, kealiran elektrik tinggi, luas permukaan tinggi dan lain lain. Kedua-dua bahan nano ini adalah bahan perancah kealiran dengan kehadiran polimer-bio untuk penyebaran bahan nano homogen yang meninggikan lagi proses pemindahan elektron. Suatu komposit nano yang terdiri daripada selulosa-nano dan tiub nano karbon multi-dinding disintesiskan, di mana selulosa-nano disintesiskan manakala tiub nano karbon multi-dinding dihidrolisiskan dengan asid untuk menghasilkan the *f*-MWCNTs/NC/GCE untuk penderiaan elektrokimia suatu ubat penghapus kesakitan, natrium diklofenak. Asimilasi selulosa-nano dan tiub nano karbon

multi-dinding meningkatkan permukaan aktif untuk penyebaran bahan nano yang meningkatkan kealiran elektrik, mempercepatkan perpindahan elektrik dan seterusnya meningkatkan tindakbalas elektrokimia terhadap penentuan kehadiran analit. Manakala komposit nano yang mengandungi grafin didopkan nitrogen, selulosa-nano dan natrium dodesil sulfat (SDS) i.e (NDG-NC)-SDS telah disediakan untuk penentuan serentak dua jenis ubat penghapus kesakitan iaitu parasetamol dan naproxen, dengan kehadiran ubat penghapus kesakitan yang lain iaitu natrium diklofenak. Dengan ciri pengikat yang kuat pada selulosa-nano, persimpanganan di antara selulosa-nano dan grafin didopkan nitrogen mempunyai ikatan yang kuat dan boleh diselitkan ke celah-celah lapisan nano grafin. Suatu komposit nano yang terdiri daripada tiub nano karbon multi-dinding, kitosan dan kuprum, *f*-MWCNTs/CTS-Cu telah disediakan untuk penentuan natirum diklofenak. Akitiviti pemangkinan tiub nano karbon multi-dinding yang tinggi, kapasiti keserapan tinggi dan pembentukan filem yang terdapat di dalam kitosan dan juga pemerbadanan kuprum secara teknik imobilasi meninggikan lagi kesan pemangkinan kompleks kitosan-kuprum. Komposit nano yang disediakan *f*-MWCNTs/CTS-Cu, adalah sesuai untuk digunakan untuk penentuan analitik natrium diklofenak. Manakala suatu polimer-bio kealiran elektrik yang terdiri daripada nanoselulos dan bahan kealiran polimer iaitu polipirol telah disediakan untuk penentuan serentak ubat parasetamol and ciprofloxacin di dalam dos komersial, media biologi dan sampel air sisa. Adalah dimaklumkan bahawa polimer-bio yang disintesiskan bersama-sama dengan struktur nano karbon adalah disediakan untuk kali pertama untuk pengesanan ubat penghapus kesakitan di dalam dos komersial dan cecair biologi.

Kata Kunci: paracetamol; natrium diklofenak; naproxen; penderia elektrokimia; polimer-bio

ACKNOWLEDGEMENTS

All praises be to Allah, for His uncountable blessings, the Allah who is the most Gracious and most Merciful, who gave me the patience and strength and granted me the capability to complete this work.

Firstly, I would like to express my deepest gratitude to my supervisors Professor Dr. Wan Jeffrey Basirun and Professor. Dr. Mohd Rafie Bin Johan for their valuable guidance, continuous support, motivation and encouragement during my PhD journey. Their valuable critical review helped me to enhance the quality of my research writing and immense knowledge.

Next, I would like to express my sincere gratitude to Dr. Samira Bagheri, who was my first supervisor and helped me to start my PhD journey. I would like to extend my gratitude to the research group members to D227 laboratory especially Shamima Akhter, Nadzirah Sofia and Magaji Ladan for their constructive discussions and sharing of knowledge and helped me in my difficult time.

Finally, my sincere gratitude goes to my deceased mother for her hard work, undemanding love, innumerable sacrifices and unconditional support throughout my life. It is possible for me to complete my studies and fulfill her dream because of her sacrifices which she made for me to reach until this point. I feel honored and deeply indebted for the support, encouragement, sacrifices, patience and prayers of my loving father, sister, brothers, aunties. I am grateful to my lovely wife Shamima Akhtetr and adorable son Mohammad Zarrar Riyon Tashreef for their inspiration and support during my difficult times. Without their love and support over the years none of this would have been possible. They have always been there for me and I am gratified for everything they have helped me to achieve. None of this would have been possible without their continuous prayers and support.

TABLE OF CONTENTS

LIST OF FIGURES

LIST OF TABLES

LIST OF SYMBOLS AND ABBREVIATIONS

°C	:	Degree Celsius
µm	:	Micrometer
Adsv	:	Adsorptive stripping differential pulse voltammetry
AA	:	Ascorbic Acid
A.C	:	Alternating current
AFM	:	Atomic force microscopy
Ag	:	Silver
AgCl	:	Silver chloride
Atm	:	Atmospheric pressure
Au	:	Gold
BIA	:	Batch injection analysis
BDDE	:	Boron doped diamond electrode
BNC	:	Bacterial nanocellulose
$CaCo_3$	:	Calcium carbonate
CdO	:	Cadmium oxide nanoparticles
CZF	:	Copper zinc ferrite
CE	:	Counter electrode
Cl	:	Chlorine
C_3N_4	:	Carbon nitride
CNPs	:	Carbon nanoparticles
CNTs	:	Carbon nanotubes
CME	:	Carbon paste electrode
CQDs	:	Carbon quantum dots
CMEs	:	Chemically modified electrodes

CNCs	:	Cellulose nanocrystals
CNFs	:	Cellulose nanofibers
CTAB	:	Cetyl trimethyl ammonium bromide
Co	:	Cobalt
CPR	:	Ciprofloxacin
CTS	:	Chitosan
Cu	:	Copper
$Cu(OH)_2$	:	Copper (II) hydroxide
$CuCl_2$	:	Copper (II) Chloride
CVD	:	Chemical vapor deposition
CV	:	Cyclic voltammetry
CWEs	:	Coated wire electrodes
DA	:	Dopamine
D.C	:	Direct current
DCF	:	Diclofenac Sodium
DDI	:	Drug-drug interactions
DI	:	Deionized
DMSO	:	Dimethyle sulfoxide
DPV	:	Differential Pulse Voltammetry
EDX	:	Energy dispersive X-ray analysis
ECP	:	Electronically conductive polymers
EIS	:	Electrochemical impedance spectroscopy
EPH	:	Epichlorohydrin
e.g	:	For example
FESEM	:	Field emission scanning electron microscopy
Fe_3O_4	:	Ferric oxide

FTO	:	Fluorine doped tin oxide
FTIR	:	Fourier transform infrared spectroscopy
f-MWCNTs	:	Functionalized multiwall carbon nanotubes
GCE	:	Glassy carbon electrode
GE	:	Graphite electrode
GO	:	Graphene oxide
AuNPs	:	Gold nanoparticles
GPES	:	General purpose electrochemical system
GP	:	Graphite paste
GR	:	Graphene
h	:	Hours
HCl	:	Hydrochloric acid
HPLC	:	High performance liquid chromatography
i.e	:	That is
$FeCl_3$	:	Iron Chloride
ISEs	:	Ion selective electrodes
IL	:	Ionic Liquid
ISFETs	:	Ion sensitive field effect transistors
ITO	:	Indium tin oxide
K	:	Kelvin
kV	:	Kilovolts
kHz	:	Kilohertz
KCl	:	Potassium chloride
K_2HPO_4	:	Di-potassium hydrogen phosphate
KH_2PO_4	:	Potassium di-hydrogen phosphate
LC	:	Liquid chromatography

LOD	:	Limit of detection
LSV	:	Linear sweep voltammetry
M	:	Molarity
Mpg	:	Mesoporous polymeric graphitic
µA	:	Microampere
mA	:	Milliampere
µg		Microgram
mHz	:	MIllihertz
µL	:	Microliter
µm	:	Micrometer
µM	:	Micromolar
Mg	:	Milligram
mL	:	Milliliter
Mm	:	Millimeter
mM	:	Millimolar
mV	:	Millivolt
Min	:	Minutes
MIP	:	Molecularly imprinted polymer
M	:	Molarity
MWCNTs	:	Multiwall carbon nanotubes
NC	:	Nanocellulose
NDG	:	Nitrogen doped graphene
NPX	:	Naproxen
Nm	:	Nanometer
NaOH	:	Sodium hydroxide
$NiMoO_4$	:	Nickel molybdate

NiONPs	:	Nickel oxide nanoparticles
N,S@GQDs	:	Nitrogen, sulphur co-doped graphene quantum dots
NSAID	:	Non-steroidal anti-inflammatory drug
OTC	:	Over the counter
PANI	:	Polyaniline
PBS	:	Phosphate buffer solution
PCT	:	Paracetamol
PEG	:	Pencil graphite electrode
PPY	:	Polypyrrole
Pt	:	Platinum
RE	:	Reference electrode
RPM	:	Rotation per minute
RSD	:	Relative standard deviation
Sm_2O_3	:	Samarium oxide
SCE	:	Standard calomel electrode
SDS	:	Sodium dodecyl sulphate
Si-GO-g	:	Silylated graphene oxide grafted chemically modified electrode
STM	:	Scanning tunneling microscope
SWCNTs	:	Single wall carbon nanotubes
SWADSV	:	Squarewave adsorptive stripping voltammetry
SWV	:	Squarewave voltammetry
H_2SO_4	:	Sulphuric acid
TEM	:	Transmission electron microscopy
TiO_2	:	Titanium dioxide
UA	:	Uric acid
TLC	:	Thin layer chromatography

WE	:	Working electrode
H_2O	:	Water
XRD	:	X-ray power diffraction

LIST OF APPENDICES

CHAPTER 1: INTRODUCTION

1.1 Background

1.1.1 Nanotechnology

The breakthrough of nanoscience and widespread implementation of nanotechnology has a revolutionary effect on the world. For the past few years, significant attention has been paid to some materials that were anticipated of being sluggish when in the bulk appearance for several technological implementations. At present, it is already validated that, at the nanostructured configuration, these bulk substances can reveal outstanding physical and chemical features (Zhang *et al*., 2008). In 1959 an American Physical Society meeting was held in Caltech in which Richard Feynman delivered a lecture on the idea of the synthesis of materials at nanoscale isolation. He said in the lecture that "There is Plenty of Room at the Bottom". Furthermore, he said that, in the case of the nanostructured components, the atomic and molecular size can be manipulated and controlled successfully for the electronics and mechanical system. The expansion of this kind of technology into a miniature system would be originated from the fusion of some specific areas such as physics, chemistry and biology. In 1974, the word "nanotechnology" was introduced for the first time by a Japanese scientist named Norio Taniguchi in The International Conference on Production Engineering, held in Tokyo (26-29th August). He stated that "nanotechnology" is the process of separation, integration and deformation of the materials by using one atom or one molecule. In 1980, Gerd Binning and Heinrich Rohrer first implemented the idea of nanotechnology by the invention of scanning the tunneling microscope (STM) and for this, they achieved the Nobel Prize in Physics in 1986(Demuth *et al*., 1986). Calvin Quate and Cristopher Gerber have also implemented the idea of nanotechnology through the invention of the atomic force microscope (AFM). Due to possessing some outstanding characteristics, many

scientists have been emphasized the development of nanostructured materials for the past few decades.

The materials which sizes are in the range between 1 to 100 nm are referred to as nanomaterials. Due to having some excellent advantages, nanomaterials worked as an effective tool for the technological revolution (Tay *et al*., 2014). The exceptional features of these materials such as

1. The expanded surface area to volume ratio with high roughness and sufficient electronic distributions enable rapid and improved interactions toward the desired analytes.
2. High thermal and mechanical integrity, lower in weight compared to other conventional materials. Along with these, they have excellent recognition capacity (Scida *et al*., 2011).
3. Due to the transfer of electrons, enhanced optical absorption or emission occurs, this feature facilitates the rapid signal conduction in electronic devices.
4. The crystallinity, morphology, structure or configuration and shape of the nanomaterials determine the catalytic effect, optic, magnetic and electronic features (Chen *et al*., 2018).

Recently, biopolymers have sparked a huge interest to the scientists the past few years due to having some unique features such as biodegradability, biocompatibility, inertness, eco-friendly and others (Gabor & Tita, 2012). In recent years, biopolymers and biopolymers-based nanocomposite have been utilized substantially in different fields of biomedical and materials science such as bioelectronics (Kim *et al*., 2010), drug delivery (Torres‐Rendon *et al*., 2015), electronic nanodevice (Shalauddin *et al*., 2019), health and environmental screening (Cao *et al*., 2017a; Tao *et al*., 2012), energy generation and storage (Jung *et al*., 2015b). The polymers which are extracted from animal or plant

sources are referred to as polysaccharides and proteins. The natural polysaccharides are termed biopolymers such as cellulose, chitin, starch and others (Mensitieri *et al*., 2011).

Among the biopolymers, cellulose and chitosan are the two most abundant biopolymers. Cellulose is the most prominent component of plants, it is considered an almost inexhaustible biopolymer with fascinating and versatile structure and features. Nanocellulose (NC) is a cost-efficient, biodegradable, eco-friendly, biocompatible and abundantly found, renewable green nanomaterials. The most interesting properties of nanocellulose as the precursor material, it does not possess the hierarchical structural defect. But it possesses most of the fascinating properties of cellulose (Kim *et al*., 2015). Recently, a substantial amount of nanocellulose has been manufactured and utilized frequently in different areas such as supercapacitors, food packaging materials, paper electrodes, electrochemical sensors and others. NC has improved mechanical integrity and thermal stability which is suitable for several host matrices. Like cellulose, NC could increase the selectivity and sensitivity of a sensor device for the electrochemical determination of specific desired analytes. NC has an excellent adsorption capability which helps to counter the leach of nanomaterials from the electrode surface. Thus, the prolonged stability of the sensor electrode can be achieved (Shalauddin *et al*., 2019). Because of the smaller particle size, the surface to volume ratio of nanocellulose is greater than cellulose which enhances the surface reaction with other nanomaterials and ultimately which is favourable for sensing performance (Moon *et al*., 2011). These combined features prepare NC fibers as perfect and potential building blocks for the attachment with other conductive polymers and carbonaceous nanomaterials such as polypyrrole (Sasso *et al*., 2010), graphene (Gr) (Malho *et al*., 2012), CNT (Koga *et al*., 2013) and others.

Chitosan (CTS), a natural biopolymer, is synthesized mainly from the exoskeleton of shellfish which is composed of D- glucosamine and N- acetyl-d-glucosamine moieties. As CTS possesses active amino and OH groups, this property provides CTS outstanding adhesion capability for organic substances, nanostructured materials and transition metals (Akhter *et al*., 2018). The presence of reactive amino groups increases the solubility of CTS in an aqueous medium. CTS becomes positively charged and reacts rapidly with the negatively charged species (Xiong *et al*., 2018). CTS possess some remarkable properties such as excellent water permeability and film formation potential, chemical inertness, less toxic, biocompatible, biodegradable and environmentally friendly (Shalauddin *et al*., 2017). Both NC and CTS have diversified applications in different fields of material science such as packaging materials (Hubbe *et al*., 2017; Yadav *et al*., 2020), conductive and craft papers (Akter *et al*., 2020; Hu *et al*., 2013), sensors (Poletti *et al*., 2020; Shalauddin *et al*., 2019; Yan *et al*., 2014), bulking agents (Bacakova *et al*., 2020; Wang *et al*., 2001), tissue engineering (Carlstrom *et al*., 2020; Liu *et al*., 2020) and others.

Biopolymers suffer from poor electrical conductivity and catalytic activity. Due to these drawbacks, only biopolymers are not sufficient to construct a successful electrochemical sensor. To increase the catalytic activity and sensing performance of an electrochemical device, other nanoparticles can be integrated into the biopolymer matrices such as carbon nanostructured materials (carbon nanotubes, nitrogen-doped graphene), mineral nanoparticles (hydroxylapatite, CaCO3), metal nanoparticles (Au, Cu) etc (Xiong *et al*., 2018).

In the study, the carbon-based nanomaterials were chosen (carbon nanotubes and nitrogen-doped graphene) to incorporate into the biopolymeric matrices. Among the carbonaceous materials, carbon nanotubes (CNT) are the important and prominent group of carbon nanostructured materials. CNTs are graphene nanosheets that are coiled within

a nanocylinder. CNTs have many attractive properties such as outstanding electrical, thermal, mechanical and enhanced electrocatalytic characteristics (Shalauddin *et al*., 2019). Since the last decades, enormous efforts have been paid on multiwall carbon nanotubes (MWCNTs) and single-wall carbon nanotubes (SWCNTs) for the application in different fields of material science (Akhter *et al*., 2018). Due to the leverages such as cost efficiency, biocompatibility, electrical properties and functionality MWCNTs have sparked enormous attention in electrochemical research fields (Alam *et al*., 2018). For the fabrication of the sensor, MWCNTs facilitate the electron transfer process and expand the active surface area of several electroactive species. They possess distinctive physical and chemical characteristics (Dehdashtian *et al*., 2019).

Graphene (Gr) a 2D carbon nanostructured material in which the atoms are arranged into a honeycomb lattice has attained enormous scientific interest due to its unique physical and chemical properties such as excellent catalytic effect and mechanical strength, extended reactive surface area (Anuar *et al*., 2018). Nitrogen-doped graphene (NDG) is synthesized by the exposure of Gr into the nitrogen plasma. NDG has remarkable electrochemical properties which could be attributed to the attachment of nitrogen functional groups and outstanding properties of Gr (Shao *et al*., 2010). Nitrogen doping plays an important role in enhancing the electrocatalytic activity of Gr based non-enzymatic electrochemical sensors (Rahsepar *et al*., 2019).

The incorporation of carbon nanostructured materials within the biopolymer matrices allow the nanocomposite intense mechanical and functional characteristics such as controlled electrical and enhanced thermal conductivity, rapid sensing capability, sufficient molecular porosity. With the presence of biopolymer matrices, the surface chemistry of carbon-based nanomaterials can be tuned which means the interfacial interactions can be controlled properly (Xiong *et al*., 2018). When biopolymer is

integrated with graphene to construct a conductive electronic device, this bionanocomposite showed very high electrical and ionic conductivity (Yu *et al*., 2017). Due to the multi-steps of intra and inter-molecular week interactions and when integrated with another complex multi-domain secondary configuration, biopolymers generally can assemble easily within the highly ordered hierarchical structures such as nanobeads (Kundu *et al*., 2010) and nanosheets (Kundu *et al*., 2010). Cao *et al* (2017) reported a highly sensitive bionanocomposite by enclosing a conductive network consist of carbon nanotubes into nanocellulose chitosan combined matrix. The bionanocomposite was proved to be fast, dynamic and repeatable which attributed to the presence of hydrogen bonding in nanocellulose and chitosan.

Painkillers are a type of therapeutic agent which are sold as over the counter (OTC) drugs mostly without restrictions and frequently administered by people who are suffering from pain and fever. The most commonly used and popular painkillers are paracetamol (Anuar *et al*., 2018), diclofenac sodium (Shalauddin *et al*., 2017) and naproxen (Tarahomi *et al*., 2019). Due to the frequent usage of these painkiller drugs, overdose can cause serious health problems such as nephrotoxicity, increased mortality, and hepatotoxicity which could be life-threatening. Thus, it is important to develop a facile, cost-effective and accurate approach for routine analysis of pharmaceutical preparations and diagnosis of drug overdose (Akhter *et al*., 2018). The focus of this study is to synthesize four nanocomposites based on the incorporation of biopolymers and carbon-based nanomaterials which has been reported for the first time and to design novel, cost-effective, facile, portable and efficient electrochemical nano-devices by employing these synthesized nanocomposites for the electrochemical determination of paracetamol, diclofenac sodium and naproxen which reflects the novelty of this present work.

1.2 Aim and objectives

NC and CTS are very potential biopolymers for the integration with carbon-based nanomaterials such as MWCNT and NDG for electrochemical sensing applications. It can be demonstrated that the combination of biopolymers and carbonaceous nanomaterials could contribute to the electrochemical sensing of desired analytes. The performance of the nanomaterials depends on the particles size, shape, crystallinity, morphology. The efficacy of the nanocomposite depends on several factors such as film formation, proper distribution of nanoparticles within the biopolymer matrices, expanded electroactive surface area, available binding sites for the chemical modifications, enhanced electrocatalytic activity, successful interactions between the carbon nanostructured material and biopolymers (such as hydrophobic-hydrophobic interactions, polar-polar interactions, hydrogen bonds, π-π interactions, van der waals forces, ionic interactions, covalent interactions and others). Nanocellulose is an ideal dispersing agent for carbon nanotubes and graphene components. The hydrophobic-hydrophobic interactions play a vital role in allowing the nanocomposite to provide a highly porous and rough appearance, improving the electrode surface for the adsorption of more analytes. Similarly, CTS helps in the dispersion of MWCNT and increase the catalytic performance with the presence of the CTS-Cu complex. This dispersion makes the fabrication of electrodes easier. The uniform coating of ppy on NC fibers following the chemical polymerization offers several advantages such as high surface area and high electrical conductivity which are highly suitable for the application of the electrochemically regulated ion-exchange process.

The specific objectives of this study are as follows:

1. To synthesize a hybrid nanocomposite of nanocellulose and functionalized multi-wall carbon nanotubes for the electrochemical determination of drug DCF in pharmaceutical drugs and biological fluids.
2. To synthesize a nanocomposite of nanocellulose, nitrogen doped graphene and sodium dodecyl sulfate for the simultaneous electrochemical determination of PCT and NPX in pharmaceutical dosage forms and biological fluids.
3. To synthesize a nanocomposite composed of functionalized multiwall carbon nanotubes, chitosan and copper modified sensor for the electrochemical detection of DCF in pharmaceutical drugs and real samples.
4. To synthesize an electroconductive nanocomposite composed of nanocellulose and polypyrrole modified sensor for the simultaneous electrochemical determination of PCT and CPR in pharmaceutical dosage forms, biological media and wastewater samples.

1.3 Structure of the thesis

This thesis is divided into seven chapters, chapter one includes the background studies of the biopolymers, carbon nanomaterials and their nanocomposites utilized for various applications based on their characteristics. Chapter one further includes the aims and objectives of the thesis. Chapter two provides a brief literature review on biopolymers, nanocellulose, chitosan and carbonaceous nanoparticles, multiwall carbon nanotubes and nitrogen dope graphene. Biopolymers based carbon nanostructured nanocomposites and their applications have also been illustrated here. Chapter three, four, five and six represents the research work and findings accomplished during the Ph.D. Candidature period which includes experimental elaborations, results and discussions including different nanocomposites consisting of nanocellulose or chitosan with the integration of carbon nanomaterials and their electrochemical applications:

1. Hybrid nanocellulose/*f*MWCNTs for the electrochemical sensing of diclofenac sodium in pharmaceutical drugs and biological fluids.
2. Nanocellulose incorporated nitrogen-doped graphene-modified electrochemical sensor for simultaneous determination of paracetamol and naproxen in pharmaceutical tablets and biological fluids.
3. Immobilized copper ions on MWCNTs-chitosan thin film: Enhanced amperometric sensor for electrochemical determination of diclofenac sodium in aqueous solution.
4. Nanocellulose and polypyrrole electroconductive nanocomposite for the simultaneous determination of paracetamol and ciprofloxacin in pharmaceutical dosage forms, biological media and wastewater samples.

The summary of the research works is included in chapter 7 which cover the significant outcomes from each study. Some probable ideas of the future arising from this research are proposed at the end of chapter 7. The flowchart of the research work is illustrated in Figure 1.1.

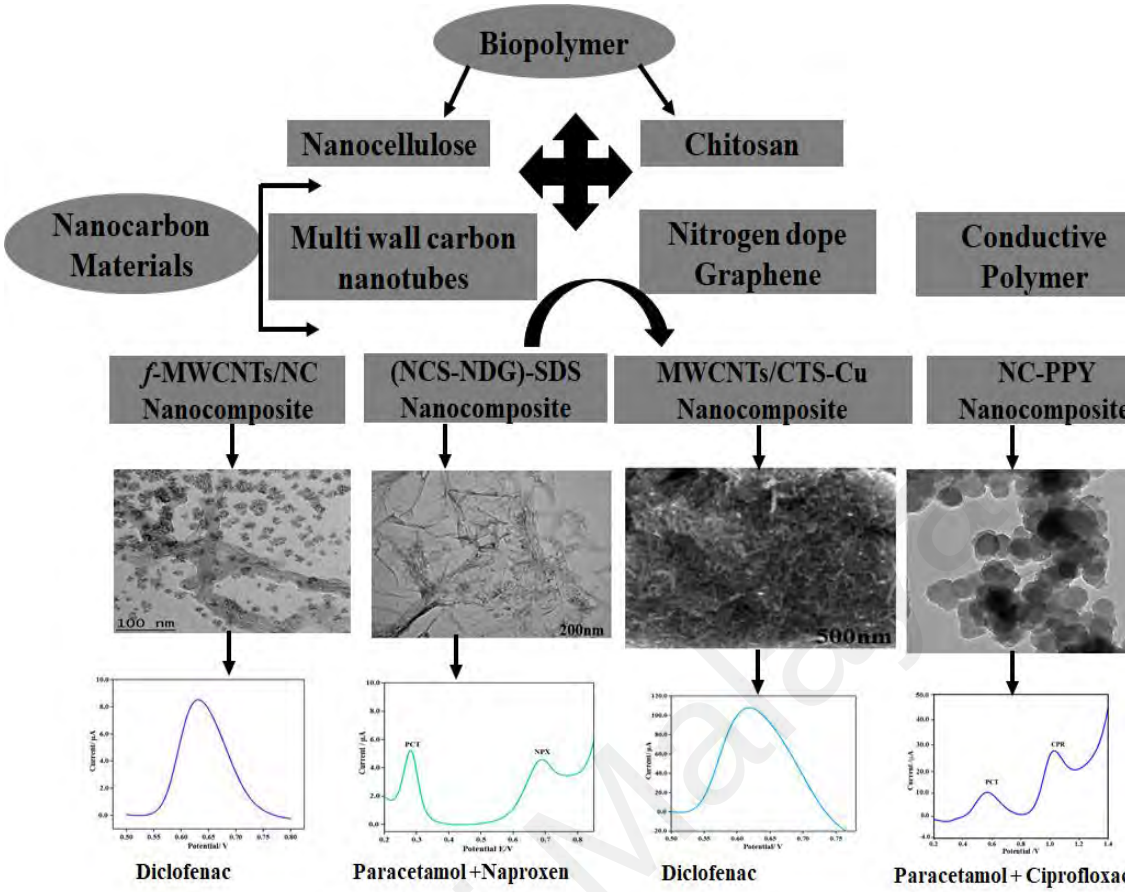

Figure.1.1: Flow chart of research studies

CHAPTER 2: LITERATURE REVIEW

2.1 Background

Human civilizations have relied extensively on biological materials (natural biopolymers) such as wool, silk, and cellulose for several purposes. For the past few decades, a vast array of biopolymers was introduced and applied in different sectors of sciences such as food packaging, textile, medicine and analytical applications. Biopolymers are not only renewable, biocompatible, biodegradable and with low toxicity but also enable sustainable and green chemistry in the manufacturing industry. With the advancements in chemistry and material sciences, the physicochemical properties of the natural biopolymers could be regulated for a beneficial output and repair the inborn defects and limitations to successfully meet the customized requirements (Aranda *et al*., 2006)

2.2 Biopolymers and their classification

Biopolymers are environmentally friendly and sustainable substances that are produced by living organisms (Ling *et al*., 2018). They have several intrinsic advantages such as renewability, mechanical robustness, biocompatibility, multifunctional characteristics, bio-degradability and others (George *et al*., 2020). Biopolymers have a wide range of diverse implementations in material science, biomedical engineering, chemical sensing, environmental and health screening, microelectronics and nano devices, fuel cells, analytical chemistry and others (Kanmani *et al*., 2017; Moohan *et al*.,). Biopolymers can be classified into different groups. Based on the chemical composition, biopolymers can be divided into different types. Cellulose and chitosan are natural polysaccharides, whereas collagen and gelatin are the common proteins. Among the biomass-based biopolymer polylactic acid, aliphatic polyesters based biopolymers

include polyhydroxybutyrate and carbohydrates (pullulan). Generally, biopolymers can be classified into three groups such as;

1. biopolymers synthesized from renewable sources,
2. chemically synthesized biopolymers
3. microbial synthesized biopolymers (Gabor & Tita, 2012)

Among the biopolymers, nanocellulose and chitosan are widely used due to their versatile advantages and facile applications.

2.3 Nanocellulose

Nanocellulose (NC) is a renewable and the most common polysaccharide (biopolymer) which possesses several outstanding properties such as biocompatibility, biodegradability, chemical inertness, low toxicity, unique physical properties and exceptional surface chemistry (Mondal, 2020). NC is extracted from the native cellulose compounds by the nanoscale isolation as shown in Figure 2.1. NC contains most of the inborn advantages of cellulose but is free from the inherent structural defects from cellulose (Dutta *et al*., 2017). Several methods are available for the extraction of NC from cellulose sources resulting in different sizes and shapes of nanocrystalline with varied mechanical features and surface chemistry (Mautner *et al*., 2019). As NC possesses a large surface area rich in hydroxyl groups and modulus structural arrangements which facilitates and offers abundant active sites for modifications of NC and is easily modified for the attachment of multiple anchoring sites for specific analytes (Xiong *et al*., 2018). These characteristics of NC make it suitable building blocks for the incorporation of other functional materials such as carbon nanostructured materials (carbon nanotubes, graphene), conductive polymers (polypyrrole) (Xiong *et al*., 2018). Although NC is not highly conductive, they assist in ion transportation by producing the pathways in the

electrochemical application. Due to the excellent binding properties of NC, it prevents the leaching of nanomaterials by forming films, thus the stability of the electrode can be extended for long times (Hebeish *et al*., 2016; Shalauddin *et al*., 2019). Recently, NC has been manufactured on a large scale and implemented in different areas of materials science such as biomedical engineering, tissue engineering, drug delivery, formulations of new therapeutics, electrochemical and bio-nanodevice (Huang *et al*., 2019).

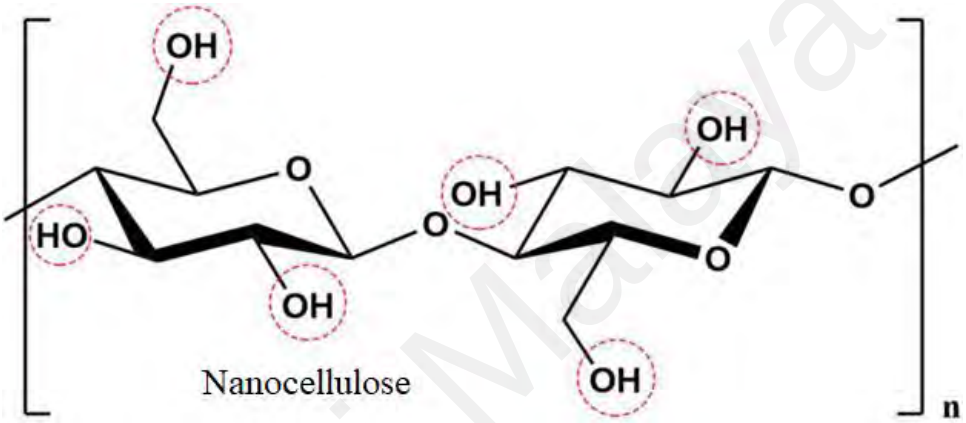

Figure 2.1: The chemical structure of nanocellulose

Generally, NC can be classified into three categories

1. Cellulose nanocrystals (CNCs)
2. Cellulose nanofibers (CNFs)
3. Bacterial nanocellulose (BNC) (Kargarzadeh *et al*., 2017)

The size, morphology, crystallinity and strength depend on the source and synthesis procedure. Generally, cellulose nanocrystals (CNCs) contain high crystalline nanostructure but cellulose nanofibers (CNFs) and bacterial nanocellulose (BNC) contain high crystalline configurations. Besides, they consist of disordered locations of amorphous regions, which provide high flexibility and more continuity (Xiong *et al*., 2018; Ferrer *et al*., 2017). Generally, CNCs are synthesized from cellulosic fibers by acid hydrolysis treatment, where the splits of the readily exposed amorphous regions occur to

produce rod-shaped crystalline cellulose (Hettrich *et al*., 2014). The acidic mixture is diluted upon reaching the appropriate level of hydrolysis and then centrifugation and dialysis were applied to eliminate residual acids and impurities. The physicochemical characteristics of CNCs firmly depend on some parameters such as the nature of the acids utilized during synthesis and their concentration, temperature and time duration of hydrolysis and cellulose source and others. Generally, CNCs of 5-10 diameter and 100-300 nm length could be synthesized from wood pulp (Wang *et al*., 2015).

Generally, the CNFs can be synthesized by several methods such as grinding, acid hydrolysis, high pressure homogenization, ultrasonication and others. The cellulosic fibers are composed of two types of macrofibers – hemicellulose and lignin. The macrofiber contains microfibrils which consist of nanofibrils of cellulose. The nanofibrils of cellulose consist of crystal and amorphous regions (Kim *et al*., 2015). As the amorphous region is responsible for the transverse split of the microfibrils and turns them into short monocrystals, thus the amorphous region is considered as the structural defect of cellulose (Rosa e*t al*., 2010). To overcome the structural defect, a recent drive of synthesizing the nanocellulose from cellulose by nanoscale synthesis has sparked the interest of scientists. Nanocellulose (NC) does not contain structural defects like cellulose (Shalauddin *et al*., 2019). Due to the nanoscale synthesis, NC has a greater surface area and porous appearance. The presence of sufficient hydroxyl groups on the surface provides NC with a prominent flexible modulus structure which could be easily modified for the specific attachment of different target analytes on the newly introduced binding sites (Nystrom *et al*., 2010)

Bacterial nanocellulose (BNC) is an exceptional biopolymer with a wide range of potential applications. BNC can be synthesized by several bacterial species such as *Acetobacter G. xylinus*. The expanded surface area and a bunch of interconnected porous

systems suggest that BNC in the form of a 3D cellulosic network structure can be utilized as a carrier for catalysts (Wesarg *et al*., 2012)

2.3.1 Synthesis process of nanocellulose

2.3.1.1 Mechanical method

In mechanical treatment, NC can be obtained by the breakdown of cellulose fibers from the lignocellulosic biomass. Generally, the derived cellulose has a diameter of less than 200 nm. Before mechanical treatment, some steps such as grinding, decrystallization, acid hydrolysis and derivatization are performed to prepare NC. NC also can be obtained from lignocellulose biomass with the application of high pressure. It is done by the suspension of biomass applying a high-speed stirrer combined with ultrasonication energy before applying the high-pressure homogenization (Wang *et al*., 2015). Ionic liquids can be applied to treat lignocellulose biomass before mechanical treatment which can penetrate through the microcrystalline cellulose and attack the hydrogen bonds between the cellulose molecules. Intra and inter molecular bonds are demolished during high-pressure homogenization and through this disintegration, NC is obtained from the biomass (Mondal, 2017). However, the main drawback of this method is the consumption of high energy and a large number of cycles are required for the defibrillation of the cellulosic biomass (Niu *et al*., 2017).

2.3.1.2 Chemical method

Acid hydrolysis is the most common technique to synthesize NC from lignocellulose biomass. The synthesis process of NC is shown in Figure 2.2. The cellulosic fibers are screened through a mill with 20 mesh screen and are transferred into 5.00 M of 250 mL NaOH solution and warmed for 3 h until the temperature reaches 80 °C. The slurry is filtered and washed thoroughly until pH 7. Then the cellulosic fibers are

air-dried properly and dimethyl sulfoxide (DMSO) is added in 80 °C water bath for 3 h. Mainly, DMSO is added to swell up the matrix of cellulosic biomass so that the concentrated acids could penetrate inside the domain configuration of lignocellulosic biomass and break down the internal bonds easily. The fibers are then filtered and washed three times with 250 mL water. The above pretreatments are performed prior to the acid hydrolysis method. The pretreated cellulosic fiber is dispersed in a combination solution containing hydrochloric acid and sulfuric acid in a 1:3 ratio and refluxed for 16 h. The obtained product is diluted by DI water with centrifugation at 2000 RCF. After several washing, NaOH is added to make it neutral. The solution is further washed three times followed by dialyzation through the membrane tube with constant stirring for 24 h. The obtained product is dried at 70 °C for 24 h and the final product (nanocellulose powder) is pale white (Zhang *et al*., 2007). In the acidic treatment, the yield of NC depends on parameters such as reaction time, acid concentration, temperature and amount of lignocellulosic biomass. The yield of NC declines with the increase of the duration of acidic treatment of cellulosic biomass. The experimental parameters are optimized to obtain the maximum yield of NC and to preserve the NC morphology (Mondal, 2017). There are several advantages in synthesizing NC following the mixed acid hydrolysis method using hydrochloric acid and sulfuric acid. In the acid hydrolysis method, due to the alkaline pre-treatment of cellulosic biomass, comparatively less energy is required to defibrillate the cellulosic nanofibrils than the mechanical method. The synergistic effect of mixed acid hydrolysis and ultrasonication energy produce NC with decreased particle size, ensure more crystallinity of the NC, effective removal of amorphous regions and increase the availability of C-OH groups than any other method. NC obtained from the acid hydrolysis method has a greater surface area and has more stability and dispersibility than the NC obtained from other methods (Niu *et al*., 2017). In this research, NC

synthesized by the chemical method can be used as a binder and film-forming agent to prevent the leaching of nanomaterials.

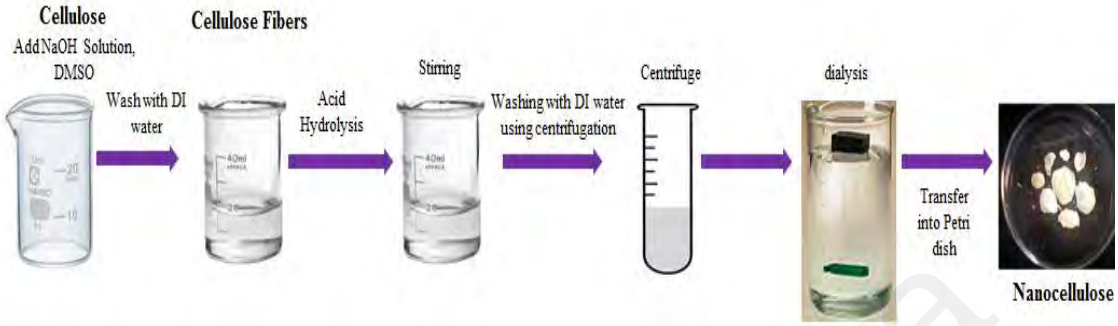

Figure 2.2: The steps of nanocellulose synthesis process

2.3.1.3 Bacterial method

NC synthesized from the bacterial method has the same chemical configuration with the NC synthesized from lignocellulosic biomass following chemical and mechanical techniques. Moreover, an ultrafine network of nanofiber is formed due to the culture medium which exhibits remarkable features such as high purity, uniform morphology, good mechanical characteristics and flexibility, good absorption capability and others (Taokaew *et al*., 2013). Bacterial nanocellulose (BNC) can be synthesized by aerobic cultivation of bacterium such as Gluconacetobacter xylinus which is a glucose enriched medium (Fu *et al*., 2013; Mondal, 2017).

2.4 Chitosan

Chitosan (CTS) is a natural polysaccharide consist of d-glucosamine and *N*-acetyl-d-glucosamine and contains abundant reactive amino and hydroxyl groups as shown in Figure 2.3. CTS possesses excellent adsorption capacity for organic substances and heavy metal cations (Honarkar & Barikani, 2009). Moreover, CTS has several distinct properties such as biodegradability, biocompatibility, non-toxicity, inertness, film formation potential (Shalauddin *et al*., 2017). CTS can be used in different fields of

applications such as tissue engineering (Nettles *et al*., 2002), biomedical applications (Jayakumar *et al*., 2010), medicine (Park & Kim, 2010; Senel & McClure, 2004) and etc. CTS has been applied enormously for the construction of electrochemical sensors. Baghayeri *et al* (2018) reported a nanocomposite of Fe_3O_4/Chitosan for the electrochemical detection of hydrogen peroxide. Shukla et al (2018) reported the effect of loading carbon nanotubes on chitosan film for the electrochemical determination of dopamine. Akhter *et al* (2018) reported an electrochemical sensor by the immobilization of cobalt oxide on MWCNT-CTS thin film for the sensitive determination of painkiller drug paracetamol. Shalauddin *et al* (2017) reported a nanocomposite by the immobilization of copper oxide on MWCNT-CTS thin film for the determination of painkiller drug diclofenac. CTS can be synthesized by the acid hydrolysis method from the skeleton of jelly fish, crabs and etc. In the current study, analytical grade CTS was purchased from Merck Malaysia and was used as the polymer, binding and film-forming agent to increase the catalytic effect of the nanocomposite.

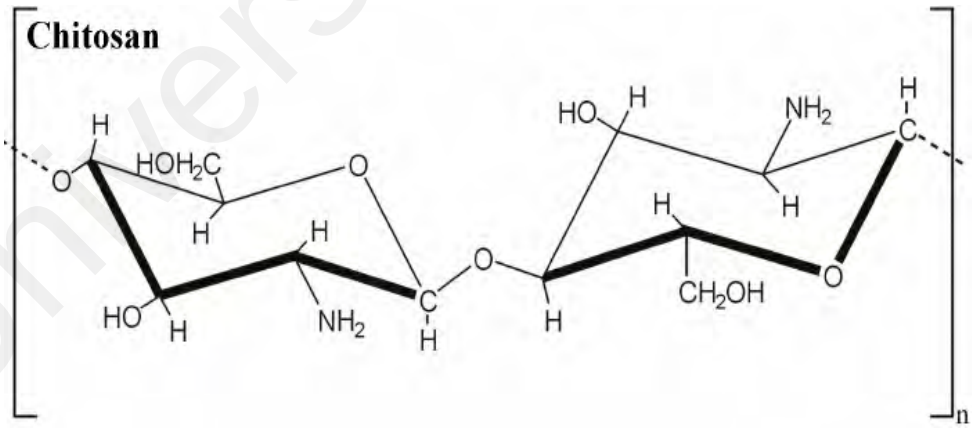

Figure 2.3: The chemical structure of chitosan

2.5 Nanomaterials

For the past two decades, extensive progress has been observed in the synthesis of nanomaterials and their applications. The materials whose size of the atoms are less than 100 nm can be defined as nanomaterials (Daniel & Astruc, 2004). Nanomaterials have several distinct properties that depend on their size and shape. There are different types of nanomaterials such as carbon-based nanomaterials, metal nanoparticles, oxide nanoparticles, composite nanomaterials which have been substantially used for the construction of electrochemical and bio-nanodevice. The main functions of nanomaterials include electrocatalyst, immobilization of targeted molecules and reactants (Vollath, 2018; Han *et al*., 2013).

2.5.1 Synthesis of nanomaterials

The successful preparation of the desired nanomaterial is a necessary prerequisite for any innovative research. The development of an efficient approach for the synthesis of nanomaterials and retaining the desired structural configuration and morphology of the synthesized nanomaterials are the challenges in the nanoscience and nanotechnology sector. However, the synthetic approach for the synthesis of nanomaterials can be categorized into three groups such as wet, dry and milling or grinding method as illustrated in Figure 2.4. In the wet and dry synthesis method, nanomaterials are synthesized from the bottom-up approach, while in the milling method the nanomaterials are synthesized from the top-down approach from the mechanical disintegration of the larger particles (Rotello, 2004). For the bottom-up approach, the nanomaterials are generally extracted from a bulk source and the desired nano-sized materials are acquired by following the progressive removal. On the other hand, nano-capsulation or nano-coatings are acquired which starts from a molecular levelled precursor, followed by the gradual mobilization of the molecules until the successful formation of the desired

composition (Hulteen, 1997). The size distribution of nanomaterials is a very crucial factor that can be changed by the proper optimization of the experiment parameters. Both of the bottom-up and top-down approaches require similar fundamentals and pre-requisites: for instance, fabrication parameters (e.g concentrations, time, energy from electrons) and surrounding conditions (e.g contaminants, temperature) need to be properly manipulated (Rotello, 2004). Thus, the nanotechnological investigation requires highly sophisticated fabrication instruments which are conducted in clean laboratory - conditions.

In the past few decades, the synthesis procedure of carbon-based nanomaterials has stimulated enormous attention due to their novel characteristics that enable the intense scientific attempt into a successful and efficient fabrication of miniaturized devices utilized in different nanoelectronics and photonics applications. In this work, the sonochemical method and microwave-assisted method have been chosen for the synthesis of nanomaterials.

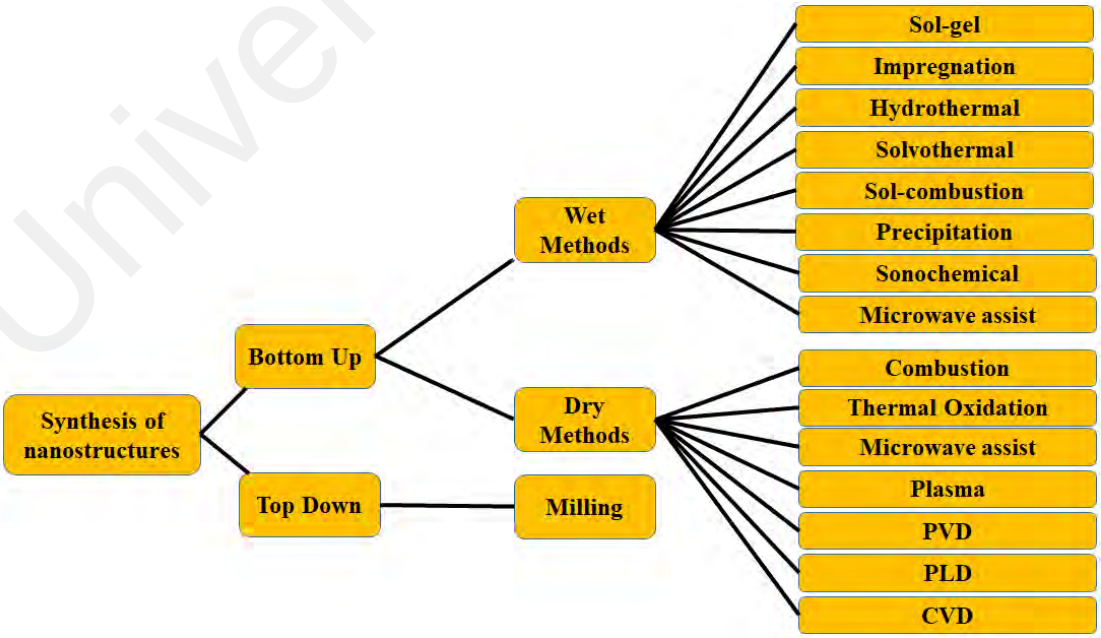

Figure 2.4: Synthetic methods of the nanoparticles (Rotello, 2004).

2.5.2 Sonochemical method

The sonochemical method for the synthesis of nanomaterials is a valuable approach for the synthesis of nanomaterials with outstanding properties. This method involves both the physical and chemical effects which offer a synergistic impact and can be utilized for the manufacturing of a broad range of nanostructured materials. The principles of sonochemistry which is responsible for the modification of nanostructures generates not from the straight interconnection between the chemical entity and sound waves, but rather from the acoustic cavitation which is considered as a physical phenomenon, which includes three phases: formation or construction, growth and collapse of the bubbles in any liquid solution (Chatel, 2019). Some extreme reaction parameters are required in this process such as high pressure of >500 atm, high temperature of >5000K and >1010 K/s of cooling rate, achieved during the collapse of the cavities. The transient and extreme conditions promote acoustic cavitation which enables the formation of materials possessing outstanding and uncommon features. The irradiation of highly intense ultrasonic energy forces the molecules to undergo high-energy chemical reactions. The high-intensity ultrasound promotes the activation of physical effects that are followed by the chemical consequences (Chen *et al*., 2011). During the ultrasonication process, microjets and shockwaves are significant physical phenomena for the fabrication of nanomaterials. When the bubbles collapse to the adjunct expanded surface, microjets occur during this period. The micro-jets at high speeds affect the surface and is responsible for the pitting and erosion which leads to the formation and modification of the surface of the nanostructures. The shock wave is another physical phenomenon that is generally formed from laser-induced collapsed bubbles. The shock wave can stimulate other physical effects along with the chemical consequences such as increased mass transportation because of strong turbulent mixing and acoustic cascade and promotes the suspending process of solid particles into the liquid medium. Inter-

particle collision of 100 m/s causes the homogenous distribution of particles, splitting, similar morphologies, surface construction and exfoliation of the multi-layered materials (Okitsu, 2010; Bang & Suslick, 2010).

2.5.3 Microwave-assisted method

The principle of microwave-assisted method is based on the aligning dipoles of any material in an external area through the excitation generated by the microwave electromagnetic radiation and is implemented along with a known synthesis approach. This is an effective wet chemical technique for the synthesis of nanostructured materials with higher reproducibility and possesses multiple merits such as controlling the size and shape by regulating the reaction parameters, rapid volumetric heating, high level of reaction rates and energy efficiency (Polshettiwar & Varma, 2010). In this approach, microwave irradiation is applied to a chemical reaction that is based on the capability of a substance to absorb the microwave generated energy and convert the energy into heat. This conversion process provides a non-equilibrium state in the system resulting in the generation of heat, thus decreasing the reaction time and ultimately improving the crystallinity of the final product. Dipolar polarization and ionic conduction are the two mechanisms that are generally activated by microwave irradiation (Motshekga *et al*., 2012).

2.6 Application of nanomaterials in electrochemical nanodevice

The outstanding physicochemical properties of nanomaterials are important for the design and construction of improved electrochemical sensors and biosensors. Different types of nanomaterials such as carbon-based nanomaterials, metal oxide nanomaterials, mineral nanoparticles and semiconductor nanoparticles have been utilized substantially for the fabrication of electrochemical sensing devices. These nanomaterials play crucial roles such as sensing of the target analytes, electrocatalyst, enhancement of

ion transfer on the electrode surface, labelling of biomolecules and etc (Guo & Wang, 2011) (Maduraiveeran & Jin, 2017).

2.7 Carbon-based nanomaterials

Carbon-based nanomaterials are a type of nanomaterials that have exceptional and tunable characteristics that enable a new dimension and technological revolution in different fields of science. These types of materials possess several advantages such as excellent mechanical integrity, surface roughness, enhanced specific surface area, thermal conductivity, exceptional electronic distributions and biological properties (Luo *et al*., 2012). The combination of these distinct properties and their remarkable sensing capabilities support the successful insertion in any electronic nano-device for significantly improved performances. For the past few years, different forms of carbon-based nanomaterials such as carbon nanotubes (CNTs), graphene (Gr), carbon nanofibers, carbon nanohorns, nanocones-disks, fullerenes, nano-diamonds and their functionalized forms have been investigated intensely and enormously applied successfully in different sectors of material science (Scida *et al*., 2011)

2.7.1 Carbon nanotubes (CNTs)

CNTs consist of graphene sheets coiled inside a nano-cylinder which exhibit several distinct properties such as outstanding mechanical integrity, electronic conductivity and catalytic activity. CNTs are composed of single or multiple layers of sp2 hybridized carbon atoms. On this basis of composition, CNTs can be classified into two groups i.e. single-walled carbon nanotubes (SWCNTs) and multi-walled carbon nanotubes (MWCNTs) (Akhter *et al*., 2018). MWCNTs are comparatively cost-efficient and have several outstanding properties such as tensile strength, good mechanical and thermal stability, flexible elasticity and high electronic conductivity and catalytic activity (Shalauddin *et al*., 2017). Due to the poor solubility, pristine CNT is not suitable for

electrode fabrication. Hence, the CNTs functionalization has been considered as a technique for activation. The functionalization technique effectively eliminates the impurities from CNTs and enhances the dispersion ability in the water and improves the electrochemical performances. Moreover, this technique provides abundant anchoring sites on CNTs which facilitates the fabrication of electrodes (Shalauddin *et al*., 2019). In recent years functionalized MWCNTs has been used enormously in different fields of material science such as electrochemical sensors (Bagheri *et al*., 2017; Shalauddin *et al*., 2017), biosensors (Gautam *et al*., 2018; Li & Lee, 2017), tissue engineering (Shrestha *et al*., 2017), energy storage (Markoulidis *et al*., 2019) and others.

2.7.2 Functionalization of CNTs

There are several methods for functionalization using the unique characteristics of CNTs. It is quite challenging to look for the best technique to improve the distinct properties such as mechanical, electrical, optical and etc. One of the challenges is to achieve the optimal functionalization of CNTs for a specific application. Functionalization is based on the covalent bonds among the functional groups on the outer wall of CNT (Ferreira *et al*., 2016). Functionalization of CNT can be done by the acid hydrolysis method which requires the presence of one or two strong acids such as hydrochloric acid, sulfuric acid, nitric acid etc. Acid hydrolysis is one of the suitable methods for CNT functionalization where CNT is used as a nanocomposite and applied for sensor fabrication (Mallakpour & Soltanian, 2016).

2.7.3 Graphene and nitrogen-doped graphene

Graphene (Gr) is composed of a monolayer of sp^2 hybridized carbon atoms and possesses several distinct features such as high active surface area, high electro-conductivity, excellent mechanical, chemical and optical features. The doping of foreign

atoms into the sp^2 hybridized carbon network modifies the intrinsic properties such as electronic distribution and surface chemistry (Choi *et al*., 2010). Doping enhances the density of free charge-carriers, electrical or thermal conductivity of carbon-based nanomaterials. Nitrogen is considered as a potential dopant for carbon nanomaterials due to the comparable size and number of valence electrons, thus forms strong bonds with the carbon atoms (Shao *et al*., 2010). Nitrogen-doped graphene (NDG) has the potential to improve electrical conductivity, due to its good biocompatibility, large surface area and excellent electrochemical response. NDG exhibits more electrocatalytic activity compared to Gr because of the unique electronic interactions between the lone–pair electrons of nitrogen and the π–system of graphitic carbon (Yu *et al*., 2016; Wang *et al*., 2010; Qu *et al*., 2010). In addition, NDG enhances the affinity towards the target analytes and improves the selectivity of Gr based sensing device. Nitrogen-doping of the Gr lattice improves the electrocatalytic activity of Gr which is suitable for electrochemical sensing (Shao *et al*., 2010). Several methods are used for the synthesis of NDG such as CVD, arc-discharge method, solvothermal method, microwave-assisted method, plasma treatment, thermal treatment and etc (Wang, *et al*., 2012). In this research, microwave assisted method was used to synthesize NDG where graphene oxide is the precursor material.

2.8 The mechanism and benefits of the incorporation of biopolymers and carbon-based nanoparticles

Depending on the desired implications, bionanocomposites can be prepared in several approaches. Different types of synthetic materials such as carbon-based nanomaterials, metal oxides, metal nanoparticles and minerals nanoparticles can be incorporated with the biopolymers and utilized in different areas of science such as bioelectronics and drug delivery (Kim *et al*., 2010; Torres-Rendon *et al*., 2015), energy generation and storage (Jung *et al*., 2015a), electrochemical sensors (Shalauddin *et al*.,

2019), health and environmental monitoring (Cao *et al*., 2017b) (Tao *et al*., 2012), lightweight structural support (George *et al*., 2020) and others. The versatile applications of biopolymer nanocomposites (biopolymers and carbon-based nanomaterials) are shown in Figure 2.5.

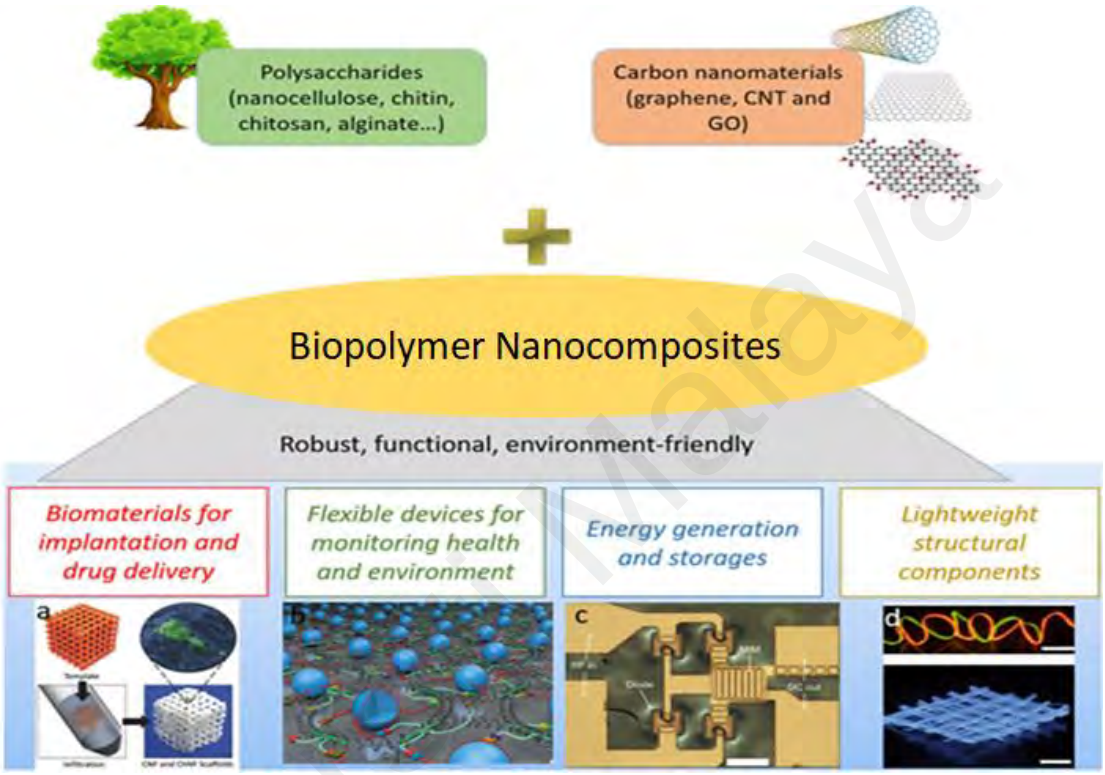

Figure 2.5: Versatile applications of biopolymer nanocomposite (biopolymers and carbon nanomaterials)

Here, the underlying mechanisms and advantages of the incorporation of biopolymers and carbon nanomaterials are described as follows. If compared to the synthetic polymer-based nanocomposite, the naturally derived bionanocomposites possess several inborn expediences such as biodegradability, biocompatibility, mechanical robustness, less toxicity, multifunctional properties and etc (Lee *et al.*, 2015). When carbon nanomaterials are introduced in biopolymer matrix, excellent properties can be achieved from this combination including excellent dispersion and highly organized configuration, high electrical conductivity, excellent catalytic activity, magnetic properties, stretch-ability, optical activity and etc (Weng *et al*., 2011; Luong *et al*., 2011).

In addition, the incorporation of carbon nanomaterials across the biopolymer matrices offers outstanding mechanical support and functional characteristics to the nanocomposite (Wan *et al*., 2016). The biointerface between the carbon nanostructured materials and bio-derived polymers (bionanocomposite) is highly desired and involves unique morphologies. These combined structural arrangements not only preserve the actual properties of the carbon nanostructures but with extra biofunctionality. Due to the highly conductive nature of the bionanocomposites, they can be used as electronic devices. For example, multiple attempts have been reported on the incorporation of highly conductive graphene materials within biopolymers (chitosan) for the fabrication of a conductive bionanocomposite (Akhter *et al*., 2020; Wen *et al*., 2016).

The research output exhibits that, the biopolymer and graphene nanocomposite possesses high ionic conductivity, unique composition and modulus structural organization. One of the impressive features of the biopolymer matrices is that the mechanical performance and functionality can be upgraded remarkably even at very low loading. The concurrent presence of the graphitic domain (hydrophobic) and oxidized domain (hydrophilic) ultimately forms a heterogeneous amphiphilic surface (Wan *et al*., 2016). This interesting phenomenon has important consequences. The GO sheets can be firmly attached with either the hydrophobic region or the hydrophilic region of the biopolymer, and the interfacial strength can be enhanced if a matching biopolymer matrix is selected. For instance, hydrogen bonding, covalent interaction and Coulombic interactions are responsible for the enhancement of the interfacial strength between GO sheets and positively charged biopolymers (chitosan) (Wan *et al*., 2015). The successful attachment of GO sheets and amphiphilic biopolymer occurs through hydrogen bonding and hydrophobic interactions of the micellar configurations. Wan *et al* reported a strong interfacial strength between GO and chitosan which ultimately enhance the tensile strength and toughness of the GO film (Wan *et al*., 2016).

Nanocellulose is a naturally derived biopolymer, composed of several molecular chains which are connected in a parallel direction and balanced by hydrogen bonds and van der Waals forces into a nanofibrillar composition. Their crystalline appearance (70-80%) provides an elastic configuration that enables them as a potential host for several materials. Due to the high aspect ratio and high stiffness, nanocellulose is utilized to reinforce a wide range of materials such as carbon matrices (Shalauddin *et al*., 2019), conductive polymers (Nystrom *et al*., 2010), inorganic nanoplates (Zhang *et al*., 2019). However, uncontrolled aggregation is one of the greatest challenges in the processing of nanomaterials which could deteriorate mechanical performance. Besides, most of the synthetic nanomaterials possess a limited number of anchoring sites, but the biocomponents usually contain a great variety of functional moieties which can form multiple hydrogen bondings, covalent bondings, hydrophobic-hydrophobic interactions, van der Waals force interactions, Coulombic interactions and covalent interactions with a wide variety of external components (Hajian *et al*., 2017). Different types of interactions between biopolymers and carbon nanomaterials are shown in Figure 2.6. These broad ranges of weak interactions not only bring benefits but also challenges in the manufacturing of novel bionanocomposites. These interactions facilitate the high efficient shift of the loads within the interfaces of the components for increased mechanical responses but the preparation becomes a challenging task because of an inconsistent clump of the nanocomponents during manufacturing. Due to the defects and clump formations, catastrophic failure could occur during the manufacturing of bionanocomposites under practical parameters (Li *et al*., 2015).

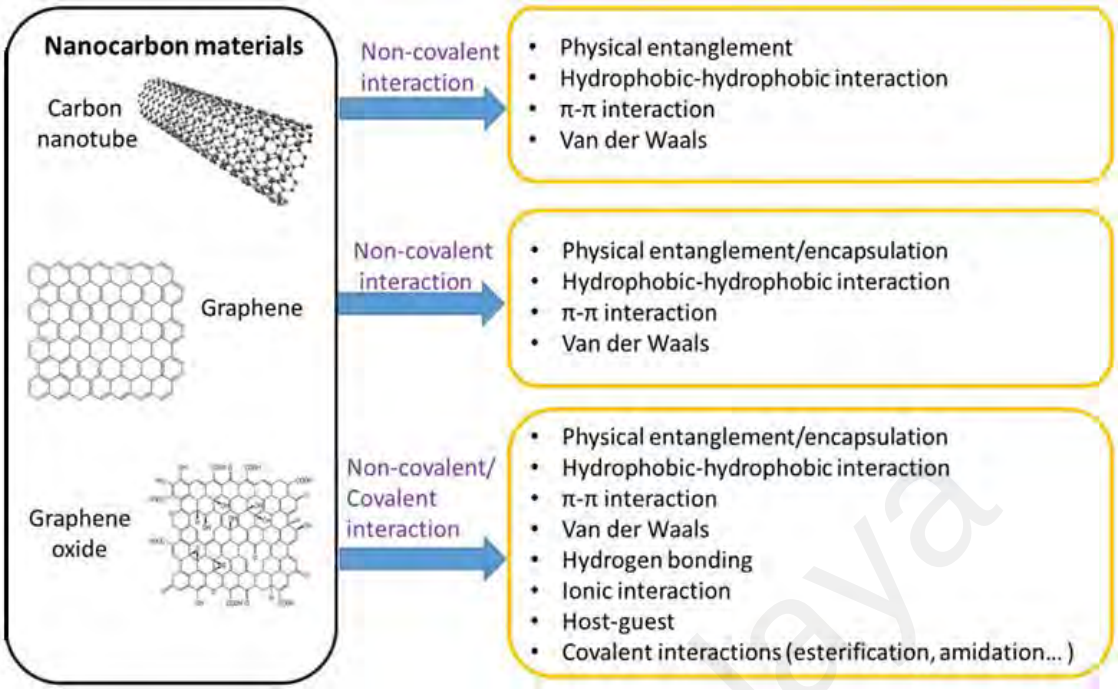

Figure.2.6: The enabling interactions between carbon nanomaterials and biopolymers

However, some of the popular synthetic nanomaterials (e.g carbon nanotubes, graphene oxide) and their interfacial interactions with specific biopolymers (nanocellulose, chitosan) have been widely exploited recently for the fabrication of neoteric bionanocomposite. The present work highlights this research scopes. Table 2.1 shows a previous report on the biopolymer-based nanocomposite for electrochemical determination.

Table 2.1: Biopolymer based nanocomposite for electrochemical sensor

Nanocomposite	Method	Electrode	Analyte	References
NC/*f*-MWCNTs	Synthesis of nanocellulose by acid hydrolysis method and functionalized MWCNTs	GCE	Diclofenac	(Shalauddin *et al*., 2019)
SWCNH/NC	Electrochemical sening of purine, guanine an adenine using single walled carbon nanohorns and nanocellulose	GCE	Purine, Adenine and Guanine	(Ortolani *et al*., 2019)
NC@N,S@GQDs/GCE	Nitrogen and sulfur co-doped graphene quantum dots/nanocellulose nanohybrid for electrochemical sensing of anti-schizophrenic drug olanzapine in pharmaceuticals and human biological fluids	GCE	Olanzapine	(Mahmoud *et al*., 2020)
CT/AuNP/MIP	An electrochemical molecularly imprinted sensor based on chitosan capped with gold nanoparticles and its application for highly sensitive butylated hydroxyanisole analysis in foodstuff products	MIP	Butylated hydroxytoluene	(Motia *et al*., 2021)
MWCNTs-CTS-Cu	Immobilization of copper ions on MWCNTS-Chitosan thin film and functionalized MWCNTs	GCE	Diclofenac	(Shalauddin *et al*., 2017)
f-MWCNTs/CTS-Co	Immobilized cobalt ion on functionalized MWCNTs - Chitosan thin film	GCE	Paracetamol	(Akhter *et al*., 2018)
(MWCNTs$_f$-NGr/CTS)-Cu	Functionalized MWCNTs and synthesis of NGr by micowave assisted method immobilization of CTS followed by Cu electrodeposition	GCE	Nilutamide	(Akhter *et al*., 2020)
$NiMoO_4$/CHIT	Sonochemical synthesis of $NiMoO_4$ and sonochemical exfoliation of CHIT	GCE	Amlodipine	(Lou *et al.*, 2020)

2.9 Painkiller drugs

2.9.1 Paracetamol

Paracetamol N-acetyl-P-aminophenol or acetaminophen (Figure 2.7) is a popular analgesic and anti-pyretic therapeutic agent which is mainly used for the relief of fever, and different types of pain such as headache, toothache, backache and etc (Akhter *et al*., 2018). As an OTC drug, paracetamol is sold randomly and used very frequently by people. However, the excess administration of this drug can cause adverse effects such as nephrotoxicity, increased mortality and liver damage (Anuar *et al*., 2018). For pharmaceutical and overdose analysis, the design and development of a facile, cost-efficient, lightweight and accurate electrochemical device are crucial and demanding in the present time (Alam *et al*., 2018). Several approaches have been introduced for the determination of paracetamol such as spectrophotometry (Sandulescu et al., 2000), chromatography (Ravisankar *et al*., 1998; Trettin *et al*., 2011) chemiluminescence (Ruengsitagoon *et al*., 2006), titrimetry (Burgot *et al*., 1997). Though these approaches have high precision, good sensitivity and selectivity, they have some disadvantages such as high price, complex operating procedure, repetitive sample preparation and etc. As electrochemical techniques can overcome the aforementioned limitations of the traditional methods, they have become the choice of preferences over other methods. Numerous electrochemical approaches have been developed for the electrochemical determination of paracetamol (Akhter *et al*., 2018; Alam *et al*., 2018).

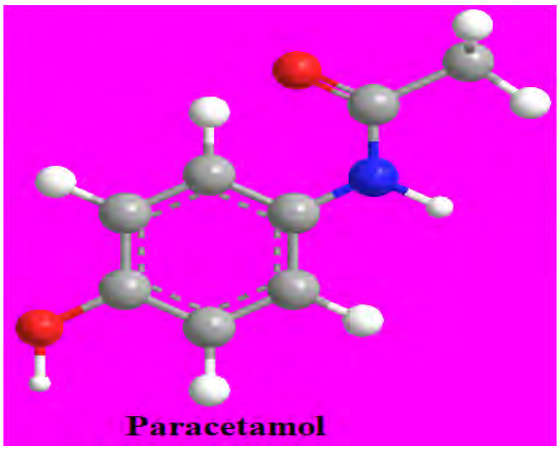

Figure. 2.7: The 3D chemical structure of paracetamol

2.9.2 Diclofenac Sodium

Diclofenac sodium (DCF) (sodium [o-(2, 6-dichloroanilino) phenyl] acetate) (shown in Figure 2.8) is a non steroidal anti-inflammatory and an analgesic drug. The drug is applied for the treatment of arthritis, menstrual pain, ankylosing spondylitis, rheumatic pain, sports injuries etc. DCF is an OTC drug for relief from different types of pain. If the patients develop the Shy Drager syndrome or diabetes, the administration of DCF drug for prolonged periods exposes the risk of heart attack or stroke. Considering the health issues and frequent administration without proper indications, it is necessary to monitor the drug in pharmaceutical dosage forms and clinical investigations (Shalauddin *et al*., 2019). Several approaches have been introduced for the detection of DCF such as thin-layer chromatography (Sun & H. Fabre, 1994), spectrofluorimetry (Arancibia *et al*., 2000), capillary zone electrophoresis (Jin & Zhang, 2000), high-performance liquid chromatography (Kole *et al.*, 2011), gas chromatography (Kadowaki *et al*., 1984), voltammetry (Shalauddin *et al*., 2017; Shalauddin *et al*., 2017; Honakerin *et al*., 2020) etc.

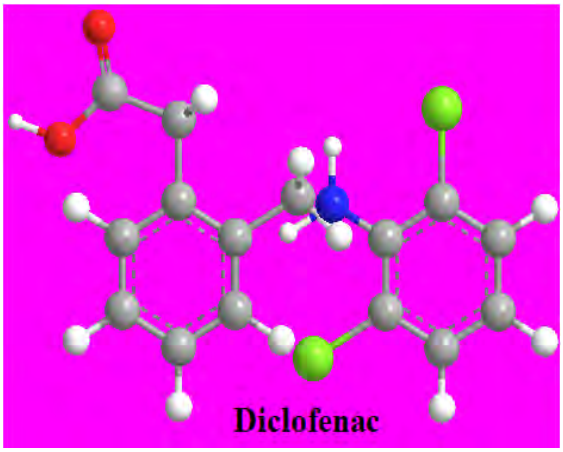

Figure. 2.8: The 3D chemical structure of diclofenac

2.9.3 Naproxen

Naproxen (NPX) is a widely used analgesic and anti-inflammatory drug mainly used for the treatment of rheumatoid arthritis, dysmenorrhea, ankylosing spondylitis, musculoskeletal injury, acute gout (shown in Figure 2.9). NPX is an OTC drug and is used frequently by patients (Tashkhourian *et al*., 2014). The prolonged consumption of NPX results in adverse health effects such as gastrointestinal lesions, kidney problems and heart disease. Considering all the health issues, a facile and simple technique should be developed for the determination of NPX from pharmaceutical preparations and biological medium for pharmaceutical quality control analysis and clinical investigations (Sarhangzadeh, 2015). Till now, different approaches have been developed for the determination of NPX such as liquid chromatography (Madikizela & Chimuka, 2017), spectrofluorimetry (Damiani *et al*., 2002), potentiometry (Lenik & Łyszczek, 2016), fluorescence (Li *et al*., 2012), spectrophotometry (El-Kommos *et al*., 2013), voltammetry (Eslami & Alizadeh, 2016; Adhoum *et al*., 2003; Soltani *et al*., 2018).

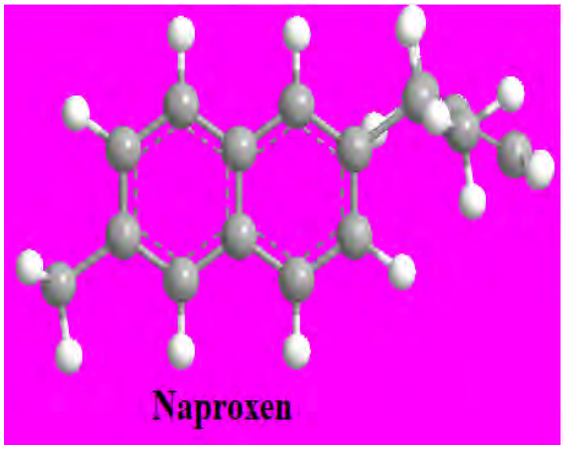

Figure. 2.9: The 3D chemical structure of naproxen

2.9.4 Ciprofloxacin

Ciprofloxacin (CPR) is a third-generation antibiotic drug from the quinolone group and is generally administered for urinary tract, skin and respiratory tract infections (shown in Figure 2.10) (Chen *et al*., 2019). The electroactivity of CPR is due to the presence of the piperazine ring. An overdose of CPR causes health problems such as liver damage, hypersensitivity and nerve problems (Fang et al., 2019). Considering all the health issues, a facile and simple technique should be developed for the determination of CPR. Several methods have been utilized for the detection of CPR such as high-performance liquid chromatography (Liu *et al*., 2018; Sultana *et al.*, 2013) capillary electrophoresis (Lecoeur *et al*., 2019; Wang *et al*., 2005), fluorimetry (Perera *et al*., 2019; Turkie & Munshid, 2019), titrimetry (D'Souza *et al*., 2015; Basavaiah *et al*., 2006) and electrochemical techniques (Anuar *et al*., 2018; Matsunaga *et al*., 2020; Bonyadi *et al*., 2020)

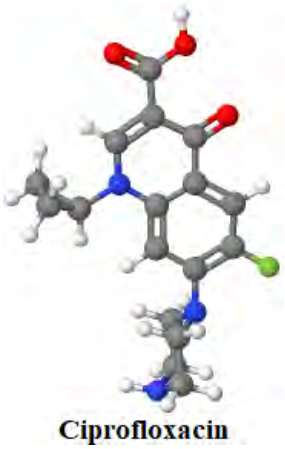

Figure. 2.10: The 3D chemical structure of ciprofloxacin

2.10 Sensors

Sensors are devices that detect analytes by the transduction of signals into a measured parameter such as current, potential and impedance in the case of electrochemical sensors. The main function of the sensing materials and signal transducers in a sensor is to transmit the signals without any magnification from any specific analyte or any reaction changes. Sensors can generate any signals as thermal, electrical and optical output signals which can be transformed into digital signals for further processing. The sensor is generally classified into two groups according to the types of output signals i.e. electrochemical sensors and biosensors. The electrochemical sensors have multiple advantages over other sensors because the electrode of this type of sensor is capable of recognising the analyte in the host without changing the parameters of the host system (Kubrusly & Malebranche, 1985). The biosensors can recognize biochemical substances such as biological proteins, tissues, nucleotides and others. The active sensing material on the electrode surface acts as a catalyst in biochemical compounds reaction and generate the output signals. The combined functions of the electrochemical sensor and biosensor give rise to another type of sensor which is known as an electrochemical biosensor. This type of sensor is constructed by the electrochemical method to perform as a biosensor. The development and proper selection of active material require great effort. Active sensing materials can act as a catalyst for the sensing

of a specific analyte or several analytes (Aznoli & Navimipour, 2017). Recently, the advancement of nanotechnology has brought new possibilities for a substantial amount of new potential materials and devices with outstanding features which have beneficial functions for several electrochemical sensor and biosensor applications. The nanostructure can manipulate the fundamental characteristics of a material without changing its chemical composition. Furthermore, the nanostructures can be used to enhance the transfer of electrons and optical excitation, as these factors play a vital role in the development of a nanoelectronic device. Nanostructured materials possess a high surface to volume ratio and enhanced electroconductivity which is favourable for the construction of nanodevice.

For the past few decades, nanoparticles have aroused a huge interest for their application in different fields of science. Generally, the synthetic methods of nanoparticles can be classified into two groups, bottom-up and top-down methods. In the bottom-up method, the smaller sized structures are integrated into a larger structure by the self-assembly process. On the other hand, the top-down approach refers to the depletion of large-sized structures to form multifunctional nanostructures (Holzinger *et al*., 2014). In this literature, the development of electrochemical sensors by the effective selection of nanostructured materials and their application as the efficient sensing of the targeted analytes have been enlighted.

2.10.1 Chemical Sensors

A chemical sensor is a device that produces information on its surrounding environment. Generally, the chemical sensor contains a receptor and a transducer. The receptor can transform the chemical information into a form of energy that can be measured by a transducer. A transducer can transform the energy which carries the chemical information about the desired analyte into the detectable useful signal through

modern instrumentation and separate the signal from its surrounding information as shown in Figure 2.11 (Hulanicki *et al*., 1991).

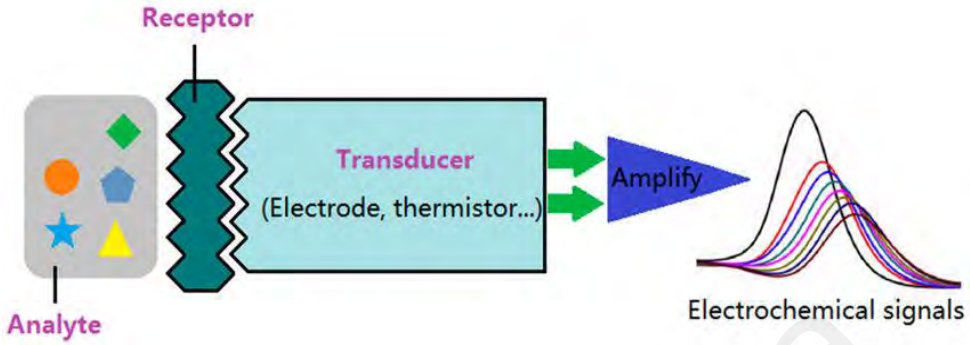

Figure 2.11: Schematic diagram of a general chemical sensor

The classification of chemical sensors depends on the characteristics such as optical, electrical, thermal or gas sensors. The advantages of these sensors are that they are capable of detecting and receiving the analyte response from solid, liquid or gaseous medium. Electrochemical sensors are a type of chemical sensor which have several advantages such as miniaturization, simple composition and operation procedure, rapid result and cost-efficient compared to other types of sensors. Electrochemical sensors are classified into three types such as potentiometric, amperometric and conductometric sensors. In amperometric sensors, the current is measured by the A.C or D.C mode. For instance, chemically inactive electrodes, chemically active electrodes and chemically modified electrodes. In a potentiometric sensor, equilibrium is established at the electrode interface and the potential of the working electrode is measured against a reference electrode. The composition of an analyte can be obtained by the difference between the working electrode and the reference electrode. Conductometric sensors are capable of measuring conductivity in multiple frequency series (Stradiotto *et al*., 2003).

2.10.2 Potentiometric Sensors

Potentiometric sensors can be categorized into three classes such as ion-selective electrodes (ISEs), coated wire electrodes (CWEs), ion-sensitive field-effect transistors (ISFETs). ISEs are the widely used potentiometric sensing electrodes. A large variety of ISEs is commercially available which are beneficial and efficient for the detection of the ion concentration in a different types of liquid specimens. In ISEs, the signal is formed at the interface by the isolation of charges. Generally, the ion-selective membrane isolates the analyte solution and an inner solution containing a continuous concentration of ionic species. Generally, a Ag/AgCl RE is surrounded by the inner solution containing a constant concentration of Cl^- ions which provide electrical contact to the ISEs. The ISE potential is measured by the addition of two RE potentials and membrane potentials composed of the boundary potential of each membrane or solution interface and a probable diffusion potential that might be generated by the concentration gradient within the membrane phase. There are different techniques to develop an electrode that is selective to a single species depending on the nature and configuration of the materials of the membranes. Research in this particular field has exposed several implementations to unlimited analytes (Goepel *et al*., 2008; Buhlmann *et al*., 1998).

Coated wire electrodes (CWEs) are another type of ion-selective electrode having a polymeric membrane that has direct contact with metal. However, the main drawback of this type of electrode is the poor signal stability. Even if no transfer of charges has occurred at the electrode interface, a parasitic capacitance affects the signal stability.

Ion sensitive field-effect transistors (ISFETs) can be potentiometric ion sensors or chemical sensors. This type of transducer works by implementing the field-effect. Due to the various advantages such as miniaturisation, facile fabrication by microelectronic technology, they are the most studied field-effect devices. ISFET contains a bare gate insulator which is composed of silicon oxide, aluminium oxide etc. Due to the

electrochemical equilibration between the protonated oxide surface and the solution containing protons, the insulator exhibits an intrinsic pH sensitivity (Bratov *et al*., 2010).

2.10.3 Amperometric sensors

In amperometric sensors, the amperometric measurements are accomplished in an electrochemical cell by measuring the amount of currents within a single applied potential. However, in the voltammetric measurements, a time-dependent potential is applied in an electrochemical cell and the resulting current is measured as a function of that specific potential. The voltammograms are recorded which contains a plot of current versus the applied potential. This voltammogram has similarity with spectroscopy which can reveal quantitative or qualitative information of a species involving in the oxidation or reduction reaction (Brett & Oliveira Brett, 1993). Initially, the basic instruments of voltammetry consist of two electrodes but the modern voltammetric techniques require a three-electrode system containing a working electrode, a platinum wire as the auxiliary or counter electrode and SCE or Ag/AgCl as the reference electrode. For working electrodes, different types of materials are used such as carbon, gold, silver, copper, cobalt etc. The desired oxidation or reduction reactions occur at the working electrode. The reference electrode provides a steady potential compared to the working electrode (Thevenot *et al*., 2001). Generally, the potential of the counter electrode is not measured. The counter electrode is adjusted to balance the reactions occurring at the working electrode. The current generating from redox reactions is called the Faradic current. A Faradic current is a cathodic current due to the reduction of an analyte and is negative by convention. On the other hand, a Faradic current is an anodic current due to the oxidation of an analyte. In voltammetric experiments, an electrolytic solution is used which is also known as a supporting electrolyte. The electrochemical cell contains the electrolytic solution and the three electrodes are immersed in the solution (Stetter *et al*., 2003). The electrolytic solution decreases the resistance of the solution, as the added resistance

declines the accuracy of the results remarkably. Some crucial experimental parameters should be controlled properly in the voltammetric measurements such as changing of the working electrode potential, time measurement of the current and stirring of the solution. The performance of the amperometric sensor is greatly influenced by the nature of the working electrode. Therefore, enormous efforts have been focussed on electrode fabrication to improve the performance of the sensor device (Bard, 1980). The trends of electrochemical determination of analytes commenced in 1922 and Heyrovsky acquired the Nobel prize for the invention of the mercury electrode (Smyth & Vos, 1992). Recently, the electrodes composed of metals such as platinum, gold, cobalt, copper, nickel and several forms of carbon have aroused huge interest due to having low background current, extended potential window, cost-effective, inertness and suitable for multiple recognition and detection of analytes. Through the expansion of chemically modified electrodes, a new approach has been generated to electrode systems, where some crucial parameters of the electrode surface can be modified by the addition of a surface modifier.

2.10.4 Conductometric sensor

A conductometric sensor is a miniaturised device of a two-electrode system that is designed to measure the conductivity of the electrolytic layer close to the electrode surface. Conductivity is the reciprocal of the resistance (Kriz *et al*., 1996). This technique is simple and cost-efficient because it does not require any reference electrode. One of the crucial parameters for the design of a conductometric transducer is the proper selection of electrode materials (Svetlicic *et al*., 1998). Several materials have been tested and utilised such as gold, silver, cobalt, platinum, carbons, copper, aluminium, nickel and others. All of these materials are electrically conductive and suitable, but the expensive materials have comparatively better properties. Efficient measurement of the conductivity facilitates the improved construction of the instrument and effective determination of the analytes of interest (Svetlicic *et al*., 1998).

2.11 Chemically modified electrodes (CMEs)

One of the special features of electrochemical techniques is the utilization of chemically modified electrodes with properties can be tailored and applied effectively for the selective determination of the desired analytes. A CME is designed through the modification of electrode surface with desired materials to develop an electrode that shows different responses compared to the unmodified electrodes. The modified electrode can exhibit similar features as the modified materials. Different types of electrodes have been used for the fabrication of CMEs such as boron-doped diamond, glassy carbon, indium tin oxide (ITO), fluorine-doped tin oxide (FTO), screen printed, gold, diamond and carbon paste electrode. At CMEs, the oxidation or reduction reaction occurs by the transfer of electrons from an electrode to a reaction substrate or a reactant (Rahman *et al*., 2017). The incorporation of CMEs in electrochemical measurements turns this method into a crucial application in materials characterization. CMEs are different compared to other classes of electrodes, as the thin layer of a suitable material is coated or bounded on the surface of the electrode to provide special chemical features. One of the distinct properties of CMEs is the electrocatalytic properties which are important in electroanalytical measurements. They have several advantages including rapid response, reusable, resistance towards fouling, limiting the effect of interference molecules in the complex solution, enhancing the electrocatalytic effects, chemically and thermally stable, cost-efficient, readily available and high sensitivity and selectivity (Linford, 1990). Due to their multiple benefits, CMEs proved eligible, reliable and ready to be implemented in amperometric sensing devices for the analysis of complex samples (Fang *et al*., 2017). There are several approaches to chemically modify the electrodes such as chemisorption, covalent bonding, self-assembly technique, polymer film coating, drop-casting and composite. CMEs have been utilized in different fields of research such as electrochemical investigations, electrochemical conductivity, electrostatic properties of

the electrode surface, ionic transportation, polymer electron transportation, development of electrochemical devices. Since 1979 the approaches of the surface modification of electrodes have been one of the most active areas of research interest in the field of electrochemistry, with important information on how the electrodes interact with the surrounding environments. Among the fabrication techniques, the drop-casting technique was utilized for the fabrication of glassy carbon electrodes (GCE) in the present study. A small quantity of the material solution is micropippetted and drop-casted on the surface of GCE and evaporated properly at ambient temperature as shown in Figure 2.12. Here, GCE is chosen as the bare electrode due to its chemical inertness, cost-efficiency, wide potential range and low background current (Wang & Taha, 1990).

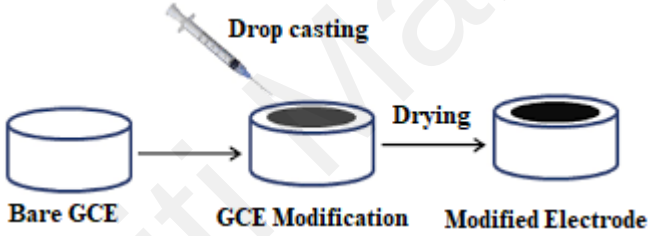

Figure 2.12: Surface modification of electrode

2.12 Electrochemical methods

The voltammetric approaches are the measurement of the current changes from the electrochemical reactions of the analyte at the surface of the electrode. Voltammetric experiments are performed in an electrochemical cell which consists of two or three electrodes, i.e working electrodes (WE), counter electrodes (CE) or auxiliary electrodes and reference electrodes (RE). The electrochemical reactions under investigation occur at the WE, where the CE is used to complete the circuit. The potential for RE should be consistent as it is the reference potential for the WE. To maintain a constant potential of the RE, the RE is introduced inside the electrochemical cell (three-electrode system) as shown in Figure 2.13. The most important function of RE is that it can maintain the potential constantly even if there are any changes in the analyte concentration in the

solution. The three electrodes are immersed inside a container containing inert supporting electrolytes which is not easily oxidized or reduced and the chemical species to be investigated. The supporting electrolyte is important because it can decrease the resistance of the solution and remove the influence the electromigration. The flow of current between the WE and CE is a function of potential and is measured by an instrument called potentiostat or galvanostat. This voltammetric measurement is drawn through the current versus potential plot which is referred to as the voltammogram (Stradiotto *et al*., 2003). Different types of voltammetric approaches are as follows.

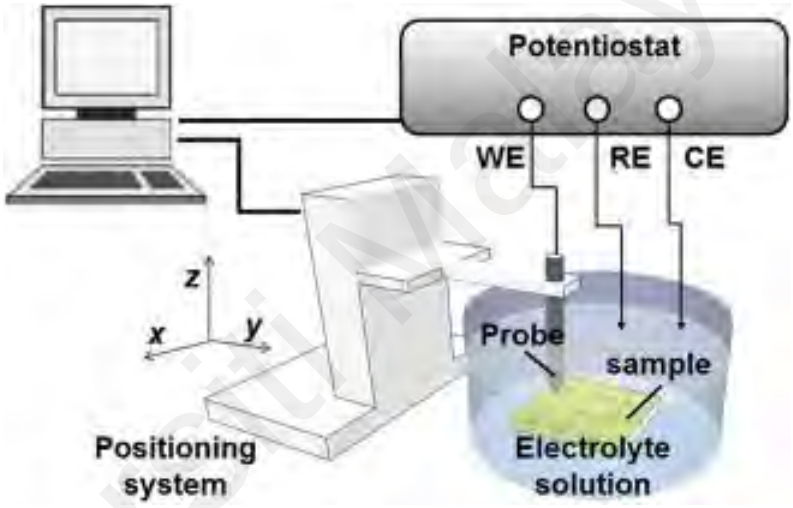

Figure 2.13: The three electrode system electrochemical cell.

2.12.1 Cyclic voltammetry

Cyclic voltammetry (CV) is a popular and effective electrochemical technique that is commonly used for the investigation of the redox reaction of molecular species. The electrochemical characteristics of an analyte in solution or a molecule that is adsorbed on the electrode surface can be investigated through a CV. CV is accomplished by cycling the potential of the WE versus the RE and measuring the current. The WE potential is usually measured against a RE which contains a stable and well-known potential. The applied potential generates an excitation signal (Farghaly *et al*., 2014). The potential scan can be negative from a more positive potential to a more negative potential. The switching

potential is a state where a sufficient voltage is reached to undergo an oxidation or reduction reaction of an analyte. For the reverse potential, the scan could be from positive to negative. When an oxidation reaction is required for some analytes, the potential could be scanned from the positive direction. The voltage rate shifts overtime during each phase is called the scan rate of that specific experiment. If the electron transfer is fast on the surface of the working electrode and when the current is limited by the diffusion of the analytes to the electrode surface, then the peak current is proportional to the square root of the scan rate (Gosser, 1993). The relationship can be explained through the Randles-Sevcik equation. Then the experiment samples a little portion of the solution such as the diffusion layer of the electrode surface. In sensor applications, the CV experiments are used to determine the electrochemical performances of the unmodified and different modified electrodes in the presence and absence of the target analytes. The influences of different pH, pH optimization, influences of different scan rates and scan rate optimization are also accomplished by this technique. The active surface area of the electrode can also be calculated using the Randles-Sevcik relationship from the CV technique. The Randles-Sevcik relationship is shown as follows:

$i_p = 2.69 \times 10^5 \, A \, C \, D^{1/2} \, (n)^{3/2} \, \upsilon^{1/2}$

i_p = redox peak current (Amp), A = surface area of the electrode (cm^2), n = number of transferred electrons, C = concentration of the ferricyanide solution (mol cm^{-3}), D = diffusion coefficient (7.60×10^{-6} cm^2 s^{-1}) and υ = scan rate (V s^{-1}) (Lether & Wenston, 1987).

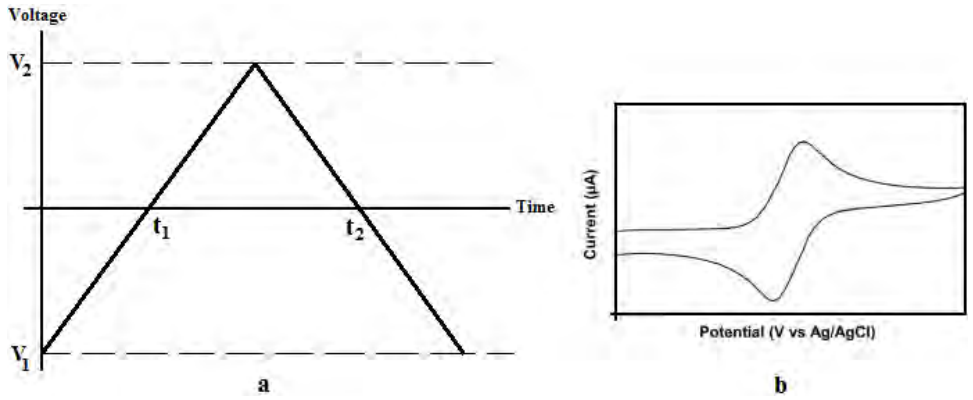

Figure 2.14: A potential time curve of cyclic voltammogram which is obtained by measuring the current at the WE during the potential scans (a). A cyclic voltammogram resulting from a single electron reduction and oxidation (b).

The voltammogram is plotted with current versus applied potential. The voltage sweeps between V_1 and V_2 at a fixed rate. During the forward scan of the reducing potential, the cathodic current is low. But when the applied potential is gradually increased, the cathodic current increases over time with the presence of a reducible analyte in the solution. When the reduction potential of the analyte reaches some point, the decline of the cathodic current occurs due to the exhaustion of the concentration of reducible analytes. When the voltage reaches V_2 the scan reverses and the voltage sweeps back to V_1. If the redox couple is reversible the reduced analyte will be re-oxidized in the reverse scan producing an anodic current. The scan rate, $(V_2 - V_1)/ (t_2 - t_1)$, is a crucial factor because an adequate time must be provided to perform the scan rates to allow for the completion of a successful chemical reaction as shown in Figure 2.14 (Streeter *et al*., 2008).

2.12.2 Differential pulse voltammetry

Differential pulse voltammetry (DPV) is an analytical tool for quantitative electrochemical analysis the investigation of the kinetics and the mechanism of the electrochemical reaction. DPV is a sensitive technique that is similar to squarewave voltammetry but offers multiple benefits over other electrochemical techniques. These techniques possess a short pulse time which enhances the measured Faradic currents. The DPV technique is applied for the evaluation of the analytical application of an electrochemical nano-device (Adeloju *et al*., 1985). The highest to lowest analytic

concentration range (linear range) and the lowest concentrations of analytes i.e limit of detection (LOD) that is possible for a WE to detect can be calculated by the corresponding curves in this technique. LOD can be calculated by the following equation.

$$LOD = 3 \times S_b/m$$

Here, 3 is the signal to noise ratio of 3, S_b denotes the standard deviation of the blank sample and m denotes the slope of the calibration curve (Akhter *et al*., 2018).

2.12.3 Squarewave voltammetry (SWV)

SWV is a sensitive, small amplitude and rapid responsive approach which is designed to identify not only the contribution of Faradic signals but also the parasitic charging currents. The analysis of the characteristics specifications of this approach also offers the investigation of the reaction kinetics and mechanism of the electrode process subjected to the study. The shape of the potential current curve is measured by the applied potentials height ΔE, which might differ corresponding to the potential steps E_{step} (mV) and duration τ. In the applied potential vs. time curve, t refers to the pulse width, and f refers to the pulse application frequency (Osteryoung & Osteryoung, 1985). The currents are measured two times, at the ending of forwarding potential pulse and reverse potential pulse and in both cases, the current is measured immediately before the reverse of the potential direction. The signals can be achieved from the intensity of differential current ΔI. The effect of the current signal generated from capacitive current is very minimal. The measurement of current at two different intervals in each squarewave sequence and two waveforms of current are gathered and saved as they have the diagnostic utility. A plot is drawn between the differential current and applied potential which indicates the redox (reduction-oxidation) processes. The peak obtained from the plot is directly proportional to the redox-active analytes. As SWV has high sensitivity and is considered as an improvement over other analytical approaches, this technique has been used frequently for several electrochemical investigations in recent years for the development

of electrochemical nano-device, analysis of pharmaceutical preparations etc (Lovrić & Komorsky-Lovric, 1988).

Selectivity, stability, real sample study are the quantitative analysis and prerequisites for the construction of any successful sensor. In this thesis, the quantitative analysis of the desired analyte was conducted by differential pulse voltammetry and square wave voltammetry.

2.13 Electrochemical impedance spectroscopy (EIS)

The EIS is an electrochemical method that measures the impedance of any system subjected to an AC potential and depend on the frequency of AC potential. It is a complex approach in electrochemical research. EIS is performed to investigate the intrinsic characteristic of a material that affects the electrical conductivity or capacity of an electrochemical system. By changing the excitation frequency for the applied potential within a frequency range, the impedance can be calculated. The impedance combines the real impedance and imaginary impedance of any system as a function of perturbation frequency which are the electrical resistance and reactance (Lasia, 2002). Generally, the Nyquist plot and Bode plot are implemented for the presentation of data in EIS, but for most electrochemical analyses, the Nyquist plot is presented as shown in Figure 2.14. The impedance technique is considered as an effective approach to investigate the electrode-electrolyte interface i.e electrical properties resulting from the reactions at the surface of the fabricated electrodes (Jorcin *et al*., 2006).

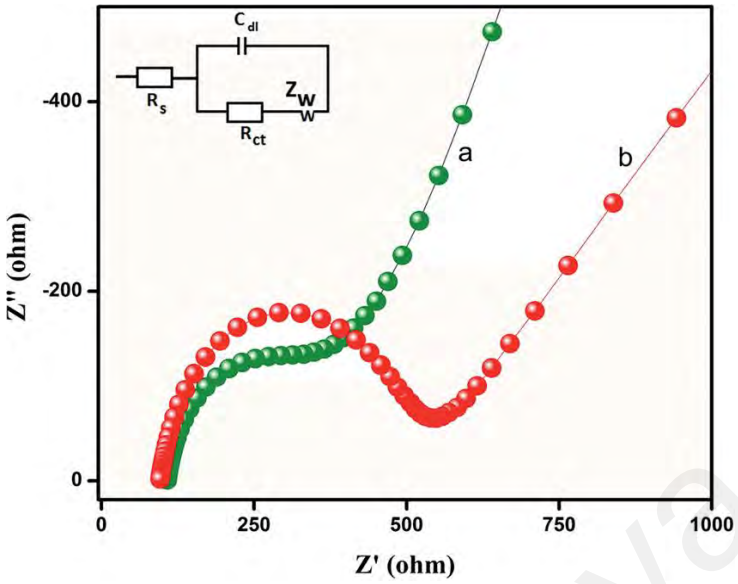

Figure. 2.15: A typical electrochemical impedance spectroscopy

2.14 Application of biopolymer-based carbon nanocomposites

2.14.1 Electrochemical sensing of the target molecules

Cellulose and chitosan are the most abundant biopolymers on earth. Their availability, biocompatibility, cost-efficiency and chemical inertness make them lucrative and a green alternative for large scale production over other commercial synthetic biopolymers. Both of them are utilized enormously in electrochemical applications such as in the fabrication of electrochemical sensors and biosensors. Cellulose and chitosan have almost a similar molecular structure except for the presence of an amine (NH_2) group as a pendant functional group in CTS. For the past few years, both cellulose or nanocellulose and CTS have been utilized enormously in different electrochemical applications such as electrochemical sensors and biosensors etc. Among the carbon nanomaterials, multiwalled carbon nanotubes and nitrogen-doped graphene possess exceptional electrical conductivity, electro-catalytic activity, cost-effectiveness and have a facile synthetic approach, suitable and widely used in the fabrication of sensors.

Mao *et al* (2015) reported a nanocomposite of MWCNT and chitosan-copper complex using the self-assembly approach for the electrochemical determination of

paracetamol in tablets and human serum samples. They modified a glassy carbon electrode (GCE) with MWCNTs/CTS-Cu by a simple and inexpensive CV and DPV method. They demonstrated that the electrode showed excellent electrocatalytic performance for the oxidation of paracetamol in pH 7.0 PBS with good stability, high selectivity and sensitivity, wide linear range and a low detection limit. Shahrokhian *et al* (2015) reported the catalytic activity of nanocellulose and carbon nanoparticles nanocomposite film toward the oxidation of metoclopramide in presence of pH 7.0. They prepared a GCE modified with NC/CNPs using electrodeposition and studied the linear sweep voltammetry (LSV) and CV of the modified electrode. The fabricated NC/CNPs is an efficient, low cost and facile approach for the electrochemical determination of metoclopramide in pharmaceuticals and clinical preparations with rapid response, good reproducibility, high stability, broad linear range and low detection limit. Mahmoud *et al* (2020) synthesized a nanohybrid composite of nitrogen and sulphur co-doped graphene quantum dots and nanocellulose for the electrochemical sensing of anti-schizophrenic drug olanzapine in pharmaceuticals and human biological fluids and the fabricated sensor was studied by CV and squarewave adsorptive stripping voltammetry (SWADSV). They reported that the fabricated electrodes exhibited good electrocatalytic activity towards the electro-oxidation of olanzapine in the presence of pH 7.0 with good selectivity, sensitivity, stability and reproducibility. Anirudhan *et al* (2018) developed a nanocomposite of silylated Graphene oxide–grafted-chemically modified nanocellulose (Si-GO-g-CMNC) for the selective sensing of cholesterol and was studied by CV and DPV. They claimed that the fabricated electrode showed good redox performance toward the electrochemical determination of cholesterol in pH 7.4 with a broad linear range, low limit of detection, good stability, high selectivity and good reproducibility.

CHAPTER 3: BIOPOLYMER BASED HYBRID (NANOCELLULOSE/*F*-MWCNTS) NANOCOMPOSITE FOR THE ELECTROCHEMICAL SENSING OF DICLOFENAC SODIUM IN PHARMACEUTICAL DRUGS AND BIOLOGICAL FLUIDS

3.1 Introduction

Diclofenac sodium (DCF) (sodium [o-(2, 6-dichloroanilino) phenyl] acetate) is a safe and widely used painkiller. The non-steroidal anti-inflammatory drug (NSAID) is generally prescribed as an anti-pyretic, anti-rheumatic, analgesic and anti-inflammatory drug for joint degenerative disease and arthritis treatment (Okoth *et al*., 2018). In addition, it is administered for the treatment of musculoskeletal injuries, ankylosing spondylitis, post-surgery analgesia, osteoarthritis and sports injuries. It inhibits the synthesis of prostaglandin through the inhibition of the cyclooxygenase enzyme and is the primary mechanism of its analgesic, anti-thermal and anti-inflammatory effect (Goyal *et al*., 2010). Usually, the sodium salt of DCF is used because of its Generally solubility. The DCF is easily metabolized by the hepatic enzyme.

DCF has a half-life ($t_{1/2}$) of 1-2 h, a protein binding capability of 99% and a volume distribution of 0.171 kg^{-1}. DCF travels easily through the synovial fluid. Thus the determination of low concentrations of DCF from pharmaceutical dosage forms and environmental samples is very important (Shalauddin *et al*., 2017). The long-term consumption of DCF by patients suffering from the Shy-Drager syndrome and diabetes could result in adverse effects such as heart attack and stroke (Aguilar-Lira *et al*., 2017). Due to these effects and the huge commercial demand in pharmaceuticals, medical and biomedical applications, it is very important to develop a facile, sensitive, selective, accurate and cost-effective technique for the detection of DCF (Mofidi *et al*., 2017).

Several analytical techniques have been developed for the quantification of DCF such as spectrophotometry (Lucas *et al*., 2014), gas chromatography-mass spectrometry (Borenstein *et al*., 1996), liquid chromatography (Elkady, 2010), and thin-layer chromatography (Sun *et al*., 1994). These conventional techniques have several disadvantages such as high cost, time-consuming, the need for chemical reagents and pre-treatment steps before the analysis, which could be complicated for the detection of certain analytes (Goyal *et al*., 2010). Electrochemical methods have drawn great attention recently because of their rapid response, simple procedure, higher sensitivities and possible miniaturization for on-site detection (Rodríguez *et al*., 2007). For example, several potentiometric (Kormosh *et al*., 2009) and voltammetric methods (Afkhami *et al*., 2016; Aguilar-Lira, Álvarez-Romero, et al., 2017) have been reported for DCF detection. Voltammetric techniques have advantages such as accuracy, simplicity, swiftness, selectivity and cost-effectiveness, even though the unmodified electrode generally shows a lower response towards DCF electro-oxidation (Yang *et al*., 2008).

Carbon nanotubes (CNT) consist of single or multiple layers of sp^2 hybridized carbon atoms which are folded into nano-cylinders (Thostenson *et al*., 2001). The two main types of CNT are the single-walled carbon nanotubes (SWCNTs) and multi-walled carbon nanotubes (MWCNTs) (Yang *et al*., 2008). Since their discovery, CNTs have gained significant attention due to their unique properties such as excellent electrical conductivity, good chemical, mechanical and thermal stability, high tensile strength and elasticity (Gooding, 2005). Among these two types of CNT, MWCNT has gathered significant attention from researchers due to their unique properties such as expanded surface area, sharp electrochemical response, good adsorption ability, better chemical stability, significant electrical conductivity and higher mechanical strength (Yang *et al*., 2015). However, pristine CNT is insoluble in water and could not be used for electrode fabrication. In recent years, the functionalization of CNT is an effective method of

activation. The functionalization process effectively removes impurities from the CNT, increases the dispersion in water and also improves the electrochemical performance. More importantly, functionalization provides stronger anchoring of the CNT which facilitates the fabrication of the modified electrode. Functionalized MWCNTs (*f*-MWCNT) have been utilized for the fabrication of nanocomposites in various applications such as electrochemical sensors, biomedical science, medicine and electronics (Hu *et al*., 2010; Perez-Lopez & Merkoci, 2012).

Cellulose is a biocompatible and prominent sustainable material, is also the most available and unlimited natural biopolymer (Taheri *et al*., 2018). It has been utilized substantially to produce nano-structured cellulose or nanocellulose (NC) by nanoscale isolation, which is free from hierarchical structural defects (Moon *et al*., 2011). NC is one of the most cost-effective, bio-degradable, biocompatible, environmentally friendly and easily available green nanomaterial (Xue *et al*., 2017). Recently, the drive towards large scale production of NC has shown advancements due to the improved mechanical characteristics and thermal stability of several host matrices (Lin *et al*., 2012). Cellulose could enhance the selectivity and sensitivity of electrochemical sensors for the detection of certain analytes. As cellulose possesses good adhesion properties, it prevents the leaching of nanoparticles from the electrode surface. Thus a remarkable improvement can be obtained for the long term stability of the modified electrode (Guiomar *et al*., 1997). Cellulose is composed of repeating cellobiose units that contain six free OH groups, an acetal linkage and a single hemiacetal linkage which are attached by strong inter and intramolecular hydrogen bondings. The hydrogen bonds also provide the NC fibers with large aspect ratios, surfaces functionalized with OH groups and a distinguished axial elastic modulus configuration. Moreover, NC possesses a large amount of OH groups which can be further modified for the incorporation of binding sites for the selective adsorption of different analyte species (Portaccio *et al*., 2007). These combined

characteristics make the nanostructured cellulose fibers an ideal building block for conjugation with other functional materials such as polypyrrole (Wang *et al*., 2014), graphene (Yan *et al*., 2014) and CNT (Wang *et al*., 2013). Furthermore, one of the interesting properties of cellulose is, without any modification cellulose fibers increase the ionic conductivity when utilized in any electrochemical applications, as they promote ionic mobility by producing ion conduction pathways (Gui *et al*., 2013).

Based on the aforementioned issues, it is reasonable to presume that a nanocomposite of NC and functionalized MWCNTs should display strong, flexible and effective electrodes with superior mechanical integrity and electrochemical performance for the detection of certain analytes. Wang *et al.* (1987) reported a modified GC electrode with cellulose acetate utilized for the detection of an antipsychotic drug, chlorpromazine (oxidizable organic compounds) by adsorptive stripping voltammetry. Shahrokhian *et al*. (2015) reported a GC electrode modified with a nanocomposite of NC and carbon nanoparticles for the sensitive electrochemical detection of the anti-emetic drug metoclopramide.

Herein, we report an electrochemical sensor based on GC electrode modified with NC and *f*-MWCNTs for the first time for the sensitive determination of DCF. The electrochemical performance of DCF at the GC electrode modified with nanocomposite of NC and *f*-MWCNTs was analysed by differential pulse voltammetry (DPV) and cyclic voltammetry (CV). This present work shows a broad linear range and low LOD for DCF detection compared to previous studies (shown in Table 3.1). The results showed an extraordinary expansion of the surface area and increased interfacial electron transfer rates which enable a new avenue for electrochemical determination of DCF. Finally, the electrode was utilized for the voltammetric determination of DCF from tablet and ampoule preparations, human blood serum and urine samples. The fabricated

nanocomposite proved to be simple, rapid and effective, with high sensitivity and selectivity for the detection of DCF in real samples.

3.2 Experimental section

3.2.1 Chemicals

Diclofenac sodium, cellulose, dopamine, ascorbic acid, K_2HPO_4 and KH_2PO_4 were procured from Sigma Aldrich (Malaysia). All chemicals were of analytical grade and used without further purification. Pristine MWCNT (> 99.9 wt% purity, diameter 8-15 nm, length 10-50 μM) was procured from Bay Tubes, Germany. The aqueous solutions were prepared in deionized water (DI). A 1.0×10^{-3} M DCF stock solution was prepared daily. The solution was kept in the dark at 4 ºC. A 0.2 M phosphate buffer solution (PBS) at pH 4 was prepared by dissolving 0.132 gm of K_2HPO_4 and 0.169 gm of KH_2PO_4 in DI water.

3.2.2 Instrumentation

Electrochemical experiments were performed on Autolab AUT72609 galvanostat/potentiostat from Ecochemie (Netherlands). Differential pulse voltammetry (DPV) and cyclic voltammetry (CV) were performed in a three-electrode single compartment electrochemical cell. The galvanostat/potentiostat was interfaced with a computer installed with the GPES (general purpose electrochemical system) software to run the electrochemical experiments. A GCE (3 mm diameter) was the working electrode, while the reference and counter electrodes were Ag/AgCl (3.0 M KCl) and a platinum wire, respectively. Field emission scanning electron microscopy (FESEM) was performed on SU8030 Hitachi (Japan) while transmission electron microscopy (TEM) was performed by Tecnai G2 F20 FEI (U.S). Atomic force microscopy (AFM) was performed by AFM5000II Hitachi (Japan) while X-ray powder diffraction (XRD)

measurement was carried out by EMPYREAN PANalytical (Netherlands). Fourier transformed infrared spectroscopy (FTIR) was performed on a Spectrum 400 PerkinElmer, (U.S.) while an Invia Raman Microscope Renishaw (UK) was used to obtain the Raman spectra.

3.2.3 Methodology

For the synthesis of NC/*f*MWCNTs nanocomposite, cellulose and pristine MWCNTs were used as the precursor materials. The source of cellulose was cotton linter. NC and *f*MWCNTs were synthesized using their precursor material followed by the acid hydrolysis method. The GC electrode was fabricated by the drop-casting technique. The morphological properties were characterized by FESEM, TEM, AFM, XRD, FTIR and Raman spectroscopy. Before the electrochemical experiments, pH and scan rate were optimized. CV and DPV methods were employed to investigate the electrochemical behaviour of NC/*f*MWCNTs/GCE sensors. Satisfactory relative standard deviation and recovery values were obtained from the real sample analysis.

3.2.4 Experimental Procedures

The stock solution was prepared by dissolving the required amounts of the analyte in DI water and stored at 4 °C. The standard solutions were prepared by diluting aliquots of the stock solution. Nitrogen gas was purged for 10-12 min to deoxygenate the solution before the cyclic voltammetry experiments. For Differential pulse voltammetry, the conditions were: step E: 0.002V, modulation amplitude: 0.05V, initial E: 0.5V and final E: 0.8V.

3.2.5 Preparation of functionalized MWCNT

The synthesis of *f*-MWCNT from pristine MWCNT was performed as described (Karthik *et al*., 2017). The pristine MWCNT (0.3gm) was dispersed in a mixture of nitric acid (70 ml) and sulfuric acid (210 ml) (1:3 ratio) and refluxed for 24 h. After this, the COOH-pristine MWCNT dispersion was diluted. Then the dispersion was filtered through a filter paper and the residue was washed several times with DI water until reaching pH 7.0. Finally, the obtained *f*-MWCNT was dried at 80 °C for 24 h and were characterized by FESEM, TEM, XRD, FTIR and Raman spectroscopy.

3.2.6 Synthesis of nanocellulose

Nanocellulose was synthesized from cellulose (source: cotton linter) as described elsewhere (Zhang *et al*., 2007). The cellulose (0.5 gm) was dispersed in a combination of hydrochloric acid (12.1N, 50ml) and sulfuric acid (36.0 N 150ml) (1:3) and refluxed for 16 h. The dispersion was diluted by DI water using a centrifuge (2000 RCF). After washing, the product was added with 0.1M NaOH until pH 7.0. Then the solution was further washed 3 times with DI water (3 x 150 mL) followed by dialyzation with the membrane tube with continuous stirring for 24 h. Finally, the product was dried in an oven at 70 ºC for 24 h. The final product was a pale white powder and analysed by FESEM, TEM, AFM, XRD, FTIR and Raman spectroscopy.

3.2.7 Fabrication of the modified glassy carbon electrode (*f*-MWCNT/NC/GC electrode)

Firstly, the surface of the bare GC electrode was polished carefully by alumina powder on a microcloth (Buehler) and washed with DI water to reach a mirror-like surface. Then, 2 mg of *f*-MWCNT was dispersed by sonication in 2 mL DI water for 30 min. The nanocellulose suspension was prepared by dissolving 2 mg of nanocellulose in

1 mL of DI water and sonicated for 30 min. First, a 5 µM of nanocellulose suspension was drop-casted onto the GC electrode surface and left to dry. This was followed by the drop-casting of 6 µM of *f*-MWCNT on the GC electrode surface and left to dry at ambient temperature (fabrication step shows in Figure 3.1). The bare GC electrode and *f*-MWCNT/NC/ GC modified electrode was studied by FESEM, TEM and AFM imaging.

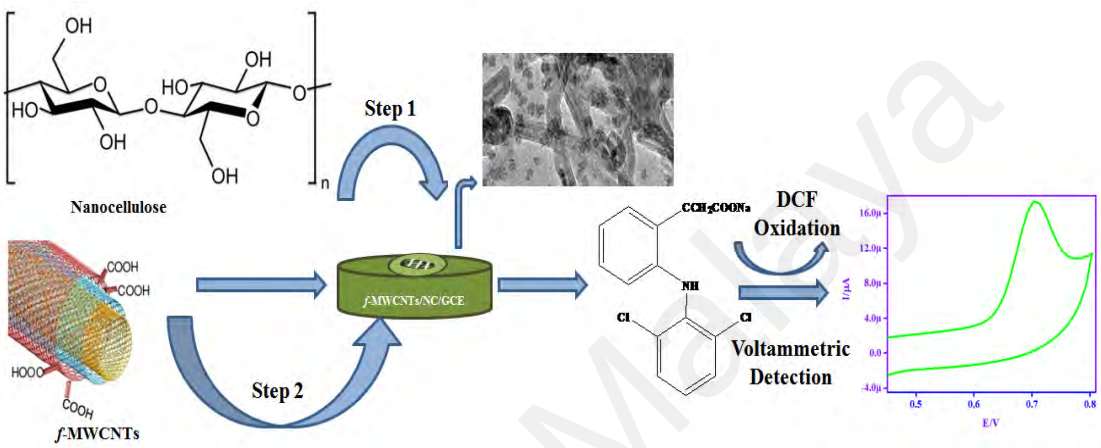

Figure 3.1: Fabrication of *f*-MWCNT/NC/ GC modified electrode for the detection of DCF

3.2.8 Preparation of real samples

To prepare the DCF tablet solution, two DCF tablets (50 mg) were completely ground and homogenized into powders. The powders were dissolved in DI water and stirred by a mechanical stirrer for 45 min. Then the solution was filtered through a syringe filter membrane (0.45 µm pore diameter). The filtrate was diluted in 0.2 M PBS to prepare a 0.1 mM stock solution of DCF. An accurately measured volume of 5 DCF sodium ampoule mixture equivalent to 15.65 mg of DCF sodium was diluted with 0.2 M PBS. Then, 1 mL of this solution was diluted with PBS and analyzed. Human serum specimens were collected from University Malaya Hospital while human urine specimens were collected from healthy volunteers. For the blood collection, we prepared a request letter with the supervisor's signature on it. After handover the letter to the head of the nurse with proper evidence, we were able to collect the human blood from them. The human

blood serum sample was centrifuged at 4000 rpm for 15 min and filtered. After filtration, it was diluted 10 times using a 0.2 M phosphate buffer solution without further treatment. The urine samples were diluted (4 times) in 0.2 M PBS. Different concentrations of DCF were added to the diluted urine samples. The recovery tests were performed using DPV for the measurement of DCF from DCF tablet dosage forms containing human blood serum and urine.

3.3 Aim of the research

This study aims to fabricate a new modified electrode based on NC and *f*-MWCNT. The combination of these two materials into a nanocomposite is expected to improve the properties of the nanocomposite compared to the single material. Thus the synergistic effect between NC and *f*-MWCNT and the excellent electrical conductivity is a hallmark for the high-performance electrochemical sensing of DCF.

3.4 Results and discussions

3.4.1 Materials characterizations

FESEM, TEM, AFM, XRD, FTIR and Raman experiments were used to characterize the key building blocks of the sensor. The surface morphology of different modified electrodes (NC/GC electrode, *f*-MWCNT/GC electrode and *f*-MWCNTs/NC/GC electrode) was studied by FESEM as illustrated in Figure 3.2 (A and B) showing a well-distributed NC and *f*-MWCNT. Figure 3.2C clearly shows a smooth surface of NC and *f*-MWCNT composite on the bare GC electrode. The NC layer is fully covered with a layer of *f*-MWCNT. Due to the presence of NC, the surface morphology of the modified electrode becomes light in colour (charging effect) compared to the *f*-MWCNT in Figure 3.2B. The excellent homogeneous distribution of NC and *f*-MWCNT is due to the porous structure and high surface to volume ratio of the NC and *f*-MWCNT.

This excellent morphology promotes higher electrical conductivity and a faster interfacial electron transfer process. Figure 3.2D presents the TEM image of the final nanocomposite NC and *f*-MWCNT, which reveals that the *f*-MWCNTs is homogeneously dispersed in the NC turning into individual or smaller *f*-MWCNT bundles. Furthermore, due to the large surface area and water dispersion of NC, *f*-MWCNTs can be strongly adsorbed on the surface of NC (Hamedi *et al*., 2014). Appendix 3.1 (Figure A, B, C) shows the TEM images of NC and *f*-MWCNTs on GCE and nanocomposite of NC/ *f*-MWCNTs in different magnifications.

AFM was used to analyse the morphology of the NC and NC/ *f*-MWCNTs thin films (topology of 2 x 2 μm) as shown in Figure 3.3. Both images indicate a homogeneous distribution of NC (Figure 3.3A) and NC/ *f*-MWCNTs (Figure 3.3B) on the GC electrode. The deposited nanoparticles are spherical and their size ranges from 5.8-78.6 nm. The 3D images (Figure 3.3C and 3.3D) revealed that the sample height has increased from 23 nm to 35 nm in the final composite (NC/ *f*-MWCNTs) compared to the first sample (NC). This confirmed the successful deposition of NC and *f*-MWCNTs on the GC electrode surface. From the topology and 3D images, it is clear that the surface roughness has been increased and became more porous in the final composite (NC/ *f*-MWCNTs). These features facilitate the charge transfer rate, catalytic performance, sensitivity and fast response time of the sensor (Siqueira *et al*., 2008).

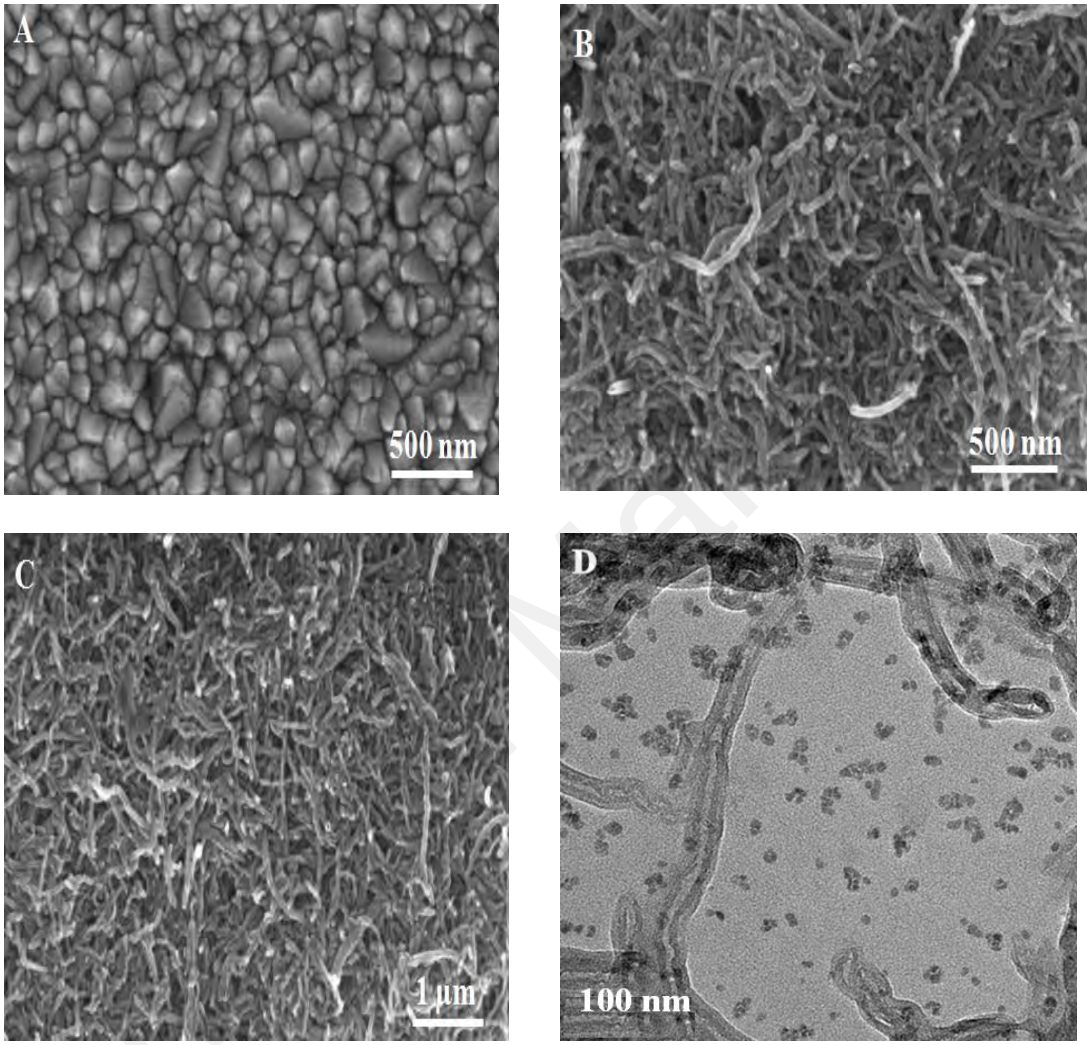

Figure 3.2: FESEM image of NC (A), *f*-MWCNTs (B), NC / *f*-MWCNTs composite (C) and TEM image of NC / *f*-MWCNTs composite (D).

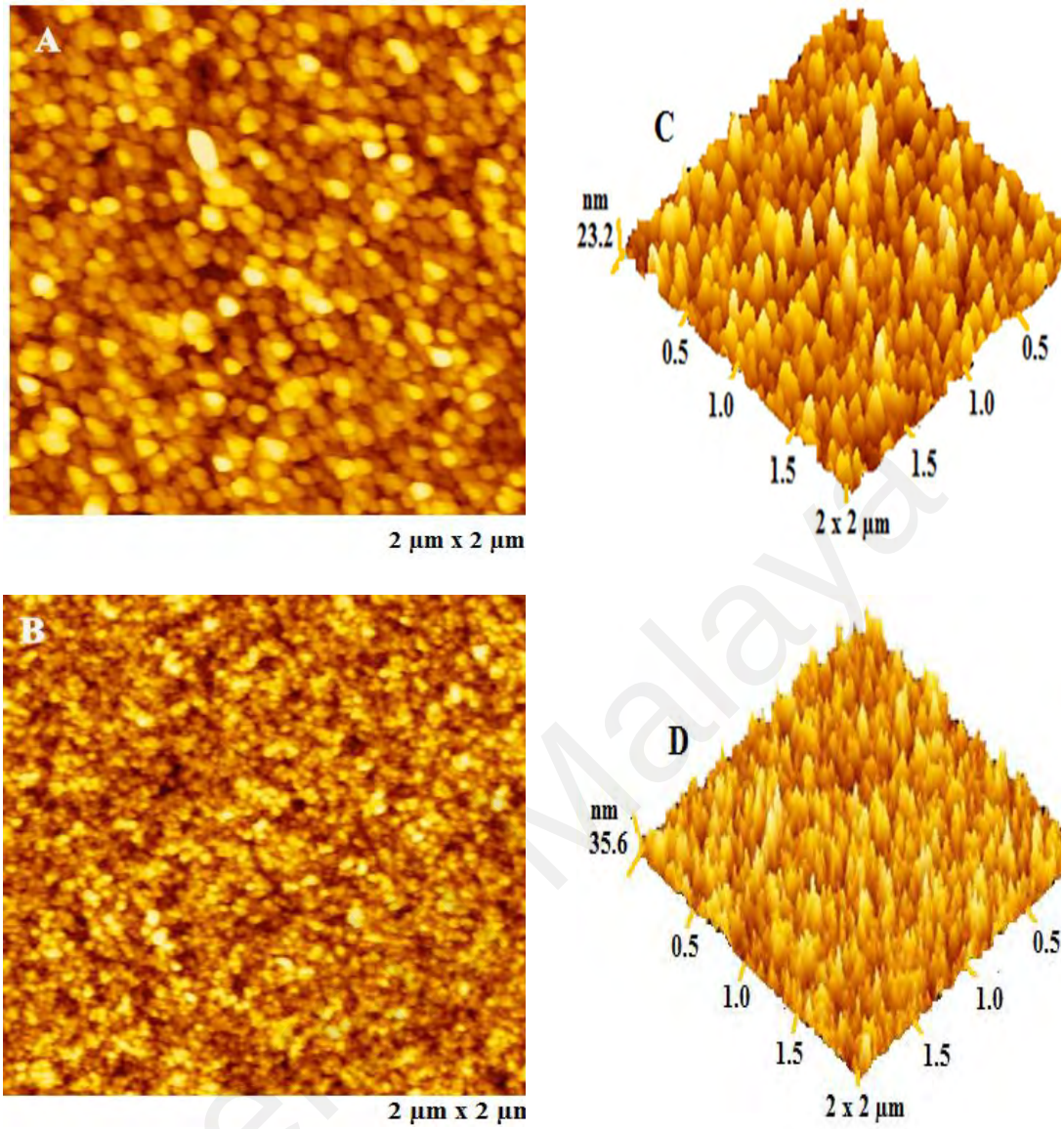

Figure 3.3: Atomic force microscopic (AFM) image of NC (A) and NC/ *f*-MWCNTs (B).

Appendix 3.2 shows the XRD patterns of NC, *f*-MWCNTs and NC/*f*-MWCNTs powders. From appendix 3.2 (curve a), the powder XRD patterns display distinct peaks at 16º and 23º. These peaks are attributed to the presence of NC (Lu & Hsieh, 2010). Curve b is the XRD of *f*-MWCNTs with peaks at 26º and 42º. This observation affirms that the MWCNT retained the same tubular structure after the functionalization process. Curve c of the NC/*f*-MWCNTs composite shows the same characteristics peaks for NC and some additional peaks at 25.8º and 42.9º which confirms the presence of NC and *f*-MWCNTs (Shanmugharaj *et al*., 2007). Therefore, the XRD data confirms the presence

of NC and *f*-MWCNTs and the successful synthesis of NC and *f*-MWCNTs nanocomposite.

FTIR spectroscopy was used to investigate the main functional groups present in Figure 3.4A cellulose (a), NC (b), and figure 3.4B pristine MWCNTs (a) and *f*-MWCNT (b). Figure 3.4A shows a broad band between 3500-3200 cm^{-1} attributed to the free OH stretch. The characteristic C-H stretch at 2900 cm^{-1} is observed for both cellulose and NC (Mandal & Chakrabarty, 2011). Nanocellulose possesses a higher density of hydroxyl groups (Stenstad *et al*., 2008). Thus after the chemical treatment, transmittance peaks were seen between 1653-1645 cm^{-1} in the NC spectrum attributed to the OH bending of absorbed water (Le Troedec *et al*., 2008). The C-O-C stretch of the pyranose ring occurs at around 1050 cm^{-1} (Pappas *et al*., 2002). The C-C stretch at 1155 cm^{-1} and C-O-C glycosidic band at around 1105 cm^{-1}, of the polysaccharide, diminishes in the NC due to the molecular weight reduction and acid hydrolysis (Garside & Wyeth, 2003). Figure 3.4B is the spectra of pristine (a) and *f*-MWCNTs (b) with methylene asymmetric/symmetric stretch at 2892 cm^{-1} and 2914 cm^{-1} (Shalauddin *et al*., 2017). But a sharper peak is observed at around 1732 cm^{-1} in the *f*-MWCNTs spectrum (curve b) due to the presence of the C=O group from the acid hydrolysis process (Afkhami *et al*., 2016).

The Raman spectra of cellulose (a) and NC (b) are shown in Figure 3.4C. The ratio of the D and G band (I_d/I_g) is used to predict the defect density of the samples. The regions below 1600 cm^{-1} and above 2700 cm^{-1} are more sensitive to the presence of cellulose backbone and hydrogen bonding, respectively. The D and G bands of cellulose occur around 1097 cm^{-1} and 1323 cm^{-1}, while the 2D band is present at 2899 cm^{-1} (H. Luo et al., 2014). The D and G bands of NC occur around 1091 cm^{-1} and 1341 cm^{-1}, respectively. The 2D band at 2905 cm^{-1} is attributed to the C-H and O-H stretching. The intensities of the D, G and 2D bands of NC are larger than cellulose due to the greater

amount of crystallinity in the NC compared to cellulose (Agarwal, 2017). Figure 3.4D is the Raman spectra of pristine MWCNTs (a) and *f*-MWCNTs (b). The G band of pristine MWCNTs occurs at 1576 cm^{-1} is attributed to the Raman active E_{2g} and is analogous to that of graphite. The peaks of the D band at 1343 cm^{-1} and the 2D band at 2680 cm^{-1} are due to the defects in the pristine MWCNTs. The increased intensity of the D and 2D bands after the acidic functionalization of *f*-MWCNTs confirms the successful attachment of the functional groups on the surface of pristine MWCNTs (Vinayan *et al*., 2012).

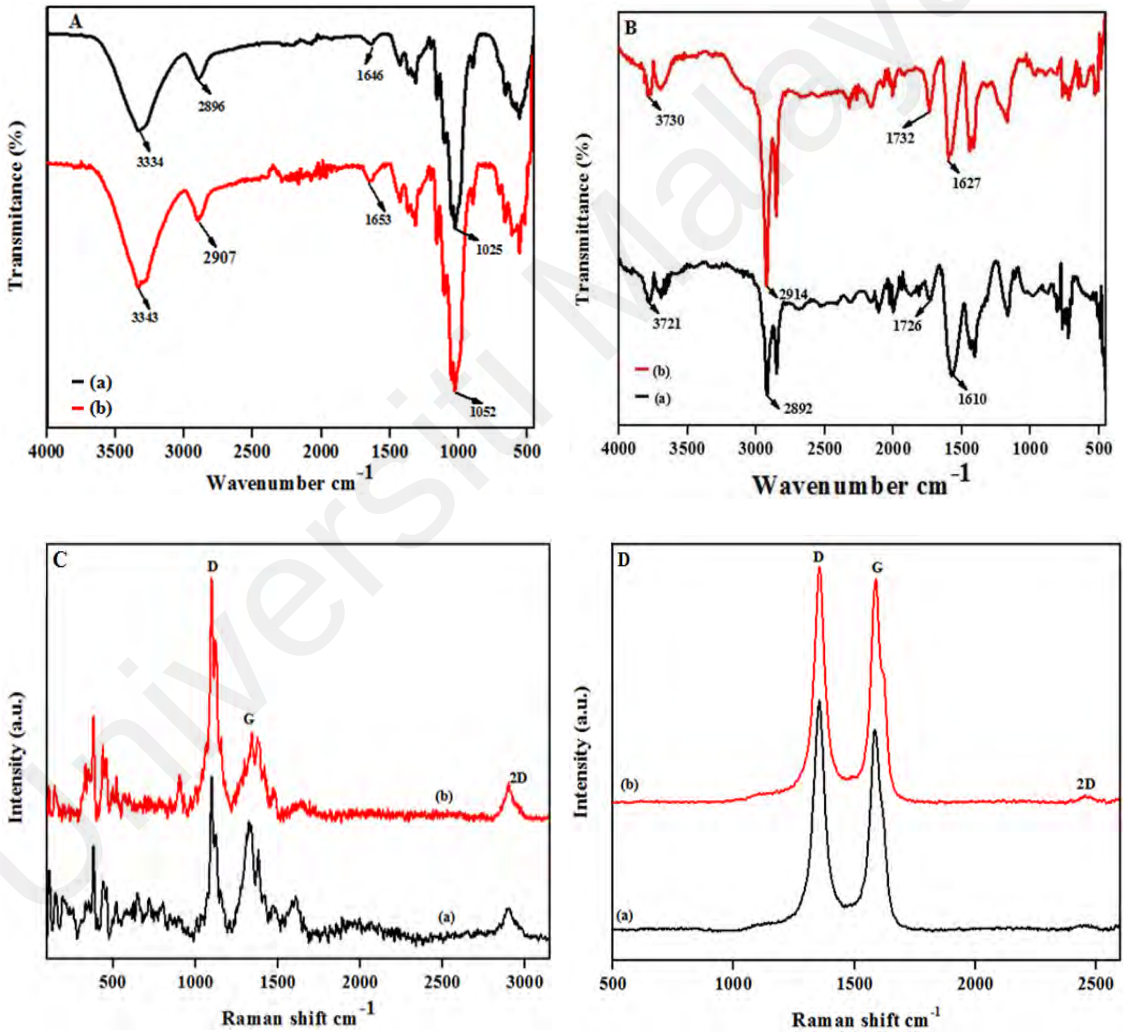

Figure 3.4: FTIR spectra of Cellulose and NC (A), Pristine and *f*-MWCNT (B). Raman spectra of Cellulose and NC (C), Pristine and *f*-MWCNT (D).

3.4.2 Surface area calculation of the modified electrode

The effective surface areas of the bare GCE, NC/GC electrode, *f*-MWCNTs/ GC electrode and *f*-MWCNTs/NC/ GC electrode were calculated to investigate the effect of surface modification. Chronocoulometry was performed in an aqueous solution of 1 mM $K_3[Fe(CN)_6]$ in 0.1 M KCl supporting electrolyte at 100 mV s^{-1}. The integrated Cottrell expression of the charge (Q) as a function of time is represented below:

$$Q = 2nFAcD^{1/2} t^{1/2} \pi^{-1/2} + Q_{dl} + nFA\Gamma_0 \quad (3.1)$$

Where the number of electrons transferred is n (n = 1), the Faraday constant is F, the working electrode surface area is A, the concentration of $K_3[Fe(CN)_6]$ is c and the diffusion coefficient of 1 mM $K_3[Fe(CN)_6]$ is D (7.6×10^{-6} cm^2 s^{-1}). Besides, $nFA\Gamma_0$ is the electrolysis of the adsorbed species, where Γ_0 is the quantity of the absorbed reactants and Q_{dl} is the capacitive charge, which can be subtracted from the background current. The chronocoulograms displays a linear relationship of Q and $t^{1/2}$, with a slope of 25 μC $s^{-1/2}$ and 272 μC $s^{-1/2}$, corresponding to the bare GC electrode and *f*-MWCNTs/ GC electrode, respectively. From the above equation, the effective surface area of the bare GC electrode, NC/ GC electrode, *f*-MWCNTs/ GC electrode and *f*-MWCNTs/ NC/ GC electrode is 0.052, 0.081, 0.078 and 0.217 cm^2, respectively. The *f*-MWCNTs/ NC/ GC electrode surface area is approximately 4.2 times larger than the bare GC electrode, which indicates that a larger electrochemically active surface area was achieved by the chemically modified GC electrode which enhances the conductivity of the modified sensor.

3.4.3 Electrochemical impedance spectroscopy

Electrochemical impedance spectroscopy (EIS) was utilized to investigate the electrical conductivity of the *f*-MWCNTs/NC/GC electrode. The electron transfer resistance (R_{ct})

at the electrode/electrolyte interface is obtained from the semicircle diameter in the Nyquist plots. Figure 3.5 shows the Nyquist plots of the unmodified GC electrode (blue dashed curve), NC/ GC electrode (red dashed curve), *f*-MWCNTs/ GC electrode (green dashed curve) and *f*-MWCNTs/NC/ GC electrode (purple dashed curve) which were performed in 0.1 M KCl with 5 mM $K_3Fe(CN)_6/K_4Fe(CN)_6$ between 100 kHz to 100 mHz. From the data fitting, the charge transfer resistance (R_{ct}) of the bare GC electrode is 1486 Ω. With the presence of NC, the R_{ct} decreases to 415 Ω due to the increase of ion transport of the NC. The R_{ct} value is 302.9 Ω for the *f*-MWCNTs/ GC electrode due to the presence of *f*-MWCNTs electrical conductor. The R_{ct} value of the modified nanocomposite decreases to 72.1 Ω due to the faster electron conductivity of *f*-MWCNTs/NC/ GC electrode compared to the NC and *f*-MWCNTs modified GC electrode. This result demonstrates that the modified electrode exhibits a lower electron transfer resistance which greatly increases the electron transfer rate.

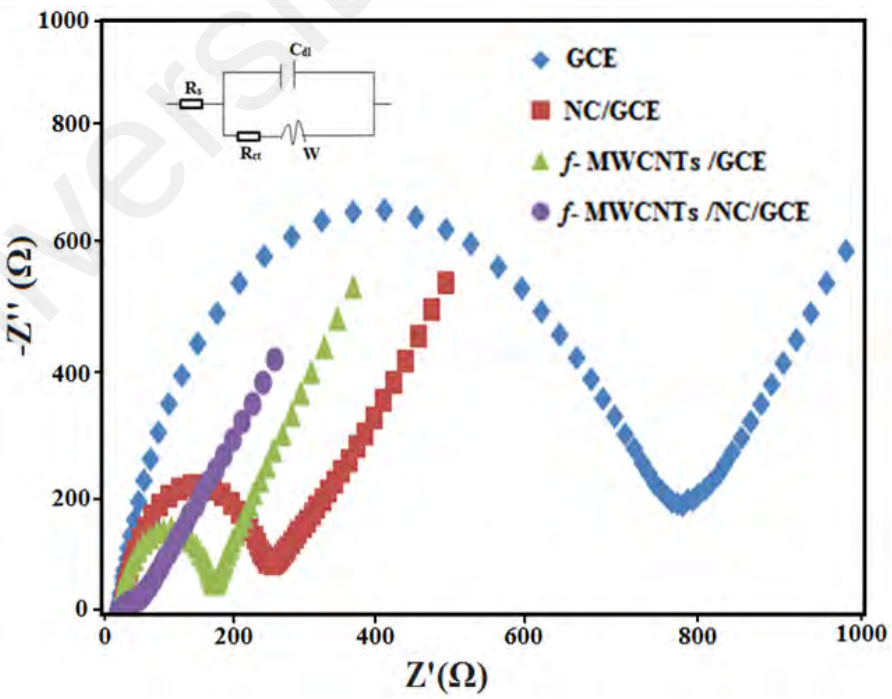

Figure 3.5: Nyquist plot of GCE (blue - dashed curve), NC/GCE (red – dashed curve), *f*-MWCNTs/GCE (green – dashed curve), *f*-MWCNTs/NC/GCE (purple – dashed curve) in 0.1 M potassium chloride solution with 5.0 mM $[Fe(CN)_6]^{3-/4-}$. Inset is the equivalent circuit for the fitting.

3.5 Electrochemical investigation of DCF at *f*-MWCNTs/NC/GC modified electrode

3.5.1 Electrochemical oxidation of DCF

To examine the electrochemical performance of the proposed sensor, CVs of DCF at *f*-MWCNTs/NC/GC electrode, *f*-MWCNTs/ GC electrode, NC/ GC electrode and unmodified GC electrode, were performed in 0.2 M PBS (pH 4) with 50 μM DCF at 100 mV s^{-1}. Figure 3.6 shows that the DCF is irreversibly oxidized at 0.69 V at the bare GC electrode (black solid curve). The NC/ GC electrode shows a broad peak at around 0.69 V (red solid curve) in the presence of DCF with a peak current of approximately 1.5 times larger compared to the bare GC electrode. This could be attributed to the anchoring sites and porous structure of NC with larger surface area (section 3.2) which allows ion transport, thus increases the accessibility of DCF. The oxygen in the DCF molecule interacts with the OH groups in NC through the intra and intermolecular hydrogen bondings. In contrast, the *f*-MWCNTs/ GC electrode (blue-solid curve) shows a sharp anodic peak (E_{pa}) at 0.68 V. The peak current for DCF oxidation at the *f*-MWCNTs/ GC electrode is remarkably improved, around three times greater compared to the bare GC electrode. This is attributed to the higher electrical conductivity of the *f*-MWCNTs. The *f*-MWCNTs/NC/ GC electrode shows a strong and well-defined anodic peak (E_{pa}) for DCF oxidation (pink-solid curve) at 0.67 V and is approximately five times greater compared to the bare GC electrode.

The improved oxidation current of DCF in the presence of NC and *f*-MWCNTs is due to two reasons. In the NC/ *f*-MWCNTs nanocomposite, NC provides a hydrophilic surface on the GC electrode, while the *f*-MWCNTs prevents the agglomeration of NC which gives a rougher surface (section 3.3.1 AFM) and larger surface area of the

nanocomposite. This results in the increased absorption of DCF on the electrode surface compared to the single layers of NC and *f*-MWCNTs, resulting in the improved electrochemical oxidation of DCF. Secondly, the increase in the peak current response of DCF indicates a synergy between the NC and *f*-MWCNTs which enhances the electrical conductivity of hybrid NC/ *f*-MWCNTs nanocomposite (section 3.3.3 EIS) and ultimately amplifies the current response. The enhancement of electrical conductivity and larger surface area of the *f*-MWCNTs/NC nanocomposite facilitate the electron transfer rate.

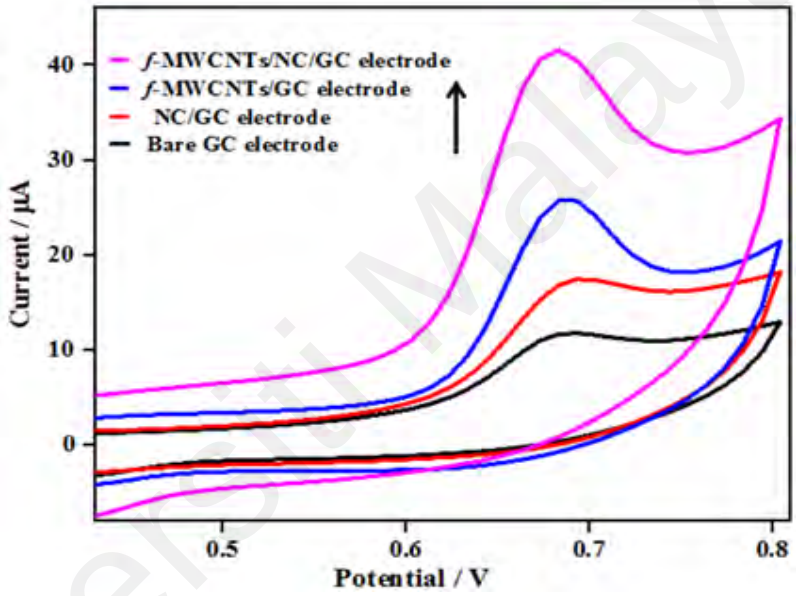

Figure 3.6: CV of the bare GC electrode (black solid curve), NC/ GC electrode (red solid curve), *f*-MWCNTs/GC electrode (blue-solid curve) and *f*-MWCNTs/ NC/GC electrode (pink- solid curve), in 50 µM DCF with 0.2 M PBS (pH 4.0) at 100 mV s^{-1}.

3.5.2 Influence of scan rate

The charge transfer is another performance indicator of the sensing electrode. This can be understood from the change of the redox peak current and peak potential with the scan rate. Figure 3.7A is the CVs of the *f*-MWCNTs/NC/ GC electrode in the presence of DCF between 10 to 400 mV s^{-1}, while Figure. 3.7B shows that the scan rate increases linearly with the oxidation peak current. The fitted regression equation is:

$$I_{pa}\ (\mu A) = 0.0592\ (\upsilon\ /mV\ s^{-1}) + 4.4236 \text{ and } (R^2 = 0.998) \quad (3.2)$$

The variation of the peak current (I_{pa}) with the scan rate (mV s^{-1}) indicates that the oxidation of DCF at *f*-MWCNTs/NC/GC electrode is a surface controlled process (Shalauddin *et al*., 2017). This observation was also confirmed by the linearity of the E_{pa} with the logarithm of the scan rate, as follows (Figure 3.6C):

$$E_{pa}\ (V) = 0.0279 \log\ (\upsilon\ /mVs^{-1}) + 0.6168 \text{ and } (R^2 = 0.999) \quad (3.3)$$

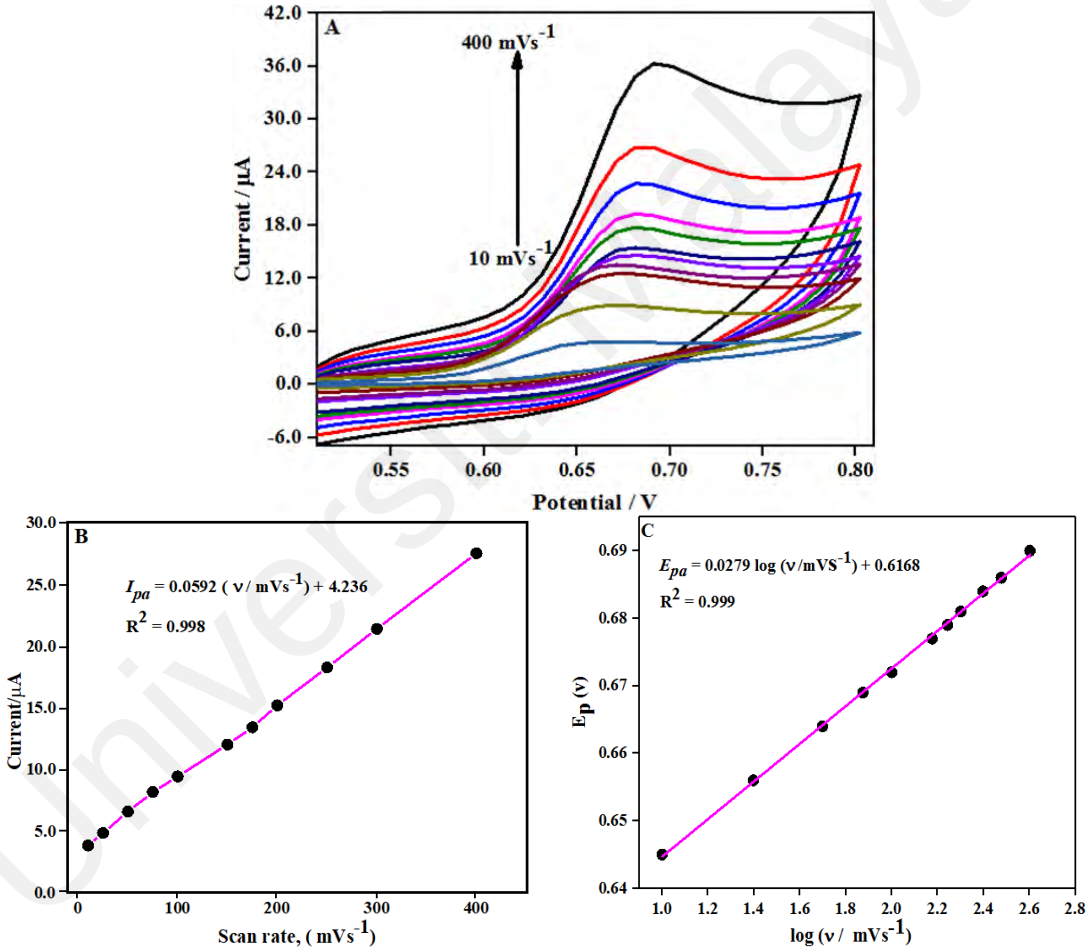

Figure 3.7: (A) CV of 50 µM DCF on *f*-MWCNTs/NC/GCE at different scan rates (10 mV s^{-1} to 400 mV s^{-1}) in 0.2 M PBS (pH 4.0). (B) the variation of the peak current of DCF with the scan rate, and (C) variation of peak potential (E_{pa}) with log υ.

3.5.3 Cyclic voltammetry at different pH

The pH of the supporting electrolyte is one of the controlling parameters for the peak potential of DCF oxidation. The pH of a solution usually influences the

electrochemical reactions by shifting the redox potential towards more positive or negative directions with varying peak currents. To obtain the maximum intensity of the oxidation peak currents at lower peak potentials, an optimum pH is required. Figure 3.8A shows the influence of pH on the oxidation of 50 µM DCF at the *f*-MWCNTs/NC/ GC electrode from pH 4 to 9 at 100 mV s^{-1}. The CVs of the *f*-MWCNTs/NC/ GC electrode show a strong dependence on the solution pH. The highest peak current is obtained at pH 4 but gradually decreases as the pH increases from 5 to 9. The highest current response for DCF determination was achieved for pH 4, thus pH 4 was considered as the optimum pH in this experiment. Figure 3.8B shows that the peak potential of DCF oxidation shifts towards a negative direction with the increase of pH, which indicates that the protons take part in the electrode reaction. The peak potential (E_p) decreases linearly with the increase of pH. The linear relationship could be expressed as follows:

$$E_{pa} \text{ (pH 4-9)} = -0.0556 \text{ pH} + 0.8168 \quad R^2 = 0.998 \tag{3.4}$$

The correlation coefficient and the slope is 0.998 and -0.0556 V/pH, respectively, which is close to a Nernstian behaviour. According to the Nernst equation, E_p (mV) = 59.16 (m/n)/pH (*n* is the electron number while *m* is the proton number), which confirms that the same number of electrons and protons were transferred in the electrochemical oxidation of DCF (Yang *et al*., 2008). Appendix 3.3 shows the proposed mechanistic pathway for the electro-oxidation of DCF at the *f*-MWCNT/NC/ GC electrode.

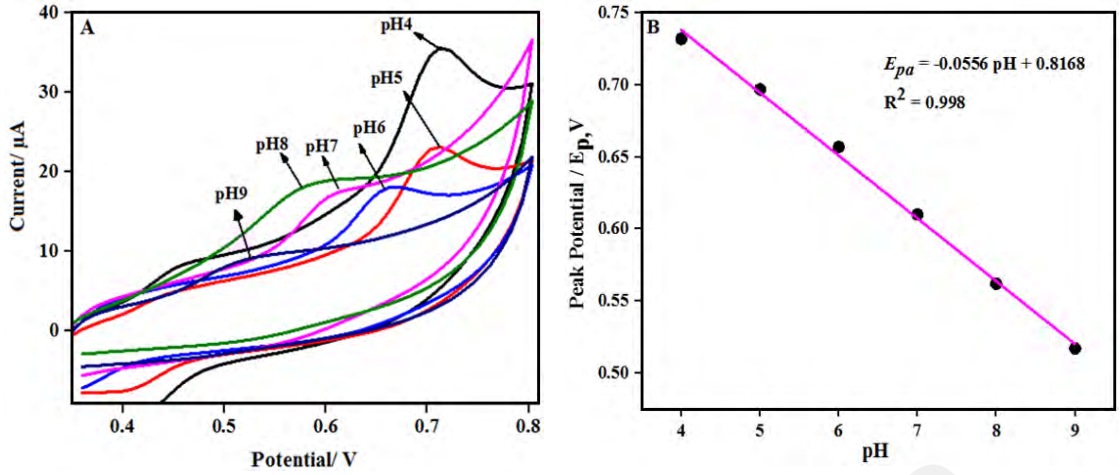

Figure 3.8: (A) Cyclic voltammetry of *f*-MWCNTs/NC/GCE in 0.2 M PBS between pH 4 to 9 with 50 µM DCF at 100 mV s^{-1}. (B) Plots of the anodic peak potential of DCF vs. pH.

3.5.4 Sensitivity and limit of detection of DCF

It is worth mentioning that the main focus of this investigation is to develop a sensing electrode to detect low concentrations of DCF. However, the outcome of sensing performance depends on the sensing technique. Due to the higher sensitivity, DPV is commonly used to detect lower concentrations of the analyte compared to the CV method. Thus DPV was used for the quantitative determination of DCF concentration at the *f*-MWCNT/NC/ GC electrode. Under optimum conditions, the peak current of oxidation increases linearly with the DCF concentration. The voltammograms showed two linear segments with different slopes at different concentration ranges of DCF, between 0.05–5 µM and 6–250 µM, as shown in Figure 3.9A and 3.9C. Similarly, Figure 3.9B and 3.9D show the plot of current vs. concentration, between 0.05–5 µM and 6–250 µM, respectively. The current values were obtained by subtracting the background current and are reported as an average of at least three replicate determinations with a standard deviation of less than 3.8% for n = 5. Thus the linear regression equations are:

$$I_p\ (\mu A) = 2.3667\ C + 0.0366\ (0.05 - 5\ \mu M) \quad R^2 = 0.998 \tag{3.5}$$

$$I_p\ (\mu A) = 0.1950\ C + 2.6471\ (6 - 250\ \mu M) \quad R^2 = 0.999 \tag{3.6}$$

Where *C* is the concentration of DCF. The correlation coefficients for the expressions are 0.999. The limit of detection (LOD) = $3S_b/m$, where S_b is the standard deviation for the blank sample and *m* is the slope of the calibration graph. The LOD for the modified electrode is 0.013 µM from the second linear segment (based on S/N = 3), where S_b was evaluated from five blank samples and 0.04 µM is the limit of quantification. The performance of the *f*-MWCNTs /NC/GC sensor towards the quantitative determination of DCF was compared with the previous works with regards to the linear range, LOD and summarized in table 3.1.

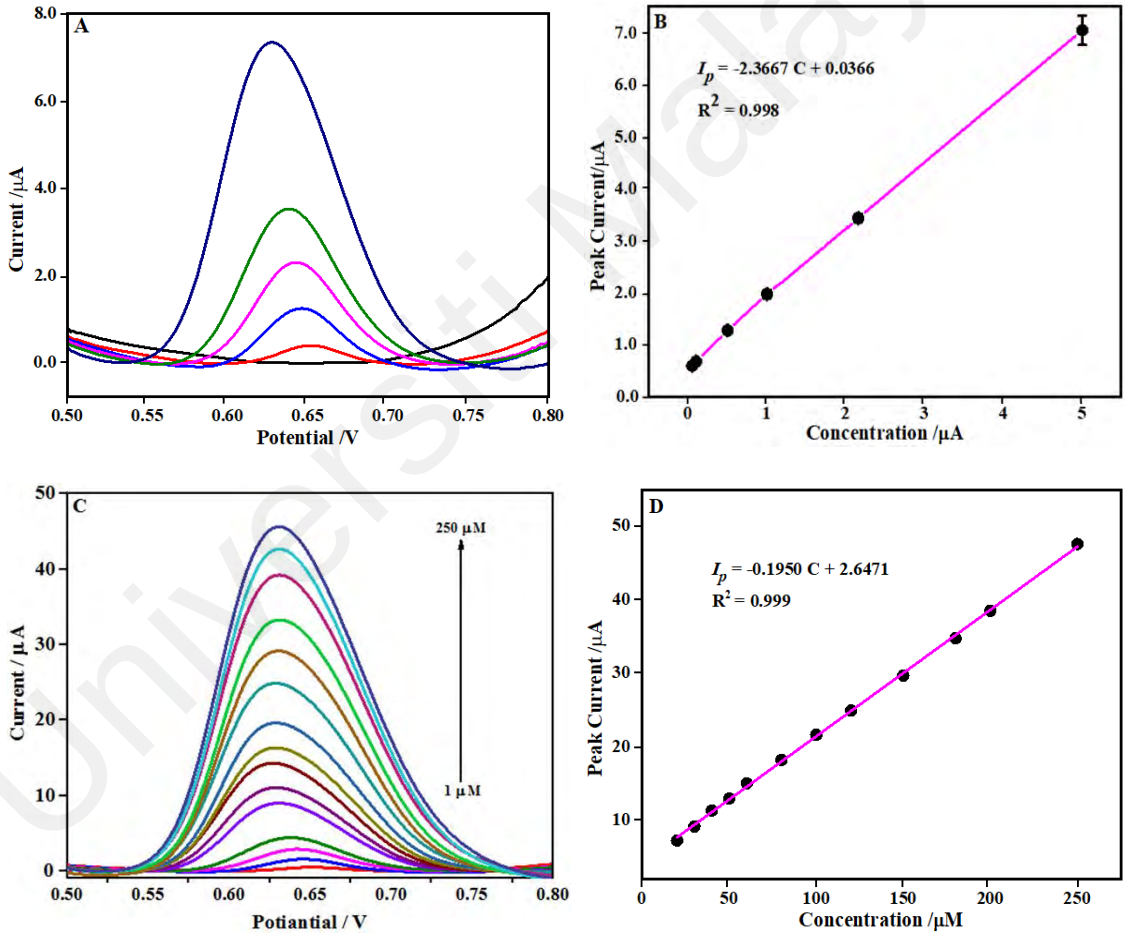

Figure 3.9: (A) DPV response at *f*-MWCNTs /NC/GC electrode in 0.2 M PBS (pH 4.0) with different concentration for DCF between 0.05 µM – 5 µM. (B) Calibration curve (i.e. peak currents vs. DCF concentration) from graph A. (C) DPV response at *f*-MWCNTs /NC/GC electrode in PBS (pH 4.0) containing different concentration for DCF between 0.05 µM – 250 µM. (D) Calibration curve (i.e. peak current vs. DCF concentration) containing different concentration for DCF between 6 µM – 250 µM.

Table 3.1: A comparison of various electrodes for the determination of DCF

Electrode	Linear Range (μM)	Detection limit (μM)	Reference
Cu/CTS/MWCNTs/GCE	0.30– 200.00	0.021	(Shalauddin *et al*., 2017)
AuNPs/MWCNT/GCE	0.03– 200.00	0.02	(Afkhami *et al*., 2016)
IL/MWCNTs paste electrode	0.30– 750.00	0.09	(Goodarzian *et al*., 2014)
Vinylferrocen/MWCNTs paste electrode	5.00– 600.00	2.00	(Mokhtari *et al*., 2012)
MWCNTs and IL-modified carbon ceramic electrode	0.05 – 50.00	0.02	(Sarhangzadeh *et al*., 2013)
MWCNTs/Cu(OH)2 nanoparticles/IL-GCE	0.18– 119.00	0.04	(Arvand *et al*., 2012)
***f*-MWCNTs/NC/GC electrode**	0.05- 250.00	0.01	This work

3.6 Performance and stability of *f*-MWCNTs/NC/GC electrode

3.6.1 Reproducibility and stability

Stability and reproducibility are the two most important factors which signify the feasibility and application of the developed sensor. The stability and reproducibility of the *f*-MWCNTs/NC/GC electrode sensor were investigated by DPV. Five different *f*-MWCNTs/NC/GC electrodes were prepared under the same conditions and tested for the electrochemical detection of 1.5 μM DCF in 0.2 M PBS. A relative standard deviation (RSD) of 4.3% was observed at five different electrodes, which confirms that the *f*-MWCNTs/NC/GC electrode possesses acceptable reproducibility. In addition, one of the five *f*-MWCNTs/NC/GC electrodes was selected for the long-term stability tests over two weeks shown in Figure 3.10. The DPV of the electrode was carried out once a week. When the *f*-MWCNTs/NC/GC electrode was stored in a dry place at ambient temperature (25 °C), the modified electrode retained approximately 96% of the initial peak current value after a week and approximately 90% after two weeks of its initial response. These results indicate that the *f*-MWCNTs/NC/GC electrode has acceptable reproducibility and stability for DCF determination.

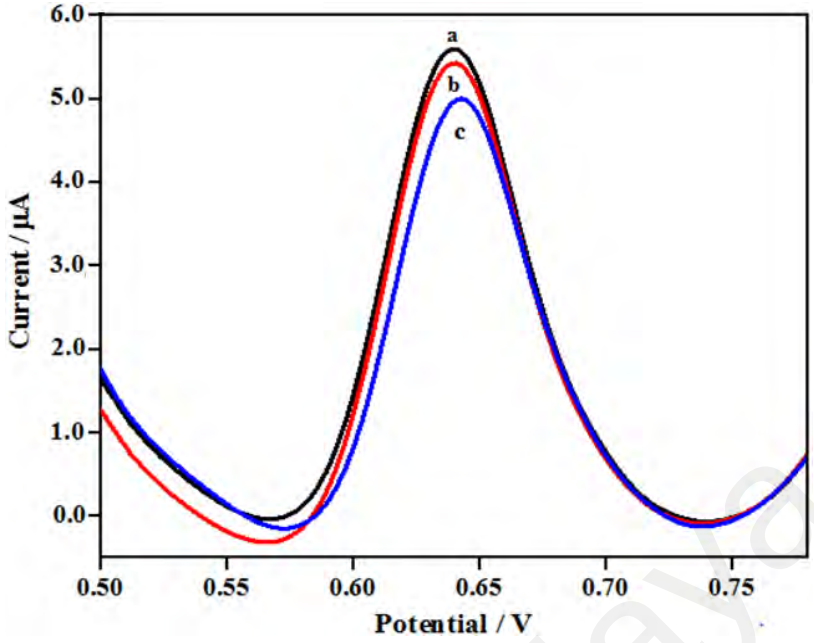

Figure 3.10: DPV signal of 1.5 µM DCF in 0.2M PBS at pH 4, (a) first day; (b) after a week; (c) after two weeks.

3.6.2 Major interferences in DCF determination

The strong affinity of the fabricated sensor towards DCF was confirmed from the voltammetric measurements performed in biological fluids with the presence of common interfering compounds. The selectivity of the fabricated sensor towards the determination of DCF was studied in the presence of interference compounds in 20 µM DCF with 0.2 M PBS. In biological samples, DCF coexists with uric acid (UA), ascorbic acid (AA), dopamine (DA), glucose, sucrose, fructose and lactose. However, no significant response was observed in the presence of 100 folds excess concentration of biological compounds such as UA, glucose, sucrose, fructose and lactose. Figure 3.11 shows that DCF (0.1 mM) has an anodic peak with a good peak separation from DA (0.1 M) and AA (0.1 M). These results reveal that there was no significant interference with the peak current of DCF at the *f*-MWCNTs/NC/GC electrode even with a 100-fold concentration of AA and DA. The *f*-MWCNTs/NC modified sensor is highly selective for the DCF detection in specific applied potential (0.5 to 0.8 Vs^{-1}). Furthermore, in the case of other interfering compounds (UA, glucose, sucrose, fructose and lactose), due to the presence of oxygen moieties on

their outer surface, they are less favourable to oxidize at pH 4.0. Higher pH is required for the oxidation of these interfering molecules. That is why no oxidation peak was observed for other interfering molecules. Therefore, it can be concluded that the fabricated sensor possesses good selectivity for the detection of DCF instead of AA, DA and other interfering compounds.

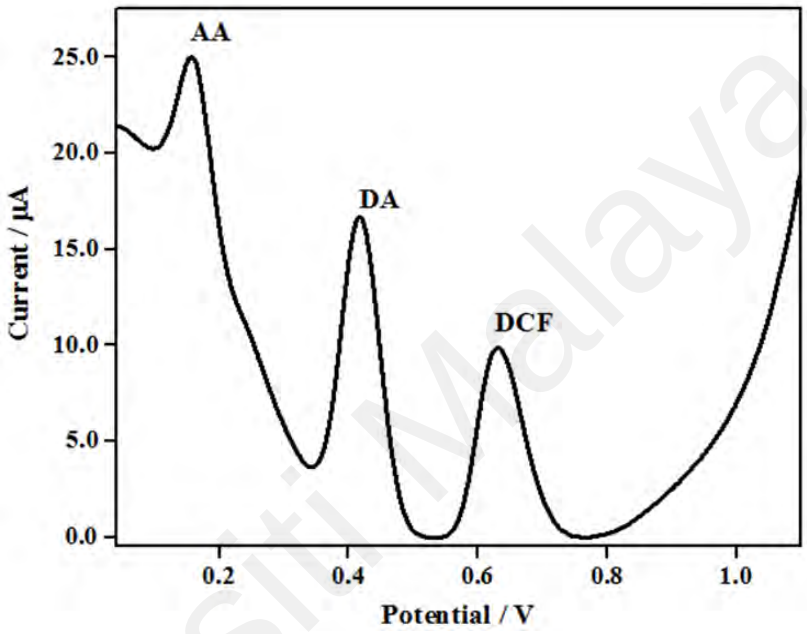

Figure 3.11: DPV on *f*-MWCNTs/NC/GC electrode with 0.1 mM DCF and 100 folds excess concentration of biological compounds such as dopamine (DA), ascorbic acid (AA), uric acid(UA), glucose, sucrose, fructose and lactose, in 0.2 M PBS

3.6.3 Determination of DCF in urine and blood serum samples

The reliability of the proposed *f*-MWCNTs/NC/GC electrode sensor was demonstrated by selecting different concentrations of DCF in a real sample analysis such as DCF tablets, DCF ampoules, human blood serum and urine. The recovery tests of DCF were performed by DPV technique under optimized experimental conditions. In this method, 0.1 mM stock solution prepared from the DCF tablets and ampoules were dissolved in 0.2 M PBS solution.

The recoveries vary in the range of 97.2% to 102% for the DCF tablets and ampoules as illustrated in table 3.2. Similarly, the standard addition method was also utilized for the determination of DCF in human blood serum and urine. The recoveries of DCF in the urine and human blood serum samples were calculated in the range of 98%−104% in table 3.3. The satisfactory recoveries of these DCF tablets and ampoules, human blood serum and urine samples indicate that *f*-MWCNTs/NC/GC electrode shows promising applications for the quantitative detection of DCF in biological fluids and pharmaceutical preparations.

Table 3.2: Determination of Diclofenac sodium in pharmaceutical preparations using differential pulse voltammetry.

Sample	Labeled Amount	Added Amount (μM)	Found (μM)	Recovery (%)	RSD (%)
Table	50 mg	0.50	0.51	102.00	1.15
		1.50	1.49	99.33	0.85
		3.00	3.05	101.60	0.66
Ampoule	75 mg/mL	0.50	0.51	102.00	0.95
		1.50	1.52	101.33	1.27
		3.00	3.03	101.00	1.35

Table 3.3: Concentration of Diclofenac sodium in human urine and serum samples at *f*-MWCNTs/NC/GCE.

Sample	Added (μM)	Found (μM)	Recovery (%)	RSD (%)
Human Urine				
Sample 1	0.50	0.52	104.00	1.75
	1.00	1.03	103.00	1.26
	1.50	1.47	98.00	0.68
Human Serum				
Sample 1	0.50	0.51	102.00	0.84
	1.00	1.01	101.00	1.17
	1.50	1.49	99.33	1.38

4. Conclusions

In this study, a hybrid of nanocellulose and *f*-MWCNTs was fabricated through a facile sonication and drop-casting method and proved to be an effective electrochemical sensor for the detection of diclofenac sodium (DCF). The presence of strong intra and intermolecular hydrogen bonding in the nanocellulose due to the abundance of OH groups is responsible for the increased anchoring sites for the analyte and also provides a distinguishing axial modulus arrangement. In addition, *f*-MWCNTs possess some extraordinary characteristics such as excellent electrochemical response, improved solubility and abundant binding sites for increased adsorption of the analyte. These synergistic effects are the main reasons for the modified GCE to achieve a higher electrochemical response for the electrooxidation of DCF with a wide linear range, better selectivity and sensitivity for DCF detection (Table 3.1). These outcomes demonstrate that the fabricated hybrid nanocomposite is scientifically interesting, practically effective and shows great promise for the determination of DCF from commercial tablets and ampoules, human blood serum and urine samples.

CHAPTER 4: SIMULTANEOUS DETERMINATION OF PARACETAMOL AND NAPROXEN SODIUM BY A NANOCOMPOSITE OF NITROGEN DOPED GRAPHENE AND NANOCELLULOSE MODIFIED WITH SODIUM DODECYL SULFATE IN PHARMACEUTICAL TABLET AND BIOLOGICAL SAMPLE.

4.1 Introduction

The analgesic and antipyretic effects of paracetamol (PCT) (N-acetyl-p-aminophenol, acetaminophen) were first introduced in the 19th century. PCT is one of the most popular, long-established and extensively utilized "over the counter" (OTC) drugs worldwide which is administered for the treatment of fever, pain, headache, backache, neuralgia etc. However, an overdose of PCT triggers the accumulation of toxic metabolites in the human body which are responsible for nephrotoxicity and hepatic necrosis leading to higher mortality and morbidity (Goyal *et al*., 2005).

Naproxen (NPX), [2-(6-methoxynaphthalen-2-yl) propionic acid is a non-steroidal anti-inflammatory drug (NSAID) that is widely used as an OTC analgesic and anti-inflammatory drug. This drug is generally used for the treatment of stiffness caused by kidney stones, rheumatoid arthritis and ankylosing spondylitis (arthritis of the spine) (Tashkhourian *et al*., 2014). The co-administration of PCT and NPX has proven effective for pain relief and is clinically validated. The combined therapy of PCT and NPX is administered to patients who suffer from rheumatic arthritis (Stefano *et al*., 2014). Both of these drugs are extensively used, thus their presence in wastewater is detrimental to the aquatic environments. Therefore, effective and fast detection of these pharmaceutical micropollutants is important in modern healthcare (Chin *et al*., 2014). The molecular structure of PCT and NPX were shown in Figure 4.1.

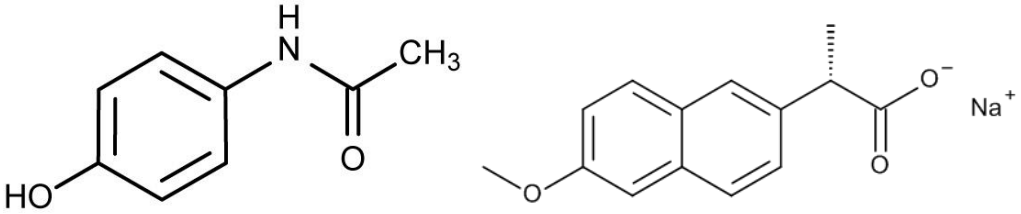

Figure 4.1: Chemical structure of PCT (left) and NPX (right)

The main focus of the present work is the simultaneous detection of PCT and NPX by a simple, facile and effective method of detection. Some of the analytical techniques for the determination of PCT and NPX are spectrophotometry (Panderi & Parissi-Poulou, 1994; Sandulescu et al., 2000), titrimetry (Burgot *et al*., 1997), high-performance liquid chromatography (Lippstone & Sherma, 1995; Ravisankar *et al*., 1998), gas chromatography (De Jong *et al*., 1989; Trettin *et al*., 2011) and capillary electrophoresis (Soini *et al*., 1992; Wu *et al*., 2015). Though these techniques have high sensitivity and selectivity, they require trained personnel and several pretreatment steps, in addition, are expensive as well. On the other hand, electrochemical techniques offer several advantages such as simple fabrication, miniaturization, portability, high sensitivity, high selectivity, rapid response, broad linear range and facile sample preparations (Bahadır & Sezgintürk, 2015; Shi *et al*., 2015).

Cellulose is a natural polysaccharide found abundantly in nature while nanocellulose (NC) is the cellulose in nanoscale dimensions. Recently, NC is produced in large quantities as it possesses improved mechanical and thermal stability, unlike the inherent structural defects present in cellulose. In addition, NC is derived from inexhaustible sources from biomass, cost-effective, biocompatible, eco-friendly, biodegradable etc. As NC possesses strong binding properties with certain nanomaterials, it prevents the leaching of electro-active materials from the electrode surface, thus increases the stability of the sensor (Shalauddin *et al*., 2019). The surface of NC contains

an abundance of OH^- groups which provides an elastic modulus arrangement suitable for the incorporation of other nanomaterials such as graphene (Yan *et al*., 2014) and carbon nanotubes (CNT) (Wang *et al*., 2013).

Nitrogen-doped graphene (NDG) has gathered significant attention in analytical sciences especially in electrochemical sensing. NDG possesses outstanding physicochemical characteristics such as expanded surface area, high catalytic activity, bio-compatibility, high electrical and thermal conductivity. Thus the doping of nitrogen into the graphene lattice enhances the electrocatalytic response for the non-enzymatic electrochemical sensing of analytes (Tajabadi *et al*., 2015; Tajabadi *et al*., 2016). Recently NDG has been used in the fabrication of electrochemical sensors for the detection of pharmaceuticals (Akhter *et al*., 2020b; Anuar *et al*., 2018; Ghadimi *et al*., 2015).

Sodium dodecyl sulphate (SDS) is an anionic surfactant that significantly enhances electrocatalytic performance and prevents the fouling of the electrode surface. Surfactants are generally used to modify the physicochemical characteristics of the electrode/electrolyte interface. The rate of electron transfer across the electrode/electrolyte interface increases with the presence of surfactants due to the lower aggregation and enhanced stability of the electro-active materials on the electrode surface (Zarei & Helli, 2015). Zheng *et al.* (2019) reported a strain sensor based on NC supported graphene dispersed in electrically conducting hydrogels. While Wand *et al.* (2020) reported a nanocomposite of NC-graphene aerogel for supercapacitor applications.

In the present study, a new nanocomposite of (NC-NDG)-SDS for the simultaneous determination of two of the most common painkillers, PCT and NPX, in the presence of diclofenac sodium (DCF) is investigated. This work explores the synergistic effect of NDG and NC for the simultaneous electrochemical detection of PCT and NPX. The inclusion of nanocarbon enhances the electrochemical performance by increasing the

surface area and electrocatalytic performance of the modified electrode. The incorporation of NDG and NC into a nanocomposite is feasible due to the good adhesion and compatibility with each other. The NC interlaces and provides a 3D network embedded with the NDG nanosheets. NC is dispersed and distributed around the NDG nanosheets as the skeleton and binder for the hybrid configuration. The SDS surfactant was introduced to enhance the dispersion of both nanomaterials and to decrease the aggregations. This ensures the successful dispersion and consequently increases the catalytic effect of the NC-NDG nanocomposite which enables a new avenue for the simultaneous electrochemical determination of PCT and NPX. The (NC-NDG)-SDS fabricated sensor showed a broad linear range and low LOD compared to previous reports (shown in Table 4.1). There are no reports on the simultaneous electrochemical determination of PCT and NPX in the presence of DCF using the (NC-NDG)-SDS nanocomposite.

4.2 Experimental methods

4.2.1 Chemicals and reagents

PCT, NPX and DCF (tablet dosage forms), and SDS were purchased from Merck (Malaysia), while graphene oxide, cellulose, K_2HPO_4, KH_2PO_4 were procured from Sigma Aldrich (Malaysia). Adequate amounts were used to prepare the stock solutions of PCT and NPX and kept in a refrigerator. The standard stock solutions of 1 x 10^{-2} M and 1 x10^{-4} M of the PCT and NPX, respectively, were prepared daily when needed. Deionized water (DI) was used as the solvent for all preparations. The phosphate buffer solution (PBS, 0.1 M, pH 7.0) was prepared by mixing K_2HPO_4 (0.662 gm) and KH_2PO_4 (0.844 gm) in DI water.

4.2.2 Instrumentation

Fourier transformed infrared (FTIR) spectroscopy was performed using an FTIR spectrometer (Spectrum 2000, Perkin Elmer) between 500 cm^{-1} and 4000 cm^{-1}. Raman spectroscopy was performed by a Horiba Xplora micro Raman Spectrometer (Japan) with a 532 nm laser source. Atomic force microscopy (AFM) was performed by AFM 5000II Hitachi (Japan) while transmission electron microscopy (TEM) was performed by Philips CH 200 LaB6-Cathode 160kV. Electrochemical experiments were performed by an Autolab PGSTAT 302N potentiostat/galvanostat (Metrohm, Netherlands) in a three-electrode electrochemical cell. A platinum wire was the counter electrode and an Ag/AgCl (3.0 M KCl) was the reference electrode.

4.2.3 Methodology

For the synthesis of (NC-NDG)-SDS/GCE nanocomposite, NC was synthesized followed by acid hydrolysis method while the NDG was synthesized by the microwave-assisted method. The GCE was fabricated by the drop-casting technique. The morphological properties were characterized by TEM, AFM, FTIR and Raman spectroscopy. Before the electrochemical experiments, pH and scan rate were optimized. CV and DPV methods were employed to investigate the electrochemical behaviour of the NC-PPY/GCE sensor. Satisfactory relative standard deviation and recovery values were obtained from the real sample analysis.

4.2.4 Synthesis of NC

The synthesis procedure of nanocellulose was explained in chapter 3, section 3.2.6.

4.2.5 Synthesis of NDG

Graphene oxide (GO) was the precursor for the synthesis of NDG and the synthesis is described by (Akhter *et al*., 2018). Initially, GO was synthesized from the Hummers method (Sookhakian *et al*., 2014). A 0.2 mg mL^{-1} of graphitic oxide suspension was ultra-sonicated for 30 min and a yellow-brown solution was obtained. Then 0.8 mL of hydrazine solution and 30 mL of GO suspension were mixed to initiate the chemical reduction via irradiation in a microwave oven for 5 min. Finally, a stable black colour suspension containing NDG sheets was obtained. The NDG suspension was centrifuged, collected and dried at 50 °C in an oven.

4.2.6 Preparation of (NC-NDG)-SDS/GCE modified electrode

Before the surface modification of the working electrode, the glassy carbon electrode (GCE) surface was polished with alumina slurry on a microcloth (Buehler) pad. The GCE was ultra-sonicated for 2 min in ethanol and followed by DI water. Initially, 1 mg of NDG and NC powders were dispersed separately in 2.5 mL DI water and ultra-sonicated for 30 min. Then, both NDG and NC solutions were mixed and sonicated again for another 30 min. Then 4.0 µL 1.0 mM SDS solution was added into the NC-NDG dispersion and ultra-sonicated for 15 min to form a uniform suspension with a final concentration of 4 µM of SDS. Finally, 7.5 µL of the suspension was drop-casted onto the surface of GCE and dried at room temperature (fabrication step shows in Figure 4.2).

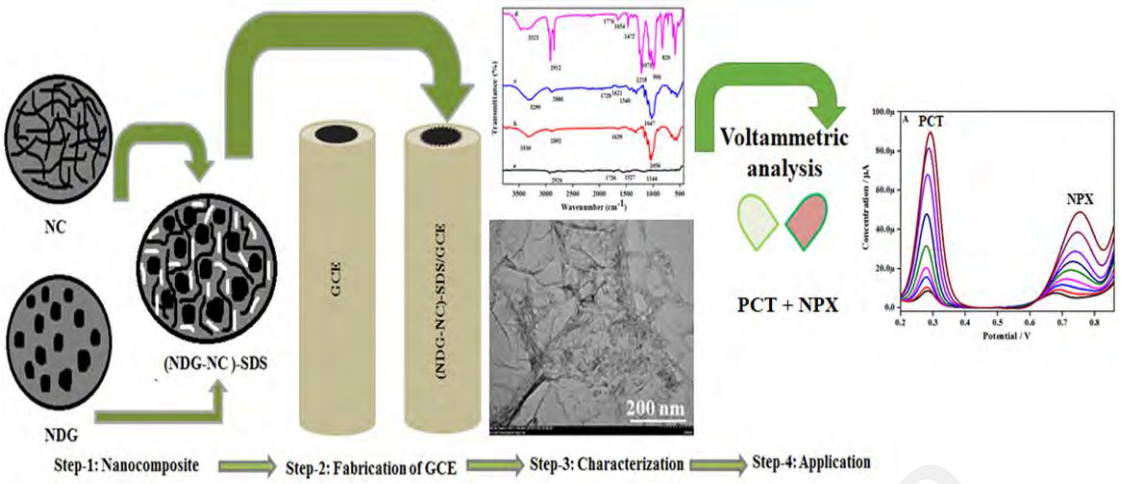

Figure 4.2: Fabrication of (NC-NDG)-SDS modified GC electrode for simultaneous detection of paracetamol and naproxen

4.2.7 Preparation of real samples

Four PCT (500 mg each) and NPX (500 mg each) tablets were selected and homogenously ground into powders by a mortar and pestle. Then the powders were weighed and dissolved in an ethanol-water mixture and filtered through a Whatman filter paper. The clear solution was then collected in a beaker and used as the stock solution. The blood collection procedure was mentioned in (section 3.2.8). The prepared sensor was utilized for the simultaneous determination of PCT and NPX in a blood serum sample from a healthy volunteer who was prescribed 500 mg PCT and 250 mg NPX tablets daily. The blood was taken from the patient at a 6 hrs interval. To prepare the blood serum sample, the blood serum sample was centrifuged and diluted to 40 mL by PBS (pH 7.0). Then 15 mL was pipetted from the stock solution and added into the electrochemical cell, followed by the addition of PCT and NPX.

4.3 Aim of the research

The study aims to fabricate a new modified sensor based on NC, NDG and anionic SDS. With the synergistic effects of NC and NDG, the proper dispersion of the nanomaterials is achieved by a certain concentration of SDS and is expected to improve

the properties of the nanocomposite and showed excellent electrochemical sensing performance for the simultaneous determination of PCT and NPX.

4.4 Results and discussions

4.4.1 Morphological properties of (NC-NDG)-SDS sensor

TEM was performed to investigate the surface morphology of the NDG/GCE (A), NC/GCE (B) and NC-NDG /GCE (C) and (NC-NDG)-SDS/GCE (D) working electrodes. Figure 4.3A is the TEM image of NDG which shows the ultrathin nanosheets of graphene with a high surface to volume ratio and retains the two-dimensional structure of graphene even after nitrogen doping. Figure 4.3B shows that the NC is present as nanofibers of 4 to 10 nm of average diameter and 20 to 80 nm of average length, while Figure 4.3C shows that the morphology of the NC-NDG nanocomposite consists of several NDG and NC layers adhered together. Few aggregations are visible on the surface of the nanocomposite which consists of the non-dispersed NC. The non-dispersed NC decreases the electrical conductivity and destabilizes the nanocomposite by disintegration. However, in the presence of SDS (Figure 4.3D), the NC are well dispersed and evenly distributed around the NDG nanosheets without any aggregation. As SDS is an anionic surfactant and a dispersive agent, the amphiphilic property of SDS facilitates the dispersion and promotes the synergistic effect between the NDG and NC.

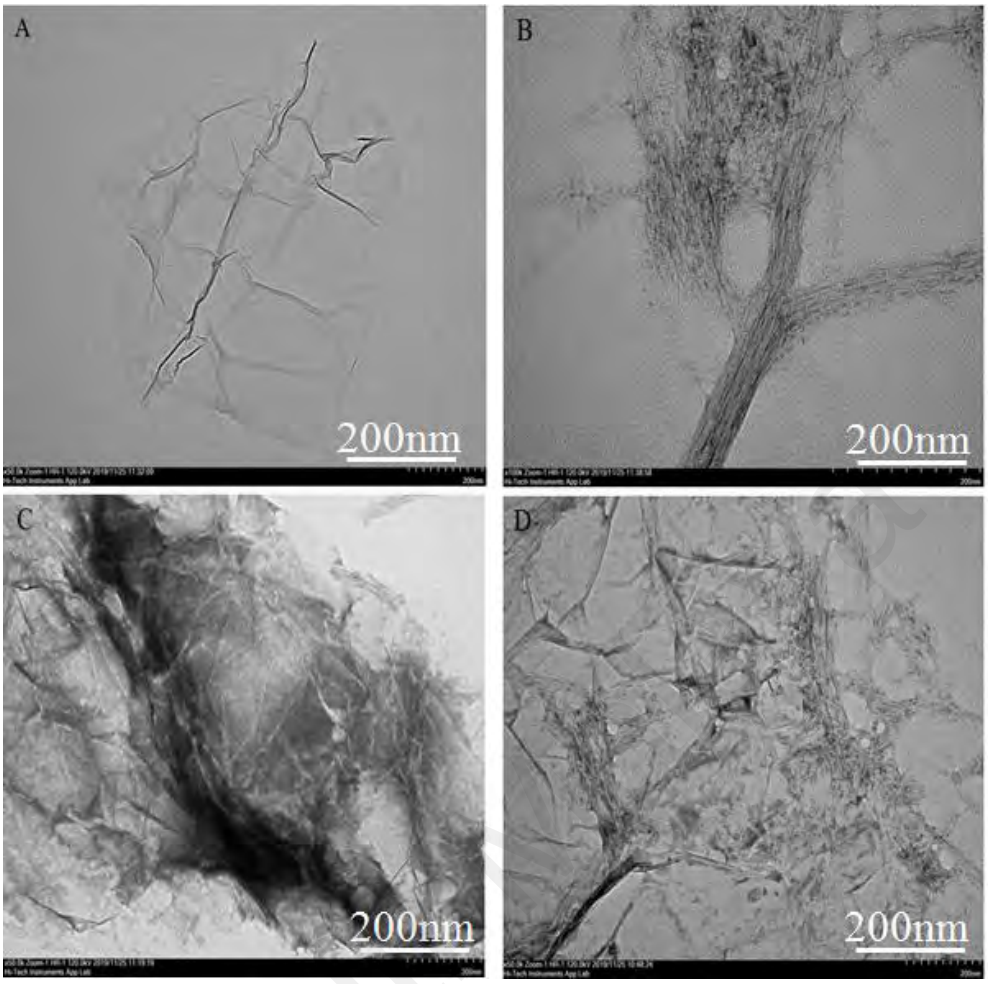

Figure 4.3: TEM images of NDG (a), NC (b), NC-NDG (c) and (NC-NDG)-SDS (d)

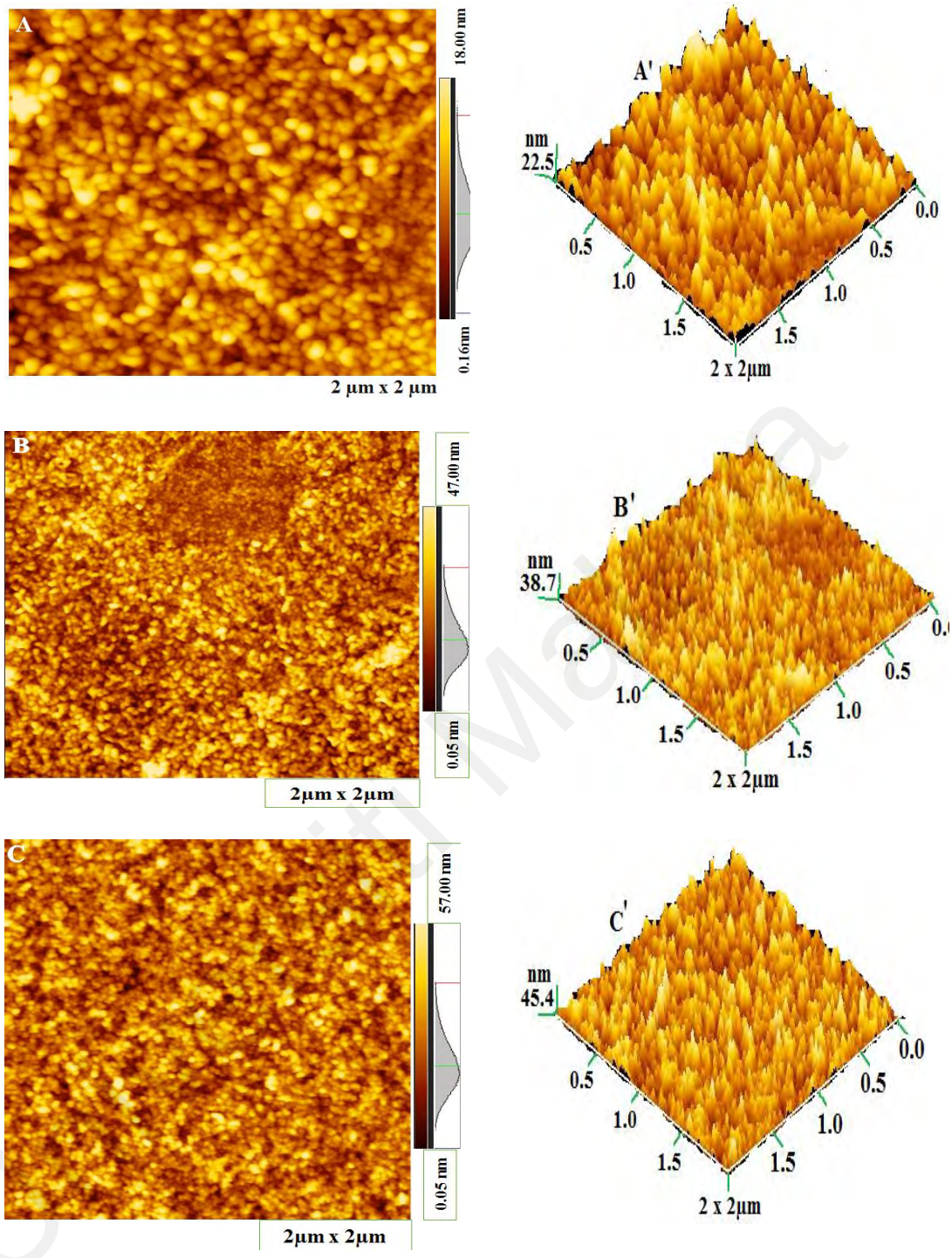

Figure 4.4: Atomic force microscopic (AFM) image of NC (A), NC-NDG(B), and (NC-NDG)-SDS (C)

Atomic force microscopy (AFM) is an effective method to obtain information about the surface of the nanocomposite where a topographic map is drawn from the information, connected through a computer. The AFM image of NC (A), NC-NDG (B) and (NC-NDG)-SDS (C) are shown in Figure 4.4 with 2µm × 2 µm topology. Figure 4.4(A) shows a homogeneous dispersion of NC with average diameters around 5.5 nm

and average lengths between 56.4 nm. Figure 4.4(B) is the AFM image of NC-NDG, where the sheets of NDG are dispersed and aggregated on the layer of NC in a random pattern. The AFM result indicates that the height of the sample increases from 18 nm to 47 nm in the NC-NDG compared to the NC sample confirming the modification occurs in the surface of NC-NDG morphology. The 3D image confirms the increase in porosity and the NDG sheets on the NC layers are approximately 7-13 nm. Figure 4.4(C) is the AFM image of (NC-NDG)-SDS nanocomposite, where the sheets of NDG are distributed homogeneously on the NC layer in the presence of the SDS surfactant. The 3D image reveals that the surface roughness increases while sample height further increases from 47 nm to 57 nm compared to the NC-NDG nanocomposite. This indicates that the presence of anionic surfactant SDS facilitates the dispersion and reduces the aggregation of both nanomaterials and enhances the porosity, electroconductivity, catalytic efficiency and response of the sensor.

4.4.2 Structural characterizations

Figure 4.5 shows the FTIR spectra of NDG (a), NC (b), NC-NDG (c) and (NC-NDG)-SDS (d). Curve (a) is the FTIR spectrum of NDG which shows the characteristic stretching vibrations of C-N and C=N, at around 1144cm^{-1} and 1527 cm^{-1}, respectively. Another peak is observed at around 1736 cm^{-1} which corresponds to the C=O stretch (Pan *et al*., 2015). Curve (b) is the FTIR spectrum of NC which clearly shows a high density of OH^- groups. After the chemical treatment, the peaks between 1648 cm^{-1} and 1638 cm^{-1} is attributed to the OH^- stretching of absorbed water. The C-O-C stretch which corresponds to the pyranose ring appears at around 1056 cm^{-1}. The decline of the C-O-C stretch of the glycosidic band at 1100 cm^{-1} and the C=C stretch of the polysaccharide at 1150 cm^{-1} is due to the acid hydrolysis treatment and shrinkage of the molecular weight (Shalauddin *et al*., 2019). The characteristic peaks for NDG are present in the curve (c).

The peaks of C=O and C=N stretch for NDG appear at around 1728 cm^{-1} and 1540 cm^{-1}, respectively, which are slightly shifted compared to the curve (a). The characteristic peak of the C-O-C stretch in NC occurs at 1047 cm^{-1} and 1621 cm^{-1} (c) which confirms the successful deposition of NDG and NC. The FTIR spectrum (d) shows additional peaks due to the presence of SDS at around 1100 cm^{-1} to 1300 cm^{-1}, attributed to the stretching vibration of the C-O and –S=O, respectively (Bhardwaj *et al*., 2014). This result concludes that both NDG and NC are present along with the SDS.

Raman spectroscopy is an effective technique for the investigation of disorder in carbonaceous compounds. The defect is represented as the ratio of I_d and I_g. Figure 4.5 B is the Raman spectrum of NDG, which shows the presence of the D and G bands. For the NDG (B), the D band occurs at around 1472 cm^{-1} while the G band at around 1580 cm^{-1}. The I_D/I_G ratio increases from 1.10 (GO) to 1.15 (NDG) from the synthesis using the GO precursor. This increment is due to the loss of the oxygen functional groups and the doping of nitrogen heteroatoms in the graphene lattice (Lin *et al*., 2010; Wei *et al*., 2009). Figure 4.5C is the Raman spectrum of NC, where the D band appears at around 1095 cm^{-1} while the G band at around 1345 cm^{-1}. The 2D band at around 2909 cm^{-1} corresponds to the C-H and O-H stretching. The bands less than 1600 cm^{-1} and more than 2700 cm^{-1} are indicators for the presence of the cellulosic backbone and hydroxyl groups. Due to the high crystallinity of NC, the intensity of the D, G and 2D bands of NC are greater compared to cellulose (Shalauddin *et al*., 2019). Figure 4.5D is the Raman spectroscopy of (NC-NDG)-SDS which shows the characteristic peaks for NDG and NC. The peaks are slightly shifted while the peak heights are reduced. The peak height of the 2D band is larger than the G band due to the presence of graphene. Smaller peaks are observed at less than 900 cm^{-1} attributed to the presence of SDS in the nanocomposite (Somasundaran *et al*., 1989).

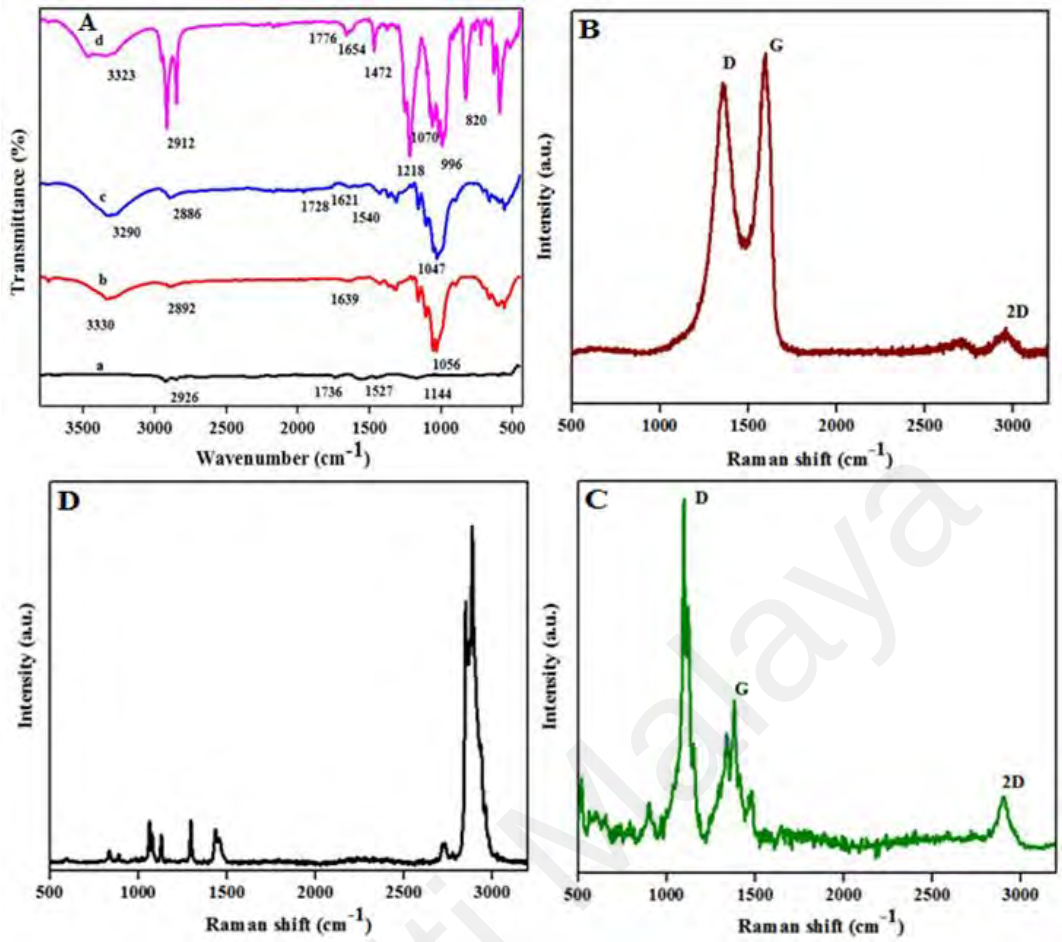

Figure 4.5: (A) FTIR spectra of NDG (a) NC (b), NC-NDG (c) and (NC-NDG)-SDS (d). Raman spectra of NDG (B), NC (C), (NC-NDG)-SDS (D).

4.5 Electrochemical characterization of (NC-NDG)-SDS sensor

Electrochemical impedance spectroscopy (Figure 4.6A) was performed to investigate the electron transfer kinetics across the electrode/electrolyte interface. The Nyquist plots (Figure 4.6A) of the bare GCE (a), GCE/NC (b), GCE/NDG (c), GCE/NC-NDG (d) and GCE/(NC-NDG)-SDS (e) were performed in the presence of 5 mM $[Fe(CN)_6]^{3-/4-}$ in 0.1 M KCl and the experimental data were fitted with the equivalent circuit model. The R_{ct} is the charge transfer resistance, Zw is the Warburg impedance, R_s is the solution resistance, R_p is electron transfer resistance and CPE is the constant phase element. The fitting of the experimental data with the circuit model gives an R_{ct} value of 415 Ω (curve a) of the bare GCE. When the GCE is modified with NC and NDG

separately, the R_{ct} declines to 285 Ω (curve b) and 135 Ω (curve c), respectively. A smaller R_{ct} value of 65 Ω (curve d) is observed for the GCE modified with the NDG-NC nanocomposite, which confirms the successful attachment of NC on the NDG nanosheets. Since NDG has high electrical conductivity while NC has good binding property, the synergistic combination of both nanomaterials provides a smaller R_{ct} value. The smallest R_{ct} value of 45 Ω (curve e) is achieved when SDS is introduced into the NDG-NC nanocomposite. This is due to the presence of SDS as an anionic surfactant that modifies the electrode/electrolyte interface to produce a faster electron transfer process. The highest electron transfer rate with the smallest R_{ct} value is attributed to the effect of SDS which is due to the efficient dispersion of both nanomaterials, producing a synergistic effect on the NC-NDG nanocomposite.

The electroactive surface area was calculated from the peak currents of the fabricated electrodes (Figure 4.6B) using the Randles-Sevcik equation (Rawool & Srivastava, 2019). The calculated electroactive surface area of the bare GCE (a), GCE/NC (b), GCE/NDG (c), GCE/NC-NDG (d) and GCE/(NC-NDG)-SDS (e) is 0.065 cm^2 (a), 0.083 cm^2 (b), 0.087 cm^2 (c),0.108 cm^2 (d) and 0.112 cm^2 (e), respectively. Thus it is confirmed that the GCE/(NC-NDG)-SDS nanocomposite possesses the largest electroactive surface area compared to the other electrodes which are attributed to the presence of SDS. This confirms the role of the SDS surfactant in increasing the dispersion of the electrode materials on the electrode surface by providing a larger surface area with increased peak currents.

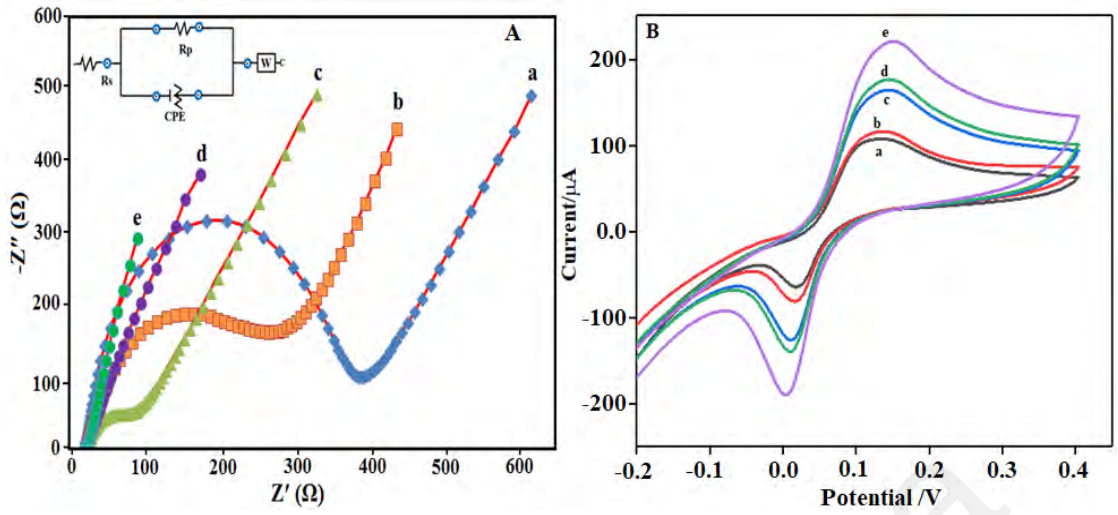

Figure 4.6: (A) The Nyquist plots of bare GCE (a), NC/GCE (b), NDG/GCE (c), NC-NDG /GCE (d) and (NC-NDG)-SDS/GCE (e) in 0.1 M KCl solution with 5.0 mM $[Fe(CN)_6]^{3-/4-}$. Inset is the equivalent circuit for the fitting. (B) CVs response of GCE (a), NC/GCE (b), NDG/GCE (c), NC-NDG/GCE (d) and (NC-NDG)-SDS/GCE (e) in 0.1 M KCl solution with 5.0 mM $[Fe(CN)_6]^{3-/4-}$ at scan rate 0.1 Vs^{-1}

4.6 Electrochemical investigation of PCT and NPX at (NC-NDG)-SDS/GCE modified electrode

4.6.1 Electrochemical behaviour of PCT and NPX

The electrochemical reaction of PCT and NPX was investigated on the bare GCE (a), NC/GCE (b), NDG/GCE (c), NC-NDG/GCE (d) and (NC-NDG)-SDS/GCE (e) by cyclic voltammetry (CV) in 0.1 M PBS (pH 7.0) at 0.1 V s^{-1}. Figure 4.7 presents the CVs for the simultaneous detection of PCT and NPX where the PCT shows a redox behaviour while NPX shows an oxidation peak. In the inset of Figure 4.7, the bare GCE does not show any reduction peak in the presence of PCT and NPX, but two weak oxidation peaks are observed at 0.42 V and 0.91 V (curve a). However, the NC/GCE and NDG/GCE modified electrodes (curve b and c, respectively) showed better electrochemical performance compared to the bare GCE. Clear oxidation and reduction peaks of PCT are observed at 0.28 V and 0.33 V (curve c), with peak currents of 3.12 µA and 4.10 µA, respectively. The NPX shows oxidation peaks at 0.80 V (curve b) and 0.79 V (curve c)

with oxidation peak currents of 8.12 μA and 12.44 μA, respectively. From these results, the GCE modified with the single components of NDG and NC did not produce the highest oxidation and reduction peak currents. In contrast, the GCE modified with the NC-NDG nanocomposite shows a distinguished redox peak for PCT and an oxidation peak for NPX (curve d). However, the GCE modified with the (NC-NDG)-SDS (curve e) shows the highest peak currents for both PCT and NPX. This is attributed to the synergistic effect of NDG and NC in the presence of the SDS. The NC is easily inserted between the NDG sheets and prevents the restacking of the graphene sheets. This ultimately expands the active surface area by increasing the basal spacing. The 3D network of NC-NDG enhances the transfer of electrons, thus increasing the electrical conductivity and electrocatalytic activity. The (NC-NDG)-SDS/GCE modified electrode shows the highest peak currents for the PCT and NPX due to the incorporation of SDS into the NDG-NC nanocomposite without a significant shift in the peak potential. With the presence of SDS in the NC-NDG nanocomposite, the sulfonic group of the SDS orientates itself towards the NC-NDG and further expands the nanocomposite. This accounts for the highest peak currents for the PCT and NPX at the (NC-NDG)-SDS nanocomposite. Thus the (NC-NDG)-SDS was selected for further experiments.

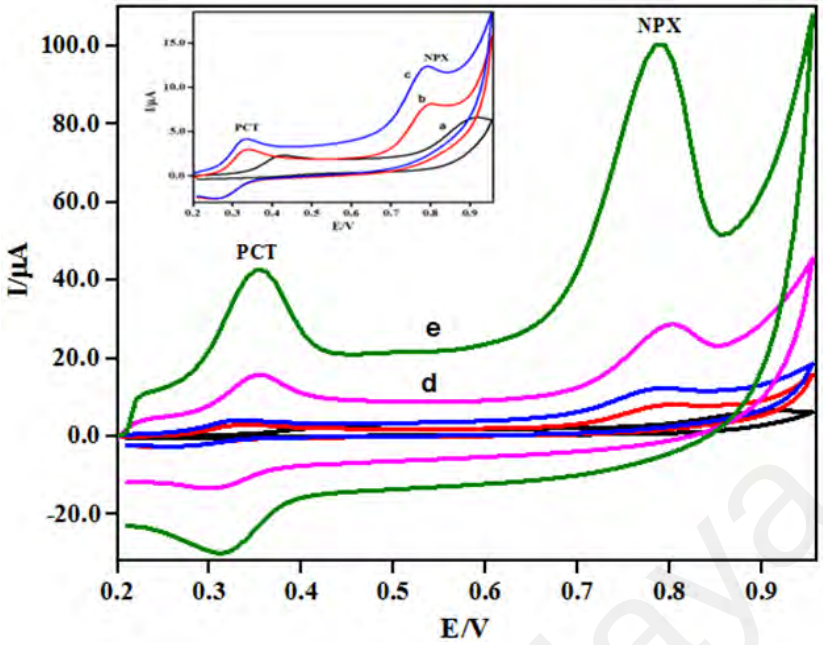

Figure 4.7: CVs of 40 μM PCT and 80 μM NPX in 0.1 MPBS (pH 7.0) at 0.1 Vs^{-1} (inset on (a) bare GCE, (b) NC/GCE and (c) NDG/GCE), NC-NDG/GCE (d) and (NC-NDG)-SDS/GCE (e)

4.6.2 Scan rate study

The influence of the scan rate on the anodic and cathodic current response of PCT and NPX at the (NC-NDG)-SDS/GCE was evaluated at different scan rates (10-400 mV s^{-1}) in PBS solution (pH 7.0) as shown in Figure 4.8. From Figure 4.8B and 4.8C, it can be observed that the redox peak current and oxidation peak current increases linearly with the scan rate for the PCT and NPX, respectively. This shows that the electrochemical reaction of PCT and NPX on the (NC-NDG)-SDS modified GCE is a surface adsorption-controlled process. The linear regression equations (Figure 4.8B, 4.8C) are expressed as follows:

$$I_{pa}\,(\text{PCT}) = 0.611\upsilon + 2.132\ (R^2 = 0.996) \quad (4.1)$$

$$I_{pc}\,(\text{PCT}) = -0.824\upsilon + 2.714\ (R^2 = 0.997) \quad (4.2)$$

$$I_{pa}\,(\text{NPX}) = 0.124\upsilon + 9.406\ (R^2 = 0.998) \quad (4.3)$$

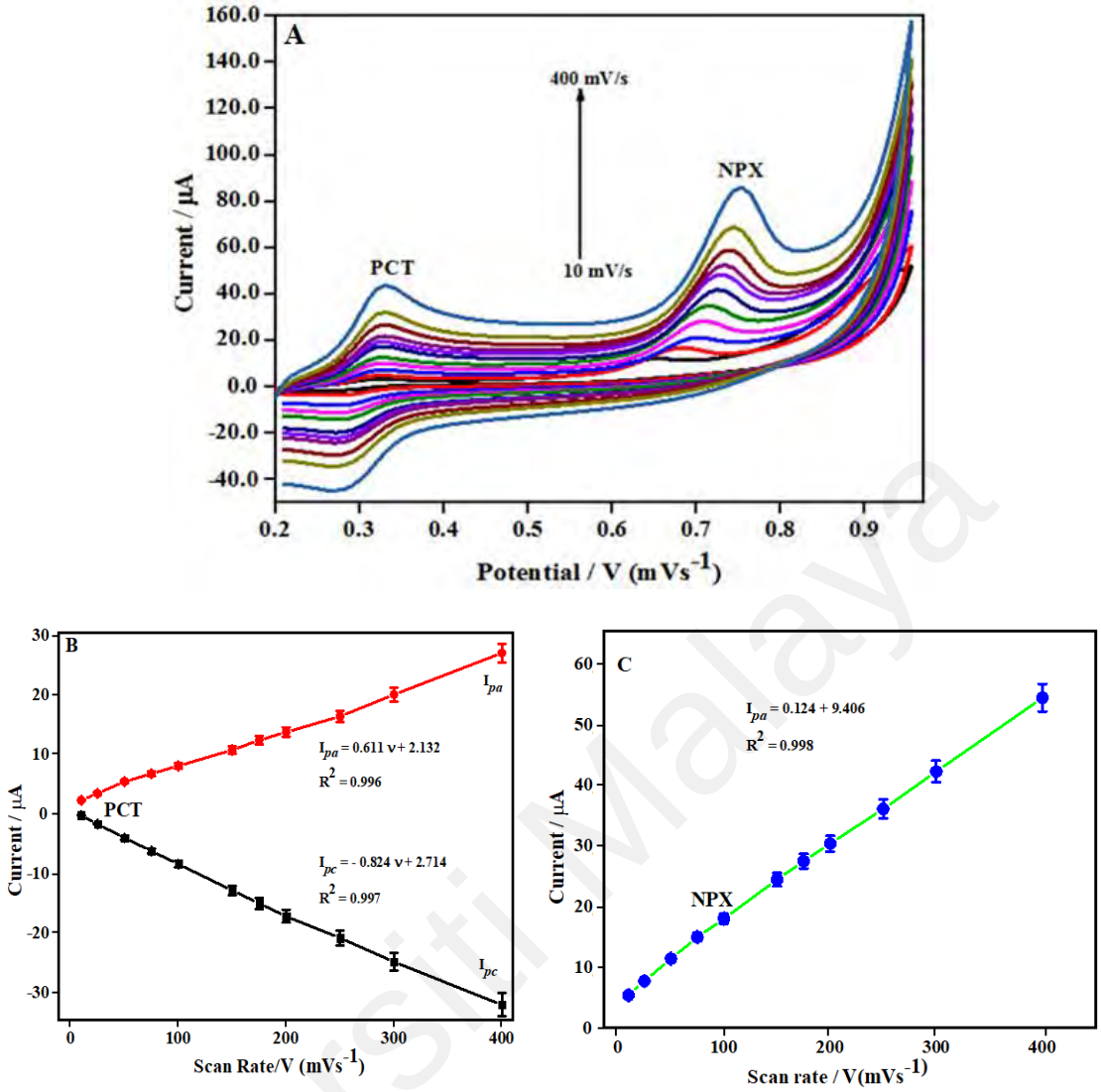

Figure 4.8: CVs of 40 µM PCT and 80 µM NPX on (NC-NDG)-SDS/GCE at 10 mV s^{-1} to 400 mV s^{-1} in 0.1 M PBS (pH 7.0). (B) The plot of redox peak current vs. scan rates of PCT. (C) The relationship between anodic peak current vs. scan rate of NPX

4.6.3 Influence of pH

The influence of pH on the current response of PCT and NPX on the (NC-NDG)-SDS modified electrode was investigated by CV between pH 5 and pH 9 in 0.1 M PBS at 0.1 V s^{-1} as shown in Figure 4.9. The highest anodic peak currents (I_{pa}) for PCT and NPX are at pH 7.0 as shown in Figure 4.10 (C, D), thus pH 7.0 was selected as the optimum pH for the electrochemical experiments. The anodic peak potentials of PCT and NPX are shifted to the negative region with increasing pH from 5.0 to 9.0 (Figure 4.10 A, B). The

anodic peak potential of PCT is shifted from 0.48 V to 0.24 V, while the shift for NPX is from 0.88 V to 0.78 V. This confirms the involvement of protons in the oxidation of PCT and NPX (Akhter *et al*., 2018; Tashkhourian *et al*., 2014). The relationship of the peak potential with the solution pH of PCT and NPX was also investigated. The linear regression equations for the oxidation peak potentials of PCT and NPX (Figure 4.10A, B) are (eq. 4.4 and eq. 4.5, respectively):

$$Ep\ (PCT) = -0.060\ pH + 0.784\ (R^2 = 0.997) \quad (4.4)$$

$$Ep\ (NPX) = -0.054\ pH + 1.024\ (R^2 = 0.995) \quad (4.5)$$

The slope values from the regression equations are 0.060 pH^{-1} and 0.054 pH^{-1} for PCT and NPX, respectively. These slope values are very close to the theoretical value of 0.059/n V from the Nernst equation, which demonstrates that the equal number of electrons and protons participate in the redox reaction of PCT (n = 2) and the oxidation reaction of NPX (n = 1), shown in Appendix 4.1 (Akhter et al., 2018; Soltani *et al*., 2018).

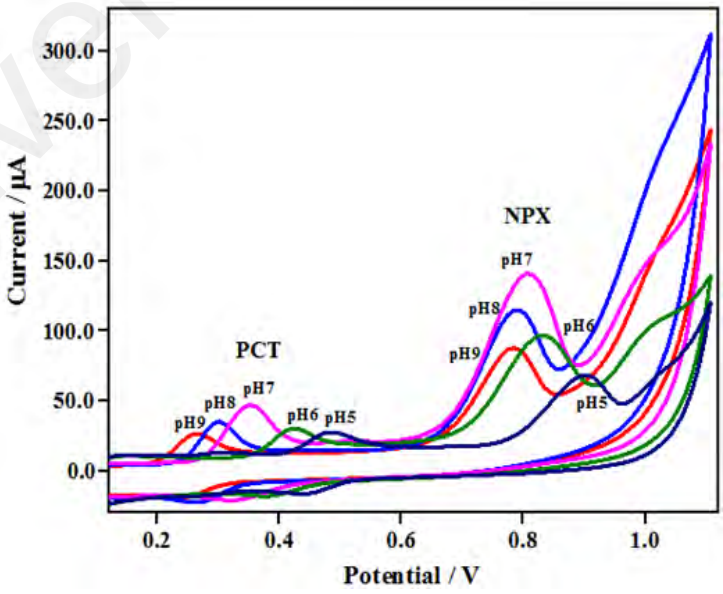

Figure 4.9: The CVs of 40 µM PCT and 80 µM NPX at the (NC-NDG)-SDS at different pH: 5.0, 6.0, 7.0, 8.0 and 9.0 at 0.1 V s^{-1}

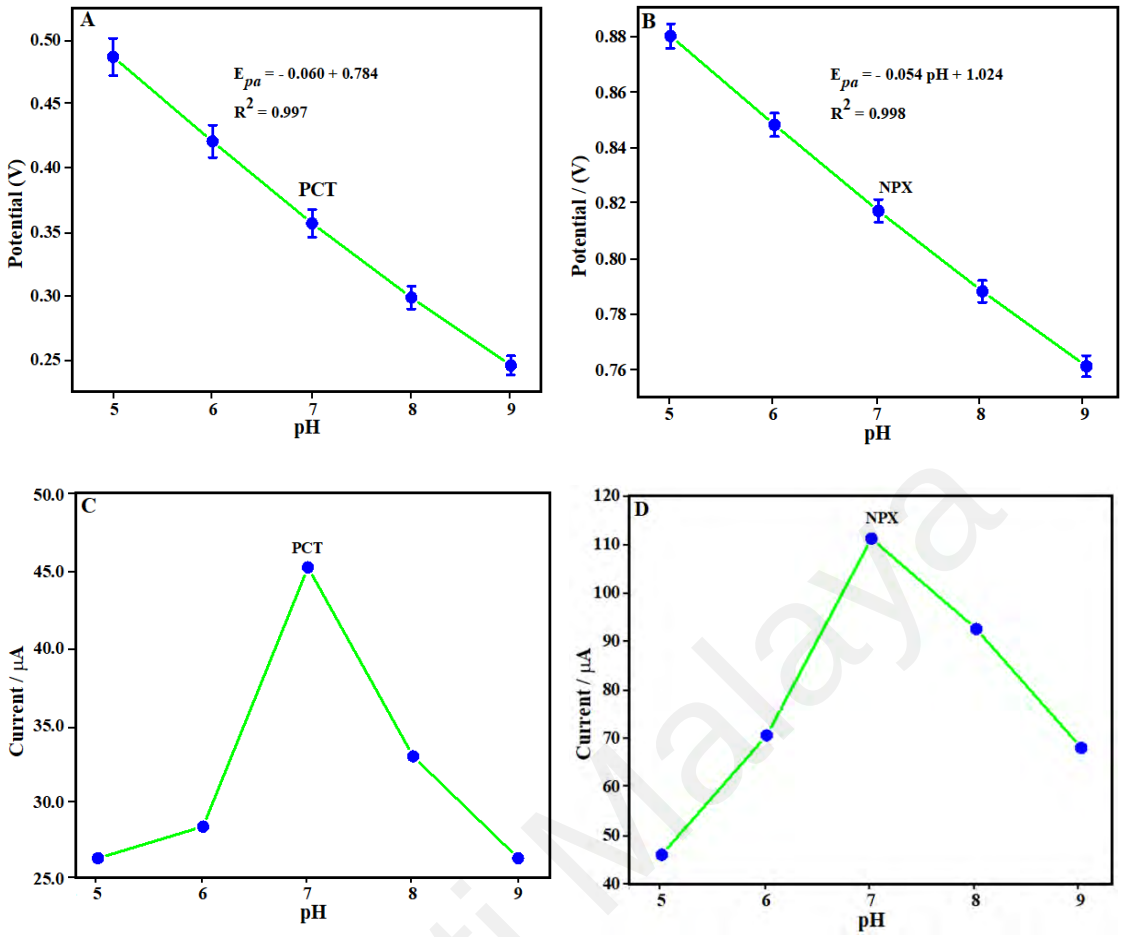

Figure 4.10: (A) The plot of oxidation peak potential vs. pH of PCT. (B) The plot of oxidation peak potential vs. pH of NPX. (C) The plot of the oxidation peak current vs. pH of PCT. (D) The plot of the oxidation peak current vs. pH of NPX

4.7 Analytical application of the (NC-NDG)-SDS sensor

4.7.1 Analysis of detection limit of sensor

Differential pulse voltammetry (DPV) is a more sensitive technique compared to CV and is generally used to investigate the linear dynamic range, sensitivity and limit of detection (LOD) of the fabricated sensor. DPV was used to evaluate the (NC-NDG)-SDS modified electrode for the simultaneous detection of PCT and NPX in 0.1 M PBS (pH 7.0) at 0.1 V s^{-1}. Figure 4.11A shows the DPV results from the electrochemical oxidation of various concentrations of PCT and NPX under optimized conditions. The oxidation peak currents of PCT and NPX increase linearly with the concentration from 0.01 to 90

μM and 0.1 to 60 μM for PCT and NPX, respectively, as shown in Figure 4.12 (A, B). The calibration plot of the anodic peak current against the concentration of PCT and NPX are presented in Figure 4.12 (A, B). The calibration equations for the PCT (Eq. 4.6) and NPX (Eq. 4.7) are:

$$I_p\,(\mu A) = 0.869\ C\ (\mu M) + 10.456\ (R^2 = 0.999) \quad (4.6)$$

$$I_p\,(\mu A) = 0.634\ C\ (\mu M) + 7.356\ (R^2 = 0.999) \quad (4.7)$$

The limit of detection (LOD) for PCT and NPX is 0.0035 μM and 0.026 μM, respectively. The results show that the simultaneous detection of PCT and NPX by DPV is achievable using the modified electrode and resembles the solitary detection of PCT and NPX as illustrated in table 4.1. It can be concluded that the two analytes do not interfere with each other in these concentration ranges. Previous studies have reported the detection of solitary analytes of PCT and NPX at different modified electrodes (Adhoum *et al*., 2003; Madrakian *et al*., 2014; Si *et al*., 2014; Tashkhourian *et al*., 2014). However, there are still no reports on the simultaneous detection of PCT and NPX analytes at the same modified electrodes. This newly developed sensor shows remarkable electrochemical performance for the simultaneous detection of PCT and NPX with low LOD, wide concentration ranges and high sensitivity. The remarkable sensing performance of this newly designed electrochemical sensor is due to the excellent catalytic activity and expanded surface area of NDG and NC, along with the effect of the anionic surfactant SDS, which increases the performance of the modified electrode for the simultaneous detection of PCT and NPX.

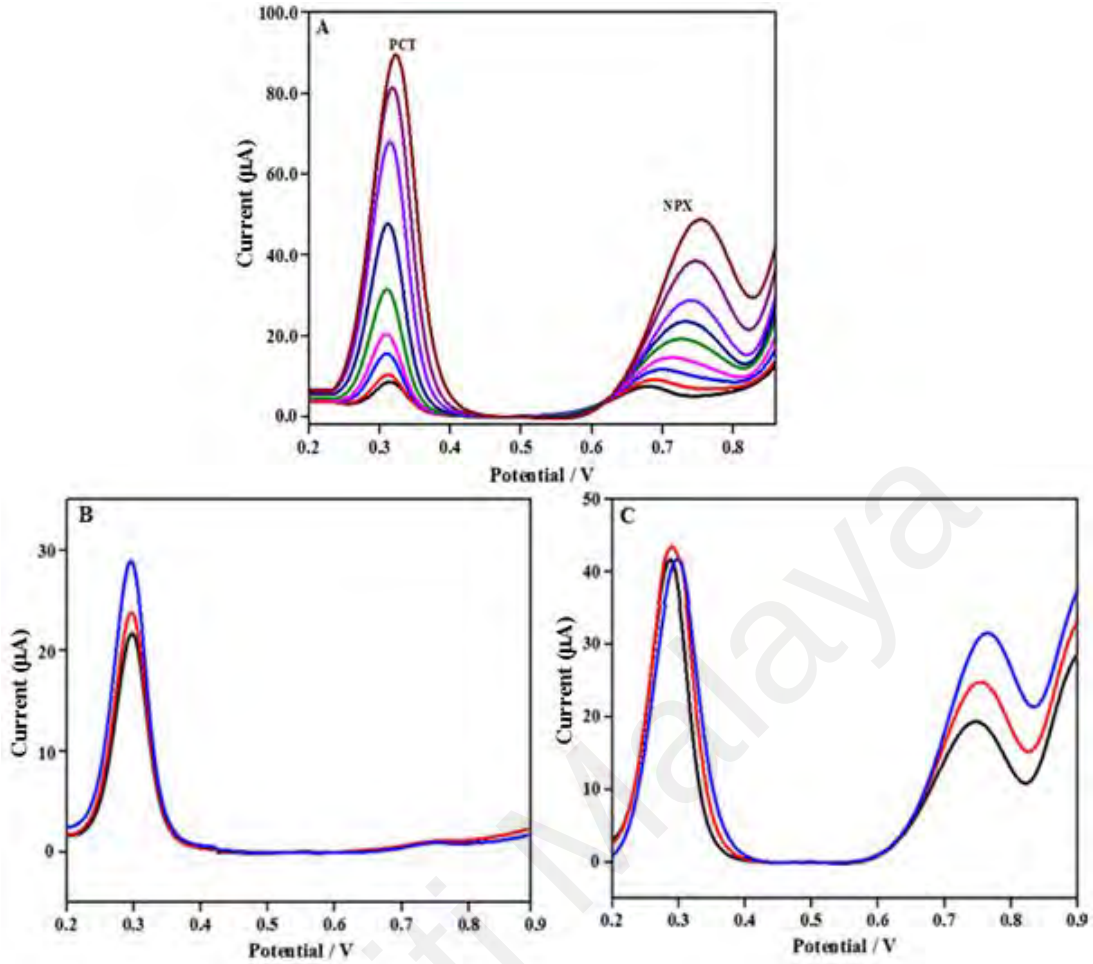

Figure 4.11: (A) DPV at (NC-NDG)-SDS at different concentrations of PCT (0.01–90 µM) and NPX (0.1–60 µM) in 0.1 M PBS (pH 7.0) at 0.1 V s^{-1}.(B) PCT concentrations of 10, 11 and 25 µM at a fixed concentration of NPX (0.5 µM). (C) NPX concentration of 15, 20, 30 µM at a fixed concentration of PCT (40 µM).

The DPV of the combined solution of PCT and NPX at the (NC-NDG)-SDS/GCE is shown in Figure 4.11 (B, C). Here, the concentration of one analyte was varied while the other was held constant. Figure 4.11B shows three well-defined peaks of PCT at 10, 11 and 25 µM, respectively, while the peak of NPX remained unchanged at 0.5 µM. Similarly, Figure 4.11C shows three well-defined peaks of NPX at 15, 20, 30 µM respectively, while the peak of PCT remained unchanged at 40 µM. These results confirm that the quantitative detection of an analyte was not influenced by the presence of the other at this modified electrode.

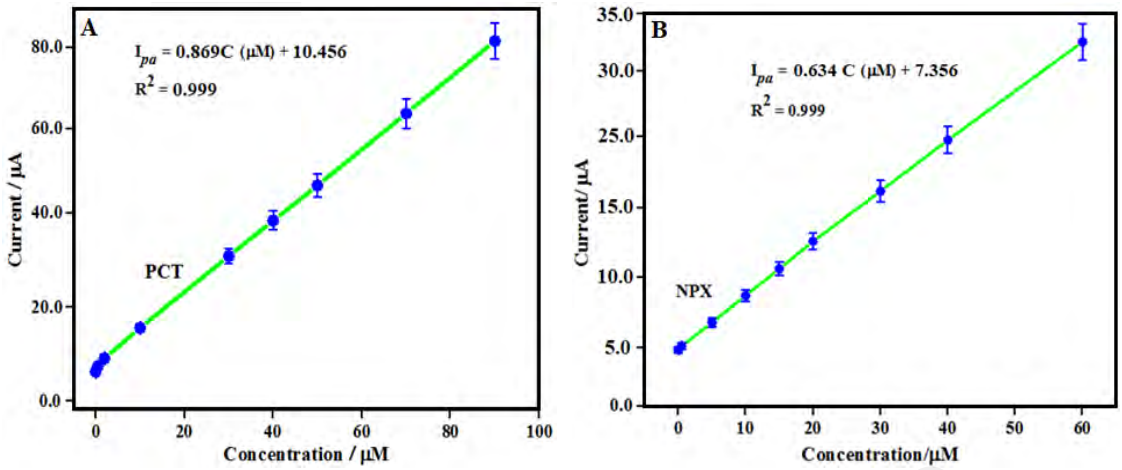

Figure 4.12: (A). Calibration plot of peak current vs. concentration of PCT. (B) Calibration plot of peak current vs. concentration of NPX.

Table 4.1: A comparison of electrodes for the individual determination of PCT and NPX.

Analyte	Electrode	Method	LOD (μM)	Linear range (μM)	Reference
PCT	Pt/NGr	SWV	0.008	0.05-90	(Anuar *et al.*, 2018)
	Co/CTS/*f*-MWCNTs/GCE	DPV	0.01	0.1 - 400	(Akhter *et al.*, 2018)
	AuNPs/MWCNT/GCE	DPV	0.03	0.09 – 35	(Madrakian *et al.*, 2014)
	PEDOT/GO/GCE	CV	0.57	10 - 60	(Si *et al.*, 2014)
NPX	ZnO/MWCNT/CPE	CV, SWV	0.23	1.0 - 200	(Tashkhourian *et al.*, 2014)
	Platinum electrode	LSV, DPV	1.0	4.0 - 100	(Adhoum *et al.*, 2003)
	GCE	BIA,	0.3	10 - 100	(Stefano *et al.*, 2012)
	BDDE	CV,DPV	30 nM	0.5 - 50	(Suryanarayanan *et al.*, 2005)
PCT and NPX	Dysprosium nanowire modified CPE	SWV	0.0003 PCT 0.0005 NPX	0.01-250 0.001-500	(Norouzi *et al.*, 2009)
	(NC-NDG)-SDS	DPV	0.0035 PCT 0.026 NPX	0.01 to 90 0.1 to 60	This work

4.7.2 Reproducibility and stability of (NC-NDG)-SDS sensor

The reproducibility of the (NC-NDG)-SDS sensor towards the simultaneous detection of 1 μM PCT and 1 μM NPX was investigated by DPV in 0.1 M PBS (pH 7) at 0.1 Vs^{-1}, using six (NC-NDG)-SDS modified electrodes. The calculated relative standard deviation (RSD) of the peak currents are 3.4% and 4.25% for PCT and NPX, respectively.

In this experiment, the RSD value was calculated from triplicate performance and the result was less than 6% which confirms the good reproducibility of the fabricated sensor. The stability of the fabricated sensor was also investigated in a separate experiment using the same concentration of PCT and NPX. The electrode was kept in pH 7.0 solution at room temperature for a week. After a week, the electrode retained 95% of the initial current response while 90% of the initial current response was retained after two weeks of storage. This confirms the stability and good reproducibility of the (NC-NDG)-SDS/GCE sensor as shown in Figure 4.13.

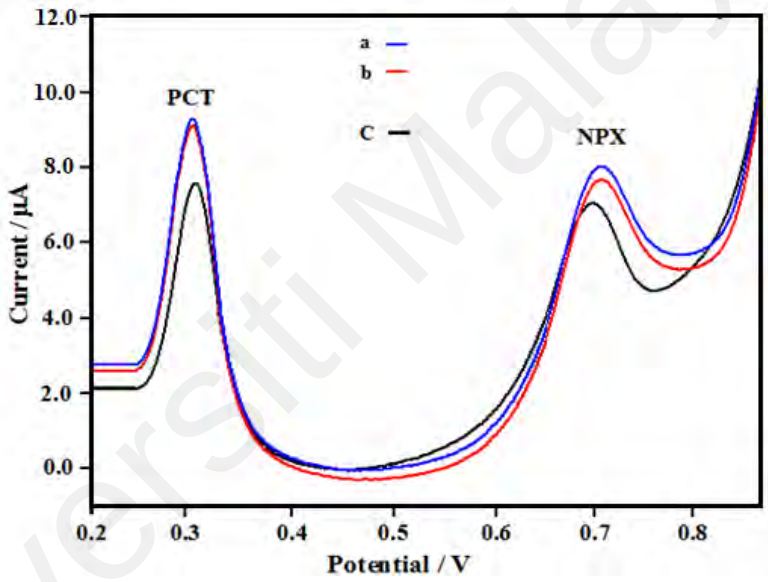

Figure 4.13: DPV signal of 1.0 µM PCT and 1.0 µM NPX in 0.1 M PBS (pH 7.0) at 0.1 V s^{-1} using (NDG-NC)-SDS modified electrodes, (a) first day; (b) 0.2 after a week; (c) after two weeks.

4.7.3 Interference study

The (NC-NDG)-SDS/GCE sensor was tested for the detection of PCT and NPX in the presence of some common interfering compounds found in biological environments. The DPV was recorded five times using the (NC-NDG)-SDS modified electrode in a solution of 1.0 µM PCT, 10 µM DCF and 0.5 µM NPX and in the presence

of 100 µM of each interfering compound (glucose, lactose, sucrose, fructose, ascorbic acid, dopamine and uric acid) as shown in Figure 4.14. A freshly prepared modified electrode was used for each measurement. The presence of interfering compounds did not influence the redox potential of the PCT, NPX and DCF except glucose. The results confirm that the peak currents of the PCT and NPX were unaffected by the presence of the interfering compounds. This suggests that the fabricated (NC-NDG)-SDS nanocomposite modified on GCE is an effective electrochemical sensor for the simultaneous determination of PCT and NPX analytes in biological environments.

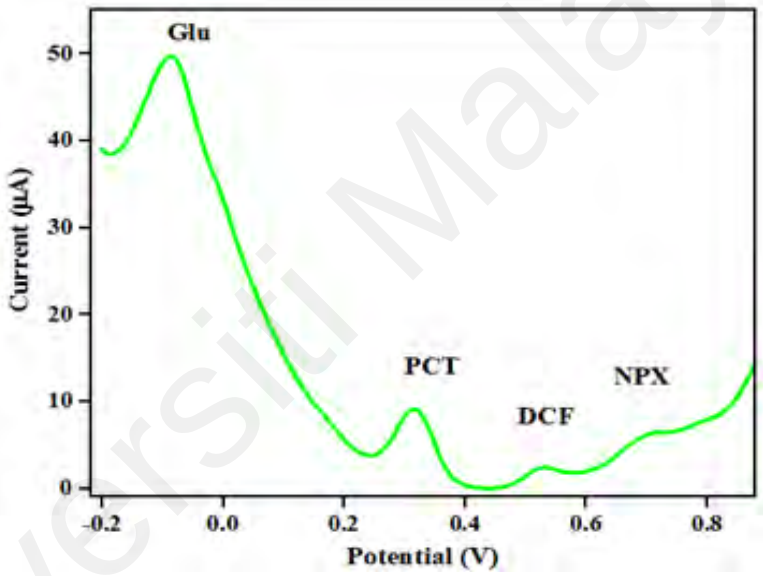

Figure 4.14: DPV signal on (NC-NDG)-SDS with 1.0 µM PCT, 10 µM DCF and 0.5 µM NPX in the presence of some common interfering compounds such as uric acid (UA), ascorbic acid (AA), dopamine (DA), lactose, fructose, sucrose and glucose, in 0.1 M PBS (pH 7.0) at 0.1 V s^{-1}

4.7.4 Determination of PCT and NPX in real samples

The practical application of the newly fabricated sensor was evaluated by the simultaneous determination of PCT and NPX in commercial tablets and human blood serum. The stock solutions of PCT and NPX were diluted 5 times using DI water and a specific amount of diluted sample and diluted blood serum sample were placed in

different electrochemical cells. The current responses for the PCT and NPX diluted solutions were recorded by the DPV technique using the (NDG-NC)-SDS electrode as shown in Tables 4.2 and 4.3. The recovery of PCT and NPX at the (NC-NDG)-SDS modified electrode (table 4.2 and 4.3) was satisfactory which confirms that the modified electrode could be used effectively for the determination of PCT and NPX in commercial dosage forms and blood serum samples.

Table 4.2: Determination of PCT and NPX in pharmaceutical preparations at (NC-NDG)-SDS using differential pulse voltammetry.

Tablet	Sample	Labelled (μM)	Found (μM)	Recovery (%)	RSD (%)
PCT	1	10	10.02	100.20	0.55
	2	15	14.95	99.66	0.84
	3	20	20.01	100.05	0.65
NPX	1	20	19.96	99.80	0.55
	2	30	30.04	100.13	0.75
	3	40	40.01	100.02	1.02

Table 4.3: Determination of PCT and NPX in human serum samples at (NC-NDG)-SDS using DPV.

Sample		Labelled (μM)	Found (μM)	Recovery (%)	RSD (%)
PCT	1	5	5.05	101.00	1.05
	2	10	9.98	99.80	0.65
	3	15	14.98	99.87	0.88
NPX	1	10	10.03	100.30	0.45
	2	20	20.04	100.20	0.74
	3	30	29.98	99.94	0.57

4.8 Effect of concentration of SDS

The effect of SDS concentration towards the detection of PCT and NPX on the NDG-NC nanocomposite was investigated as shown in Figure 4.15. It is observed that the introduction of SDS enhances the oxidation currents of PCT and NPX, with a low LOD. The oxidation currents of PCT and NPX were enhanced due to the expanded

surface area with the presence of SDS. In addition, the presence of SDS promotes interaction between the nanomaterials and ultimately contribute to enhanced capability of sensing. The attachment of SDS with NDG-NC nanocomposite improves the overall sensing performance of the sensor which is a new finding. The effect of different concentrations of SDS on the oxidation peak currents of PCT and NPX is shown in Figure 4.15. The peak currents increase with the SDS concentration from 0.5 µM to 4.0 µM. The maximum peak currents of PCT and NPX are achieved in the presence of 4 µM SDS but decreases at concentrations higher than 4 µM (shows in appendix 4.2). This could be due to the overcrowding of the surfactant on the electrode surface which decreases the active surface area for the transfer of electrons. Another reason for the declining peak currents at higher SDS concentrations is the formation of SDS micelles on the electrode surface which block the electron transfer process. As a result, the peak currents decrease at higher SDS concentrations. Therefore, 4.0 µM SDS was selected as the optimum concentration in these experiments for the simultaneous determination of PCT and NPX.

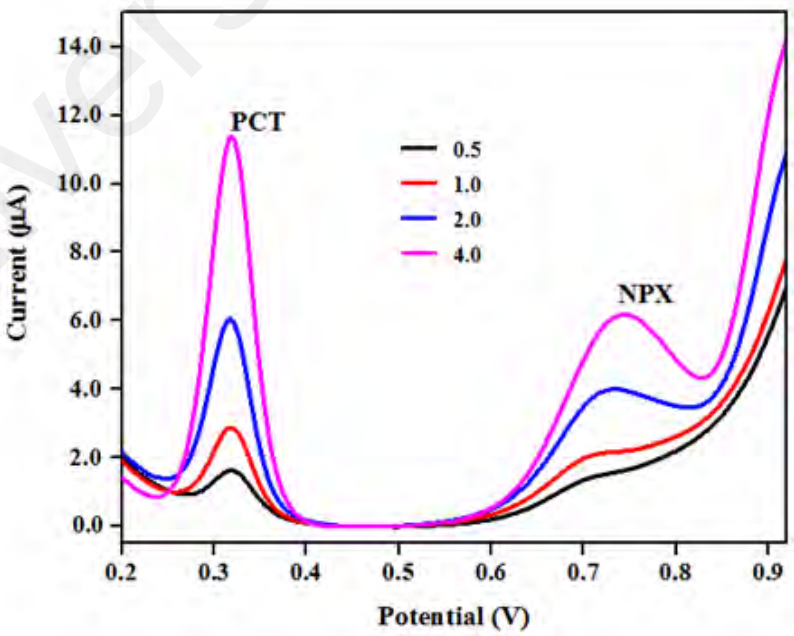

Figure 4.15: Optimization of SDS (0.5 µM to 4.0 µM) for the simultaneous determination of 2.0 µM PCT and0.5 µM NPX by DPV

4.9 Simultaneous determination of PCT, NPX in presence of DCF

Patients are sometimes administered different types of NSAIDs such as PCT, NPX and DCF to reduce fever and inflammation. Thus it is important to monitor the drug dosage to decrease the drug-drug interactions (DDI) and adverse drugs reactions (Moore *et al*., 2015). An electrochemical sensor facilitates the quantitative detection of a specific drug, but the detection of different types of drugs utilizing the same sensor is becoming the focus of biomedical research. Therefore, the simultaneous detection of PCT, NPX in presence of DCF was performed in PBS (pH 7.0) at the (NC-NDG)-SDS at 0.1 Vs^{-1}. Figure 4.16 shows a clear separation of PCT (0.312 V), NPX (0.528 V) and DCF (0.710 V) peak currents, which represents that the (NC-NDG)-SDS modified GCE sensor can detect PCT and NPX simultaneously in presence of DCF.

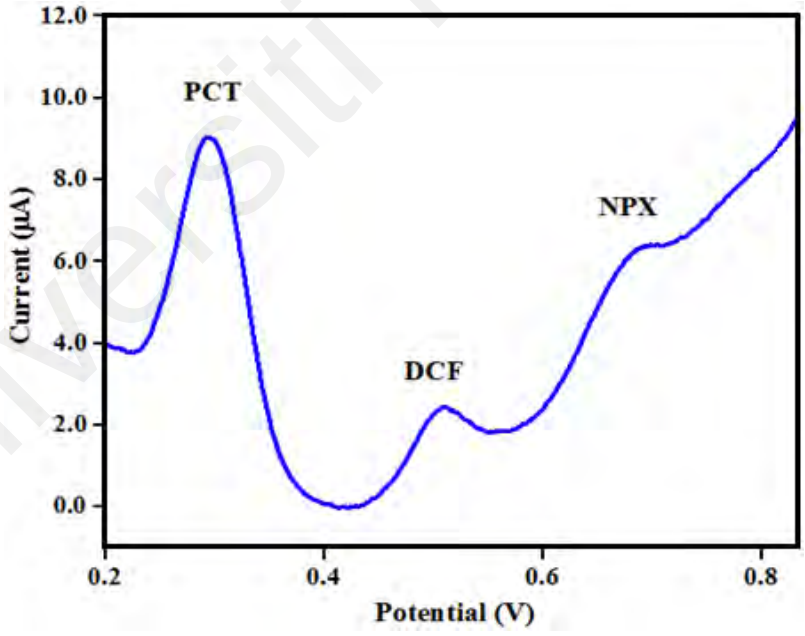

Figure 4.16: DPV on (NC-NDG)-SDS for the simultaneous determination of 1.0 µM PCT, 10 µM DCF and 0.5 µM NPX, in 0.1 M PBS (pH 7.0) at 0.1 V s^{-1}

5. Conclusions

A (NC-NDG)-SDS electrochemical sensor was fabricated for the simultaneous detection of PCT and NPX in presence of DCF with the presence of an anionic surfactant SDS. A clear peak separation between the PCT and NPX was achieved which confirms the effectiveness of the (NC-NDG)-SDS nanocomposite for the simultaneous detection of PCT and NPX. The fabricated sensor exhibited good sensitivity and selectivity at broad concentration ranges from 0.01 to 90 μM (PCT) and from 0.1 to 60 μM (NPX), with a low LOD of 0.0035 μM and 0.026 μM for the detection of PCT and NPX, respectively. The analytical determination of the drugs in tablets and human blood serum confirms the feasibility of the sensor in analysing real samples. Thus the fabricated sensor could be utilized for the simultaneous determination of PCT and NPX with satisfactory results.

CHAPTER 5: IMMOBILIZED COPPER IONS ON MWCNTS-CHITOSAN THIN FILM: ENHANCED AMPEROMETRIC SENSOR FOR THE DETERMINATION OF DICLOFENAC SODIUM IN AQUEOUS SOLUTION

5.1 Introduction

Diclofenac sodium (DCF) (sodium [o-(2,6-dichloroanilino) phenyl] acetate) Figure 5.1, is a safe and well known non-steroidal anti-inflammatory drug (NSAIDs). Besides, it is applied as an analgesic, anti-rheumatic, anti-inflammatory and anti-thermal and for the treatment of arthritis and degenerative joint disease (Iliescu *et al*., 2004). After oral administration, DCF is absorbed very well and undergoes a huge hepatic metabolism. Its half-life ($t_{1/2}$) is 1-2 hours, protein binding affinity is approximately 99% and volume of distribution (V_D) is 0.171/kg. This drug enters through the synovial fluid. As this drug is frequently used for the treatment of several diseases, it is essential to determine the concentration of DCF from pharmaceuticals preparations and also from the environment (Sanati *et al*., 2014). Prolonged administration of DCF can be responsible for life-threatening cardiac problems such as heart attack and stroke with diabetic patients and also with patients suffering from the Shy-Drager syndrome (Goodarzian *et al*., 2014). When the concentration of DCF is more than 1 mg/L, then it is considered harmful for various environmental flora and fauna (Vieno & Sillanpaa, 2014). Therefore, a simple, accurate, fast, cost-effective and selective technique for the detection of DCF is needed. Voltammetric techniques have these benefits although electro-oxidation for DCF generally shows a low response when using unmodified electrodes (Yang *et al*., 2008).

Several methods have been reported for the quantitative determination of diclofenac, for example spectrophotometric (Souza & Tubino, 2005; Tubino & de Souza, 2006), fluorometry (Moncrieff, 1992), and chromatography (Chmielewska *et al*., 2006; Chmielewska *et al*., 2006). However, there are limitations to these techniques. They are

very time consuming and chemical reagents are required to perform these techniques, therefore the focus has been diverted towards electrochemical methods of analysis due to their fast response, higher sensitivities, simple operation and the possibilities of miniaturization (Rodríguez et al., 2007; Xu *et al*., 2004). Among the electrochemical method, various voltammetric/amperometric (Blanco-Lopez *et al*., 2003; Daneshgar *et al*., 2009) and potentiometric techniques (Kormosh *et al*., 2007; Kormosh *et al*., 2009) have been reported for the determination of diclofenac (Manea *et al*., 2010).

In recent years, chemically modified electrodes have attracted huge attention because of their versatile approaches in several analyses (Kannan & Sevvel, 2017; Meenakshi *et al*., 2016; Montes *et al*., 2016). Carbonaceous nanostructured materials include carbon nanofibers (McKnight *et al*., 2003), mesoporous carbons (You *et al*., 2009) and carbon nanotubes (CNTs) (Madrakian *et al*., 2014; TermehYousefi & Kadri, 2016). These materials have been used substantially for the fabrication of modified electrodes which have several applications not only in analytical measurements but also in industrial electrochemistry (TermehYousefi *et al*., 2017). They are widely recognized due to some advantages such as cost-effectiveness, wide potential range, possess suitable electrocatalytic response for several redox reactions, are compatible and possess inert electrochemistry (Bard & Faulkner, 2001; McCreery & Bard, 1991). CNT is a type of carbonaceous material and is composed of folding the graphene layers into carbon nanocylinders (TermehYousefi *et al*., 2017). CNTs are comprised of single-walled nanotubes (SWCNTs) (Iijima & Ichihashi, 1993) and multi-walled nanotubes (MWCNTs) (Iijima, 1991). CNTs have drawn the attention of researchers due to their unique characteristics such as good mechanical strength, higher electrical conductivity and higher chemical stability (Lu & Tsai, 2011). One of the crucial approaches of this kind of material is the early electrochemical detection of cancer by employing advantageous and suitable biosensors in clinical diagnostics (Jemal *et al*., 2005; Syafiqah

et al., 2017). Since their breakthrough, CNTs have drawn significant attention for several types of investigations (Pandey *et al*., 2017; Wang, 2005). CNTs possess some exceptional properties such as remarkable structural, chemical, electrical and mechanical characteristics (Yousefi *et al*., 2015). They possess superconducting and metallic properties, in addition to semiconducting transport of electrons and it contains a hollow core suitable for the storage of guest molecules. Moreover, CNTs possess the largest elastic modulus configuration among all of the known materials (Davis *et al*., 2003). These extraordinary properties of CNTs have made them a sensing platform for the electrochemical detection and chemical detection of analytes (Gonzalez-Dominguez *et al*., 2012; Zhao *et al*., 2002).

Chitosan (CTS) is a linear copolymer composed of d-glucosamine and N-acetyl-d-glucosamine. CTS contains active amino and hydroxyl groups which are responsible for the high capacity of adsorption for organic compounds and heavy metal ions (Honarkar & Barikani, 2009). Furthermore, CTS displays many outstanding characteristics such as biocompatibility, the ability of film formation, biodegradability, low toxicity and high electrical conductivity (Song *et al*., 2011). Based on these benefits, chitosan matrix incorporated sensors have been fabricated for the detection of NSAIDs paracetamol (Babaei *et al*., 2010; Delolo *et al*., 2014; Kianipour & Asghari, 2013). The chitosan and metal complexes consisting of an annulus chelating configuration possess similar features with natural enzymes. This is the reason for the high catalytic activity for many types of chemical reactions (Hassaninejad–Darzi, 2014; Yousefi *et al*., 2015).

Numerous attempts for the determination of DCF were reported such as thin-layer chromatography (TLC) (Sun & H. Fabre, 1994), spectrophotometry (Botello & Perez-Caballero, 1995; Mazurek & Szostak, 2008), high-performance liquid chromatography (HPLC) (Kole *et al*., 2011; Sparidans *et al*., 2008), gas chromatography (Kadowaki *et al*.,

1984; Yilmaz *et al*., 2015), spectrofluorimetry (Arancibia *et al*., 2000), liquid chromatography (LC) (Demetri *et al*., 2002), capillary zone electrophoresis (Jin & Zhang, 2000), voltammetry (Chethana *et al*., 2012; Fard *et al*., 2016) from the biological fluids.

Spectrophotometry requires extensive preparations of samples by the extraction process or chemical reaction. Gas chromatography requires many extraction steps and also derivatization before the separation and detection (Goyal *et al*., 2010). These techniques have some drawbacks such as high cost, time-consumption and often requires pretreatment step, which sometimes affects the sensitivity and selectivity in the specific detections (Ramimoghadam *et al*., 2015). Electrochemical methods have advantages that could overcome the limitations of the conventional techniques of analysis as they possess high sensitivity and outstanding characteristics such as high selectivity, simplicity, reproducibility and is cost-effective (Baghayeri *et al*., 2014; Baghayeri *et al*., 2014; Madrakian *et al*., 2014; Vahedi *et al*., 2013).

Electrochemical techniques have been proved to be highly sensitive for the determination of drugs from pharmaceutical preparations and human body fluids. However, electrochemical methods are simple and dynamic because they possess rapid response, high sensitivity and selectivity, cheap instrumentation and a wide range of linearity (Goyal *et al*., 2010; Karuppiah *et al*., 2015). Mao *et al*., (2015) fabricated chitosan–copper modified electrode for the determination of paracetamol. Yu *et al*. (2011) reported a chitosan-copper complex modified with MWCNTs ionic liquid electrode for the detection of hydrogen peroxide. To the best of our knowledge, an electrochemical sensor for the detection of diclofenac sodium based on chitosan-copper complex modified with multi-walled carbon nanotubes has not been reported.

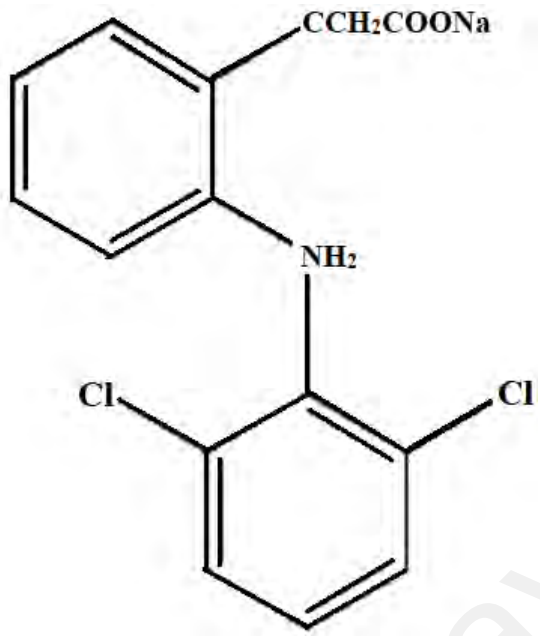

Figure 5.1: Chemical structure of Diclofenac sodium

In the current study, *f*-MWCNTs/CTS-Cu modified GCE was fabricated for the detection of DCF. The electrochemical response of DCF for the *f*-MWCNTs/CTS-Cu/GCE nanocomposite was analyzed by using cyclic voltammetry (CV) and square wave voltammetry (SWV) techniques. The outcomes of the experiment demonstrated that the *f*-MWCNTs/CTS-Cu/GCE sensor shows the incredible capability of extended active surface area and also increases the transfer of electrons between the electrode and analytes which enable a new avenue for the electrochemical determination of DCF. The *f*-MWCNTs/CTS-Cu/GCE sensor showed a broad linear range and low LOD compared to previous studies (shown in Table 5.1). To investigate the efficacy of the prepared electrode for analytical determinations, the voltammetric detection of DCF from real samples such as pharmaceuticals tablet preparations and human urine samples were attempted. The proposed method was simple, sensitive, rapid and selective for the detection of DCF from real samples.

5.2 Experimental methods

5.2.1 Chemical Reagents

MWCNTs was procured from Baytubes (Germany), while diclofenac sodium (DCF), chitosan (CTS), $CuCl_2.2H_2O$ and phosphate buffer solution (PBS) were procured from Sigma-Aldrich (Malaysia). The rest of the chemicals used in the experiment were of analytical grade and used without further purification. De-ionized (DI) water was used to prepare the standard and buffer solutions. The stock standard solution was prepared by 0.001 M concentration of Diclofenac sodium. The DCF solution was preserved in a refrigerator at 4 ºC. DI water was used for repeated dilutions. 0.2 M PBS solution was prepared by dissolving specific amounts of di-potassium hydrogen phosphate (K_2HPO_4) and potassium di-hydrogen phosphate (KH_2PO_4) in a 250 mL volumetric flask. Finally, 0.2 M PBS (pH 4.0) was used in the electrochemical experiments for the detection of DCF.

5.2.2 Instrumentation

An Autolab potentiostat/galvanostat (EcoChemie, The Netherlands) was used to perform the voltammetric technique such as cyclic voltammetry (CV), square wave voltammetry, and electrochemical impedance spectroscopy (EIS). A three-electrode electrochemical cell was used in the electrochemical experiments. A glassy carbon electrode GCE (3 mm diameter) modified with the (*f*-MWCNTs/CTS-Cu/GCE) composite was used as a working electrode (WE), while a platinum wire as the counter electrode (CE) and an Ag/AgCl/KCl (3.0 M) was the reference electrode (RE). All electrodes were also from Metrohm (Switzerland).

5.2.3 Methodology

For the synthesis of *f*-MWCNTs/CTS-Cu nanocomposite, *f*-MWCNTs was synthesized followed by the acid hydrolysis method and drop-casted on GCE. The CTS was immobilized on *f*-MWCNTs/GCE, while the Cu was immobilized by the self-assembly method on *f*-MWCNTs/CTS surface. The morphological properties were characterized by FESEM and FTIR spectroscopy. Before the electrochemical experiments, pH and scan rate were optimized. CV and SWV methods were employed to investigate the electrochemical behaviour of *f*-MWCNTs/CTS-Cu/GCE sensor. Satisfactory relative standard deviation and recovery values were obtained from the real sample analysis.

5.2.4 Purification methods of *f*-MWCNTs

The synthesis procedure of *f*-MWCNTs was explained in chapter 3, section 3.2.6.

5.2.5 Fabrication of GCE/ *f*-MWCNTs /CTS-Cu modified electrode

The bare GCE was polished on a polishing kit (Buehler) with alumina slurry and washed with doubly distilled water, then sonicated for 10 min in an aqueous HNO_3 and acetone mixture (ratio 1:10), and finally with DI water. The *f*-MWCNTs suspension was formulated by dispersing 1.0 mg *f*-MWCNTs in a 2.0 mL (v/v) mixture of doubly distilled water, ethanol and sodium dodecyl sulphate (3:1:1) and then sonicated for 30 min. Then 10.0 μL of a black suspension was drop-casted onto the surface of GCE and dried in air to form a film of *f*-MWCNTs on the surface of GCE for the preparation of *f*-MWCNTs modified GCE. The chitosan solution was prepared by dissolving 0.25 mg of chitosan powder in 50 mL 0.10 ML^{-1} acetic acid and sonicated for 30 min, then the electrode was dipped into the chitosan solution for 30 min. 0.1 gm of $CuCl_2$.$6H_20$ were mixed in 100 mL doubly distilled water to prepare a copper solution and subsequently sonicated for 30

min and then again dipped the electrode in the copper solution for 30 min. The modified GCE (GCE/ *f*-MWCNTs /CTS-Cu) was prepared by the following steps (shown in figure 5.2). At first, 5µL of MWCNTs suspension was taken into a micropipette and drop-casted to establish a coating on the surface of GCE to form the *f*-MWCNTs /GCE and then dried in air. Then the dried electrode was immersed into the chitosan solution for 30 min and the positively charged chitosan was self-assembled with the negatively charged *f*-MWCNTs. After 30 min the electrode was removed from the solution and slightly rinsed with DI water to prepare for the next step. Finally, the *f*-MWCNTs/CTS/GCE was immersed in the copper solution for 30 min. The Cu^{2+} was adsorbed onto the chitosan surface by the self-assembly method. The modified electrode was removed from the copper solution and washed with DI water and air-dried.

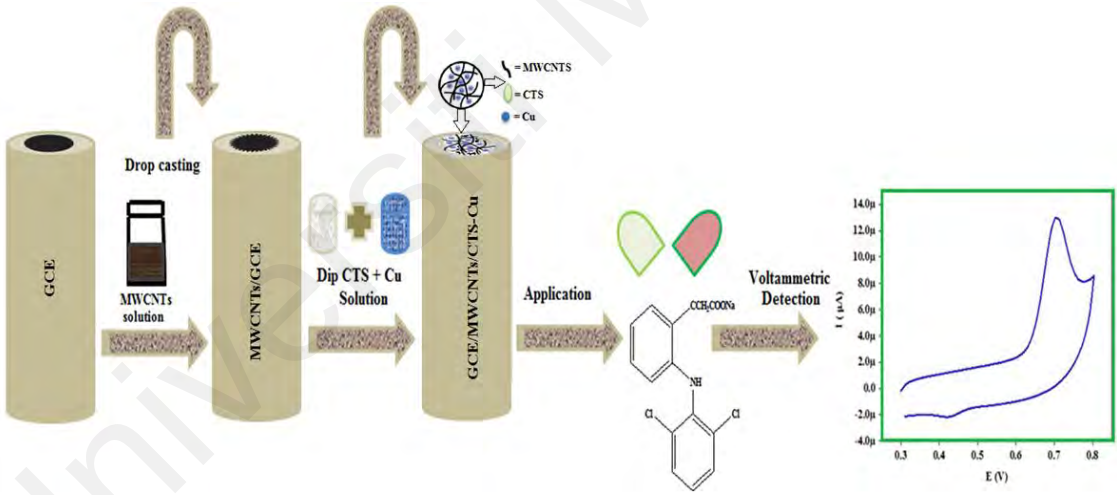

Figure 5.2: Fabrication of *f*-MWCNTs/CTS-Cu modified GC electrode for the detection of DCF

5.2.6 Preparation of pharmaceutical samples

5 tablets of diclofenac sodium (DCF) were taken and crushed in a mortar pestle to obtain a fine powder. The required amount of DCF was transferred into a 50 mL volumetric flask and then dissolved in PBS (pH 4.0). Then the mixture was sonicated for

5 min to obtain the DCF solution. After sonication, the solution was filtered to obtain the suitable aliquot and then stored in the refrigerator before use.

5.2.7 Preparation of urine specimens

A healthy volunteer was chosen to collect the urine specimen, after consuming an adequate sample kept it at a cool temperature for the next experiment. The sample (35.0 mL) was centrifuged at 2500 rpm for 15 min. By using a filter paper the supernatant was filtered two times and diluted with PBS in a volumetric flask (100 mL). Then the solution was used in the electrochemical analysis.

5.3 Aim of the research

This study aims to develop a new nanocomposite of *f*-MWCNTs and CTS with Cu. The combination of *f*-MWCNTs and CTS exhibits an extended electroactive surface area, with the electro-catalytic effect of Cu is expected to improve the properties of the nanocomposite. Thus, the synergistic effect is a hallmark of good electrochemical sensing of DCF.

5.4 Results and Discussions

5.4.1 Morphologies of different electrodes

The morphological studies of different electrodes are shown in the FESEM and EDX images in Figure 5.3. Figure 5.3C shows a clear morphology of the *f*-MWCNTs/CTS-Cu modified electrode which was characterized by FESEM. It shows that $CuCl_2$ was distributed successfully on the surface of *f*-MWCNTs and it did not affect the morphology of *f*-MWCNTs and CTS. For a detailed understanding, some portion of the images was encircled to indicate the distribution of copper. Figure 5.3B shows that the CTS polymer was distributed homogeneously on the surface of *f*-MWCNTs. The morphology of the

CTS polymer is different from the morphology of *f*-MWCNTs (Figure 5.3A). This result reveals that a successful composite (*f*-MWCNTs /CTS-Cu) was prepared on the GCE surface, as a consequence, the surface area was increased which enhanced the analyte (DCF) adsorption.

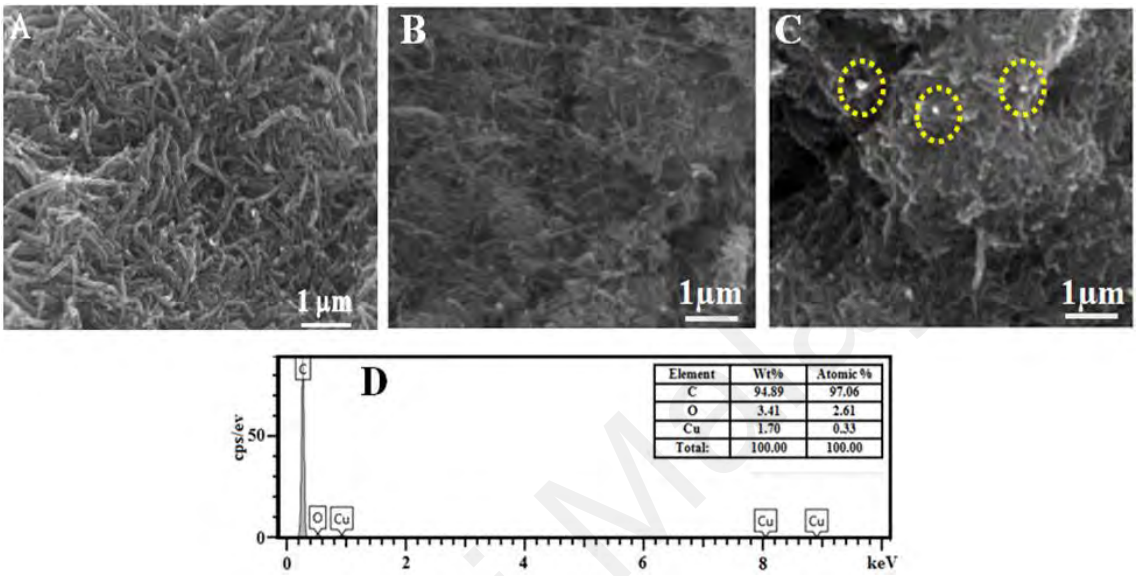

Figure 5.3: The FESEM image of (A) *f*-MWCNTs/GCE, (B) *f*-MWCNTs/CTS/GCE and (C) *f*-MWCNTs /CTS-Cu/GCE. (D) EDX analysis of *f*-MWCNTs /CTS-Cu/GCE.

The EDX result (5.3D) indicates that the nanocomposite contains carbon, oxygen and copper elements with 98.94 wt.%, 3.41 wt.%, and 1.70 wt.% respectively. This result confirms the presence of copper on the surface of the modified electrode.

5.4.2 FTIR Studies

The FTIR spectra of pristine (a), *f*-MWCNTs (b), *f*-MWCNTs-CTS (c), and *f*-MWCNTs-CTS-Cu (d) are shown in Figure 5.4. The pristine spectrum (curve a) and *f*-MWCNTs (curve b) show the same vibrations of the functional groups such as the asymmetric/symmetric methylene bands at 2923 cm^{-1} and 2852 cm^{-1} (Gonzalez-Dominguez *et al*., 2012) and the stretching vibrations of COOH- at 1740 cm^{-1} (Abdullahi, *et al*., 2015). The peaks for *f*-MWCNTs are sharper than the pristine peaks as shown in Figure 5.4.

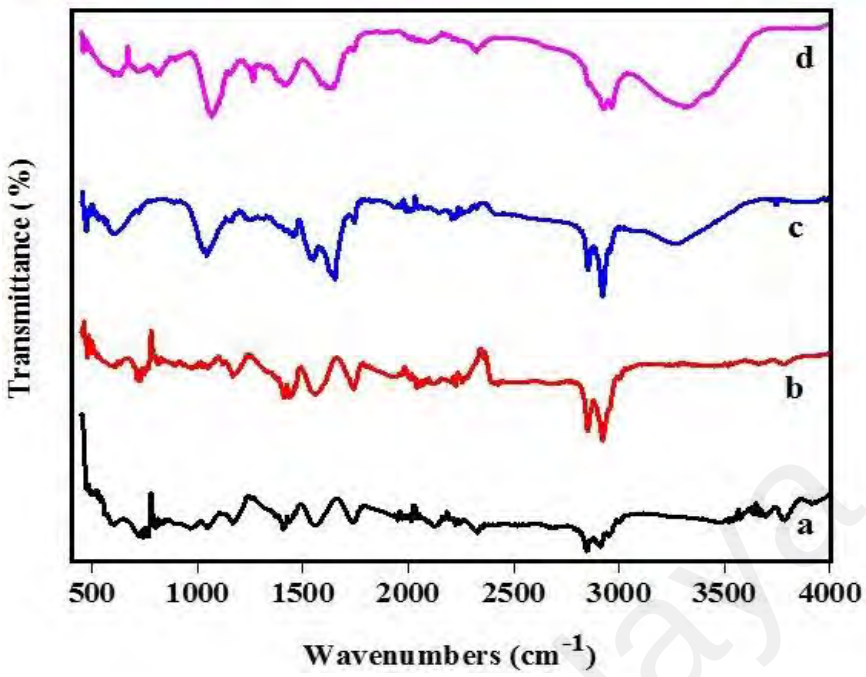

Figure 5.4: FTIR spectra of pristine (a), *f*-MWCNTs (b), *f*-MWCNTs and Chitosan (c), *f*-MWCNTs, Chitosan and Copper (d).

Curve 3 illustrates the combination of *f*-MWCNTs and chitosan. For *f*-MWCNTs, the peaks at 2920 cm^{-1} and 1746 cm^{-1} is attributed to the presence of $=CH_2$ and –COOH group. The absorption band for chitosan was found at 3370 cm^{-1} (O-H and N-H stretching vibrations), 1558 cm^{-1} (N-H bending vibrations), and 1082 cm^{-1} (C-O-C stretching vibrations) (Anicuta *et al*., 2010). The presence of these functional groups proved that the sample contained *f*-MWCNTs and Chitosan. Simultaneously, curve 4 shows the same bands for the *f*-MWCNTs and chitosan that are present in curve 3, but curve 4 shows some extra bands attributed to the presence of copper at around 456 cm^{-1} (Secco & Worth, 1987).

5.5 Electrochemical Impedance Spectroscopy (EIS) study

Electrochemical impedance spectroscopy (EIS) is commonly used for the measurement of the impedance changes of the modified electrode surface. The electrode transfer resistance (R_{ct}) value depends on the dielectric and insulating features at the

electrode/electrolyte interface, from the semicircle diameters of the Nyquist plot. The impedance spectra of the bare GCE (a), *f*-MWCNTs/GCE (b), and *f*-MWCNTs/CTS-Cu/GCE (c) were obtained in 0.1 M KCl which contained 5 mM $K_3Fe(CN)_6$/ $K_4Fe(CN)_6$ at a frequency range of 100 kHz to 100 mHz, shown in Figure 5.5. From the data fitting, the charge transfer resistance (R_{ct}) value of the bare GCE was 820 Ω. The R_{ct} value decreases to 120 Ω after the incorporation of the *f*-MWCNTs, which is attributed to the enhanced electrical conductivity of the *f*-MWCNTs. For the final composite *f*-MWCNTs/CTS-Cu/GCE, the R_{ct} value further decreases to 38 Ω, due to the smaller electron transfer resistance of the *f*-MWCNTs/CTS-Cu/GCE compared to the *f*-MWCNTs/GCE. This result indicates that the electrode was modified effectively with the proposed composite and improved the electrical conductivity.

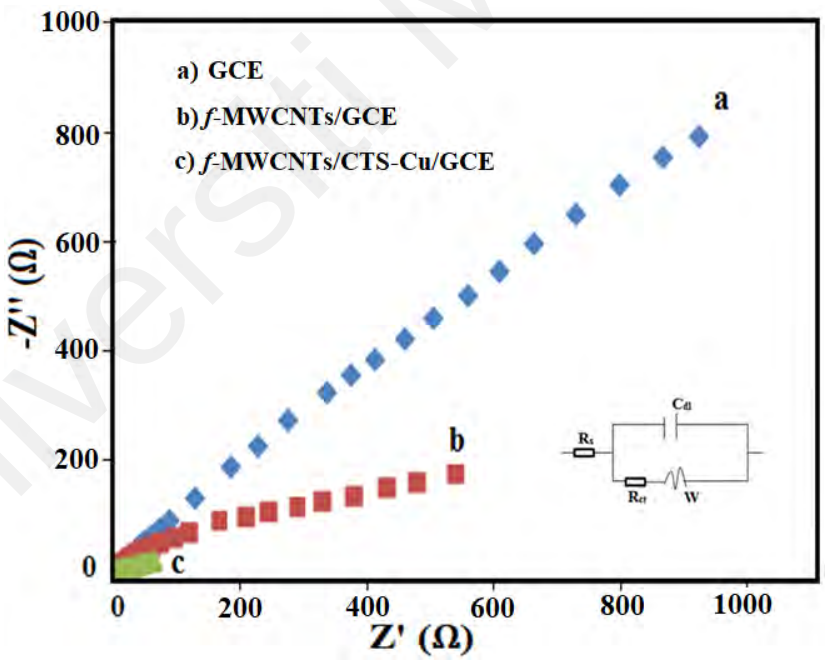

Figure 5.5: The representative impedance spectrum of the bare GCE (curve a), *f*-MWCNTs/GCE (curve b) and *f*-MWCNTs/CTS-Cu/GCE (curve c) in 5.0 mM $K_3Fe(CN)_6$ / $K_4Fe(CN)_6$ (1:1) containing 0.1 M KCl. Inset is the equivalent circuit for the fitting.

5.6 Electrochemical behaviour of DCF at *f*-MWCNTs/CTS-Cu/GCE thin film

5.6.1 Electrochemical oxidation of DCF

The electrochemical behaviour of 50 µM DCF was investigated by CV on the bare GCE (Figure 5.6a), *f*-MWCNTs/GCE (Figure 5.6b) and *f*-MWCNTs /CTS-Cu/GCE modified electrode (Figure 5.6c), respectively, in PBS (pH 4.0) between 0.3 and 0.8 V (vs. Ag/AgCl) at 100 mV s^{-1}. Figure 5.6a clearly shows the presence of an oxidation peak, without the presence of the reduction peak due to the lower conductivity of GCE. An increase in the current density was observed after modification of the GCE (Figure 5.6b and Figure 5.6c as the extended surface area possesses the excellent electro-catalytic effect of the Cu. This remarkable change of current occurred due to the presence of Cu and it demonstrates that this modification influenced the electrochemical reactions and also promoted the electron transfer rate.

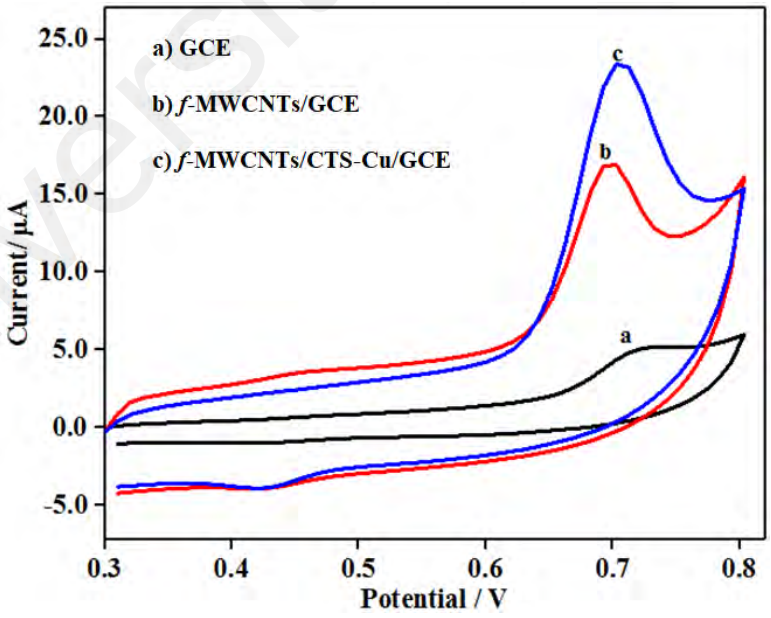

Figure 5.6: CV of the bare GCE (curve a), *f*-MWCNTs/GCE (curve b) and *f*-MWCNTs/CTS-Cu/GCE (curve c) in the solution containing 50 µM diclofenac sodium in 0.2 mol L^{-1} PBS (pH 4.0) at 100 mV s^{-1}.

5.6.2 Influence of scan rate

The effect of the potential scan rate of the modified electrode on the oxidation reaction of DCF was investigated by CV. The CVs for 50 µM concentrations of DCF in a phosphate buffer solution of pH 4.0 at the *f*-MWCNTs/CTS-Cu/GCE composite at scan rates from 10 to 250 mV s^{-1} was investigated and shown in Figure. 5.7A. From the Figure. 5.7A, the anodic peak current increases with the potential scan rate. Furthermore, Figure. 5.7B shows that the anodic peak current is proportional to the scan rate and the linear regression equation is:

$$I_{pa}\ (\mu A) = 0.292\ \nu\ (mVs^{-1}) + 2.524 \quad (R^2 = 0.987) \tag{5.1}$$

This demonstrates that the electrochemical oxidation of DCF at *f*-MWCNTs/CTS-Cu/GCE is a surface controlled process.

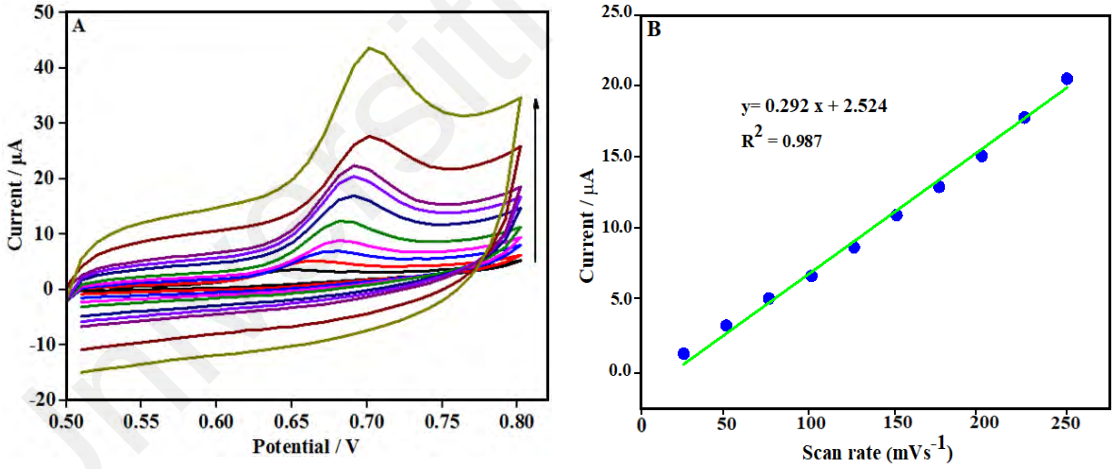

Figure 5.7: (A) CV of 50 µmol L^{-1} diclofenac sodium on the *f*-MWCNTs/CTS-Cu/GCE at different scan rate (10 mVs^{-1} to 250 mVs^{-1}) in PBS (pH 4.0). (B) a variation on the peak current with the scan rate.

5.6.3 Influence of pH

The electrochemical behaviour of DCF is directly influenced by the pH of the electrolyte. To study the effect of pH on the electro-oxidation of DCF at the *f*-MWCNTs/CTS-Cu/GCE modified electrode, CV of 50 µM DCF were recorded at different pH from 4.0 to 9.0 (Figure. 5.8A). The peak potential shifts towards the negative

region as the pH increases, due to the participation of proton in the oxidation reaction which is shown in Figure. 5.8A. The plot of E_{pa} vs pH shows a linear relationship (Figure. 5.8B) with the subsequent regression equation:

$$E_{pa}\ (V) = -0.032\ pH + 0.853 \quad (R^2 = 0.998) \qquad (5.2)$$

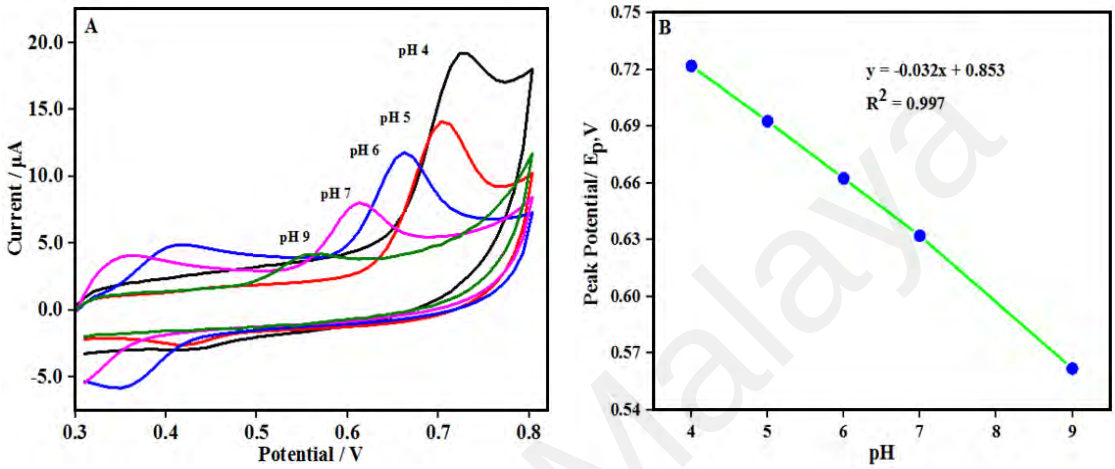

Figure 5.8: (A) Effect of the pH in the range 4 to 9 using PBS on the cyclic voltammetric response for 50 µM DCF at *f*-MWCNTs/CTS-Cu/GCE. (B) anodic peak potential as a function of pH

Besides, the current of the anodic peak of DCF increases gradually when the pH increases from 4.0 to 9.0. The highest peak current is achieved at pH 4.0, and the decline of the peak current is observed as the pH is increased to pH 9.0. Thus, pH 4.0 was considered as the optimum pH for the supporting electrolyte and was used for all subsequent experiments.

5.7 Performance evaluation of *f*-MWCNTs/CTS-Cu/GCE

5.7.1 Analysis of limit of detection of sensor

The calibration curve was constructed and described using *f*-MWCNTs/CTS-Cu/GCE under optimum conditions. Figure 5.9A shows the square wave voltammograms (SWV) for several concentrations of DCF at optimum conditions. In Figure. 5.9, a linear range 0.3 to 200 µM was observed with a regression equation (Figure. 5.9B)

$$I_p\,(\mu A) = 1.139\ C_{DCF}\,(\mu M) + 12.822\ (R^2 = 0.997) \quad (5.3)$$

The limit of detection (LOD) = $3S_b/m$, where LOD is the limit of detection, S_b for a standard deviation for the blank sample and m for the slope of the calibration graph, thus the LOD for the modified electrode is calculated as 0.021 µM. The S_b was evaluated from six blank samples. Table 5.1 presents the comparison of different modified electrodes and also analytical parameters for the evaluation of DCF from the literature (Arvand *et al*., 2012; Ensafi *et al*., 2013; Fard *et al*., 2016; Goodarzian *et al*., 2014; Mokhtari *et al*., 2012; Sarhangzadeh *et al*., 2013).

Table 5.1: The comparison of various electrodes for the determination of DCF

Electrode	Linear range(µM)	Detection limit(µM)	Reference
MWCNTs/$Cu(OH)_2$/Nanoparticles/IL-GCE	0.180 to 119.00	0.04	(Arvand *et al*., 2012)
MWCNT/ PGE	0.047 to 12.95	0.017	(Fard *et al*., 2016)
IL/MWCNTs paste electrode	0.300 to 750.00	0.09	(Goodarzian *et al*., 2014)
Vinylferrocen/MWCNTs paste electrode	5.00 to 600.00	2.00	(Mokhtari *et al*., 2012)
MWCNTs and IL-modified carbon ceramic electrode	0.050 to 50.00	0.018	(Sarhangzadeh *et al*., 2013)
IL-modified CNT paste electrode	0.500 to 300.00	0.20	(Ensafi *et al*., 2013)
***f*-MWCNTs/CTS-Cu/GCE**	0.300 to 200.00	0.021	This work

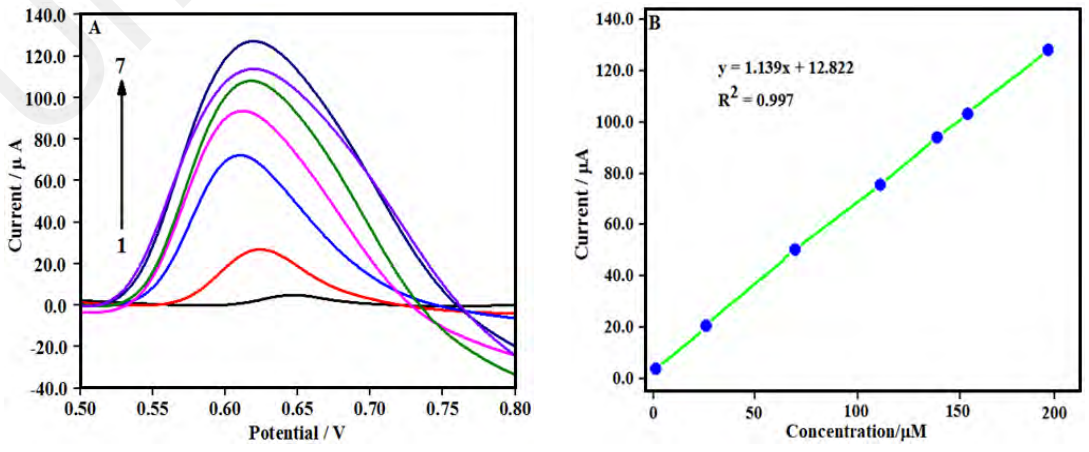

Figure 5.9: (A) SWVs response at *f*-MWCNTs/CTS-Cu/GCE in PBS (pH 4.0) at different concentration of DCF in the range of 0.3 – 200 µM (B) calibration curve for the plot for the oxidation peak current vs DCF concentration.

5.7.2 Repeatability, reproducibility, and stability

The primary requirement for a successful sensor depends on its repeatability, reproducibility and stability. The repeatability of the newly modified electrode for the measurement of DCF was studied by performing six measurements with the same DCF standard solutions using the same electrode. The relative standard deviation (RSD) of the modified electrode response toward the DCF solution (50.0 μM) is 2.55% which assures good repeatability of *f*-MWCNTs/CTS-Cu/GCE sensor. The reproducibility of the modified electrode was also investigated. Six different electrodes were prepared with the same *f*-MWCNTs/CTS-Cu nanocomposite and were studied using the DCF solution (50.0 μM). For the responses between electrodes, the relative standard deviation is 2.88%. The result demonstrated that the reproducibility of the proposed *f*-MWCNTs/CTS-Cu/GCE sensor for the measurement of DCF was satisfactory. The electrode remained stable for 9 weeks. However, after 9 weeks, the response of the electrode deteriorated. The stability of the electrode was satisfactory. It is demonstrated that the fabricated electrode was acceptable for the evaluation of real samples.

5.7.3 Interference study

Generally, DCF suffers interference in the presence of some biological molecules. The effect of various substances which interferes with the determination of DCF was studied under the optimum conditions. The interference study was done by adding various biological compounds and ions into PBS (pH 4.0) with the presence of 20.00 μM of DCF. The study showed that common ions such as sodium, potassium and chloride ion did not interfere with the determination of DCF. To investigate the interference of the biological compounds for the detection of DCF, various concentrations of fructose, glucose, citric acid, sucrose and urea were experimented with but did not interfere with the current

response of DCF. The results confirm that the fabricated electrode is highly selective for the detection of DCF in pharmaceutical dosage forms and biological samples.

Table 5.2: Diclofenac sodium detection in tablet samples (n=3)

Sample	Labeled (mg/tablet)	Found (mg/tablet)	Recovery (%)	RSD (%)	HPLC (mg)
10 mg	10 mg	10.01	100.10	2.65	10.10
50 mg	50 mg	49.40 mg	98.80	2.80	50.20
100 mg	100 mg	97.60 mg	97.60	2.20	100.80

Table 5.3: Recovery test results for Diclofenac sodium by using human urine samples (n=3)

Added (µM)	Found (µM)	Recovery (%)	RSD (%)	HPLC (µM)
0	ND[a]	-	-	ND[a]
10	9.97	99.70	1.80	10.13
50	49.20	98.40	2.60	50.34
100	98.88	98.88	2.40	98.44

[a] Not detected.

5.7.4 Real sample analysis

To evaluate the acceptability of the fabricated electrode (*f*-MWCNTs/CTS-Cu/GCE) for real sample analysis, different strengths of diclofenac sodium tablets and human urine specimens were used. The samples were diluted adequately according to the previous description. The square wave voltammetric technique was used in the determination of DCF concentration from tablets and human urine samples. The DCF was detected after its addition into human urine and the recovery values were calculated and presented in Tables 5.2 and 5.3. From table 5.2, the recovery results between 98.4 and 99.7 are considered acceptable. The comparative study reveals the feasibility of the present technique with the previous methods, in terms of the LOD. This remarkable performance is responsible for the immobilization of *f*-MWCNTs/CTS-Cu composite onto the surface of GCE which ensure the extended surface area, synergistic electrocatalytic effect and excellent conductivity.

6. Conclusions

In this work, *f*-MWCNTs-CTS-Cu was fabricated by a simple sonication and drop-casting method and utilized as a novel sensing platform for the electrochemical determination of diclofenac sodium (DCF). *f*-MWCNTs showed superior electrocatalytic activity and chitosan had excellent adsorption and film-forming capacity. Chitosan and the metal complex contain chelating groups similar to the properties of natural enzymes. Due to these reasons, the chitosan and copper complex has a synergistic effect on electrocatalytic activity. That is the main reason for the high electrocatalytic performance of the GCE modified with *f*-MWCNTs-CTS-Cu nanocomposite toward the electro-oxidation of diclofenac sodium which gave a good linear range, low detection limit and high selectivity for DCF detection. These results demonstrated that the fabricated electrode has significant potential for the determination of diclofenac sodium from the pharmaceutical dosage forms and real samples.

CHAPTER 6: BIOPOLYMER BASED CONDUCTIVE NANOCOMPOSITE: AN EFFICIENT SENSING PLATFORM FOR THE SIMULTANEOUS DETERMINATION OF PAINKILLER AND ANTIBIOTIC DRUG IN PHARMACEUTICAL TABLET, BIOLOGICAL FLUID AND WATER SAMPLE

6.1 Introduction

Paracetamol (PCT) (N-acetyl-p-aminophenol) is a very popular and extensively used "over the counter drug" in the world. PCT is a safe drug and possesses antipyretic and analgesic effects. Generally, it is used for fever, backache, cold, headache, muscle pain, osteoarthritis etc (Akhter *et al*., 2018). The overconsumption of a large dosage of PCT can cause some serious health issues such as hepatotoxicity, inflammation, nephrotoxicity, anorexia, skin rashes etc (Anuar *et al*., 2018).

Ciprofloxacin (CPR) is a third-generation antibiotic drug belonging to the quinolone group and is generally administered for urinary tract infection, skin infection, respiratory tract infection and so on (Chen *et al*., 2019). CPR shows its electroactive nature through the electrochemical oxidation of the piperazine ring which is present in the CPR structure. Overdose of CPR can cause severe health problems such as liver damage, hypersensitivity reactions, permanent nerve problems and so on (Fang *et al*., 2019).

Because of the extensive production and usage of the PCT and CPR, they are seldom detected in water resources. However, the presence of several hundred to thousands ng L^{-1} concentrations of PCT has been detected in wastewater (Alam *et al*., 2018). While the presence of CPR in pharmaceutical wastewater is around 28,000-31,000 µg L^{-1}, municipal waste water 0.255-0.568 µg L^{-1} and for hospital > 10 µg L^{-1}, have been reported (Fang *et al*., 2019). The quinolones group of drugs are less decomposed by the

bacterial metabolism process, thus it takes a long time to be eliminated from the environment compared to other classes of antibiotics (Turiel *et al*., 2005). Considering the adverse effects and water contamination by high concentrations of PCT and CPR which are associated with severe health problems, it is very crucial to monitor the concentrations of these drugs from biological fluids, commercial tablet dosage forms and water for environmental and clinical purposes. Up-to-date, several methods have been employed for the detection of PCT and CPR such as high-performance liquid chromatography (Liu *et al*., 2018; Sultana *et al*., 2013) capillary electrophoresis (Wang *et al*., 2005; Lecoeur *et al*., 2019), fluorimetry (Perera *et al*., 2019; Turkie & Munshid, 2019), titrimetry (D'Souza *et al*., 2015; Basavaiah *et al*., 2006), electrochemical techniques (Anuar *et al*., 2018; Matsunaga *et al*., 2020; Bonyadi *et al*., 2020) etc.

Nanocellulose (NC) is a derivative of cellulose, which is obtained from the nanoscale synthesis of cellulose. Cellulose is considered as the inexhaustible natural biopolymer which possesses some attractive features such as high porosity, large surface area, cost-effectiveness, excellent adhesion characteristics, biocompatibility etc. Mainly, NC is synthesized from cellulose to overcome hierarchical structural imperfections (Wang *et al*., 2014). Due to these advantages, NC has been produced on large scale in recent years and utilized in different fields of electrochemistry. In addition, NC possesses some unique features such as improved mechanical characteristics, thermal stability, biodegradability, biocompatibility and is eco-friendly. NC is comprised of several cellobiose units which have free six hydroxyl groups, one acetal linkage and one hemiacetal linkage that are inter-connected through strong hydrogen bonds. These hydrogen bonds help to provide NC with an axial elastic modulus structure and a surface sufficed with hydroxyl groups. As NC contains a substantial amount of hydroxyl groups, it facilitates the modification and penetration of new binding sites for the attachment of specific analytes (Shalauddin *et al*., 2019). Due to these physicochemical properties, NC

is considered a potential candidate to be conjugated with other functional materials such as graphene (Hou *et al*., 2019), polypyrrole (Shahnaz *et al*., 2020), carbon nanotubes (Xu *et al*., 2020) etc. Among the electronically conductive polymers (ECP), polypyrrole (PPY) has gathered particular interest due to its high electrical conductivity, biocompatibility, good stability, proper redox characteristics and ease of polymerization process compared to other ECP (Tasrin *et al*., 2020).

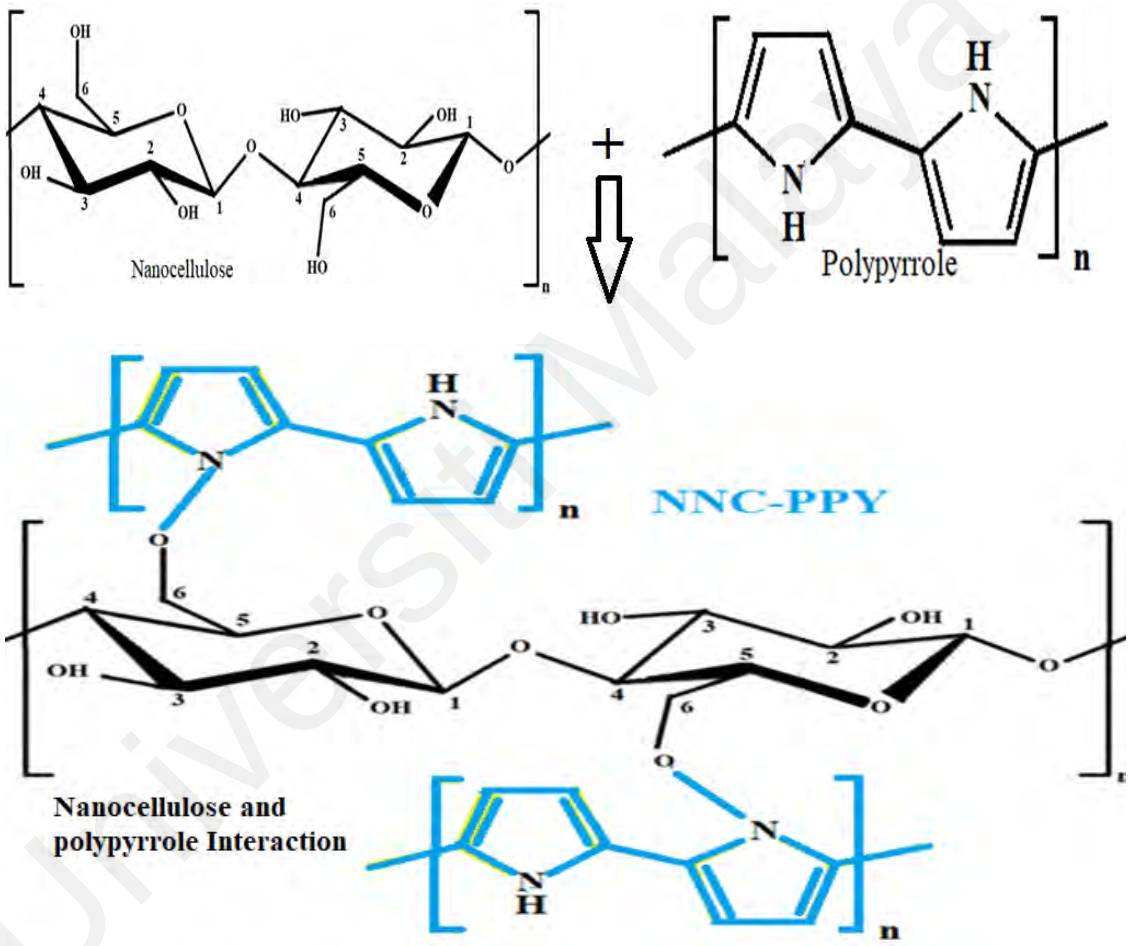

Figure 6.1: Nanocellulose polypyrrole interaction through hydrogen bonding.

The chemical polymerization procedure was chosen for the formation of NC-PPY nanocomposite. There are several reasons behind choosing chemical polymerization over other procedures. Unlike electrochemical polymerization, this process does not require any conducting substrate and is easy to scale up. Chemical polymerization of PPY on NC substrate has several advantages such as process ability, cost-efficiency and eco-

friendliness of the substrate (Nystrom *et al*., 2010). The NC-PPY nanocomposite is electroactive and shows good electroconductivity which retains the fibrous configuration of the nanocellulose with a high surface area compared to pure cellulose. This nanocomposite can be synthesized with approximately 98% of porosities which increases the surface areas ultimately (Hebeish *et al*., 2016). The PPY coating on the NC fibers surface can be demonstrated by some characteristics, where the fibers of NC are properly immersed and wetted by the PPY. Both NC and PPY can form hydrogen bonds through OH- and NH- groups, respectively, which demonstrates that both NC and PPY could be interconnected by strong hydrogen bonds (shown in Figure 6.1). During the chemical process, the inclusion of PPY on the NC fibers ultimately provide a mechanically robust configuration and a high porosity of the nanocomposite with a large active surface area (Mondal, 2018). Moreover, the addition of PPY on NC fibers creates more conductive paths through the material which might accelerate the transport of charge and ions and thus enhance the electro-conductive backbone of the nanocomposite which can actively and spontaneously interact with the specific analyte. The fibers of NC are encapsulated by the layers of PPY which provide a 3D structure and contribute to the enhanced electrochemical response by allowing absorption of more analytes on the surface of NC-PPY nanocomposite (Wang *et al*., 2015). Dulaimi *et al* and his team reported the nanocomposite of nanocellulose/polypyrrole to investigate the electrochemical characteristics (Al-Dulaimi *et al*., 2018). While another work has been reported on freestanding nanocellulose-composite fiber reinforced 3D polypyrrole electrodes for energy storage applications Wang *et al*. (2014).

Herein, we reported a nanocomposite of NC-PPY modified sensor for the first time for the simultaneous determination of PCT and CPR. The excellent and improved electrochemical conductivity with porous appearance enables a new avenue for the detection of PCT and CPR simultaneously. The NC-PPY/GCE sensor showed excellent

stability, repeatability and reproducibility with broad linear ranges and low LOD for the detection of PCT compared to previous reports (shown in Table 6.1). The NC-PPY/GCE sensor was applied for the simultaneous detection of PCT and CPR in biological fluid and pharmaceutical preparations with great recoveries.

6.2 Experimental section

6.2.1 Chemicals and Instrumentation

Paracetamol (PCT), Ciprofloxacin (CPR), Nanocellulose (NC), Sulphuric acid (H_2SO_4) and Hydrochloric acid (HCl) were purchased from Sigma Aldrich (Malaysia). Cellulose powder (microfibrillated cellulose source: cotton linter) and Pyrrole were obtained from Fischer scientific (Malaysia), Iron chloride ($FeCl_3$), Dipotassium hydrogen phosphate (K_2HPO_4), Potassium dihydrogen phosphate (KH_2PO_4) were purchased from Fluka (Malaysia). Adequate amounts of PCT and CPR were used and dissolved in deionized water (DI) to prepare the individual stock solutions. All reagents were of analytical grade and utilized as received without any further treatment. 0.1 M phosphate buffer solution pH 7.0 was prepared by mixing 0.662 gm of K_2HPO_4 and 0.844 gm of KH_2PO_4. Human blood serum was collected from a healthy volunteer from University Malaya Hospital.

An Autolab PGSTAT 302N electrochemical workstation was utilized as the electrochemical detection platform with a glassy carbon electrode (GCE) as the working electrode with 3 mm diameter, a platinum wire as counter electrode and Ag/AgCl (3.0 M KCl) as a reference electrode. All the electrochemical experiments were performed at room temperature. Deionized water (18.2 MΩ cm) was purified by a PURELAB flex system (Elga Water, Veolia, France) and used to prepare an aqueous solution throughout the experiment. A pH meter (Cyberscan 500 digital) connected with a glass electrode

(EUTECH Instruments, USA) was used to prepare and adjust the pH of the solution. Sonic 3 ultrasonic bath (Polsonic, Poland) and vortex (IKA, Germany) were used for proper dispersion of the nanomaterials. Fourier transformed infrared (FTIR) spectroscopy was performed FTIR spectrometer (Spectrum 2000, Perkin Elmer) between 500–4000 cm^{-1}. X-ray diffraction (XRD) patterns were analyzed using a Rigaku DMAX 2000 diffractometer equipped with Cu-Kα radiation (λ = 0.15405 nm, 40 kV, 40 mA). The morphological image was recorded by transmission electron microscopy (TEM) (JEM 1400, JEOL, Japan)

6.2.2 Methodology

For the synthesis of NC, the acid hydrolysis method was used while the NC-PPY nanocomposite was synthesized by the chemical polymerization method and drop-casted on GCE. The morphological properties were characterized by TEM, XRD and FTIR spectroscopy. Before the electrochemical experiments, pH and scan rate were optimized. CV and SWV methods were employed to investigate the electrochemical behaviour of the NC-PPY/GCE sensor. Satisfactory relative standard deviation and recovery values were obtained from the real sample analysis.

6.2.3 Synthesis of NC

The synthesis procedure of nanocellulose was explained in chapter 3, section 3.2.6.

6.2.4 Synthesis of NC-PPY nanocomposite

The nanocomposite of NC-PPY was synthesized according to the previous literature (Tasrin et al., 2020). The micro fibrillated cellulose powder and pyrrole were used as the starting materials for the synthesis of NC-PPY nanocomposite. Firstly, 12 gm of 2 wt % micro fibrillated cellulose hydrogel (240 mg of dry cellulose content) was

dispersed in 100 mL of DI water and mixed homogenously. Then the PPY solution was prepared by mixing 3 mL of pyrrole solution (0.043 M) in 100 mL of water. The PPY solution was added gradually to the cellulosic suspension. To prepare the $FeCl_3$ solution, 8 gm of $FeCl_3$ (0.030 M) was dissolved in 100 mL of water and mixed well. Next, the $FeCl_3$ solution was added to the cellulose-PPY dispersion to initiate the polymerization process. 160 µL of 37% HCl was added gradually in the reaction beaker. After 15 min of polymerization, the resulting PPY coated cellulosic fibers were rinsed thoroughly in DI water in a Buchner funnel using a filter paper. Finally, the PPY-NC cake was obtained after the removal of filter paper which was placed on a petri dish and air-dried properly to turn into a constant mass.

6.2.5 Fabrication of NC-PPY /GCE modified electrode

Before the fabrication step, a glassy carbon electrode (GCE) was polished to obtain a mirror-like surface, on the micro-cloth pad with alumina slurry. Then the GCE was ultra-sonicated in ethanol and then in DI water for 2 min and dried properly in ambient temperature. 1 mg of synthesized NC-PPY solid mass was dissolved in 2 mL of DI water to form a homogeneous suspension applying ultra-sonication energy for 30 min. 6 µL of NC-PPY suspension was micro-pipetted and drop-casted on the GCE surface and dried properly at ambient temperature (electrode fabrication shows in Figure 6.2).

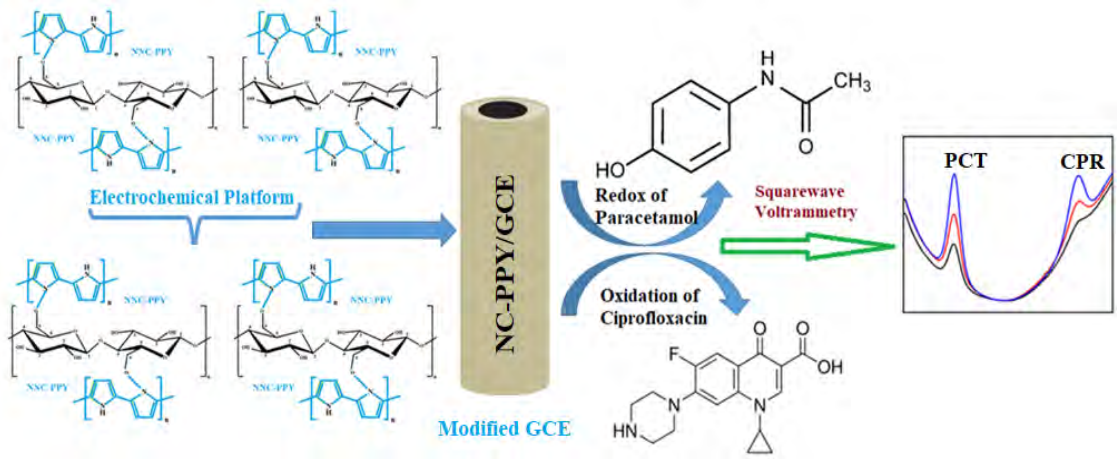

Figure 6.2: Fabrication of NC-PPY modified GC electrode for the detection of PCT and CPR

6.3 Aim of the research

This study aims to develop an electrochemical sensor based on the NC and conductive polymer PPY. The combination of NC-PPY nanocomposite showed high electro-conductivity with an increased porosity of the surface area compared to the NC alone. The proposed fabricated sensor showed excellent selectivity toward the detection of PCT and CPR.

6.4 Results and Discussions

6.4.1 Surface Morphology of modified electrode

Scanning electron microscopy (SEM) and transmission electron microscopy (TEM) were employed to investigate the morphology of the modified electrode. Figure 6.3A shows the dispersion of NC. Figure 6.3B shows a uniform mixture of NC-PPY fibers with a porous foam-like network composed of NC-PPY. Figure 6.3C, clearly exhibits that the fibers of NC entangled and embedded on the layer of PPY and formed a 3D network (Wang *et al*., 2014). The layer of PPY was coated on the NC fibers. Figure 6.3D is the magnified image of Figure 6.3C.

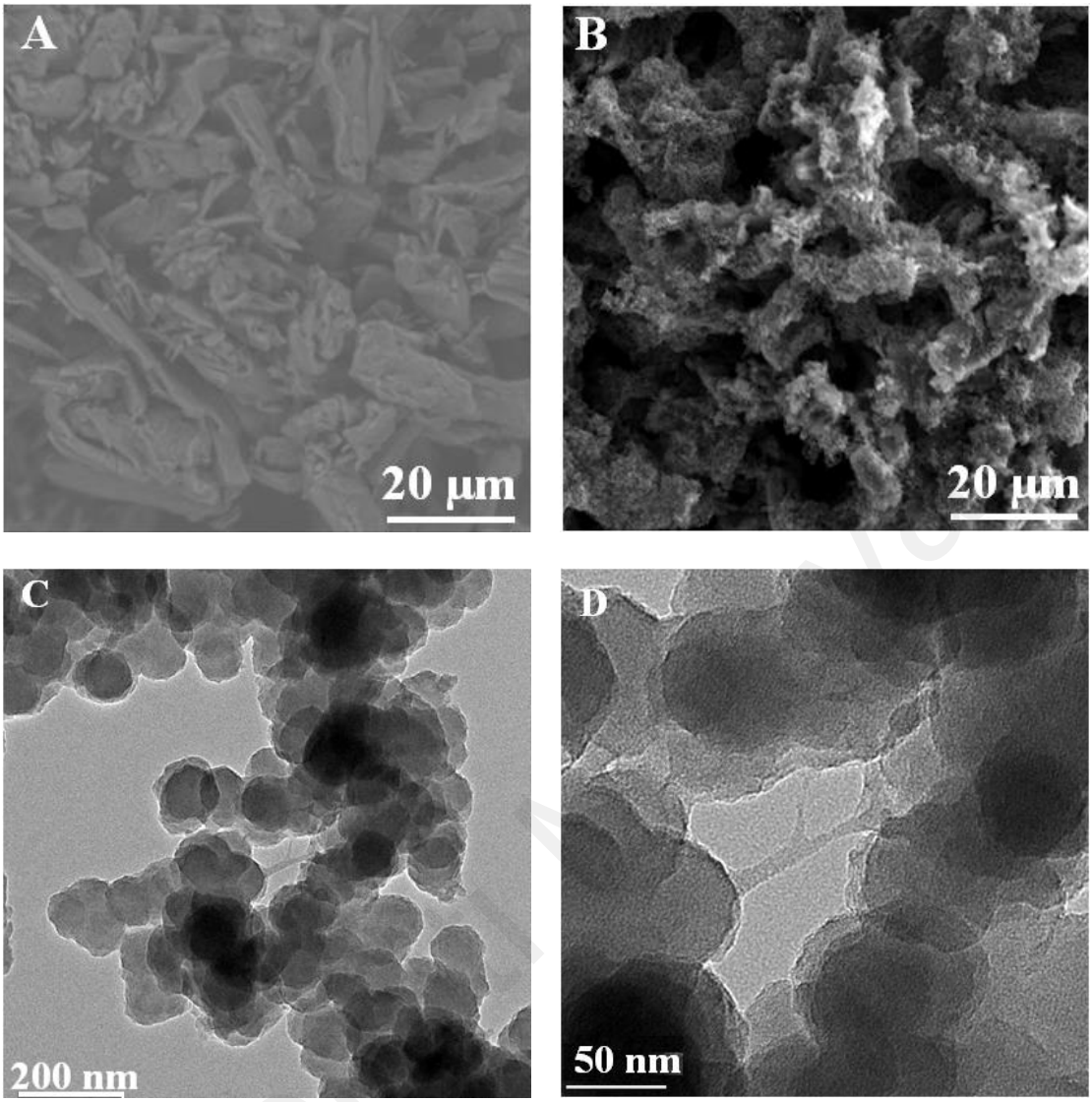

Figure 6.3: SEM image of (A) NC, (B) NC-PPY and TEM images of (C) NC-PPY, (D) NC-PPY (higher resolution).

6.4.2 Structural Characterizations NC-PPY nanocomposite

The as-prepared NC and NC-PPY nanocomposites were studied by different techniques to investigate their morphological and structural compositions to determine their properties. The FTIR was performed to determine the presence of functional groups and chemical compositions of NC and NC-PPY. Figure 6.4A shows the FTIR spectra of cellulose (a), NC (b) and (c) NC-PPY. Curve a and b shows broad FTIR peaks between 3326 and 3339 cm^{-1} which confirms the free OH stretch. Both the cellulose and NC showed a characteristic peak at around 2900 cm^{-1} that is attributed to the C-H stretch. NC

contains a higher density of OH groups than cellulose. Due to the chemical treatment, the spectrum of NC contains the transmittance peaks that appear around 1645 cm^{-1} and confirms the bending vibration of the absorbed H_2O. In curve b, the characteristic peaks are sharper than curve a (Shalauddin *et al*., 2019). Some characteristic C-C stretch, C-O-C Stretch from the pyranose ring appear around approximately 1155 cm^{-1} and 1050 cm^{-1}. Curve c shows the characteristic bands at 1540 and 1450 cm^{-1} which could be assigned to the C-C and C-N stretching vibrations present in the pyrrole ring. It is noted that the bands assigned for the free OH groups of cellulose are weakened in the NC-PPY nanocomposite. In addition, the increase of the C-C and C-N bands are observed which indicates the layer of PPY on the surface of NC (Muller *et al*., 2013).

The crystalline properties of NC (a) and NC-PPY (b) nanocomposite were studied by XRD and illustrated in Figure 6.4B. The diffraction pattern for the powdered NC shows some distinct peaks at $2\Theta = 15.44°$, 22.62° and 34.66° and which could be assigned to the presence of NC (Shalauddin *et al*., 2019). The broad peak at 15.44° and 22.62° is attributed to the amorphous and crystalline regions of the NC respectively. Typically, the peak of PPY appears at $2\Theta = 26.05°$ which is distinctly shown in curve b but this peak is absent in curve a. The distinctive peak of curve a is present in curve b but is slightly shifted with decreased peak intensity. From this result, it is confirmed that the crystalline structure of the NC is not hampered by the acid hydrolysis treatment and the presence of PPY through chemical polymerization (Shahnaz *et al*., 2020).

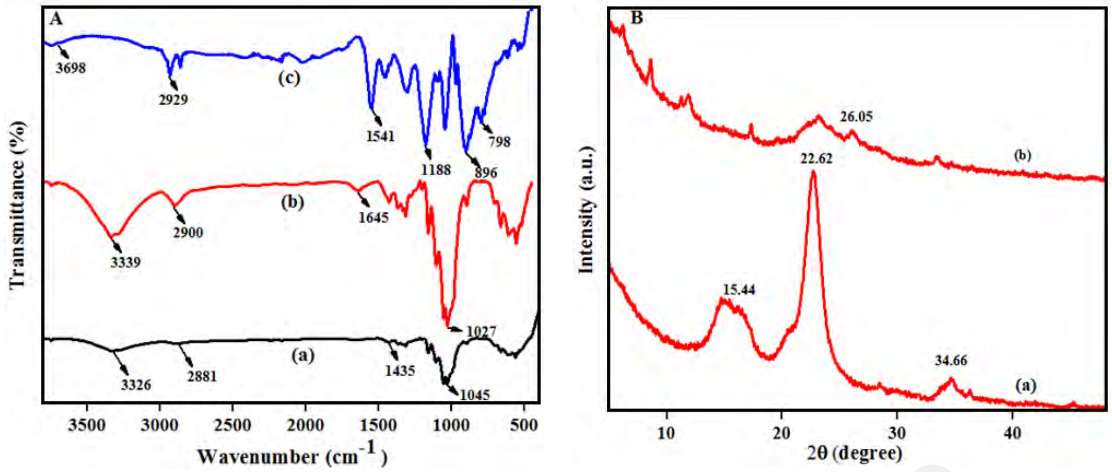

Figure 6.4: FTIR spectra of (A) cellulose (a), NC (b), NC-PPY(c) and XRD spectra of (B) NC (a), NC-PPY (b)

6.4.3 Electrochemical Characterization of sensor

The EIS study was conducted to investigate the interfacial electron transfer properties on the electrode-electrolyte interface. The optimized operational parameters for the study were; the frequency ranges from 100 kHz to 100 mHz and V_{rms} potential of 10 mV. The data is shown in Figure 6.5 as the Nyquist plot of different electrodes, the bare GCE (a), NC/GCE (b), NC-PPY/GCE in the presence of 0.1M KCl and 5mM $[Fe(CN)_6]^{3-/4-}$. The GCE possesses the largest R_{ct} value of 280 Ω which could be attributed to the very poor interfacial electrons transfer. The R_{ct} value for NC/GCE is 185 Ω which is due to the comparatively lower electrical conductivity of the GCE and 63 Ω for NC-PPY/GCE. The smallest R_{ct} value is achieved by the NC-PPY/GCE which is due to the extra-ordinary electrical conductivity and improved electrons transfer across the surface of the electrode showing the smallest charge transfer resistance. The R_{ct} values can be represented by the decreasing order of: GCE > NC/GCE > NC-PPY/GCE: 280 Ω > 185 Ω > 63 Ω. The plots have a semi-circular segment which is at a higher frequency and the linear segment comparatively at a lower frequency. The Nyquist plot is presented in the form of Randle's equivalent circuits (shown in inset). Here, the components of this

circuit are the electron transfer resistance (R_p), constant phase element (CPE), solution resistance (R_s) and Warburg impedance (W).

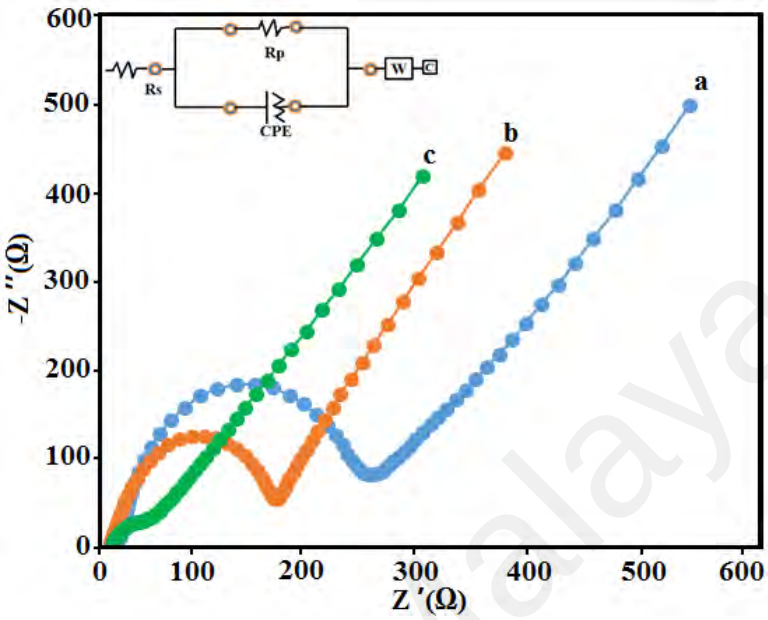

Figure 6.5: The Nyquist plots of bare GCE (a), NC/GCE (b) and NC-PPY/GCE (c) in 0.1 M KCl solution with 5.0 mM $[Fe(CN)_6]^{3-/4-}$. Inset is the equivalent circuit for the fitting.

6.5 Electrochemical behaviour of NC-PPY/GCE modified electrode

6.5.1 Electrochemical investigation of PCT and CPR

The electrochemical response of an electrode towards the target analyte is measured by the redox potential and the corresponding current. Cyclic voltammetry was performed to investigate the electrochemical response of bare GCE (a), NC/GCE (b), NC-PPY/GCE (c) in the presence of 45 µM PCT, 30 µM CPR and 0.1 M PBS pH 7.0 at 0.1 V s^{-1}. In Figure 6.66, the bare GCE shows very little irreversible oxidation peak for PCT and CPR at 0.56 V and 1.02 V, respectively. No reduction peak was obtained for the PCT at the bare GCE in the applied potential window. The electron transfer on the surface of the electrode is poor due to the lower conductivity of the bare GCE. On the other hand, when the surface of GCE is modified with NC, a couple of slightly increased oxidation

peaks for PCT and CPR are appeared at 0.51 V and 0.99 V, compared to bare GCE. No reduction peak of PCT was observed. This could be because, NC is not so conductive and could not sufficiently promote the electron transfer process alone (Wang *et al*., 2014). In addition, when the GCE is fabricated with NC-PPY, the voltammetric responses for PCT and CPR are increased dramatically. The NC-PPY/GCE exhibits high background current response which indicates a better electrochemical response than the bare GCE and NC/GCE. A pair of distinct redox peaks and an oxidation peak for PCT and CPR are appeared at 0.47 V and 0.98 V, respectively. The redox peak of PCT is shifted negatively at 0.47 V, while the oxidation peak of CPR is shifted in the same direction at 0.98 V. The NC-PPY/GCE nanocomposite exhibits the highest background current response towards the redox peak of PCT and oxidation peak of CPR compared to the bare GCE and NC/GCE, which could be due to the porous appearance of the surface with an extended surface area that allows access of more analyte on the surface of the electrode and faster electrons transfer process (Wang *et al*., 2015). The current response of PCT and CPR are reinforced due to the excellent conductivity and higher active surface area of the NC-PPY/GCE. Thus, this indicates that the NC-PPY/GCE has greater electrocatalytic efficiency towards the redox peak current of PCT and oxidation peak current of CPR.

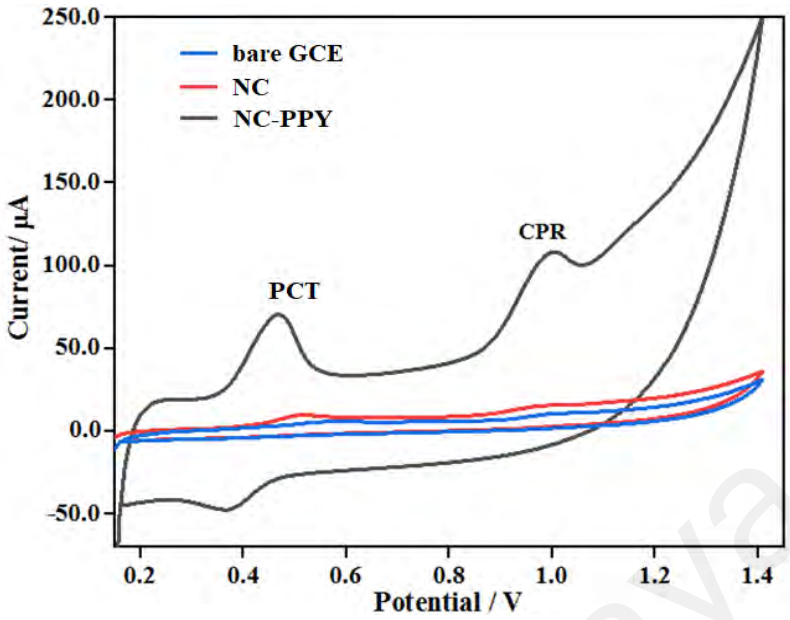

Figure 6.6: CVs of 45 µM PCT and 30 µM CPR in 0.1 M PBS (pH 7.0), potential range 0.2 V to 1.4 V and scan rate at 0.1 Vs^{-1} on (a) bare GCE, (b) NC/GCE and (c) NC-PPY/GCE.

6.5.2 Scan rate study

To investigate the mechanism of reactions for PCT and CPR, the influence of the scan rate on the peak current and peak potential was studied. The CV of 45 µM of PCT and 30 µM of CPR at NC-PPY/GCE in the presence of 0.1M PBS pH 7.0 was recorded at different scan rates from 50- 500 mV s^{-1} (Figure 6.7A). The result shows a linear increment of the redox peak current of PCT and oxidation peak current of CPR with the scan rate. This entailed that the electrochemical reactions of PCT and CPR on the NC-PPY/GCE follow an adsorption controlled mechanism (Pollap *et al*., 2020). PCT and CPR are organic compounds in nature and both contain benzene rings in their structure. Thus, the van der Waals force is formed between the PCT and NC-PPY while electrostatic interactions are formed between the CPR and NC-PPY and both are absorbed on the surface of NC-PPY/GCE (Anuar *et al*., 2018; Matsunaga *et al*., 2020). In addition, a variation of the redox peak current of PCT and the oxidation peak current of CPR are observed with the changes of scan rates, which reveals that the electrochemical redox

reaction of PCT and oxidation reaction of CPR is surface controlled process on the NC-PPY nanocomposite (Pollap *et al*., 2020). The oxidation currents of PCT and CPR are shifted toward the positive direction which is due to the kinetic effect of the NC-PPY on the oxidation of PCT and CPR (Figure 6.7 B & C). The obtained regression relationship for PCT and CPR is as follows

$$I_{pa}\,(\mu A) = 0.676\,\upsilon + 14.142\ (R^2 = 0.989)\quad (PCT) \tag{6.1}$$

$$I_{pc}\,(\mu A) = -0.087\,\upsilon + 4.989\ (R^2 = 0.975)\ (PCT) \tag{6.2}$$

$$I_{pa}\,(\mu A) = 1.409\,\upsilon + 13.026\ (R^2 = 0.996)\ (CPR) \tag{6.3}$$

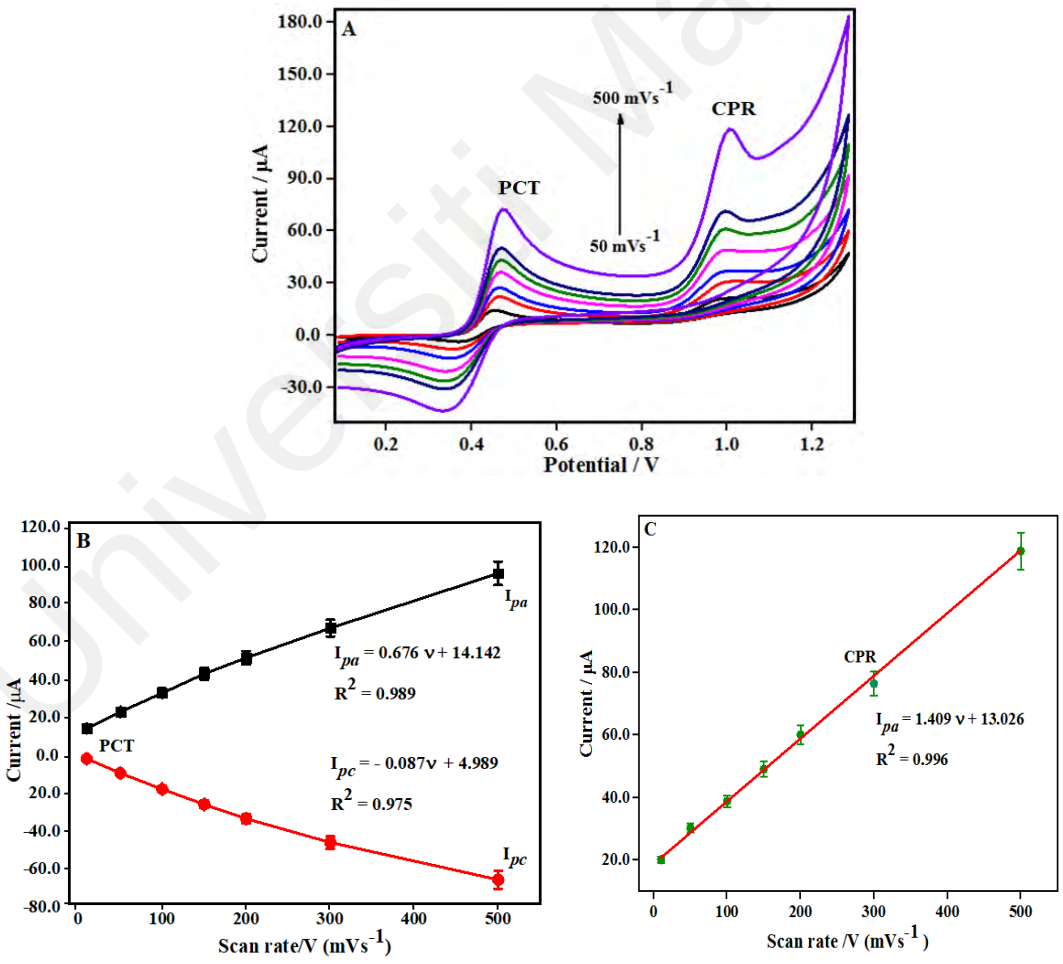

Figure 6.7: (A) CVs of 45 µM PCT and 30 µM CPR on NC-PPY/GCE at 50 mV s^{-1} to 500 mV s^{-1} in 0.1 M PBS (pH 7.0). (B). the plot of redox peak current vs. scan rates of PCT (black line for oxidation of PCT and red line for reduction of PCT). (C). the relationship between anodic peak current vs. scan rate of CPR.

6.5.3 Influence of different pH values

As both PCT and CPR are oxidizable and electroactive compounds, the electrochemical behaviour of PCT and CPR at NC-PPY/GCE is greatly influenced by the presence of different pH (Anuar *et al*., 2018; Bonyadi *et al*., 2020). To investigate the influence of different pH values, cyclic voltammograms of 45 µM PCT and 30 µM CPR was recorded at 0.1 V s^{-1} in the presence of 0.1 M PBS pH 7.0 in different pH ranges from pH 4-10 as shown in Fig. 6.8A. It is observed that the most intense anodic peak potential for PCT and CPR were obtained at pH 7.0 (Fig 6.6A). In addition, when the pH increases from 4-10, the redox peak potential of PCT and oxidation peak potential of CPR are gradually shifted to the negative region. The oxidation peak potential of PCT is shifted from 0.66 V to 3.7 V, while the oxidation peak potential of CPR is shifted from 1.18 V to 0.7 V. This indicates that the oxidation of PCT and CPR, and the electrochemical reactions of PCT and CPR require proton transport (Pollap *et al*., 2020). Figure 6.8B and 6.8C show the relationship between the anodic peak potential (E_{pa}) and different pH for PCT and CPR, respectively. From both of the graphs (6.8B and 6.8C), a linear relationship between E_{pa} and different pH values was observed with a slope value of -0.051 V pH^{-1} and -0.050 V pH^{-1} for PCT and CPR respectively. The linear regression equations for the oxidation peak potential of PCT and CPR (Figure 6.8 B and C) are as following:

$$E_p \text{ (PCT)} = -0.051 \text{ pH} + 0.771 \ (R^2 = 0.998) \quad (6.4)$$

$$E_p \text{ (CPR)} = -0.050 \text{ pH} + 1.374 \ (R^2 = 0.992) \quad (6.5)$$

From the equations 6.4 and 6.5, it was observed that both the slope value of PCT and CPR are very close to the Nernst equation value (0.059 V pH^{-1}), indicating that the number of exchanged electrons and protons are similar in the reactions of PCT and CPR (n= 2) which is shown in Appendix 6.1 (Pollap *et al*., 2020). From Fig. 6.8D and 6.8E for

PCT and CPR, an enhancement of the peak current is observed when the pH changes from 4.0 to 7.0 but declined beyond the pH 7.0. Due to low current detection, the oxidation reactions for both PCT and CPR seemed to be less favourable in low and high pH values. Based on the experiments, pH 7.0 was chosen as the optimum pH for the determination of PCT and CPR in the following experiments. This investigation reveals that the electrochemical reactions of PCT and CPR at NC-PPY/GCE is dependent on the pH and NC-PPY exhibited great improvement of the oxidation peak current of PCT and CPR and minimized the overpotential.

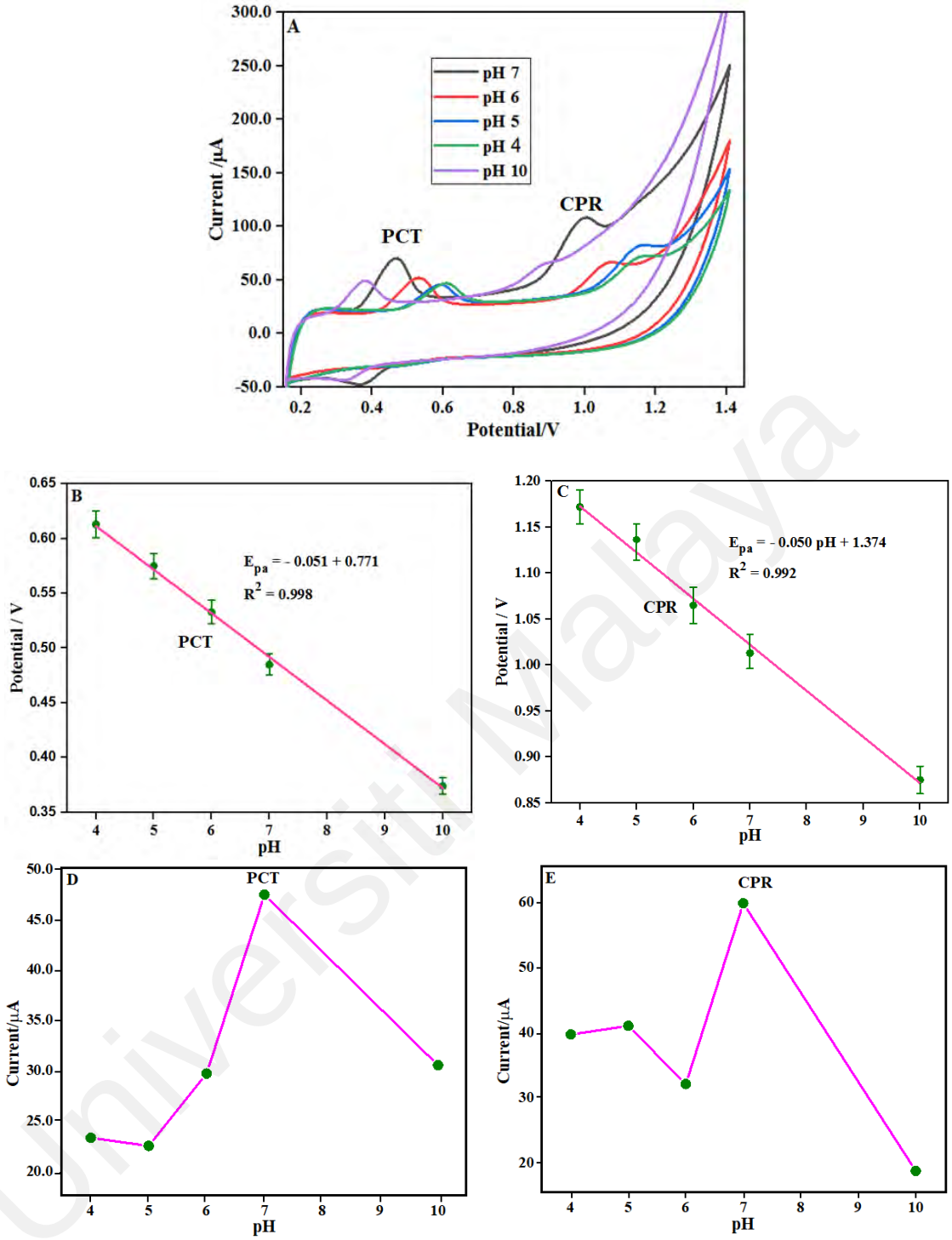

Figure 6.8: The CVs of 45 µM PCT and 30 µM CPR at the NC-PPY/GCE at different pH: 4.0, 5.0, 6.0, 7.0, and 10.0 at 0.1 V s^{-1}. (B) The plot of oxidation peak potential vs. pH of PCT. (C) the plot of oxidation peak potential vs. pH of CPR. (D) the plot of the oxidation peak current vs. pH of PCT. (E) the plot of the oxidation peak current vs. pH of CPR.

6.6 performance Evaluation of NC-PPY/GCE sensor

6.6.1 Analysis of limit of detection of sensor

The quantitative analysis of the proposed NC-PPY/GCE sensor was performed for the simultaneous determination of PCT and CPR using the squarewave voltammetric method by measuring some crucial analytical parameters such as linear range, the limit of detection, reproducibility and selectivity test. SWV is a more sensitive technique than a CV in terms of low detection limits and resolution. Some functional parameters such as frequency (*f*), amplitude (a) and step potential (Es) were optimized during the experiments by changing a single parameter while the other two parameters remained unchanged. The optimized functional parameters were frequency (*f*) = 23 Hz, (a) = 45 mV and (Es) = 2 mV. Figure 6.9A shows the effect of the various concentration range of PCT (0.05-70.0 μM) and CPR (0.01-80 μM) at NC-PPY/GCE in the presence of 0.1M PBS pH 7.0 at 0.1 V s^{-1}. A gradual increment of the oxidation peak currents of PCT and CPR are observed with the increment of the concentrations of PCT and CPR. The calibration plot was drawn between the oxidation peak current and varied concentrations of PCT using a linear segment, from 0.05 - 70 μM (Fig. 6.9B). Similarly, for the CPR, the linear segment of the calibration plot starts from 0.01 – 80 μM (Fig. 6.9C). The linear regressions for the calibrated ranges are the following:

$$I_p\,(\mu A) = 1.245C + 13.423 \quad (0.50\text{-}70\ \mu M)\ \ (PCT)\ \ (R^2 = 0.998) \tag{6.4}$$

$$I_p\,(\mu A) = 1.706C + 52.572 \quad (0.01\text{-}80\ \mu M) \quad (CPR)\ \ (R^2 = 0.998) \tag{6.5}$$

The LOD value of PCT and CPR are calculated as the linear regression equation (Eq. 6.4 and 6.5) respectively, by applying a signal to noise ratio S/N = 3. A comparison is summarized in table 1, based on the present work and previous studies in terms of LOD and linear ranges. It is observed that the NC-PPY fabricated GCE showed impressive

results with lower detection limits and broad linear ranges compared to the other modified electrodes. These results show that the excellent electro-conductivity with porous configuration and a mechanically robust structure of the 3D network greatly enhance the electrochemical performance of the NC-PPY/GCE fabricated sensor for the simultaneous determination of PCT and CPR with very low concentration ranges.

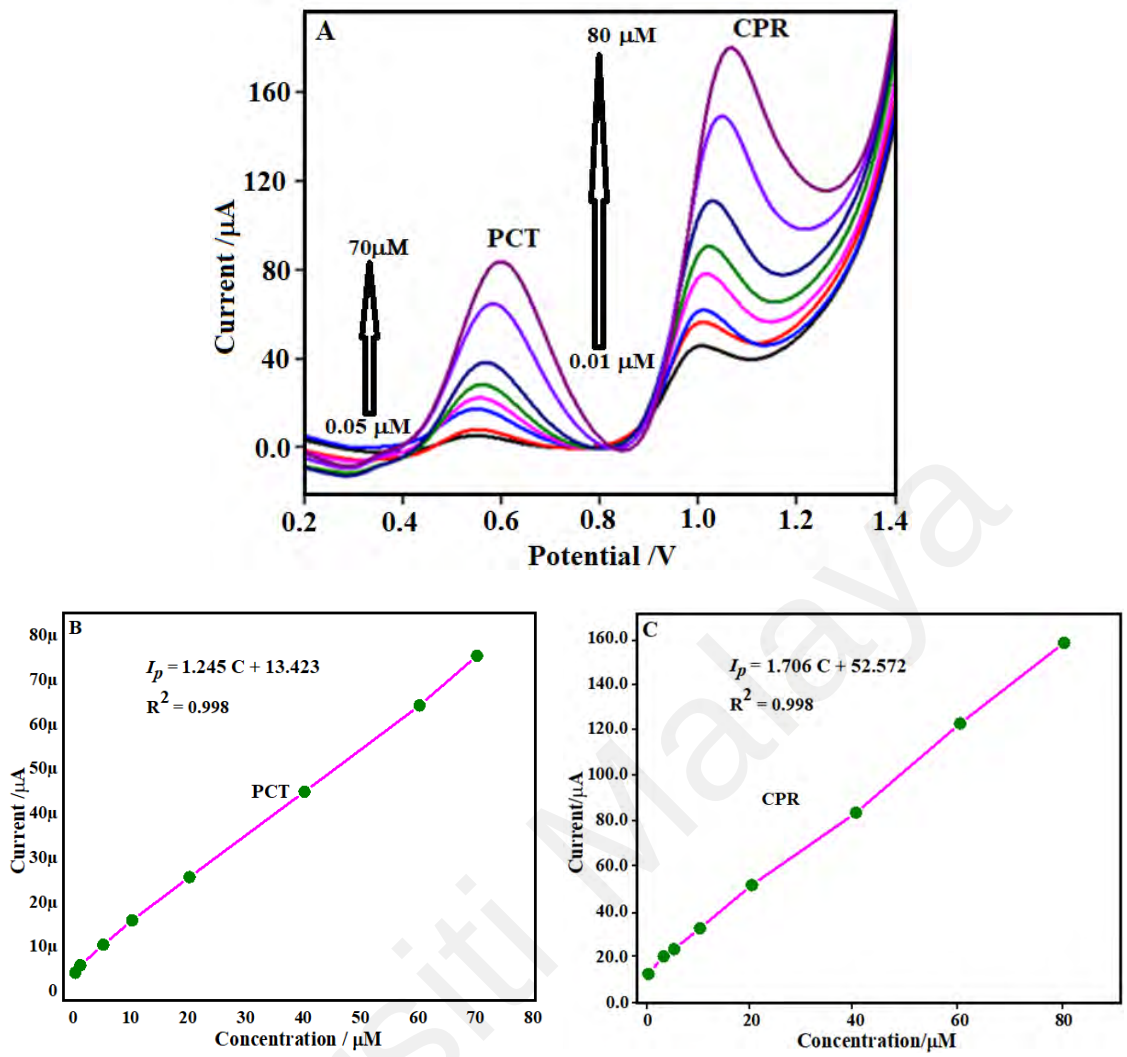

Figure 6.9: (A) SWV at NC-PPY/GCE at different concentrations of PCT (0.05–70 µM) and CPR (0.01–80 µM) in 0.1 M PBS (pH 7.0) at 0.1 V s^{-1}, (B) Calibration curve of PCT concentration vs current (0.05 –70 µM), (C) Calibration curve of CPR concentration vs current (0.01 – 80 µM)

The performance of the NC-PPY/GCE sensor for the sensitive determination of PCT and CPR was compared with previous reports in terms of linear range and LOD as illustrated in table 1. It is observed that the linear range and LOD of NC-PPY/GCE sensor exhibited remarkable outcomes compared to other fabricated sensors such as biopolymer-based nanocomposites (Baccarin *et al*., 2017; Kalambate *et al*., 2020; Hu *et al*., 2018), biopolymer and conductive polymer-based nanocomposites (Kushwaha & Shukla, 2020; Bonyadi *et al*., 2020), graphene and CNT based nanocomposite (Baccarin et al., 2017; Yang *et al*., 2020; Hareesha & Manjunatha, 2020; Jin et al., 2020). These results suggest

that the extra-ordinary electrochemical conductivity and extended surface area with high porosity could greatly increase the electrochemical performance of the NC-PPY/GCE sensor for the sensitive determination of PCT and CPR at very low concentrations.

Table 6.1: A comparison of various electrodes for the simultaneous determination of PCT and CPR

Electrode	Methods	Linear range (PCT & CPR) (μM)	Detection limit (PCT & CPR) (nM)	Reference
CQDs/ZnO-NFs/Poly (CTAB)/GCE	DPV	0.05–30.0 & 0.01–30.0	2.47 & 1.97	(Hatamluyi *et al*., 2020)
Sm_2O_3-9-3/GP	DPV	0.01 – 300 & 0.05 – 170	0.1 & 5	(Biswas *et al*., 2020)
mpg-C_3N_4/PANI/CdO	DPV	0.1 – 790 & 0.01 – 250	26 & 5	(Bonyadi *et al*., 2020)
NiONPs-GO-CTS: EPH/GCE	SWV	0.10-2.9 & 0.040–0.97	6.7 & 6.0	(Santos *et al*., 2017)
Tio2/PB/AuNPs/CMK3 /Nafion/GE	CV	1–10 & 10–52	108 & 210	(Pollap *et al*., 2020)
CZF-CME	Adsv	0.909 - 4700 & 0.185 – 476	2.58 & 88.5	(Kingsley *et al*., 2016)
NC-PPY/GCE	SWV	0.05 – 70 & 0.01 – 80	1.5 & 0.95	**This work**

6.6.2 Repeatability, reproducibility and stability

The individual solutions of PCT and CPR were prepared freshly and analysed six times using NC-PPY/GCE. The corresponding relative standard deviation values for PCT are 2.75% and for CPR were 3.65%, respectively confirms the NC-PPY/GCE sensor has good repeatability. The fabricated sensor was kept in a clean environment and the electrochemical signal was investigated for three consecutive weeks (Fig. 6.10). After three consecutive weeks, the current responses of the NC-PPY/GCE electrode are 98.97%, 96.22%, 91.06% for PCT and 98.66%, 97.57%, 91.51% for CPR, from its initial current response. Furthermore, the reproducibility was investigated from the response of

another six individual electrodes using the above concentrations of PCT and CPR. The calculated RSD values for PCT and CPR solutions are 3.55% and 4.35%, respectively which confirms the good reproducibility of the NC-PPY/GCE electrode.

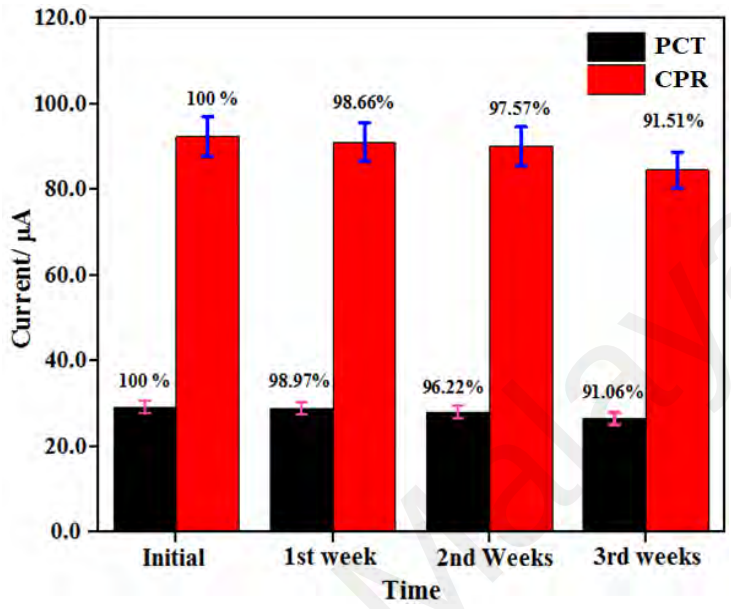

Figure 6.10: Bar diagram shows the stability of NC-PPY/GCE modified electrodes for the determination of PCT and CPR for three consecutive weeks.

6.6.3 Interference Study

The selectivity of the fabricated sensor is an important parameter for a successful sensor which is investigated by the interference test (Akhter et al., 2020a). Under identical conditions, the test was performed in the presence of a wide range of interfering compounds with a similar structure to PCT, such as para-aminophenol and acetanilide, antibiotics such as penicillin, tetracycline and metronidazole and ions such as NO_3^-, SO_4^-, CO_3^- and ascorbic acid (AA), dopamine (DA) and uric acid (UA) etc. Furthermore, the spiked concentrations of PCT and CPR are 8 µM and 12 µM, while 45 µM of para-aminophenol and acetanilide, 50 µM of the antibiotics, 40 µM of ions and 60 µM of AA, DA and UA were utilized. From Figure 6.11, it is clear that the peak currents of PCT, CPR and DA are well-separated, which demonstrated that the presence of the potential

interfering compounds did not interfere with the current responses of PCT and CPR. The results confirmed that the fabricated NC-PPY/GCE sensor is highly specific and selective for the detection of PCT and CPR from the biological media and pharmaceutical dosage forms.

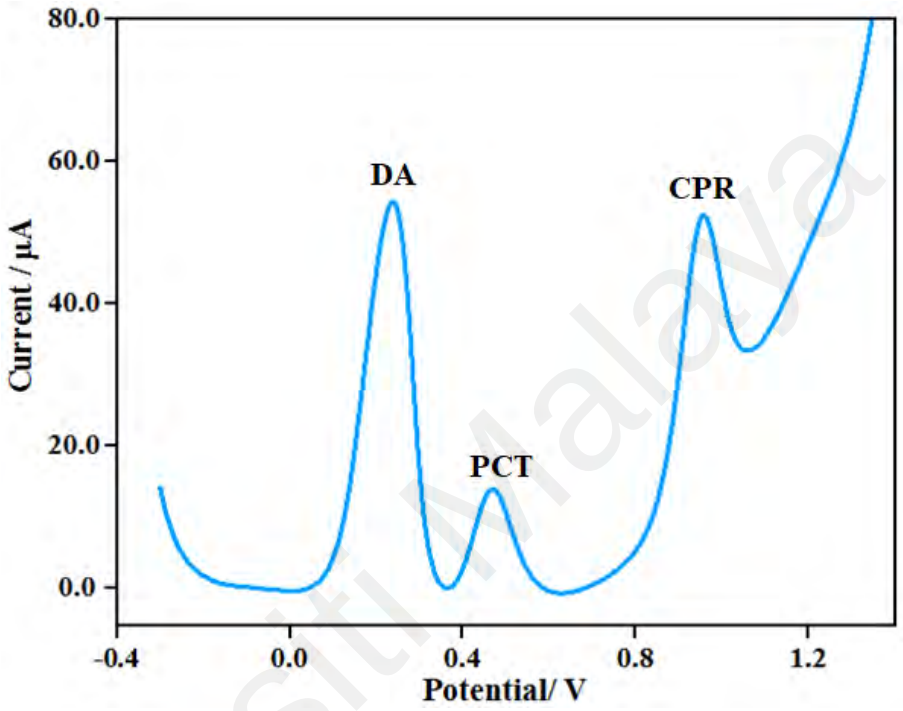

Figure 6.11: SWV signal on NC-PPY/GCE with 8.0 µM PCT and 12µM CPR and 100 fold excess concentration of common interfering compounds such as uric acid (UA), ascorbic acid (AA), dopamine (DA), lactose, fructose, sucrose and glucose, in 0.1 M PBS (pH 7.0) at 0.1 V s^{-1}.

6.6.4 Analysis of the real samples

The drug-free human blood serum and urine samples from the University of Malaya Hospital (Kuala Lumpur, Malaysia), was preserved properly in a refrigerator. The blood collection procedure was mentioned in (section 3.2.8). 10 mL of human blood serum was centrifuged at 2000 rpm for 15 minutes. The supernatant was filtered by a filter paper (0.45 mm). 0.1 M PBS pH 7.0 was added to the filtered solution for dilution. The tablet dosage forms of PCT and CPR were collected from a local pharmacy and crushed into fine powder to prepare the solution by dissolving DI water. Then the

solutions of PCT and CPR were filtered and diluted using 0.1 M PBS. The investigation of the practical application of the fabricated NC-PPY/GCE sensor was studied using the human blood sample and pharmaceutical tablet dosage forms. The SWV method was utilized to determine the known concentrations of PCT and CPR using the standard addition approach. The recovery and relative standard deviation values (RSD %) for real samples of pharmaceutical tablets and blood serums were calculated from this experiment and shown in Table 6.2 and 6.3 respectively. The good recovery results and low RSD values confirm the suitability, efficiency and practical application of the NC-PPY/GCE sensor towards the detection of PCT and CPR.

Table 6.2: Determination of PCT and CPR in pharmaceutical preparations at NC-PPY/GCE using squarewave voltammetry.

Tablet	Sample	Labelled (μM)	Found (μM)	Recovery (%)	RSD (%)
PCT	1	5	5.05	101.00	0.55
	2	10	10.05	100.50	0.68
	3	15	14.96	99.73	0.96
CPR	1	5	5.06	101.20	0.75
	2	10	9.96	99.60	1.25
	3	20	20.05	100.25	1.15

Table 6.3: Determination of PCT and CPR in blood serum at NC-PPY/GCE using squarewave voltammetry.

Sample	Labelled (μM)	Found (μM)	Recovery (%)	RSD (%)	Sample
PCT	1	15	15.08	100.53	1.05
	2	20	20.02	100.10	1.46
	3	35	34.98	99.94	0.88
CPR	1	10	10.04	100.40	0.78
	2	20	20.0	100.25	1.35
	3	30	29.96	99.86	0.86

6.6.5 Determination of PCT and CPR in the water sample

The electrochemical performance of the NC-PPY fabricated sensor was further evaluated in real water samples using the standard addition approach. The sample lake water was collected from Tasek Varsiti Lake located in the University of Malaya campus, Kuala Lumpur, Malaysia. The lake water was preserved and filtered through 0.30 μm

membrane filters to eliminate the impurities. Then different concentrations of PCM and CPR (0.3 and 0.8 μM) were injected at the same time in the filtered lake water. The electrochemical response of the NC-PPY/GCE sensor in the detection of PCT and CPR is illustrated in table 3 in terms of recovery (%) and RSD (%). The excellent electrochemical response with the great recovery of 98 – 105 % for PCT, and 99 – 102% for CPR, with RSD values of 0.75 – 2.35% for PCT and 0.85 – 1.55% for CPR, confirming the feasibility and applicability of the proposed NC-PPY/GCE sensor for the simultaneous determination of PCT and CPR in the water samples.

Table 6.4: Analytical performance of NC-PPY/GCE sensors for the detection of PCT and CPR in water sample using squarewave voltammetry.

Sample		Spiked (μM)	Found (μM)	Recovery (%)	RSD (%)
Lake water sample	PCT	0.1	0.105	105.00	2.35
		0.5	0.490	98.00	1.05
		1.0	1.010	101.00	0.75
	CPR	0.5	0.510	102.00	1.25
		1.0	0.990	99.00	0.85
		2.0	2.010	100.50	1.55

7. Conclusions

In summary, a facile and selective electrochemical sensor electrode was prepared via drop cast dispersion method on the GCE surface by NC-PPY nanocomposite. The sensor showed excellent analytical response for the simultaneous determination of PCT and CPR in pharmaceutical preparations, biological fluids and water sample with a broad concentration range from 0.05 – 70 μM for PCT and 0.01 – 80 μM for CPR with great recoveries and a low detection limit of 1.5 nM for PCT and 0.95 nM for CPR. The NC-PPY/GCE sensor showed significant selectivity, reproducibility, repeatability and stability. All these acquired results proved that the NC-PPY/GCE sensor has great potential for the simultaneous determination of PCT and CPR in biological media, pharmaceutical dosage forms and water samples.

CHAPTER 7: CONCLUSIONS AND FUTURE WORK

7.1 Conclusions

The present research focuses the finding on the four research works which are as the following:

1. The synthesis of nanocellulose and functionalized multiwall carbon nanotubes, followed by the preparation of nanocomposite via drop-casting onto the surface of glassy carbon electrode for the electrochemical detection of painkiller drugs diclofenac sodium. The nanocellulose and functionalized multiwall carbon nanotubes were synthesized by the acid hydrolysis method. The electrochemical performances were investigated using cyclic voltammetry, electrochemical impedance spectroscopy and differential pulse voltammetry. The synthesized nanomaterials and nanocomposites were investigated for their structure and surface morphology using Fourier transformed infrared spectroscopy (FTIR), Raman spectroscopy, powder X-ray diffraction (XRD), atomic force microscopy (AFM), transmission electron microscopy (TEM), field emission scanning electron microscopy (FESEM). The morphological assessment confirms the spherical shapes of nanocellulose and functionalized multiwall carbon nanotubes, which are homogeneously distributed with a smooth and extended surface area with a porous appearance and high surface to volume ratio of the functionalized multiwall carbon nanotubes and nanocellulose. The outstanding electroconductivity of *f*-MWCNTs/NC/GCE facilitates the rapid electron transfer process. Here, NC not only prevents the leaching of nanomaterials but also promotes the ionic conductivity and promote more binding site with the presence of hydroxyl groups that could adsorb increased number of moieties efficiently. The *f*-MWCNTs/NC/GCE nanocomposite was utilized for the sensitive detection of DCF in biological fluids and pharmaceutical preparations. The electrode response was linear towards the DCF concentration range of 0.05 to 250 μM, and linear

range divided into two segments from 0.05 to 5.00 μM and 6.00 to 250 μM and a low limit of detection of 0.013 μM. The fabricated sensor showed good sensitivity and selectivity toward the electrochemical determination of DCF. The selectivity of the sensor was also investigated in the presence of various interfering substances mentioned in chapter 3. There was no signal detected except ascorbic acid and dopamine interference species which indicates that the proposed sensor electrode has high selectivity toward the electro-oxidation of DCF and is a potential candidate for the determination of DCF from pharmaceutical preparations and biological specimens with good stability and recoveries.

2. Another nanocomposite of nitrogen-doped graphene (NDG) and nanocellulose (NC) (NDG-NC) was fabricated for the simultaneous electrochemical determination of paracetamol (PCT) and naproxen (NPX). Here, NC was synthesized followed by the same acid hydrolysis method while NDG was synthesized by the microwave-assisted method. An anionic surfactant sodium dodecyl sulfate (SDS) was added with the NDG-NC dispersion to ensure the homogeneous dispersion of both nanomaterials and the electrocatalytic performance of the synthesized nanocomposite was investigated upon increasing the concentration of SDS. The combination of NDG and NC exhibited good biocompatibility with each other. NC provided a 3D network and dispersed it around the nanosheets of NDG. Here, NC functions as a skeleton and also as a binder. The presence of SDS reduced the agglomeration of NDG and NC ultimately enhanced the electrochemical performance of the nanocomposite. The morphological properties of (NDG-NC)-SDS nanocomposite were studied by FTIR, TEM, FESEM and Raman spectroscopy. The electrochemical performance of (NDG-NC)-SDS modified GCE sensor was investigated by CV, EIS and DPV technique and showed enhanced electrocatalytic response towards the redox peak of PCT and oxidation peak of NPX between 0.2 V to 0.9 V at 0.1 Vs^{-1} with a broad linear range from 0.01 to 90 μM and 0.1 to 60 μM for PCT and NPX, respectively. The limit of detection is 0.0035 μM and 0.026

μM for PCT and NPX, respectively, while the limit of quantification is 0.035μM and 0.26 μM, respectively. The (NC-NDG)-SDS sensor showed good stability, reproducibility and repeatability for the electrochemical determination of PCT and NPX in the presence of diclofenac sodium. To investigate the selectivity of the (NC-NDG)-SDS sensor, an interference study was performed in presence of some common interfering molecules. There was no signal except glucose detected for the interference species which indicates that the proposed sensor electrode has high selectivity toward the redox reaction of PCT and oxidation of NPX. The real sample analysis was performed on commercial preparations and human serum to assess the practical applicability of the proposed sensor with satisfactory results for the simultaneous determination of PCT and NPX. The results demonstrated that the fabricated (NDG-NC)-SDS sensor is a promising candidate for the simultaneous determination of PCT and NPX in pharmaceuticals and biological preparations.

3. Another work has been reported on this contribution, which highlights the synthesis of functionalized multiwall carbon nanotubes by acid hydrolysis method and followed by the sonication and drop-casting onto the surface of GCE. The chitosan solution was sonicated and drop-casted on *f*-MWCNTs and copper ions were immobilized on the multiwall carbon nanotubes and chitosan to prepare *f*-MWCNTs/CTS-Cu nanocomposite for the electrochemical determination of a common painkiller drug diclofenac sodium (DCF) from the pharmaceutical dosage forms and real samples. The morphology of the nanocomposite was studied by FT-IR, FESEM and EDX. The electrochemical performances were investigated by cyclic voltammetry, electrochemical impedance spectroscopy and square wave voltammetry. The *f*-MWCNTs/CTS-Cu nanocomposite showed excellent response toward the electro-oxidation of DS which is attributed to the outstanding electro-catalytic effect and electro-conductivity of *f*-MWCNTs and Cu^{2+} ions and the excellent film formation and adsorption ability of CTS.

Hence, the combination of CTS and Cu showed synergistic electro-catalytic activity and exhibited a remarkable performance for the electrochemical detection of DCF with a good linear range between 0.3 to 200 μM and a low detection limit of 0.021 μM was obtained. The sensor material was tested in the presence of various interfering molecules mentioned in chapter 4. There was no signal detected for the interference species which indicates that the modified sensor has good selectivity. The proposed sensor showed good stability and reproducibility and was suitable for the determination of DCF from the pharmaceutical dosage forms and real samples.

4. Another nanocomposite of nanocellulose (NC) and polypyrrole (PPY) was synthesized followed by the chemical polymerization for the simultaneous determination of paracetamol (PCT) and ciprofloxacin (CPR) in the pharmaceutical preparations, biological fluids and water samples. Here, NC has been synthesized by the same acid hydrolysis method. The layers of PPY were distributed homogeneously on NC fibers through chemical polymerization. The presence of OH- groups in NC and NH- groups of PPY are interconnected with each other through a strong hydrogen bond which demonstrates that the incorporation of PPY with the NC ultimately offers a 3D network with a mechanically stretchable structure. The nanocomposite of NC-PPY possesses a large surface area with a porous appearance. The attachment of NC and PPY generate more ionic pathways which accelerate the ion transportation and ultimately enhance the electroconductivity and electrocatalytic performance of NC. The morphological characteristics of NC-PPY nanocomposite were investigated by SEM, TEM, FTIR and Raman spectroscopy. The electrochemical performance of the NC-PPY nanocomposite was investigated by CV, EIS and SWV methods. The proposed NC-PPY modified GCE sensor showed a sharp electrochemical response towards the redox of PCT and oxidation of CPR with a dynamic linear range of 0.05 to 70 μM for PCT and 0.01 to 80 μM for CPR. The calculated LOD was 1.5 nM μM for PCT and 0.95 nM for CPR. The selectivity

of NC-PPY modified GCE sensor was assessed through the interference test in the presence of some common interfering molecules. From the interference test, it was shown that except for dopamine (DA) and ascorbic acid (AA), the interfering molecules did not interfere with the redox peak current of PCT and the oxidation peak of CPR. It could be demonstrated that the NC-PPY modified GCE sensor has high selectivity towards the PCT and CPR. Moreover, the fabricated electrode is also efficient for the simultaneous determination of PCT and CPR from the wastewater sample. The real sample analysis was performed in pharmaceutical dosage forms and biological fluids to evaluate the practical application of the proposed electrode with satisfactory recovery. The results demonstrated that the NC-PPY modified GCE is a potential candidate for the simultaneous determination of PCT and CPR in pharmaceutical dosage forms and biological fluids.

The present study represents different electrochemical sensing platforms for the quantitative detection of painkiller drugs. Furthermore, the study explores the different applications of the proposed sensors in clinical, pharmaceutical and environmental monitoring aspects which proves the potential of this research investigation and could contribute to the research community. By comparing the advantages and sensing performances, *f*-MWCNTs/NC/GCE sensing platform might be selected for commercialization purposes for pharmaceutical routine analysis due to its simple and fewer fabrication steps, cost-effectivity, very low LOD and broad linear ranges.

7.2 Future Work

The current research work focuses on the incorporation of biopolymers such as nanocellulose and chitosan with carbon-based nanostructured materials such as multiwall carbon nanotubes and nitrogen doped graphene for the preparation of bionanocomposite with enhanced catalytic effect and electrochemical response. In this work, the synthesized

bionanocomposite was utilized as a sensing platform for the electrochemical determination of common painkillers in pharmaceutical dosage preparations and biological fluids. The attachment of carbon-based nanomaterials and biopolymers facilitated the efficient electron transfer at the electrode and electrolyte interface, provides synergy in the catalytic effect, thus enhances the electrochemical signals. From these results it can be demonstrated that some future works can be explored based on improved and novel concepts which are listed below:

1. The scope of electrochemical sensors could be expanded with the synthesis of novel bionanocomposite. In this work, multiwall carbon nanotubes and nitrogen-doped graphene were utilized as carbon-based nanomaterials. Other types of carbon nanomaterials such as nanorods, nanotubes, nanobeads, nanoribbons, nanofibers and others are yet to be explored.
2. The electrochemical performances of the bionanocomposite could be further improved by the selection of other doping elements on the graphene support.
3. The bionanocomposite could be synthesized further by the incorporation of metal oxide, metal nanoparticles, mineral nanoparticles, with the incorporation of nanocellulose and chitosan which is still open to investigation.
4. The sensitivity and flexibility of the bionanocomposite could be further improved by the combination of nanocellulose and chitosan, with the incorporation of carbon nanomaterials. Both approaches contribute to an improvement in the electrocatalytic activity of the nanocomposite towards analyte detection.
5. The proposed bionanocomposites along with other nanomaterials could be used for the electrochemical determination of other analytes, supercapacitors and solar cell applications. However, more studies are needed for the synthesis and

preparation of different types of bionanocomposites for the fabrication of advanced electrochemical sensors.

REFERENCES

Abdullahi, N., Saion, E., Shaari, A. H., Al-Hada, N. M., & Keiteb, A. (2015). Optimisation of the photonic efficiency of TiO 2 decorated on MWCNTs for Methylene Blue photodegradation. *PloS one, 10*(5), e0125511.

Adeloju, S., Bond, A., & Briggs, M. (1985). Multielement determination in biological materials by differential pulse voltammetry. *Analytical chemistry, 57*(7), 1386-1390.

Adhoum, N., Monser, L., Toumi, M., & Boujlel, K. (2003). Determination of naproxen in pharmaceuticals by differential pulse voltammetry at a platinum electrode. *Analytica chimica acta, 495*(1-2), 69-75.

Afkhami, A., Bahiraei, A., & Madrakian, T. (2016). Gold nanoparticle/multi-walled carbon nanotube modified glassy carbon electrode as a sensitive voltammetric sensor for the determination of diclofenac sodium. *Materials Science and Engineering: C, 59*, 168-176.

Agarwal, U. P. (2017). Raman Spectroscopy of CNC-and CNF-Based Nanocomposites. *Handbook of Nanocellulose and Cellulose Nanocomposites*, 609-625.

Aguilar-Lira, G., Álvarez-Romero, G., Zamora-Suárez, A., Palomar-Pardavé, M., Rojas-Hernández, A., Rodríguez-Ávila, J., & Páez-Hernández, M. (2017). New insights on diclofenac electrochemistry using graphite as working electrode. *Journal of Electroanalytical Chemistry, 794*, 182-188.

Aguilar-Lira, G., Gutiérrez-Salgado, J., Rojas-Hernández, A., Rodríguez-Ávila, J., Páez-Hernández, M., & Álvarez-Romero, G. (2017). Artificial neural network for the voltamperometric quantification of diclofenac in presence of other nonsteroidal anti-inflammatory drugs and some commercial excipients. *Journal of Electroanalytical Chemistry, 801*, 527-535.

Akhter, S., Basirun, W. J., Alias, Y., Johan, M. R., Bagheri, S., Shalauddin, M., . . . Anuar, N. S. (2018). Enhanced amperometric detection of paracetamol by immobilized cobalt ion on functionalized MWCNTs-Chitosan thin film. *Analytical biochemistry, 551*, 29-36.

Akhter, S., Basirun, W. J., Shalauddin, M., Johan, M. R., Bagheri, S., Akbarzadeh, O., & Anuar, N. S. (2020a). Hybrid nanocomposite of functionalized multiwall carbon nanotube, nitrogen doped graphene and chitosan with electrodeposited copper for the detection of anticancer drug nilutamide in tablet and biological samples. *Materials Chemistry and Physics, 253*, 123393.

Akter, T., Nayeem, J., Quadery, A. H., Razzaq, M. A., Uddin, M. T., Bashar, M. S., & Jahan, M. S. (2020). MICROCRYSTALLINE CELLULOSE REINFORCED CHITOSAN COATING ON KRAFT PAPER. *CELLULOSE CHEMISTRY AND TECHNOLOGY, 54*(1-2), 95-102.

Al-Dulaimi, A. A., Wanrosli, W., Abdulrazak, L. F., & Husham, M. (2018). Preparation of nanocomposite polypyrrole/cellulose nanocrystals for conductive paper. *Nordic Pulp & Paper Research Journal, 33*(2), 309-316.

Alam, A. U., Qin, Y., Howlader, M. M., Hu, N.-X., & Deen, M. J. (2018). Electrochemical sensing of acetaminophen using multi-walled carbon nanotube and β-cyclodextrin. *Sensors and Actuators B: Chemical, 254*, 896-909.

Anicuta, S.-G., Dobre, L., Stroescu, M., & Jipa, I. (2010). Fourier transform infrared (FTIR) spectroscopy for characterization of antimicrobial films containing chitosan. *University Politehnica of Bucharest, Faculty Applied Chemistry and Material Science*. 2010, 1234-40.

Anuar, N. S., Basirun, W. J., Ladan, M., Shalauddin, M., & Mehmood, M. S. (2018). Fabrication of platinum nitrogen-doped graphene nanocomposite modified electrode for the electrochemical detection of acetaminophen. *Sensors and Actuators B: Chemical, 266*, 375-383.

Arancibia, J. A., Boldrini, M. A., & Escandar, G. M. (2000). Spectrofluorimetric determination of diclofenac in the presence of α-cyclodextrin. *Talanta, 52*(2), 261-268.

Aranda, P., Darder, M., Fernández-Saavedra, R., López-Blanco, M., & Ruiz-Hitzky, E. (2006). Relevance of polymer–and biopolymer–clay nanocomposites in electrochemical and electroanalytical applications. *Thin Solid Films, 495*(1-2), 104-112.

Arvand, M., Gholizadeh, T. M., & Zanjanchi, M. A. (2012). MWCNTs/Cu (OH) 2 nanoparticles/IL nanocomposite modified glassy carbon electrode as a voltammetric sensor for determination of the non-steroidal anti-inflammatory drug diclofenac. *Materials Science and Engineering: C, 32*(6), 1682-1689.

Aznoli, F., & Navimipour, N. J. (2017). Deployment strategies in the wireless sensor networks: systematic literature review, classification, and current trends. *Wireless Personal Communications, 95*(2), 819-846.

Babaei, A., Afrasiabi, M., & Babazadeh, M. (2010). A glassy carbon electrode modified with multiwalled carbon nanotube/chitosan composite as a new sensor for simultaneous determination of acetaminophen and mefenamic acid in pharmaceutical preparations and biological samples. *Electroanalysis, 22*(15), 1743-1749.

Bacakova, L., Pajorova, J., Tomkova, M., Matejka, R., Broz, A., Stepanovska, J., . . . Kallio, P. (2020). Applications of Nanocellulose/Nanocarbon Composites: Focus on Biotechnology and Medicine. *Nanomaterials, 10*(2), 196.

Baccarin, M., Santos, F. A., Vicentini, F. C., Zucolotto, V., Janegitz, B. C., & Fatibello-Filho, O. (2017). Electrochemical sensor based on reduced graphene oxide/carbon black/chitosan composite for the simultaneous determination of dopamine and paracetamol concentrations in urine samples. *Journal of Electroanalytical Chemistry, 799*, 436-443.

Baghayeri, M., Maleki, B., & Zarghani, R. (2014). Voltammetric behavior of tiopronin on carbon paste electrode modified with nanocrystalline Fe 50 Ni 50 alloys. *Materials Science and Engineering: C, 44*, 175-182.

Baghayeri, M., Zare, E. N., & Lakouraj, M. M. (2014). A simple hydrogen peroxide biosensor based on a novel electro-magnetic poly (p-phenylenediamine)@ Fe 3 O 4 nanocomposite. *Biosensors and Bioelectronics, 55*, 259-265.

Bagheri, H., Hajian, A., Rezaei, M., & Shirzadmehr, A. (2017). Composite of Cu metal nanoparticles-multiwall carbon nanotubes-reduced graphene oxide as a novel and high performance platform of the electrochemical sensor for simultaneous determination of nitrite and nitrate. *Journal of hazardous materials, 324*, 762-772.

Bahadır, E. B., & Sezgintürk, M. K. (2015). Electrochemical biosensors for hormone analyses. *Biosensors and Bioelectronics, 68*, 62-71.

Bard, A. (1980). Electrochemical Merhods. *Fundamentals and applications, 290*.

Bard, A. J., & Faulkner, L. R. (2001). Fundamentals and applications. *Electrochemical Methods, 2nd ed.; Wiley: New York*.

Basavaiah, K., Nagegowda, P., Somashekar, B., & Ramakrishna, V. (2006). Spectrophotometric and titrimetric determination of ciprofloxacin based on reaction with cerium (IV) sulphate. *Science Asia, 32*(4), 403-409.

Bhardwaj, V., Chauhan, S., & Sharma, P. (2014). Probing effect of lipophilic butylated hydroxytoluene on anionic surfactant properties for potential food and pharmaceutical applications: Thermo-acoustic and spectroscopic study. *Fluid Phase Equilibria, 373*, 63-71.

Biswas, S., Naskar, H., Pradhan, S., Chen, Y., Wang, Y., Bandyopadhyay, R., & Pramanik, P. (2020). Sm 2 O 3 nanorod-modified graphite paste electrode for trace level voltammetric determination of acetaminophen and ciprofloxacin. *New Journal of Chemistry, 44*(5), 1921-1930.

Blanco-López, M. C., Lobo-Castañón, M.-J., Miranda-Ordieres, A. J., & Tuñón-Blanco, P. (2003). Voltammetric response of diclofenac-molecularly imprinted film modified carbon electrodes. *Analytical and bioanalytical chemistry, 377*(2), 257-261.

Bonyadi, S., Ghanbari, K., & Ghiasi, M. (2020). All-electrochemical synthesis of a three-dimensional mesoporous polymeric gC 3 N 4/PANI/CdO nanocomposite and its application as a novel sensor for the simultaneous determination of epinephrine, paracetamol, mefenamic acid, and ciprofloxacin. *New Journal of Chemistry, 44*(8), 3412-3424.

Borenstein, M. R., Xue, Y., Cooper, S., & Tzeng, T.-B. (1996). Sensitive capillary gas chromatographic-mass spectrometric-selected-ion monitoring method for the determination of diclofenac concentrations in human plasma. *Journal of Chromatography B: Biomedical Sciences and Applications, 685*(1), 59-66.

Botello, J. C., & Pérez-Caballero, G. (1995). Spectrophotometric determination of diclofenac sodium with methylene blue. *Talanta, 42*(1), 105-108.

Bratov, A., Abramova, N., & Ipatov, A. (2010). Recent trends in potentiometric sensor arrays—A review. *Analytica chimica acta, 678*(2), 149-159.

Brett, C., & Oliveira Brett, A. M. (1993). *Electrochemistry: principles, methods, and applications*.

Burgot, G., Auffret, F., & Burgot, J.-L. (1997). Determination of acetaminophen by thermometric titrimetry. *Analytica chimica acta, 343*(1-2), 125-128.

Cao, J., Lu, C., Zhuang, J., Liu, M., Zhang, X., Yu, Y., & Tao, Q. (2017a). Multiple hydrogen bonding enables the self-healing of sensors for human–machine interactions. *Angewandte Chemie International Edition, 56*(30), 8795-8800.

Cao, J., Lu, C., Zhuang, J., Liu, M., Zhang, X., Yu, Y., & Tao, Q. (2017b). Multiple hydrogen bonding enables the self-healing of sensors for human–machine interactions. *Angewandte Chemie, 129*(30), 8921-8926.

Carlström, I. E., Rashad, A., Campodoni, E., Sandri, M., Syverud, K., Bolstad, A. I., & Mustafa, K. (2020). Cross-Linked Gelatin-Nanocellulose Scaffolds for Bone Tissue Engineering. *Materials Letters*, 127326.

Chatel, G. (2019). Sonochemistry in nanocatalysis: the use of ultrasound from the catalyst synthesis to the catalytic reaction. *Current Opinion in Green and Sustainable Chemistry, 15*, 1-6.

Chen, D., Sharma, S. K., & Mudhoo, A. (2011). *Handbook on applications of ultrasound: sonochemistry for sustainability*: CRC press.

Chen, T., Liu, Y., Lu, J., Xing, J., Li, J., Liu, T., & Xue, Q. (2019). Highly efficient detection of ciprofloxacin in water using a nitrogen-doped carbon electrode fabricated through plasma modification. *New Journal of Chemistry, 43*(38), 15169-15176.

Chen, Y., Fan, Z., Zhang, Z., Niu, W., Li, C., Yang, N., . . . Zhang, H. (2018). Two-dimensional metal nanomaterials: synthesis, properties, and applications. *Chemical reviews, 118*(13), 6409-6455.

Chethana, B., Basavanna, S., & Arthoba Naik, Y. (2012). Voltammetric determination of diclofenac sodium using tyrosine-modified carbon paste electrode. *Industrial & Engineering Chemistry Research, 51*(31), 10287-10295.

Chin, C.-J. M., Chen, T.-Y., Lee, M., Chang, C.-F., Liu, Y.-T., & Kuo, Y.-T. (2014). Effective anodic oxidation of naproxen by platinum nanoparticles coated FTO glass. *Journal of hazardous materials, 277*, 110-119.

Chmielewska, A., Konieczna, L., Plenis, A., Bieniecki, M., & Lamparczyk, H. (2006). Determination of diclofenac in plasma by high-performance liquid chromatography with electrochemical detection. *Biomedical chromatography, 20*(1), 119-124.

Chmielewska, A., Konieczna, L., Plenis, A., & Lamparczyk, H. (2006). Sensitive quantification of chosen drugs by reversed-phase chromatography with electrochemical detection at a glassy carbon electrode. *Journal of Chromatography B, 839*(1-2), 102-111.

Choi, W., Lahiri, I., Seelaboyina, R., & Kang, Y. S. (2010). Synthesis of graphene and its applications: a review. *Critical Reviews in Solid State and Materials Sciences, 35*(1), 52-71.

D'Souza, O. J., Mascarenhas, R. J., Thomas, T., Basavaraja, B. M., Saxena, A. K., Mukhopadhyay, K., & Roy, D. (2015). Platinum decorated multi-walled carbon nanotubes/Triton X-100 modified carbon paste electrode for the sensitive amperometric determination of Paracetamol. *Journal of Electroanalytical Chemistry, 739*, 49-57.

Damiani, P., Bearzotti, M., & Cabezón, M. A. (2002). Spectrofluorometric determination of naproxen in tablets. *Journal of pharmaceutical and biomedical analysis, 29*(1-2), 229-238.

Daneshgar, P., Norouzi, P., Ganjali, M. R., Dinarvand, R., & Moosavi-Movahedi, A. A. (2009). Determination of diclofenac on a dysprosium nanowire-modified carbon paste electrode accomplished in a flow injection system by advanced filtering. *Sensors, 9*(10), 7903-7918.

Daniel, M.-C., & Astruc, D. (2004). Gold nanoparticles: assembly, supramolecular chemistry, quantum-size-related properties, and applications toward biology, catalysis, and nanotechnology. *Chemical reviews, 104*(1), 293-346.

Davis, J. J., Coleman, K. S., Azamian, B. R., Bagshaw, C. B., & Green, M. L. (2003). Chemical and biochemical sensing with modified single walled carbon nanotubes. *Chemistry–A European Journal, 9*(16), 3732-3739.

De Jong, E., Kiffers, J., & Maes, R. (1989). The determination of non-steroidal anti-inflammatory drugs by GC—MS—MS in equine urine. *Journal of pharmaceutical and biomedical analysis, 7*(12), 1617-1622.

Dehdashtian, S., Behbahanian, N., Mohammadi Taherzadeh, K., & Hashemi, B. (2019). Development of electrochemical sensor based on multiwall carbon nanotube for determination of anticancer drug idarubicin in biological samples. *Advances in Nanochemistry, 1*(1), 22-28.

Delolo, F. G., Rodrigues, C., Silva, M. M. d., Dinelli, L. R., Delling, F. N., Zukerman-Schpector, J., & Batista, A. A. (2014). A new electrochemical sensor containing a film of chitosan-supported ruthenium: detection and quantification of sildenafil citrate and acetaminophen. *Journal of the Brazilian Chemical Society, 25*(3), 540-549.

Demetri, G. D., Von Mehren, M., Blanke, C. D., Van den Abbeele, A. D., Eisenberg, B., Roberts, P. J., . . . Janicek, M. (2002). Efficacy and safety of imatinib mesylate in advanced gastrointestinal stromal tumors. *New England Journal of Medicine, 347*(7), 472-480.

Demuth, J., Hamers, R., Tromp, R., & Welland, M. (1986). A scanning tunneling microscope for surface science studies. *IBM journal of research and development, 30*(4), 396-402.

Dutta, S., Kim, J., Ide, Y., Kim, J. H., Hossain, M. S. A., Bando, Y., . . . Wu, K. C.-W. (2017). 3D network of cellulose-based energy storage devices and related emerging applications. *Materials Horizons, 4*(4), 522-545.

El-Kommos, M. E., Mohamed, N. A., & Abdel Hakiem, A. F. (2013). Extractive spectrophotometric determination of some nonsteroidal anti-inflammatory drugs using methylene blue. *Journal of AOAC International, 96*(4), 737-744.

Elkady, E. F. (2010). Simultaneous determination of diclofenac potassium and methocarbamol in ternary mixture with guaifenesin by reversed phase liquid chromatography. *Talanta, 82*(4), 1604-1607.

Ensafi, A. A., Izadi, M., & Karimi-Maleh, H. (2013). Sensitive voltammetric determination of diclofenac using room-temperature ionic liquid-modified carbon nanotubes paste electrode. *Ionics, 19*(1), 137-144.

Fang, J., Xie, Z., Wallace, G., & Wang, X. (2017). Co-deposition of carbon dots and reduced graphene oxide nanosheets on carbon-fiber microelectrode surface for selective detection of dopamine. *Applied Surface Science, 412*, 131-137.

Fang, X., Chen, X., Liu, Y., Li, Q., Zeng, Z., Maiyalagan, T., & Mao, S. (2019). Nanocomposites of Zr (IV)-based metal–organic frameworks and reduced graphene oxide for electrochemically sensing ciprofloxacin in water. *ACS Applied Nano Materials, 2*(4), 2367-2376.

Fard, G. P., Alipour, E., & Sabzi, R. E. A. (2016). Modification of a disposable pencil graphite electrode with multiwalled carbon nanotubes: application to electrochemical determination of diclofenac sodium in some pharmaceutical and biological samples. *Analytical Methods, 8*(19), 3966-3974.

Farghaly, O. A., Hameed, R. A., & Abu-Nawwas, A.-A. H. (2014). Analytical application using modern electrochemical techniques. *Int. J. Electrochem. Sci, 9*(1), 3287-3318.

Ferreira, F. V., Cividanes, L. D. S., Brito, F. S., de Menezes, B. R. C., Franceschi, W., Simonetti, E. A. N., & Thim, G. P. (2016). Functionalization of carbon nanotube and applications *Functionalizing Graphene and Carbon Nanotubes* (pp. 31-61): Springer.

Gabor, D., & Tita, O. (2012). Biopolymers used in food packaging: a review. *Acta Universitatis Cinbinesis, Series E: Food Technology, 16*(2).

Garside, P., & Wyeth, P. (2003). Identification of cellulosic fibres by FTIR spectroscopy-thread and single fibre analysis by attenuated total reflectance. *Studies in Conservation, 48*(4), 269-275.

Gautam, V., Singh, K. P., & Yadav, V. L. (2018). Polyaniline/multiwall carbon nanotubes/starch nanocomposite material and hemoglobin modified carbon paste electrode for hydrogen peroxide and glucose biosensing. *International journal of biological macromolecules, 111*, 1124-1132.

George, A., Sanjay, M., Sriusk, R., Parameswaranpillai, J., & Siengchin, S. (2020). A comprehensive review on chemical properties and applications of biopolymers and their composites. *International Journal of Biological Macromolecules*. 154, 329-338.

Ghadimi, H., Nasiri-Tabrizi, B., Nia, P. M., Basirun, W. J., Tehrani, R. M., & Lorestani, F. (2015). Nanocomposites of nitrogen-doped graphene decorated with a palladium silver bimetallic alloy for use as a biosensor for methotrexate detection. *RSC advances, 5*(120), 99555-99565.

Gonzalez-Dominguez, J., Castell, P., Bespin-Gascon, S., Anson-Casaos, A., Diez-Pascual, A., Gomez-Fatou, M., . . . Martinez, M. (2012). Covalent functionalization of MWCNTs with poly (p-phenylene sulphide) oligomers: a route to the efficient integration through a chemical approach. *Journal of Materials Chemistry, 22*(39), 21285-21297.

Goodarzian, M., Khalilzade, M. A., Karimi, F., Gupta, V. K., Keyvanfard, M., Bagheri, H., & Fouladgar, M. (2014). Square wave voltammetric determination of diclofenac in liquid phase using a novel ionic liquid multiwall carbon nanotubes paste electrode. *Journal of Molecular Liquids, 197*, 114-119.

Gooding, J. J. (2005). Nanostructuring electrodes with carbon nanotubes: A review on electrochemistry and applications for sensing. *Electrochimica Acta, 50*(15), 3049-3060.

Gosser, D. K. (1993). *Cyclic voltammetry: simulation and analysis of reaction mechanisms* (Vol. 43): VCH New York.

Goyal, R. N., Chatterjee, S., & Rana, A. R. S. (2010). The effect of modifying an edge-plane pyrolytic graphite electrode with single-wall carbon nanotubes on its use for sensing diclofenac. *Carbon, 48*(14), 4136-4144.

Goyal, R. N., Gupta, V. K., Oyama, M., & Bachheti, N. (2005). Differential pulse voltammetric determination of paracetamol at nanogold modified indium tin oxide electrode. *Electrochemistry communications, 7*(8), 803-807.

Gui, Z., Zhu, H., Gillette, E., Han, X., Rubloff, G. W., Hu, L., & Lee, S. B. (2013). Natural cellulose fiber as substrate for supercapacitor. *ACS nano, 7*(7), 6037-6046.

Guiomar, A. J., Evans, S. D., & Guthrie, J. T. (1997). Immobilization of glucose oxidase onto a Langmuir-Blodgett ultrathin film of a cellulose derivative deposited on a self-assembled monolayer. *Supramolecular Science, 4*(3-4), 279-291.

Guo, S., & Wang, E. (2011). Noble metal nanomaterials: controllable synthesis and application in fuel cells and analytical sensors. *Nano Today, 6*(3), 240-264.

Hajian, A., Lindstr m, S. B., Pettersson, T. r., Hamedi, M. M., & W gberg, L. (2017). Understanding the dispersive action of nanocellulose for carbon nanomaterials. *Nano letters, 17*(3), 1439-1447.

Hamedi, M. M., Hajian, A., Fall, A. B., H kansson, K., Salajkova, M., Lundell, F., . . . Berglund, L. A. (2014). Highly conducting, strong nanocomposites based on nanocellulose-assisted aqueous dispersions of single-wall carbon nanotubes. *ACS nano, 8*(3), 2467-2476.

Hareesha, N., & Manjunatha, J. G. (2020). Surfactant and polymer layered carbon composite electrochemical sensor for the analysis of estriol with ciprofloxacin. *Materials Research Innovations, 24*(6), 349-362.

Hassaninejad–Darzi, S. K. (2014). A novel, effective and low cost catalyst for formaldehyde electrooxidation based on nickel ions dispersed onto chitosan-modified carbon paste electrode for fuel cell. *Journal of Electroceramics, 33*(3-4), 252-263.

Hatamluyi, B., Modarres Zahed, F., Es' haghi, Z., & Darroudi, M. (2020). Carbon quantum dots co-catalyzed with ZnO nanoflowers and Poly (CTAB) nanosensor for simultaneous sensitive detection of Paracetamol and Ciprofloxacin in biological samples. *Electroanalysis, 32*(8), 1818-1827.

Hebeish, A., Farag, S., Sharaf, S., & Shaheen, T. I. (2016). Advancement in conductive cotton fabrics through in situ polymerization of polypyrrole-nanocellulose composites. *Carbohydrate Polymers, 151*, 96-102.

Hettrich, K., Pinnow, M., Volkert, B., Passauer, L., & Fischer, S. (2014). Novel aspects of nanocellulose. *Cellulose, 21*(4), 2479-2488.

Holzinger, M., Le Goff, A., & Cosnier, S. (2014). Nanomaterials for biosensing applications: a review. *Frontiers in chemistry, 2*, 63.

Honarkar, H., & Barikani, M. (2009). Applications of biopolymers I: chitosan. *Monatshefte für Chemie-Chemical Monthly, 140*(12), 1403.

Hou, M., Xu, M., Hu, Y., & Li, B. (2019). Nanocellulose incorporated graphene/polypyrrole film with a sandwich-like architecture for preparing flexible supercapacitor electrodes. *Electrochimica acta, 313*, 245-254.

Hu, L., Hecht, D. S., & Gruner, G. (2010). Carbon nanotube thin films: fabrication, properties, and applications. *Chemical reviews, 110*(10), 5790-5844.

Hu, L., Zheng, G., Yao, J., Liu, N., Weil, B., Eskilsson, M., . . . Bloking, J. T. (2013). Transparent and conductive paper from nanocellulose fibers. *Energy & Environmental Science, 6*(2), 513-518.

Huang, J., Dufresne, A., & Lin, N. (2019). *Nanocellulose: From fundamentals to advanced materials*: John Wiley & Sons.

Hubbe, M. A., Ferrer, A., Tyagi, P., Yin, Y., Salas, C., Pal, L., & Rojas, O. J. (2017). Nanocellulose in thin films, coatings, and plies for packaging applications: A review. *BioResources, 12*(1), 2143-2233.

Hulanicki, A., Glab, S., & Ingman, F. (1991). Chemical sensors: definitions and classification. *Pure and applied chemistry, 63*(9), 1247-1250.

Hulteen, J. (1997). A general template-based method for the preparation of nanomaterials. *Journal of Materials Chemistry, 7*(7), 1075-1087.

Iijima, S. (1991). Helical microtubules of graphitic carbon. *nature, 354*(6348), 56-58.

Iijima, S., & Ichihashi, T. (1993). Single-shell carbon nanotubes of 1-nm diameter, *Nature* 363(6430), 603-605.

Iliescu, T., Baia, M., & Miclăuş, V. (2004). A Raman spectroscopic study of the diclofenac sodium–β-cyclodextrin interaction. *European journal of pharmaceutical sciences, 22*(5), 487-495.

Jayakumar, R., Prabaharan, M., Nair, S., Tokura, S., Tamura, H., & Selvamurugan, N. (2010). Novel carboxymethyl derivatives of chitin and chitosan materials and their biomedical applications. *Progress in Materials Science, 55*(7), 675-709.

Jemal, A., Murray, T., Ward, E., Samuels, A., Tiwari, R. C., Ghafoor, A., . . . Thun, M. J. (2005). Cancer statistics, 2005. *CA: a cancer journal for clinicians, 55*(1), 10-30.

Jin, W., & Zhang, J. (2000). Determination of diclofenac sodium by capillary zone electrophoresis with electrochemical detection. *Journal of Chromatography A, 868*(1), 101-107.

Jin, Y., Li, X., Ge, C., Ma, J., Li, Y., Zhao, E., . . . Li, D. (2020). Carbon nanotube hollow polyhedrons derived from ZIF-8@ ZIF-67 coupled to electro-deposited gold nanoparticles for voltammetric determination of acetaminophen. *Microchimica Acta, 187*(1), 1-9.

Jorcin, J.-B., Orazem, M. E., Pébère, N., & Tribollet, B. (2006). CPE analysis by local electrochemical impedance spectroscopy. *Electrochimica Acta, 51*(8-9), 1473-1479.

Jung, Y. H., Chang, T.-H., Zhang, H., Yao, C., Zheng, Q., Yang, V. W., . . . Park, D.-W. (2015a). High-performance green flexible electronics based on biodegradable cellulose nanofibril paper. *Nature communications, 6*(1), 1-11.

Kadowaki, H., Shiino, M., Uemura, I., & Kobayashi, K. (1984). Sensitive method for the determination of diclofenac in human plasma by gas chromatography-mass spectrometry. *Journal of Chromatography B: Biomedical Sciences and Applications, 308*, 329-333.

Kannan, A., & Sevvel, R. (2017). A highly selective and simultaneous determination of paracetamol and dopamine using poly-4-amino-6-hydroxy-2-mercaptopyrimidine (Poly-AHMP) film modified glassy carbon electrode. *Journal of Electroanalytical Chemistry, 791*, 8-16.

Kargarzadeh, H., Ahmad, I., Thomas, S., & Dufresne, A. (2017). *Handbook of nanocellulose and cellulose nanocomposites*: Wiley Online Library.

Karthik, R., Karikalan, N., Chen, S.-M., Gnanaprakasam, P., & Karuppiah, C. (2017). Voltammetric determination of the anti-cancer drug nilutamide using a screen-printed carbon electrode modified with a composite prepared from β-cyclodextrin, gold nanoparticles and graphene oxide. *Microchimica Acta, 184*(2), 507-514.

Karuppiah, C., Cheemalapati, S., Chen, S.-M., & Palanisamy, S. (2015). Carboxyl-functionalized graphene oxide-modified electrode for the electrochemical determination of nonsteroidal anti-inflammatory drug diclofenac. *Ionics, 21*(1), 231-238.

Kianipour, S., & Asghari, A. (2013). Room temperature ionic liquid/multiwalled carbon nanotube/chitosan-modified glassy carbon electrode as a sensor for simultaneous determination of ascorbic acid, uric acid, acetaminophen, and mefenamic acid. *IEEE Sensors Journal, 13*(7), 2690-2698.

Kim, D.-H., Viventi, J., Amsden, J. J., Xiao, J., Vigeland, L., Kim, Y.-S., . . . Contreras, D. (2010). Dissolvable films of silk fibroin for ultrathin conformal bio-integrated electronics. *Nature materials, 9*(6), 511-517.

Kim, J.-H., Shim, B. S., Kim, H. S., Lee, Y.-J., Min, S.-K., Jang, D., . . . Kim, J. (2015). Review of nanocellulose for sustainable future materials. *International Journal of Precision Engineering and Manufacturing-Green Technology, 2*(2), 197-213.

Kingsley, M. P., Kalambate, P. K., & Srivastava, A. K. (2016). Simultaneous determination of ciprofloxacin and paracetamol by adsorptive stripping voltammetry using copper zinc ferrite nanoparticles modified carbon paste electrode. *RSC advances, 6*(18), 15101-15111.

Koga, H., Saito, T., Kitaoka, T., Nogi, M., Suganuma, K., & Isogai, A. (2013). Transparent, conductive, and printable composites consisting of TEMPO-oxidized nanocellulose and carbon nanotube. *Biomacromolecules, 14*(4), 1160-1165.

Kole, P. L., Millership, J., & McElnay, J. C. (2011). Determination of diclofenac from paediatric urine samples by stir bar sorptive extraction (SBSE)–HPLC–UV technique. *Talanta, 85*(4), 1948-1958.

Kormosh, Z., Hunka, I., Bazel, Y., Laganovsky, A., Mazurenko, I., & Kormosh, N. (2007). Determination of diclofenac in pharmaceuticals and urine samples using a membrane sensor based on the ion associate of diclofenac with Rhodamine B. *Open Chemistry, 5*(3), 813-823.

Kormosh, Z. A., Hunka, I., & Bazel, Y. R. (2009). A potentiometric sensor for the determination of diclofenac. *Journal of Analytical Chemistry, 64*(8), 853-858.

Kriz, D., Kempe, M., & Mosbach, K. (1996). Introduction of molecularly imprinted polymers as recognition elements in conductometric chemical sensors. *Sensors and Actuators B: Chemical, 33*(1-3), 178-181.

Kubrusly, C. S., & Malebranche, H. (1985). Sensors and controllers location in distributed systems—A survey. *Automatica, 21*(2), 117-128.

Kundu, J., Chung, Y.-I., Kim, Y. H., Tae, G., & Kundu, S. (2010). Silk fibroin nanoparticles for cellular uptake and control release. *International journal of pharmaceutics, 388*(1-2), 242-250.

Lasia, A. (2002). Electrochemical impedance spectroscopy and its applications *Modern aspects of electrochemistry* (pp. 143-248): Springer.

Le Troedec, M., Sedan, D., Peyratout, C., Bonnet, J. P., Smith, A., Guinebretiere, R., . . . Krausz, P. (2008). Influence of various chemical treatments on the composition and structure of hemp fibres. *Composites Part A: Applied Science and Manufacturing, 39*(3), 514-522.

Lecoeur, M., Rabenirina, G., Schifano, N., Odou, P., Ethgen, S., Lebuffe, G., & Foulon, C. (2019). Determination of acetaminophen and its main metabolites in urine by capillary electrophoresis hyphenated to mass spectrometry. *Talanta, 205*, 120108.

Lee, M., Jeon, H., & Kim, S. (2015). A highly tunable and fully biocompatible silk nanoplasmonic optical sensor. *Nano letters, 15*(5), 3358-3363.

Lenik, J., & Łyszczek, R. (2016). Functionalized β-cyclodextrin based potentiometric sensor for naproxen determination. *Materials Science and Engineering: C, 61*, 149-157.

Lether, F., & Wenston, P. (1987). An algorithm for the numerical evaluation of the reversible Randles-Sevcik function. *Computers & chemistry, 11*(3), 179-183.

Li, J., & Lee, E.-C. (2017). Functionalized multi-wall carbon nanotubes as an efficient additive for electrochemical DNA sensor. *Sensors and Actuators B: Chemical, 239*, 652-659.

Li, Y., Tamilavan, V., & Hyun, M. H. (2012). A fluorescent chiral chemosensor for the recognition of the two enantiomers of chiral carboxylates. *Chirality, 24*(5), 406-411.

Li, Y., Zhu, H., Shen, F., Wan, J., Lacey, S., Fang, Z., . . . Hu, L. (2015). Nanocellulose as green dispersant for two-dimensional energy materials. *Nano energy, 13*, 346-354.

Lin, N., Bruzzese, C. c., & Dufresne, A. (2012). TEMPO-oxidized nanocellulose participating as crosslinking aid for alginate-based sponges. *ACS applied materials & interfaces, 4*(9), 4948-4959.

Lin, Z., Yao, Y., Li, Z., Liu, Y., Li, Z., & Wong, C.-P. (2010). Solvent-assisted thermal reduction of graphite oxide. *The Journal of Physical Chemistry C, 114*(35), 14819-14825.

Linford, R. G. (1990). *Electrochemical science and technology of polymers* (Vol. 2): Springer.

Ling, S., Chen, W., Fan, Y., Zheng, K., Jin, K., Yu, H., . . . Kaplan, D. L. (2018). Biopolymer nanofibrils: Structure, modeling, preparation, and applications. *Progress in polymer science, 85*, 1-56.

Liu, J., Yang, B., Li, M., Li, J., & Wan, Y. (2020). Enhanced dual network hydrogels consisting of thiolated chitosan and silk fibroin for cartilage tissue engineering. *Carbohydrate Polymers, 227*, 115335.

Liu, Y. y., Hu, X. l., Bao, Y. f., & Yin, D. q. (2018). Simultaneous determination of 29 pharmaceuticals in fish muscle and plasma by ultrasonic extraction followed by SPE–UHPLC–MS/MS. *Journal of separation science, 41*(10), 2139-2150.

Lou, B.-S., Rajaji, U., Chen, S.-M., & Chen, T.-W. (2020). A simple sonochemical assisted synthesis of NiMoO4/chitosan nanocomposite for electrochemical sensing of amlodipine in pharmaceutical and serum samples. *Ultrasonics Sonochemistry, 64*, 104827.

Lovrić, M., & Komorsky-Lovric, Š. (1988). Square-wave voltammetry of an adsorbed reactant. *Journal of electroanalytical chemistry and interfacial electrochemistry, 248*(2), 239-253.

Lu, P., & Hsieh, Y.-L. (2010). Preparation and properties of cellulose nanocrystals: rods, spheres, and network. *Carbohydrate Polymers, 82*(2), 329-336.

Lu, T.-L., & Tsai, Y.-C. (2011). Sensitive electrochemical determination of acetaminophen in pharmaceutical formulations at multiwalled carbon nanotube-alumina-coated silica nanocomposite modified electrode. *Sensors and Actuators B: Chemical, 153*(2), 439-444.

Lucas, F. W. d. S., Mascaro, L. H., Fill, T. P., Rodrigues-Filho, E., Franco-Junior, E., Homem-de-Mello, P., . . . Correia, A. N. (2014). Diclofenac on boron-doped diamond electrode: from electroanalytical determination to prediction of the electrooxidation mechanism with HPLC-ESI/HRMS and computational simulations. *Langmuir, 30*(19), 5645-5654.

Luo, B., Liu, S., & Zhi, L. (2012). Chemical approaches toward graphene-based nanomaterials and their applications in energy-related areas. *Small, 8*(5), 630-646.

Luo, H., Xiong, G., Yang, Z., Raman, S. R., Si, H., & Wan, Y. (2014). A novel three-dimensional graphene/bacterial cellulose nanocomposite prepared by in situ biosynthesis. *RSC Advances, 4*(28), 14369-14372.

Madikizela, L. M., & Chimuka, L. (2017). Simultaneous determination of naproxen, ibuprofen and diclofenac in wastewater using solid-phase extraction with high performance liquid chromatography. *Water Sa, 43*(2), 264-274.

Madrakian, T., Haghshenas, E., & Afkhami, A. (2014). Simultaneous determination of tyrosine, acetaminophen and ascorbic acid using gold nanoparticles/multiwalled carbon nanotube/glassy carbon electrode by differential pulse voltammetric method. *Sensors and Actuators B: Chemical, 193*, 451-460.

Maduraiveeran, G., & Jin, W. (2017). Nanomaterials based electrochemical sensor and biosensor platforms for environmental applications. *Trends in Environmental Analytical Chemistry, 13*, 10-23.

Mahmoud, A. M., Mahnashi, M. H., Alkahtani, S. A., & El-Wekil, M. M. (2020). Nitrogen and sulfur co-doped graphene quantum dots/nanocellulose nanohybrid for electrochemical sensing of anti-schizophrenic drug olanzapine in pharmaceuticals and human biological fluids. *International journal of biological macromolecules, 165*, 2030-2037.

Malho, J.-M., Laaksonen, P. i., Walther, A., Ikkala, O., & Linder, M. B. (2012). Facile method for stiff, tough, and strong nanocomposites by direct exfoliation of multilayered graphene into native nanocellulose matrix. *Biomacromolecules, 13*(4), 1093-1099.

Mallakpour, S., & Soltanian, S. (2016). Surface functionalization of carbon nanotubes: fabrication and applications. *RSC advances, 6*(111), 109916-109935.

Mandal, A., & Chakrabarty, D. (2011). Isolation of nanocellulose from waste sugarcane bagasse (SCB) and its characterization. *Carbohydrate Polymers, 86*(3), 1291-1299.

Manea, F., Ihos, M., Remes, A., Burtica, G., & Schoonman, J. (2010). Electrochemical Determination of Diclofenac Sodium in Aqueous Solution on Cu-Doped Zeolite-Expanded Graphite-Epoxy Electrode. *Electroanalysis, 22*(17-18), 2058-2063.

Markoulidis, F., Todorova, N., Grilli, R., Lekakou, C., & Trapalis, C. (2019). Composite Electrodes of Activated Carbon and Multiwall Carbon Nanotubes Decorated with Silver Nanoparticles for High Power Energy Storage. *Journal of Composites Science, 3*(4), 97.

Matsunaga, T., Kondo, T., Osasa, T., Kotsugai, A., Shitanda, I., Hoshi, Y., . . . Yuasa, M. (2020). Sensitive electrochemical detection of ciprofloxacin at screen-printed diamond electrodes. *Carbon, 159*, 247-254.

Mautner, A., Rocha, I., Sirviö, J. A., Kluge, M., Herrera, M. A., & Nigmatullin, R. (2019). Advances in Nanocellulose. *Advances in Nanocellulose*, 342.

Mazurek, S., & Szostak, R. (2008). Quantitative determination of diclofenac sodium in solid dosage forms by FT-Raman spectroscopy. *Journal of pharmaceutical and biomedical analysis, 48*(3), 814-821.

McCreery, R. L., & Bard, A. (1991). Electroanalytical chemistry. *Marcel Dekker, Inc., New York, 17*, 221-374.

McKnight, T. E., Melechko, A. V., Guillorn, M. A., Merkulov, V. I., Doktycz, M. J., Culbertson, C. T., . . . Simpson, M. L. (2003). Effects of microfabrication processing on the electrochemistry of carbon nanofiber electrodes. *The Journal of Physical Chemistry B, 107*(39), 10722-10728.

Meenakshi, S., Pandian, K., Jayakumari, L., & Inbasekaran, S. (2016). Enhanced amperometric detection of metronidazole in drug formulations and urine samples based on chitosan protected tetrasulfonated copper phthalocyanine thin-film modified glassy carbon electrode. *Materials Science and Engineering: C, 59*, 136-144.

Mensitieri, G., Di Maio, E., Buonocore, G. G., Nedi, I., Oliviero, M., Sansone, L., & Iannace, S. (2011). Processing and shelf life issues of selected food packaging materials and structures from renewable resources. *Trends in Food Science & Technology, 22*(2-3), 72-80.

Mofidi, Z., Norouzi, P., Seidi, S., & Ganjali, M. R. (2017). Determination of diclofenac using electromembrane extraction coupled with stripping FFT continuous cyclic voltammetry. *Analytica chimica acta, 972*, 38-45.

Mokhtari, A., Karimi-Maleh, H., Ensafi, A. A., & Beitollahi, H. (2012). Application of modified multiwall carbon nanotubes paste electrode for simultaneous voltammetric determination of morphine and diclofenac in biological and pharmaceutical samples. *Sensors and Actuators B: Chemical, 169*, 96-105.

Moncrieff, J. (1992). Extractionless determination of diclofenac sodium in serum using reversed-phase high-performance liquid chromatography with fluorimetric detection. *Journal of Chromatography B: Biomedical Sciences and Applications, 577*(1), 185-189.

Mondal, S. (2017). Preparation, properties and applications of nanocellulosic materials. *Carbohydrate polymers, 163*, 301-316.

Mondal, S. (2018). Review on nanocellulose polymer nanocomposites. *Polymer-Plastics Technology and Engineering, 57*(13), 1377-1391.

Mondal, S. (2020). Nanocellulose reinforced polymer nanocomposites for sustainable packaging of foods, cosmetics, and pharmaceuticals *Sustainable Nanocellulose and Nanohydrogels from Natural Sources* (pp. 237-253): Elsevier.

Montes, R. H., Lima, A. P., Cunha, R. R., Guedes, T. J., dos Santos, W. T., Nossol, E., . . . Munoz, R. A. (2016). Size effects of multi-walled carbon nanotubes on the electrochemical oxidation of propionic acid derivative drugs: Ibuprofen and naproxen. *Journal of Electroanalytical Chemistry, 775*, 342-349.

Moon, R. J., Martini, A., Nairn, J., Simonsen, J., & Youngblood, J. (2011). Cellulose nanomaterials review: structure, properties and nanocomposites. *Chemical Society Reviews, 40*(7), 3941-3994.

Moore, N., Pollack, C., & Butkerait, P. (2015). Adverse drug reactions and drug–drug interactions with over-the-counter NSAIDs. *Therapeutics and clinical risk management, 11*, 1061.

Motia, S., Bouchikhi, B., & El Bari, N. (2021). An electrochemical molecularly imprinted sensor based on chitosan capped with gold nanoparticles and its application for highly sensitive butylated hydroxyanisole analysis in foodstuff products. *Talanta, 223*, 121689.

Motshekga, S. C., Pillai, S. K., Sinha Ray, S., Jalama, K., & Krause, R. (2012). Recent trends in the microwave-assisted synthesis of metal oxide nanoparticles supported on carbon nanotubes and their applications. *Journal of Nanomaterials, 2012*.

Muller, D., Silva, J. P., Rambo, C., Barra, G., Dourado, F., & Gama, F. (2013). Neuronal cells' behavior on polypyrrole coated bacterial nanocellulose three-dimensional (3D) scaffolds. *Journal of Biomaterials Science, Polymer Edition, 24*(11), 1368-1377.

Nettles, D. L., Elder, S. H., & Gilbert, J. A. (2002). Potential use of chitosan as a cell scaffold material for cartilage tissue engineering. *Tissue engineering, 8*(6), 1009-1016.

Niu, F., Li, M., Huang, Q., Zhang, X., Pan, W., Yang, J., & Li, J. (2017). The characteristic and dispersion stability of nanocellulose produced by mixed acid hydrolysis and ultrasonic assistance. *Carbohydrate polymers, 165*, 197-204.

Norouzi, P., Dousty, F., Ganjali, M. R., & Daneshgar, P. (2009). Dysprosium nanowire modified carbon paste electrode for the simultaneous determination of naproxen and paracetamol: application in pharmaceutical formulation and biological fluid. *Int. J. Electrochem. Sci, 4*(10), 1373-1386.

Nystrom, G., Mihranyan, A., Razaq, A., Lindstrom, T., Nyholm, L., & Strømme, M. (2010). A nanocellulose polypyrrole composite based on microfibrillated cellulose from wood. *The Journal of Physical Chemistry B, 114*(12), 4178-4182.

Okoth, O. K., Yan, K., Feng, J., & Zhang, J. (2018). Label-free photoelectrochemical aptasensing of diclofenac based on gold nanoparticles and graphene-doped CdS. *Sensors and Actuators B: Chemical, 256*, 334-341.

Ortolani, T. S., Pereira, T. S., Assumpção, M. H., Vicentini, F. C., de Oliveira, G. G., & Janegitz, B. C. (2019). Electrochemical sensing of purines guanine and adenine using single-walled carbon nanohorns and nanocellulose. *Electrochimica acta, 298*, 893-900.

Osteryoung, J. G., & Osteryoung, R. A. (1985). Square wave voltammetry. *Analytical chemistry, 57*(1), 101-110.

Pan, Y., Yang, N., Chen, Y., Lin, Y., Li, Y., Liu, Y., & Liu, C. (2015). Nickel phosphide nanoparticles-nitrogen-doped graphene hybrid as an efficient catalyst for enhanced hydrogen evolution activity. *Journal of Power Sources, 297*, 45-52.

Panderi, I., & Parissi-Poulou, M. (1994). Second-derivative spectrophotometric determination of naproxen in the presence of its metabolite in human plasma. *Analyst, 119*(4), 697-701.

Pandey, R. R., Fukumori, M., TermehYousefi, A., Eguchi, M., Tanaka, D., Ogawa, T., & Tanaka, H. (2017). Tuning the electrical property of a single layer graphene nanoribbon by adsorption of planar molecular nanoparticles. *Nanotechnology, 28*(17), 175704.

Pappas, C., Tarantilis, P., Daliani, I., Mavromoustakos, T., & Polissiou, M. (2002). Comparison of classical and ultrasound-assisted isolation procedures of cellulose from kenaf (Hibiscus cannabinus L.) and eucalyptus (Eucalyptus rodustrus Sm.). *Ultrasonics Sonochemistry, 9*(1), 19-23.

Park, B. K., & Kim, M.-M. (2010). Applications of chitin and its derivatives in biological medicine. *International journal of molecular sciences, 11*(12), 5152-5164.

Perera, G., de Costa, M., & Mahanama, K. (2019). Development of a fluorimetric method for assessing paracetamol in pharmaceuticals tablets. *Journal of Photochemistry and Photobiology A: Chemistry, 368*, 248-253.

Perez-Lopez, B., & Merkoçi, A. (2012). Carbon nanotubes and graphene in analytical sciences. *Microchimica Acta, 179*(1-2), 1-16.

Poletti, F., Favaretto, L., Kovtun, A., Treossi, E., Corticelli, F., Gazzano, M., . . . Melucci, M. (2020). Electrochemical sensing of glucose by chitosan modified graphene oxide. *JPhM, 3*(1), 014011.

Pollap, A., Baran, K., Kuszewska, N., & Kochana, J. (2020). Electrochemical sensing of ciprofloxacin and paracetamol in environmental water using titanium sol based sensor. *Journal of Electroanalytical Chemistry, 878*, 114574.

Polshettiwar, V., & Varma, R. S. (2010). *Aqueous microwave assisted chemistry: synthesis and catalysis*: Royal Society of Chemistry.

Portaccio, M., Durante, D., Viggiano, A., Di Martino, S., De Luca, P., Di Tuoro, D., . . . De Luca, B. (2007). Amperometric glucose determination by means of glucose oxidase immobilized on a cellulose acetate film: dependence on the immobilization procedures. *Electroanalysis, 19*(17), 1787-1793.

Rahman, M. M., Lopa, N. S., Ju, M. J., & Lee, J.-J. (2017). Highly sensitive and simultaneous detection of dopamine and uric acid at graphene nanoplatelet-modified fluorine-doped tin oxide electrode in the presence of ascorbic acid. *Journal of Electroanalytical Chemistry, 792*, 54-60.

Rahsepar, M., Foroughi, F., & Kim, H. (2019). A new enzyme-free biosensor based on nitrogen-doped graphene with high sensing performance for electrochemical detection of glucose at biological pH value. *Sensors and Actuators B: Chemical, 282*, 322-330.

Ramimoghadam, D., Bagheri, S., Yousefi, A. T., & Abd Hamid, S. B. (2015). Statistical optimization of effective parameters on saturation magnetization of nanomagnetite particles. *Journal of Magnetism and Magnetic Materials, 393*, 30-35.

Rawool, C. R., & Srivastava, A. K. (2019). A dual template imprinted polymer modified electrochemical sensor based on Cu metal organic framework/mesoporous carbon for highly sensitive and selective recognition of rifampicin and isoniazid. *Sensors and Actuators B: Chemical, 288*, 493-506.

Rodríguez, J. A., Barrado, E., Castrillejo, Y., Santos, J. R., & Lima, J. L. (2007). Validation of a tubular bismuth film amperometric detector: Determination of diclofenac sodium by multisyringe flow injection analysis. *Journal of pharmaceutical and biomedical analysis, 45*(1), 47-53.

Rosa, M., Medeiros, E., Malmonge, J., Gregorski, K., Wood, D., Mattoso, L., . . . Imam, S. (2010). Cellulose nanowhiskers from coconut husk fibers: Effect of preparation conditions on their thermal and morphological behavior. *Carbohydrate Polymers, 81*(1), 83-92.

Rotello, V. M. (2004). *Nanoparticles: building blocks for nanotechnology*: Springer Science & Business Media.

Ruengsitagoon, W., Liawruangrath, S., & Townshend, A. (2006). Flow injection chemiluminescence determination of paracetamol. *Talanta, 69*(4), 976-983.

Sanati, A. L., Karimi-Maleh, H., Badiei, A., Biparva, P., & Ensafi, A. A. (2014). A voltammetric sensor based on NiO/CNTs ionic liquid carbon paste electrode for determination of morphine in the presence of diclofenac. *Materials Science and Engineering: C, 35*, 379-385.

Săndulescu, R., Mirel, S., & Oprean, R. (2000). The development of spectrophotometric and electroanalytical methods for ascorbic acid and acetaminophen and their applications in the analysis of effervescent dosage forms. *Journal of pharmaceutical and biomedical analysis, 23*(1), 77-87.

Santos, A. M., Wong, A., Almeida, A. A., & Fatibello-Filho, O. (2017). Simultaneous determination of paracetamol and ciprofloxacin in biological fluid samples using a glassy carbon electrode modified with graphene oxide and nickel oxide nanoparticles. *Talanta, 174*, 610-618.

Sarhangzadeh, K. (2015). Application of multi wall carbon nanotube–graphene hybrid for voltammetric determination of naproxen. *Journal of the Iranian Chemical Society, 12*(12), 2133-2140.

Sarhangzadeh, K., Khatami, A. A., Jabbari, M., & Bahari, S. (2013). Simultaneous determination of diclofenac and indomethacin using a sensitive electrochemical sensor based on multiwalled carbon nanotube and ionic liquid nanocomposite. *Journal of Applied Electrochemistry, 43*(12), 1217-1224.

Sasso, C., Zeno, E., Petit-Conil, M., Chaussy, D., Belgacem, M. N., Tapin-Lingua, S., & Beneventi, D. (2010). Highly conducting polypyrrole/cellulose nanocomposite films with enhanced mechanical properties. *Macromolecular Materials and Engineering, 295*(10), 934-941.

Scida, K., Stege, P. W., Haby, G., Messina, G. A., & García, C. D. (2011). Recent applications of carbon-based nanomaterials in analytical chemistry: critical review. *Analytica chimica acta, 691*(1-2), 6-17.

Secco, E. A., & Worth, G. G. (1987). Infrared spectra of unannealed and of annealed Cu4 (OH) 6 (NO3) 2. *Canadian journal of chemistry, 65*(10), 2504-2508.

Senel, S., & McClure, S. J. (2004). Potential applications of chitosan in veterinary medicine. *Advanced drug delivery reviews, 56*(10), 1467-1480.

Shahnaz, T., Padmanaban, V., & Narayanasamy, S. (2020). Surface modification of nanocellulose using polypyrrole for the adsorptive removal of Congo red dye and chromium in binary mixture. *International journal of biological macromolecules, 151*, 322-332.

Shalauddin, M., Akhter, S., Bagheri, S., Abd Karim, M. S., Kadri, N. A., & Basirun, W. J. (2017). Immobilized copper ions on MWCNTS-Chitosan thin film: Enhanced amperometric sensor for electrochemical determination of diclofenac sodium in aqueous solution. *International Journal of Hydrogen Energy, 42*(31), 19951-19960.

Shalauddin, M., Akhter, S., Basirun, W. J., Bagheri, S., Anuar, N. S., & Johan, M. R. (2019). Hybrid nanocellulose/f-MWCNTs nanocomposite for the electrochemical sensing of diclofenac sodium in pharmaceutical drugs and biological fluids. *Electrochimica acta, 304*, 323-333.

Shanmugharaj, A., Bae, J., Lee, K. Y., Noh, W. H., Lee, S. H., & Ryu, S. H. (2007). Physical and chemical characteristics of multiwalled carbon nanotubes functionalized with aminosilane and its influence on the properties of natural rubber composites. *Composites science and technology, 67*(9), 1813-1822.

Shao, Y., Zhang, S., Engelhard, M. H., Li, G., Shao, G., Wang, Y., . . . Lin, Y. (2010). Nitrogen-doped graphene and its electrochemical applications. *Journal of Materials Chemistry, 20*(35), 7491-7496.

Shi, S., Reisberg, S., Anquetin, G., Noël, V., Pham, M., & Piro, B. (2015). General approach for electrochemical detection of persistent pharmaceutical micropollutants: Application to acetaminophen. *Biosensors and Bioelectronics, 72*, 205-210.

Shrestha, B. K., Shrestha, S., Tiwari, A. P., Kim, J.-I., Ko, S. W., Kim, H.-J., . . . Kim, C. S. (2017). Bio-inspired hybrid scaffold of zinc oxide-functionalized multi-wall carbon nanotubes reinforced polyurethane nanofibers for bone tissue engineering. *Materials & Design, 133*, 69-81.

Si, W., Lei, W., Han, Z., Zhang, Y., Hao, Q., & Xia, M. (2014). Electrochemical sensing of acetaminophen based on poly (3, 4-ethylenedioxythiophene)/graphene oxide composites. *Sensors and Actuators B: Chemical, 193*, 823-829.

Siqueira, J., Jos R, Gasparotto, L. H., Oliveira, J., Osvaldo N, & Zucolotto, V. (2008). Processing of electroactive nanostructured films incorporating carbon nanotubes and phthalocyanines for sensing. *The Journal of Physical Chemistry C, 112*(24), 9050-9055.

Smyth, M. R., & Vos, J. G. (1992). *Analytical voltammetry*: Elsevier.

Soini, H., Novotny, M. V., & Riekkola, M. L. (1992). Determination of naproxen in serum by capillary electrophoresis with ultraviolet absorbance and laser-induced fluorescence detection. *Journal of Microcolumn Separations, 4*(4), 313-318.

Soltani, N., Tavakkoli, N., Mosavimanesh, Z. S., & Davar, F. (2018). Electrochemical determination of naproxen in the presence of acetaminophen using a carbon paste electrode modified with activated carbon nanoparticles. *Comptes Rendus Chimie, 21*(1), 54-60.

Somasundaran, P., Kunjappu, J. T., Kumar, C. V., Turro, N. J., & Barton, J. K. (1989). Excited-state resonance Raman spectroscopy as a probe of alumina-sodium dodecyl sulfate hemimicelles. *Langmuir, 5*(1), 215-218.

Song, Q., Zhang, Z., Gao, J., & Ding, C. (2011). Synthesis and property studies of N-carboxymethyl chitosan. *Journal of Applied Polymer Science, 119*(6), 3282-3285.

Sookhakian, M., Amin, Y., Baradaran, S., Tajabadi, M., Golsheikh, A. M., & Basirun, W. (2014). A layer-by-layer assembled graphene/zinc sulfide/polypyrrole thin-film electrode via electrophoretic deposition for solar cells. *Thin Solid Films, 552*, 204-211.

Souza, R. L. d., & Tubino, M. (2005). Spectrophotometric determination of diclofenac in pharmaceutical preparations. *Journal of the Brazilian Chemical Society, 16*(5), 1068-1073.

Sparidans, R. W., Lagas, J. S., Schinkel, A. H., Schellens, J. H., & Beijnen, J. H. (2008). Liquid chromatography–tandem mass spectrometric assay for diclofenac and three primary metabolites in mouse plasma. *Journal of Chromatography B, 872*(1), 77-82.

Stefano, J. S., Lima, A. P. d., Montes, R. H., Richter, E. M., & Muñoz, R. A. (2012). Fast determination of naproxen in pharmaceutical formulations by batch injection analysis with pulsed amperometric detection. *Journal of the Brazilian Chemical Society, 23*(10), 1834-1838.

Stefano, J. S., Montes, R. H., Richter, E. M., & Muñoz, R. A. (2014). Flow-injection analysis with multiple-pulse amperometry for simultaneous determination of paracetamol and naproxen using a homemade flow cell for screen-printed electrodes. *Journal of the Brazilian Chemical Society, 25*(3), 484-491.

Stenstad, P., Andresen, M., Tanem, B. S., & Stenius, P. (2008). Chemical surface modifications of microfibrillated cellulose. *Cellulose, 15*(1), 35-45.

Stetter, J. R., Penrose, W. R., & Yao, S. (2003). Sensors, chemical sensors, electrochemical sensors, and ECS. *Journal of The Electrochemical Society, 150*(2), S11.

Stradiotto, N. R., Yamanaka, H., & Zanoni, M. V. B. (2003). Electrochemical sensors: a powerful tool in analytical chemistry. *Journal of the Brazilian Chemical Society, 14*(2), 159-173.

Streeter, I., Wildgoose, G. G., Shao, L., & Compton, R. G. (2008). Cyclic voltammetry on electrode surfaces covered with porous layers: an analysis of electron transfer kinetics at single-walled carbon nanotube modified electrodes. *Sensors and Actuators B: Chemical, 133*(2), 462-466.

Sultana, N., Arayne, M. S., & Ali, S. N. (2013). An ultra-sensitive LC method for the simultaneous determination of paracetamol, carbamazepine, losartan and ciprofloxacin in bulk drug, pharmaceutical formulation and human serum by programming the detector. *American Journal of Analytical Chemistry,* 4, 24-33.

Sun, S.-W., & Fabre, H. (1994). Practical approach for validating the TLC assay of an active ingredient in a pharmaceutical formulation. *Journal of Liquid Chromatography & Related Technologies, 17*(2), 433-445.

Sun, S.-W., Fabre, H., & Maillols, H. (1994). Test procedure validation for the TLC assay of a degradation product in a pharmaceutical formulation. *Journal of Liquid Chromatography & Related Technologies, 17*(11), 2495-2509.

Sun, S., & Fabre, H. (1994). Practical approach for validating the TLC assay of an active ingredient in a pharmaceutical formulation. *Journal of Liquid Chromatography & Related Technologies, 17*(2), 433-445.

Suryanarayanan, V., Zhang, Y., Yoshihara, S., & Shirakashi, T. (2005). Voltammetric assay of naproxen in pharmaceutical formulations using boron-doped diamond electrode. *Electroanalysis: An International Journal Devoted to Fundamental and Practical Aspects of Electroanalysis, 17*(11), 925-932.

Svetlicic, V., Schmidt, A. J., & Miller, L. L. (1998). Conductometric sensors based on the hypersensitive response of plasticized polyaniline films to organic vapors. *Chemistry of materials, 10*(11), 3305-3307.

Syafiqah, N. A., Termeh Yousefi, A., & Kadri, N. A. (2017). Continuous synthesis of well-crystalline VACNTs using CVD method for engineering applications. *Materials Research Innovations, 21*(6), 379-385.

Taheri, M., Ahour, F., & Keshipour, S. (2018). Sensitive and selective determination of Cu 2+ at d-penicillamine functionalized nano-cellulose modified pencil graphite electrode. *Journal of Physics and Chemistry of Solids*. 117, 180-187.

Tajabadi, M., Basirun, W. J., Lorestani, F., Zakaria, R., Baradaran, S., Amin, Y. M., . . . Sookhakian, M. (2015). Nitrogen-doped graphene-silver nanodendrites for the non-enzymatic detection of hydrogen peroxide. *Electrochimica acta, 151*, 126-133.

Tajabadi, M., Sookhakian, M., Zalnezhad, E., Yoon, G. H., Hamouda, A., Azarang, M., . . . Alias, Y. (2016). Electrodeposition of flower-like platinum on electrophoretically grown nitrogen-doped graphene as a highly sensitive electrochemical non-enzymatic biosensor for hydrogen peroxide detection. *Applied Surface Science, 386*, 418-426.

Tao, H., Brenckle, M. A., Yang, M., Zhang, J., Liu, M., Siebert, S. M., . . . Rogers, J. A. (2012). Silk-based conformal, adhesive, edible food sensors. *Advanced materials, 24*(8), 1067-1072.

Taokaew, S., Seetabhawang, S., Siripong, P., & Phisalaphong, M. (2013). Biosynthesis and characterization of nanocellulose-gelatin films. *Materials, 6*(3), 782-794.

Tarahomi, S., Rounaghi, G. H., & Daneshvar, L. (2019). A novel disposable sensor based on gold digital versatile disc chip modified with graphene oxide decorated with Ag nanoparticles/β-cyclodextrin for voltammetric measurement of naproxen. *Sensors and Actuators B: Chemical, 286*, 445-450.

Tashkhourian, J., Hemmateenejad, B., Beigizadeh, H., Hosseini-Sarvari, M., & Razmi, Z. (2014). ZnO nanoparticles and multiwalled carbon nanotubes modified carbon paste electrode for determination of naproxen using electrochemical techniques. *Journal of Electroanalytical Chemistry, 714*, 103-108.

Tasrin, S., Fazil, S. M. M., Senthilmurugan, S., & Selvaraju, N. (2020). Facile preparation of nanocellulose embedded polypyrrole for dye removal: unary and binary process optimization and seed toxicity. *International Journal of Environmental Science and Technology*, 1-14.

Tay, C. Y., Setyawati, M. I., Xie, J., Parak, W. J., & Leong, D. T. (2014). Back to basics: Exploiting the innate physico-chemical characteristics of nanomaterials for biomedical applications. *Advanced functional materials, 24*(38), 5936-5955.

TermehYousefi, A., Azhari, S., Khajeh, A., Hamidon, M. N., & Tanaka, H. (2017). Development of haptic based piezoresistive artificial fingertip: Toward efficient tactile sensing systems for humanoids. *Materials Science and Engineering: C, 77*, 1098-1103.

TermehYousefi, A., & Kadri, N. A. (2016). Morphology optimization of highly oriented carbon nanotubes for bioengineering applications. *Materials Research Innovations, 20*(4), 268-271.

TermehYousefi, A., Tateno, K., Bagheri, S., & Tanaka, H. (2017). Development of frequency based taste receptors using bioinspired glucose nanobiosensor. *Scientific Reports, 7*(1), 1-9.

Thevenot, D. R., Toth, K., Durst, R. A., & Wilson, G. S. (2001). Electrochemical biosensors: recommended definitions and classification. *Biosensors and Bioelectronics, 16*(1-2), 121-131.

Thostenson, E. T., Ren, Z., & Chou, T.-W. (2001). Advances in the science and technology of carbon nanotubes and their composites: a review. *Composites science and technology, 61*(13), 1899-1912.

Torres-Rendon, J. G., Femmer, T., De Laporte, L., Tigges, T., Rahimi, K., Gremse, F., . . . Wessling, M. (2015). Bioactive gyroid scaffolds formed by sacrificial templating of nanocellulose and nanochitin hydrogels as instructive platforms for biomimetic tissue engineering. *Advanced materials, 27*(19), 2989-2995.

Trettin, A., Zoerner, A. A., Böhmer, A., Gutzki, F.-M., Stichtenoth, D. O., Jordan, J., & Tsikas, D. (2011). Quantification of acetaminophen (paracetamol) in human plasma and urine by stable isotope-dilution GC–MS and GC–MS/MS as pentafluorobenzyl ether derivative. *Journal of Chromatography B, 879*(23), 2274-2280.

Tubino, M., & de Souza, R. L. (2006). Determination of diclofenac in pharmaceutical preparations by diffuse reflectance photometry. *Talanta, 68*(3), 776-780.

Turiel, E., Bordin, G., & Rodríguez, A. R. (2005). Study of the evolution and degradation products of ciprofloxacin and oxolinic acid in river water samples by HPLC-UV/MS/MS-MS. *Journal of Environmental Monitoring, 7*(3), 189-195.

Turkie, N. S., & Munshid, H. Q. (2019). New Approach for the determination of ciprofloxacin hydrochloride using fluorescence resonance energy transfer (FRET) and continuous flow injection analysis via ISNAG-fluorimeter. *Journal of pharmaceutical sciences and research, 11*(4), 1563-1570.

Vahedi, J., Karimi-Maleh, H., Baghayeri, M., Sanati, A. L., Khalilzadeh, M. A., & Bahrami, M. (2013). A fast and sensitive nanosensor based on MgO nanoparticle room-temperature ionic liquid carbon paste electrode for determination of methyldopa in pharmaceutical and patient human urine samples. *Ionics, 19*(12), 1907-1914.

Vieno, N., & Sillanpaa, M. (2014). Fate of diclofenac in municipal wastewater treatment plant—a review. *Environment international, 69*, 28-39.

Vinayan, B., Jafri, R. I., Nagar, R., Rajalakshmi, N., Sethupathi, K., & Ramaprabhu, S. (2012). Catalytic activity of platinum–cobalt alloy nanoparticles decorated functionalized multiwalled carbon nanotubes for oxygen reduction reaction in PEMFC. *International Journal of Hydrogen Energy, 37*(1), 412-421.

Wan, S., Peng, J., Jiang, L., & Cheng, Q. (2016). Bioinspired graphene-based nanocomposites and their application in flexible energy devices. *Advanced materials, 28*(36), 7862-7898.

Wan, S., Peng, J., Li, Y., Hu, H., Jiang, L., & Cheng, Q. (2015). Use of synergistic interactions to fabricate strong, tough, and conductive artificial nacre based on graphene oxide and chitosan. *ACS nano, 9*(10), 9830-9836.

Wang, H., Maiyalagan, T., & Wang, X. (2012). Review on recent progress in nitrogen-doped graphene: synthesis, characterization, and its potential applications. *Acs Catalysis, 2*(5), 781-794.

Wang, H., Zhang, X., Jiang, Z., Li, W., & Yu, Y. (2015). A comparison study on the preparation of nanocellulose fibrils from fibers and parenchymal cells in bamboo (Phyllostachys pubescens). *Industrial Crops and Products, 71*, 80-88.

Wang, J. (2005). Carbon-nanotube based electrochemical biosensors: A review. *Electroanalysis, 17*(1), 7-14.

Wang, J., & Taha, Z. (1990). Catalytic oxidation and flow detection of carbohydrates at ruthenium dioxide modified electrodes. *Analytical chemistry, 62*(14), 1413-1416.

Wang, L., Wu, X., & Xie, Z. (2005). Determination of enrofloxacin and its metabolite ciprofloxacin by high performance capillary electrophoresis with end-column amperometric detection. *Journal of separation science, 28*(11), 1143-1148.

Wang, M., Anoshkin, I. V., Nasibulin, A. G., Korhonen, J. T., Seitsonen, J., Pere, J., . . . Ikkala, O. (2013). Modifying native nanocellulose aerogels with carbon nanotubes for mechanoresponsive conductivity and pressure sensing. *Advanced materials, 25*(17), 2428-2432.

Wang, X., Ma, J., Wang, Y., & He, B. (2001). Structural characterization of phosphorylated chitosan and their applications as effective additives of calcium phosphate cements. *Biomaterials, 22*(16), 2247-2255.

Wang, Y., Wei, X., Li, J., Wang, F., Wang, Q., Chen, J., & Kong, L. (2015). Study on nanocellulose by high pressure homogenization in homogeneous isolation. *Fibers and Polymers, 16*(3), 572-578.

Wang, Z., Tammela, P., Strømme, M., & Nyholm, L. (2015). Nanocellulose coupled flexible polypyrrole@ graphene oxide composite paper electrodes with high volumetric capacitance. *Nanoscale, 7*(8), 3418-3423.

Wang, Z., Tammela, P., Zhang, P., Huo, J., Ericson, F., Strømme, M., & Nyholm, L. (2014). Freestanding nanocellulose-composite fibre reinforced 3D polypyrrole electrodes for energy storage applications. *Nanoscale, 6*(21), 13068-13075.

Wang, Z., Tammela, P., Zhang, P., Strømme, M., & Nyholm, L. (2014). Efficient high active mass paper-based energy-storage devices containing free-standing additive-less polypyrrole–nanocellulose electrodes. *Journal of Materials Chemistry A, 2*(21), 7711-7716.

Wei, D., Liu, Y., Wang, Y., Zhang, H., Huang, L., & Yu, G. (2009). Synthesis of N-doped graphene by chemical vapor deposition and its electrical properties. *Nano letters, 9*(5), 1752-1758.

Wesarg, F., Schlott, F., Grabow, J., Kurland, H.-D., Heßler, N., Kralisch, D., & Müller, F. A. (2012). In situ synthesis of photocatalytically active hybrids consisting of bacterial nanocellulose and anatase nanoparticles. *Langmuir, 28*(37), 13518-13525.

Wu, X.-Y., Niu, W.-J., Cosnier, S., Deng, S.-Y., Zhang, X.-J., & Shan, D. (2015). Ferricyanide confined into the integrative system of pyrrolic surfactant and SWCNTs: The enhanced electrochemial sensing of paracetamol. *Electrochimica Acta, 186*, 16-23.

Xiong, R., Grant, A. M., Ma, R., Zhang, S., & Tsukruk, V. V. (2018). Naturally-derived biopolymer nanocomposites: Interfacial design, properties and emerging applications. *Materials Science and Engineering: R: Reports, 125*, 1-41.

Xu, H., Xie, Y., Zhu, E., Liu, Y., Shi, Z., Xiong, C., & Yang, Q. (2020). Supertough and ultrasensitive flexible electronic skin based on nanocellulose/sulfonated carbon nanotube hydrogel films. *Journal of Materials Chemistry A, 8*(13), 6311-6318.

Xu, M., Chen, L., & Song, J. (2004). Polarographic behaviors of diclofenac sodium in the presence of dissolved oxygen and its analytical application. *Analytical Biochemistry, 329*(1), 21-27.

Xue, Y., Mou, Z., & Xiao, H. (2017). Nanocellulose as a sustainable biomass material: structure, properties, present status and future prospects in biomedical applications. *Nanoscale, 9*(39), 14758-14781.

Yadav, S., Mehrotra, G., Bhartiya, P., Singh, A., & Dutta, P. (2020). Preparation, physicochemical and biological evaluation of quercetin based chitosan-gelatin film for food packaging. *Carbohydrate Polymers, 227*, 115348.

Yan, C., Wang, J., Kang, W., Cui, M., Wang, X., Foo, C. Y., . . . Lee, P. S. (2014). Highly stretchable piezoresistive graphene–nanocellulose nanopaper for strain sensors. *Advanced Materials, 26*(13), 2022-2027.

Yang, K., Wu, W., Jing, Q., & Zhu, L. (2008). Aqueous adsorption of aniline, phenol, and their substitutes by multi-walled carbon nanotubes. *Environmental science & technology, 42*(21), 7931-7936.

Yang, L., Zhang, B., Xu, B., Zhao, F., & Zeng, B. (2020). Ionic liquid functionalized 3D graphene-carbon nanotubes–AuPd nanoparticles–molecularly imprinted copolymer based paracetamol electrochemical sensor: Preparation, characterization and application. *Talanta, 224*, 121845.

Yang, N., Chen, X., Ren, T., Zhang, P., & Yang, D. (2015). Carbon nanotube based biosensors. *Sensors and Actuators B: Chemical, 207*, 690-715.

Yang, X., Wang, F., & Hu, S. (2008). Enhanced oxidation of diclofenac sodium at a nano-structured electrochemical sensing film constructed by multi-wall carbon nanotubes–surfactant composite. *Materials Science and Engineering: C, 28*(1), 188-194.

Yilmaz, B., Kaban, S., Akcay, B. K., & Ciltas, U. (2015). Differential pulse voltammetric determination of diclofenac in pharmaceutical preparations and human serum. *Brazilian Journal of Pharmaceutical Sciences, 51*(2), 285-294.

You, C., Xu, X., Tian, B., Kong, J., Zhao, D., & Liu, B. (2009). Electrochemistry and biosensing of glucose oxidase based on mesoporous carbons with different spatially ordered dimensions. *Talanta, 78*(3), 705-710.

Yousefi, A., Bagheri, S., Kadri, N. A., Mahmood, M. R., & Ikeda, S. (2015). Constant glucose biosensor based on vertically aligned carbon nanotube composites. *International Journal of Electrochemical Science, 10*(5), 4183-4192.

Yousefi, A. T., Tanaka, H., Bagheri, S., Kadri, N. A., Ikeda, S., Mahmood, M. R., & Miyake, M. (2015). Possible high efficiency platform for biosensors based on optimum physical chemistry of carbon nanotubes. *Chemical Vapor Deposition, 21*(10-11-12), 263-266.

Yu, X., Cheng, H., Zhang, M., Zhao, Y., Qu, L., & Shi, G. (2017). Graphene-based smart materials. *Nature Reviews Materials, 2*(9), 1-13.

Zarei, K., & Helli, H. (2015). Electrochemical determination of aminopyrene on glassy carbon electrode modified with multi-walled carbon nanotube–sodium dodecyl sulfate/Nafion composite film. *Journal of Electroanalytical Chemistry, 749*, 10-15.

Zhang, J., Elder, T. J., Pu, Y., & Ragauskas, A. J. (2007). Facile synthesis of spherical cellulose nanoparticles. *Carbohydrate Polymers, 69*(3), 607-611.

Zhang, Q., Chen, C., Chen, W., Pastel, G., Guo, X., Liu, S., . . . Yu, H. (2019). Nanocellulose-enabled, all-nanofiber, high-performance supercapacitor. *ACS applied materials & interfaces, 11*(6), 5919-5927.

Zhang, Y., Chen, Y., Wang, T., Zhou, J., & Zhao, Y. (2008). Synthesis and magnetic properties of nanoporous Co3O4 nanoflowers. *Microporous and Mesoporous Materials, 114*(1-3), 257-261.

Zhao, Q., Gan, Z., & Zhuang, Q. (2002). Electrochemical sensors based on carbon nanotubes. *Electroanalysis, 14*(23), 1609-1613.